6-29-2021

The Coordination Chemistry of the Rhodizonate Dianion and Its Decomposition Products

Joshua A. Silverman
Florida International University, jsilv023@fiu.edu

FLORIDA INTERNATIONAL UNIVERSITY

Miami, Florida

THE COORDINATION CHEMISTRY OF THE RHODIZONATE DIANION AND ITS DECOMPOSITION PRODUCTS

A dissertation submitted in partial fulfillment of

the requirements for the degree of

DOCTOR OF PHILOSOPHY

in

CHEMISTRY

by

Joshua Allen Silverman

2021

To: Dean Michael R. Heithaus
College of Arts, Sciences and Education

This dissertation, written by Joshua Allen Silverman, and entitled The Coordination Chemistry of the Rhodizonate Dianion and its Decomposition Products, having been approved in respect to style and intellectual content, is referred to you for judgment.

We have read this dissertation and recommend that it be approved.

Werner Boeglin

Watson Lees

Christopher Dares

Raphael Raptis

Konstantinos Kavallieratos, Major Professor

Date of Defense: June 29, 2021

The dissertation of Joshua Allen Silverman is approved.

Dean Michael R. Heithaus
College of Arts, Sciences and Education

Andrés G. Gil
Vice President for Research and Economic Development
and Dean of the University Graduate School

Florida International University, 2021

DEDICATION

I dedicate this dissertation to my parents, JoAnn and Richard, for their love and support, my brother, Andrew, my sister, Rachel, and my cuddly dog, Ginger.

ACKNOWLEDGMENTS

First, I wish to thank the US Nuclear Regulatory Commission for sponsoring me throughout my time pursuing a graduate degree at Florida International University with grant numbers NRC-HQ-84-14-G-0040 and NRC-HQ-84-15-G-0038/0038B.

Second, I wish to thank the members of my committee for their support, aid, and advice. In particular, I would like to thank Dr. Raphael Raptis for helping me with inorganic structure determination, and Dr. Christopher Dares for his assistance with X-ray Photoelectron Spectroscopy. I would be remiss without giving an extra special thanks to my major professor Dr. Konstantinos Kavallieratos for not only putting up with my production delays, but also for giving me the extraordinarily rare privilege of permitting me to pursue the research project of my choice and adding it to the research portfolio of our group.

Third, I would like to thank Drs. Indranil Chakraborty and Logesh Mathivathanan for their work in X-ray crystallography and single crystal structure determination.

Finally, I would like to extend a special thanks to the two undergraduates, Shannon Saluga (summer REU student) and Cristian Nodarse, whose work helped completion of Chapters 4 and 3, respectively.

ABSTRACT OF THE DISSERTATION

COORDINATION CHEMISTRY OF THE RHODIZONATE DIANION AND ITS DECOMPOSITION PRODUCTS

by

Joshua Allen Silverman

Florida International University, 2021

Miami, Florida

Professor Konstantinos Kavallieratos, Major Professor

The rhodizonate dianion is of importance for forensic testing, specifically with regard to the sodium rhodizonate test for lead in gunpowder residues. In an effort to understand this test from a chemical perspective, the coordination of rhodizonate and its decomposition products, croconate and oxalate, with several metals has been investigated with many structural and spectroscopic methods.

FT-IR data of the three sequential steps of the sodium rhodizonate test show coordination between Pb(II) atoms, tartrate anions, and rhodizonate dianions, with the tartrate being substituted for Cl^- once a 5% HCl solution is added to produce the confirmatory blue-purple color for Pb. XPS data confirms the coordination of Cl^- to Pb(II) with a shift from the major XPS peak of the Pb $4f_{7/2}$ peak from 138.6 eV to 139.0 eV. UV-Vis titrations show that Pb(II) and rhodizonate bind in a 1:1 ratio in water/ethanol (50/50 by volume).

Rhodizonate was also shown to complex with lanthanides and to form complexes between toxic metals, such as lead, cadmium and mercury, and N-donating co-ligands. UV-Vis titrations show that rhodizonate coordinates to lanthanides in 1:1 ratio in

water/ethanol (50/50 by volume), and to toxic metals forming metal-rhodizonate-N-donating co-ligand complexes in 1:1:1 ratio in water/ethanol (50/50 by volume).

Crystals of the five-member croconate, a decomposition product of rhodizonate, with Pb(II) and Cd(II) show marked differences. Pb(II)-croconate crystals feature 3D-layers of alternating Pb(II) and croconate, while Cd(II)-croconate crystals feature 1D-layers of alternating Cd(II) and croconate held together through a hydrogen bonding network. Metal-rhodizonate solutions left over longer times will further decompose into oxalates, which form 3D metal-oxalate frameworks, unique among metal oxalates, forming large pores, in contrast to 1D and 2D metal-oxalates reported in the literature.

TABLE OF CONTENTS

CHAPTER PAGE

LIST OF TABLES

TABLE PAGE

LIST OF FIGURES

FIGURE PAGE

ABBREVIATIONS AND ACRONYMS

Bipy	2,2’-bipyridine
Cro	Croconate
FT-IR	Fourier Transform Infrared Spectroscopy
Imid	Imidazole
Ln	Lanthanide
MOF	Metal Oxide Framework
OAc	Acetate
Ox	Oxalate
NMR	Nuclear Magnetic Resonance Spectroscopy
Phen	1,10-phenanthroline
Rho	Rhodizonate
Tart	Tartrate
UV-Vis	Ultraviolet-Visible Spectroscopy
XPS	X-ray Photoelectron Spectroscopy

CHAPTER I. INTRODUCTION: THE CHEMICAL AND SPECTROSCOPIC PROPERTIES OF RHODIZONATE AND CROCONATE

1.1 Oxocarbons and Rhodizonate

Rhodizonate ($C_6O_6^{2-}$) is the six-carbon member of a class of cyclic compounds known as oxocarbons. Oxocarbon anions are cyclic carbon and oxygen containing compounds in which the carbons are each part of a carbonyl group. They have the general form $C_nO_n^{2-}$. The first oxocarbon compound was synthesized by Leopold Gmelin in 1825 after reacting carbon dioxide with hot potassium hydroxide. The reaction was later discovered to be more efficient by reacting potassium metal with carbon monoxide [1]. This reaction produces potassium dihydroxyacetylene, which then trimerizes to make $K_6C_6O_6$, which oxidizes in air in an aqueous solution to form dipotassium rhodizonate [1].

$$2K + 2CO \rightarrow 2K_2C_2O_2$$

$$3K_2C_2O_2 \rightarrow K_6C_6O_6 \rightarrow K_2C_6O_6 + 4K^+ + 4OH^-$$

The compound that Gmelin actually isolated and characterized, however, was potassium croconate, $K_2C_5O_5$ [2]. In aqueous solution, rhodizonate undergoes oxidative ring contraction to form croconate, the five-carbon ring oxocarbon [1]. An illustration of the mechanism for this process is shown in Figure 1.1 below.

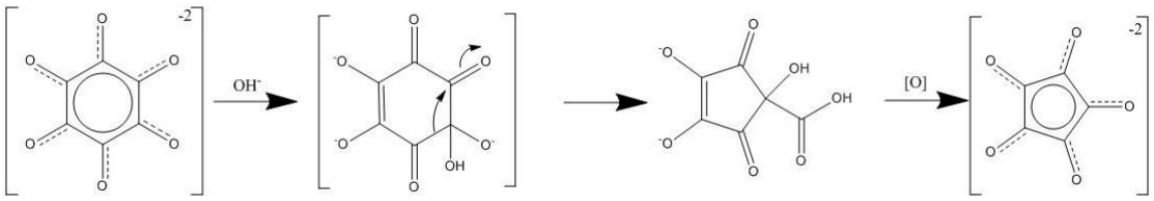

Figure 1.1: The mechanism of oxidative ring contraction in aqueous solution for the transformation of rhodizonate to croconate.

Other oxocarbons have also been synthesized and characterized. Squaric acid, the four member ring oxocarbon, was synthesized in 1969, yet despite the relative newness of

squarate and its difficulty in synthesizing it, there are far more reported compounds involving squarate and its derivatives than for rhodizonate or croconate [3-5]. Deltic acid, the three membered oxocarbon, was synthesized in the 1970s, but its properties and derivatives are still little known [1]. Higher order oxocarbons have been theorized [6] and experimentally discovered, but their extremely low stabilities have led to a scarcity of information about them [7].

1.2 The Sodium Rhodizonate Forensic Test

The most well-known application of rhodizonate is the Sodium Rhodizonate Test [8]. The Sodium Rhodizonate Test (which is somewhat of a misnomer, as potassium rhodizonate works just as well) is a qualitative colorimetric test for lead in gunpowder residues. When a firearm is discharged, the bullet and a cloud of combusted gunpowder, not-combusted gunpowder, and gunpowder primers shoot out of the barrel. This cloud of particulate matter contains lead from the lead styphnate ($PbC_6HN_3O_8$) and lead azide ($Pb(N_3)_2$) found in the gunpowder primer [9]. Rhodizonate anions interact with Pb(II) deposited on the shot surface and display a distinct color. To perform the Sodium Rhodizonate Test, three solutions are required: i) An aqueous solution of sodium (or potassium) rhodizonate, ii) a pH 2.8 buffer solution of tartaric acid with sodium bitartrate, and iii) a 5% HCl solution. The amount of sodium rhodizonate used is nominally 1 g of rhodizonate per 100 mL of deionized water, but conversations with forensic analysts revealed that common practice is to dissolve enough sodium rhodizonate in approximately 100 mL of deionized water to turn the solution to the color of strong tea. This solution is sprayed (about two or three sprays from an ordinary spray bottle) on a shot surface and then two or three sprays of the pH 2.8 buffer are sprayed over the sodium rhodizonate

solution. If lead is present, the surface will turn to a deep red color. To confirm the presence of lead (as other heavy metals also turn red when bound to rhodizonate under acidic conditions), two or three sprays of 5% HCl follow on the red surface. Lead, and only lead, will give a color change into a bluish-purple color [9,10].

Figure 1.2: Pictures of the sodium rhodizonate test for Pb in action: The left picture shows a square of white denim that was shot by a Glock-17 9mm pistol at a distance of 6 inches. The middle picture shows that same cloth after 3 sprays from a spray bottle containing a concentrated aqueous sodium rhodizonate solution and a 0.1 M pH 2.8 sodium bitartrate/tartaric acid buffer in aqueous solution. The Pb from the gunpowder turns a deep red color. The right picture shows that same cloth after 3 sprays of 5% HCl. This confirmatory step makes the Pb, and only the Pb, turn a blue-purple color (pictures taken by the author J. A. Silverman).

The analytical use of Na-rho test has been known for decades [11,12]. Several patents have been filed for detection of lead in a variety of materials, from gasoline [13] to paint [12,14] to the air itself [15]. Further research has been reported on improvements of the sodium rhodizonate test [16], and in applying it to different fabrics [17], skin [18], and even plant materials [19,20]. However, this complex, while routinely formed, has not been isolated and its chemical structure is unknown. The reactivity of rhodizonate in solution that can help elucidate the chemistry behind the Na-rho test has also not been studied and largely remains unknown. Understanding the chemistry and reactivity of rhodizonate is therefore a critical step in efforts to understand and improve this critical forensic test.

1.3 Chemistry and Reactivity of Rhodizonate

There have been relatively few examples of reported fully characterized rhodizonate complexes in the literature. Specifically, there are eight crystal structures with transition metals [21-25] (and none of those are binary complexes), three structures with alkali metals [26-28] (all of which are binary complexes), and four structures that contain no metal [29-32]. The relatively small number of isolated rhodizonate complexes, and the lack of knowledge about rhodizonate reactivity is mainly due to its instability in water. In aqueous solution, the rhodizonate anion rapidly undergoes oxidative ring contraction, as described in Figure 1.1. An aqueous solution of 0.01 M sodium rhodizonate will completely decompose to the carboxy intermediate after about 36 hours. The transition to the five-membered croconate takes about one week. The decomposition of rhodizonate can be shown spectroscopically by the loss of its characteristic 482 nm UV-Vis absorption band. Likewise, the formation of croconate is shown by the increase in its absorbance at 368 nm [33]. This formation of croconate from rhodizonate anion is so straightforward, that it is the standard method for preparing croconate [1].

1.4 Spectroscopy of rhodizonate, other oxocarbons, and their complexes.

1.4.1 UV-Vis and fluorescence

Alkali metal rhodizonate salts are somewhat soluble in water and are typically only soluble in water, and insoluble in common organic solvents, unless they are mixed with water. Water-miscible solvents, such as ethanol, methanol, and acetone can be added to dilute aqueous solutions of alkali metal rhodizonates without precipitating the rhodizonate salts [33]. The molar absorptivity of rhodizonate at 482 nm is 3.3×10^4 L mol^{-1} cm^{-1} [35]. This high molar absorptivity necessitates very dilute solutions of rhodizonate (in the order

of 10^{-5} M) for conducting UV-Vis spectroscopic studies, as deviations from Beer's Law become apparent for higher concentrations ($>10^{-4}$ M). Even though rhodizonate has high absorptivity, it has very low fluorescence emission. Less than 1% of the excited state of rhodizonate in de-oxygenated solutions gives fluorescence emission [35].

Squarate, croconate, and rhodizonate all have a "shoulder" in their UV-Vis spectra at higher frequencies [1]. The intense primary absorption band is caused by an allowed $\pi \rightarrow \pi^*$ transition. The shoulder is caused by a Jahn-Teller distortion in the excited $\pi \rightarrow \pi^*$ state, which is doubly degenerate in oxocarbon systems [36]. This shoulder is not necessarily present in rhodizonate complexes with non-alkali metals. Complexes of rhodizonate with Hg(I), Hg(II), Tl(I), Cd(II), Sr(II), Ba(II), and Zn(II) do display the Jahn-Teller shoulder in aqueous solutions. It should be noted that the relative intensities of the shoulder and primary band differ for each complex. Complexes of Ag(I), Cu(II), and Pb(II) in aqueous solutions do not display the shoulder [33].

In solid form, rhodizonate salts exhibit a wide variety of colors: Solid alkali metal rhodizonates show a marked difference in color from their colors in solution. Na(I) rhodizonate powder is greenish-blue, while K(I) and Cs(I) rhodizonates are dark purple, and Rb(I) rhodizonate is black. In contrast, Ba(II) rhodizonate has the same brown color in both solid form and in solution [37]. While many metal-rhodizonate complexes have been reported, only few X-ray crystal structures are known. Many metal salts, when added to aqueous rhodizonate solutions form colored precipitates. A summary of the precipitated rho complexes is shown in Table 1.1.

Table 1.1: Known precipitates of metal rhodizonates in aqueous solution under two different pHs [33].

Cation	Precipitate in Water at pH 2.8	Precipitate in Water at pH 7.0
Ag^{+}	Black	Black
Hg_2^{2+}	Brownish-red	Brownish-red
Tl^{+}	Dark brown	Dark brown
Pb^{2+}	Deep red	Bluish-purple
Cu^{2+}	None	Orange-red
Hg^{2+}	None	Orange-red
Cd^{2+}	Brownish-red	Brownish-red
Zn^{2+}	None	Brownish-purple
Ba^{2+}	Reddish-brown	Reddish-brown
Sr^{2+}	Reddish-brown	Reddish-brown
Sn^{2+}	Purple	None
UO_2^{2+}	None	Brown
Bi^{3+}	None	Brownish-red

The stability of rhodizonate in aqueous solution is especially low under acidic conditions. Using a mixed solvent system, such as water/ethanol or water/acetone, improves the stability of the rhodizonate anion. Reactions in solution between rhodizonate and various metals in mixed solvent systems, such as water/ethanol or water/acetone, tend to give colored solutions that may or may not give precipitates. A summary of the colors of these metal-rhodizonate solutions in water/ethanol or water/acetone (both 50/50 by volume) is shown in Table 1.2, below:

Table 1.2: A summary of colored solutions of metal-rhodizonates in water/ethanol (50/50 by volume). Using water/methanol or water/acetone (50/50 by volume) yields similar results [33].

Cation	Color
Ag^{+}	Purplish-black
Hg_2^{2+}	Blue
Tl^{+}	Brown
Ba^{2+}	Reddish-brown precipitate
Sr^{2+}	Reddish-brown precipitate
Pb^{2+}	Purple
Cu^{2+}	Orange-red
Cd^{2+}	Reddish-brown
Hg^{2+}	Purple
Zn^{2+}	Brown

1.4.2 Vibrational spectroscopy

1.4.2.1 Binary complexes

The near infrared and Raman spectra of rhodizonate show a few significant features and are dominated by C=O stretches. A few other stretches in the fingerprint region are attributed to various C-C stretches. A list of all the significant IR and Raman-active stretches and their assignments for rhodizonate are shown in Table 1.3 below:

Table 1.3: A list of significant Raman and IR active stretches for the rhodizonate anion [38].

Wavenumber (cm^{-1})	Type	Strength	Assignment
1051	Infrared	Strong	C-C stretch
1252	Raman	Strong	C-C stretch
1449	Infrared	Very Strong	C=O stretch
1546	Raman	Strong	C=O stretch
1669	Raman	Medium	Symmetric C=O stretch

Binding rhodizonate to metals shifts the frequency of these significant stretches, but these shifts are not in a uniform direction and are not easily explained. A summary of the changes of the five vibrational stretches shown in Table 1.3 above when bound to different cations is depicted in Table 1.4 below:

Table 1.4: A summary of important stretches for various rhodizonates. All values are expressed in wavenumbers [38].

$C_6O_6^{-2}$ (cm^{-1})	$K_2C_6O_6$ (cm^{-1})	$(NH_4)_2C_6O_6$ (cm^{-1})	BaC_6O_6 (cm^{-1})	$Ag_2C_6O_6$ (cm^{-1})	$Tl_2C_6O_6$ (cm^{-1})
IR: 1051	1051	1054	1069	1060	1049
Ram.: 1252	1257	1255	1277	1257	1250
IR: 1449	1500	1510	1483	1470	1453
Ram.: 1546	1534 & 1553	1553	1543	1534	1535 & 1550
Ram.: 1669	1661	1659	1676	1661	1661

1.4.2.2 Mixed-Ligand Complexes

There are relatively few reports on metal rhodizonate complexes with N-donor ligands, such as 1,10-phenanthroline (phen) and 2,2'-bipyridine (bipy). Studies performed using resonance Raman spectroscopy on Cu(II)-(phen)-rhodizonate and Cu(II)-(bipy)-rhodizonate complexes show that the charge-transfer transition shown in their electronic spectra exist primarily within the rhodizonate segments of the complexes. In the adducts, the Raman C=O stretches are enhanced in intensity, relative to the unbound rhodizonate. A list of the important Raman-active bands for the free rhodizonate anion and the Cu(II) complexes is shown in Table 1.5 below [39].

Table 1.5: The Raman shifts (in cm^{-1}) of free rhodizonate anion, Cu(bipy)rhodizonate, and Cu(phen)rhodizonate [39].

$C_6O_6^{-2}$	Strength	$Cu(bipy)C_6O_6$	Strength	$Cu(phen)C_6O_6$	Strength	Assignment
352	Very Strong	348	Very Strong	350	Very Strong	Ring Bend
427	Strong	414	Strong	416	Strong	C=O Bend
550	Strong	553	Medium	548	Medium	Ring Breathe
		1040	Medium			Bipy Mode
				1050	Medium	Phen Mode
1253	Medium	1234	Weak	1237	Weak	C-C Stretch
		1431	Weak			Bipy Mode
				1434	Weak	Phen Mode
1553	Strong	1587	Strong	1585	Medium	C=O Stretch
1601	Very Weak	1608	Strong	1606	Medium	C=O Stretch
1661	Medium	1659	Medium	1664	Medium	C=O Stretch

1.4.3 Mass Spectrometry

The mass spectrum of rhodizonate is rather unremarkable. Like all oxocarbons, rhodizonate will eventually fragment during a mass spectrometry experiment into several corresponding carbon monoxide monomers as shown below:

$$C_nO_n \rightarrow n\ CO$$

It is no surprise, then, that ions formed through the loss of CO dominate the rhodizonate and croconate mass spectra. There is some presence of fragments with unequal numbers of carbon and oxygen, such as C_3O_2 or C_2O, formed most likely as a result of losing a CO_2 group sometime during fragmentation. For pseudo-oxocarbons (oxocarbons that substitute other group VI elements for oxygen around the carbon ring, such as C_6S_6), fragments with equal numbers of carbon and a heavier group VI elements are rare. This is most likely due to the instability of compounds such as CS, CSe, and CTe, while CO is highly stable [40].

1.4.4 NMR Spectroscopy

Consisting of only carbon and oxygen, rhodizonate cannot be studied via ^{1}H-NMR. It can be studied with ^{13}C-NMR or ^{17}O-NMR, but neither of these techniques produce a particularly interesting spectrum. The ^{13}C-NMR of rhodizonate produces a singlet at δ = 174 ppm. Compared to ^{13}C-NMR chemical shifts of squarate (δ = 204 ppm) and croconate (δ = 189 ppm), rhodizonate shows stronger shielding, which suggests that the C=O bonds are less polarized, consistent with theoretical predictions [41]. Theoretical studies of rhodizonate ^{17}O-NMR spectrum estimate one singlet at δ = 452 ppm. Compared to the standard ketone ^{17}O-NMR chemical shift of δ = 463 ppm, the small difference suggests that very little π-electron magnetic shielding is taking place. This lack of shielding suggests that rhodizonate, despite the conclusions of earlier studies, is non-aromatic [42].

1.5 Theoretical Studies and Structure

Given the relative scarcity of experimental structural studies on rhodizonate and its complexes, it follows that much of the earlier work in understanding rhodizonate structures was done computationally. While earlier computational studies assumed the bond lengths and geometries of the rhodizonate anion [43], later computational studies, with their improved methods, were able to determine the geometry, bond lengths, and aromaticity of rhodizonate. Initial studies of rhodizonate assumed it had planar shape, giving it a D_{6h} symmetry [44]. However, many computational (and some experimental) studies show that the rhodizonate ring is twisted about 23°, giving it a C_2 symmetry [26, 45].

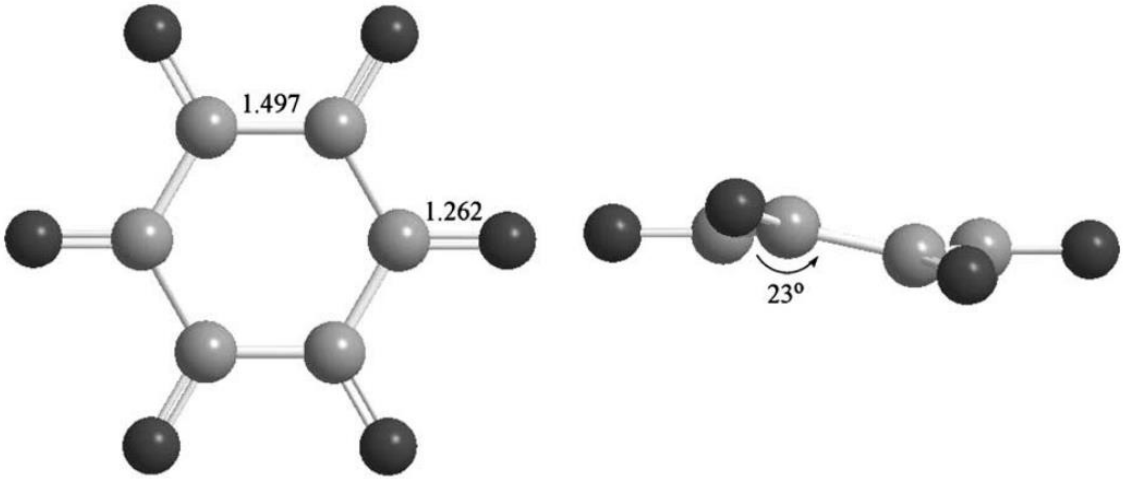

Figure 1.3: The MP2/6-31+G(d) optimized structures for the rhodizonate anion in its D_{6h} planar form (left) and its C_2 twisted conformation (right). The twisted C_2 conformation is shown to be more energetically favorable. Reprinted from [45].

This was demonstrated by the existence of several imaginary frequencies in the structural calculations of rhodizonate anions in planar configurations [45]. Attempting to fit a vertical symmetry plane, σ_v, to force a C_{2v} symmetry, also spawns imaginary frequencies when performing these calculations at several levels of theory [45]. The bond lengths calculated from these computational studies vary depending on the level of theory used. The average

bond lengths for C-C and C-O bonds of the rhodizonate anion in its energetically favored twisted C_2 conformation were calculated to be 1.470 Å and 1.240 Å, respectively [30,46].

1.6 X-ray Crystallography

The first known X-ray crystal structures of metal rhodizonate complexes were reported by Neumann in 1965 [47]. However, Neumann's work in characterizing the crystal structures of potassium rhodizonate and rubidium rhodizonate never made it to the Cambridge Structural Database [28]. Two other studies were published over three decades later, added potassium rhodizonate [28] and rubidium rhodizonate [27] to the database. Soon thereafter, a powder diffraction study of sodium rhodizonate was published [26]. The bond lengths for each compound are found in Table 1.6, below:

Table 1.6: The bond lengths of the different alkali metal rhodizonates in Å [38]. The lithium compounds are theoretically calculated using the B3LYP/6-311+G* basis set [48].

Compound	C-C bond length	C-C bond length	C=O bond length	C=O bond length
$Na_2C_6O_6$	1.451	1.466	1.250	1.253
$K_2C_6O_6$	1.481	1.479	1.255	1.255
$Rb_2C_6O_6$	1.469	1.470	1.253	1.255
$Li_4C_6O_6$	1.409	1.526	1.278	1.381
$Li_6C_6O_6$	1.411	1.411	1.390	1.390

Both sodium and potassium rhodizonate salts have each metal coordinated with eight oxygen atoms from four different rhodizonates. The rhodizonate anion itself has a twisted conformation, much like the free rhodizonate. The root-mean-square deviation from planarity for these compounds is 0.113 Å [26]. In contrast, rubidium rhodizonate has a planar conformation [27].

The many oxygens of rhodizonate permit a high degree of hydrogen bonding, allowing for many organic inclusion complexes. A 2001 study by Lam and Mak shows that rhodizonate can be used to link urea and bis-urea into a crystalline structural network. In

the same study, it was also shown that this structure allows for tautomerization between the D_{6h} and C_{2v} symmetries of rhodizonate, with C-C bond lengths shorter than in rhodizonate complexes of heavier alkali metals [29]. A 2004 study by Wang *et al.,* reported the crystal structures of Cd(II)-rhodizonate-bipyrimidine and Mn(II)-rhodizonate-bipyrimidine. Each metal is in the center of a distorted pentagonal bipyramid, coordinated to two nitrogen atoms from the 2,2'-bipyrimidine (bpym) and four oxygen atoms from the rhodizonate anion (Fig. 1.4).

The rhodizonates coordinate in a bis-bidentate bridging mode with two metal cations, creating a zig-zag pattern between metal and rhodizonate. Measuring the bond lengths in the crystal reveals that the two uncoordinated oxygen atoms have ketone-like character with their adjoining carbon atoms. To date, this is the first reported complex featuring rhodizonate as a bridging ligand while coordinating with a metal cation [24].

All the aforementioned rhodizonate complexes were formed using aqueous rhodizonate anion, $C_6O_6^{-2}$. Until recently, any attempt to grow crystals using rhodizonic acid, $C_6O_6H_2$, had failed. A 2013 study was the first successful experiment growing rhodizonic acid crystals on a metal substrate. By dehydrating the rhodizonic acid under high vacuum, evaporating, and then depositing it on gold or copper, two-dimensional metal-rhodizonic acid structures formed. When deposited on a gold surface, rhodizonic acid forms hexagonal gold clusters. When deposited on the more reactive copper surface, rhodizonic acid coordinates with either three or six copper atoms in a two to one ratio. Since the rhodizonic acid molecules in these clusters still have their hydrogens, it is thought that these complexes would have ferroelectric properties [49].

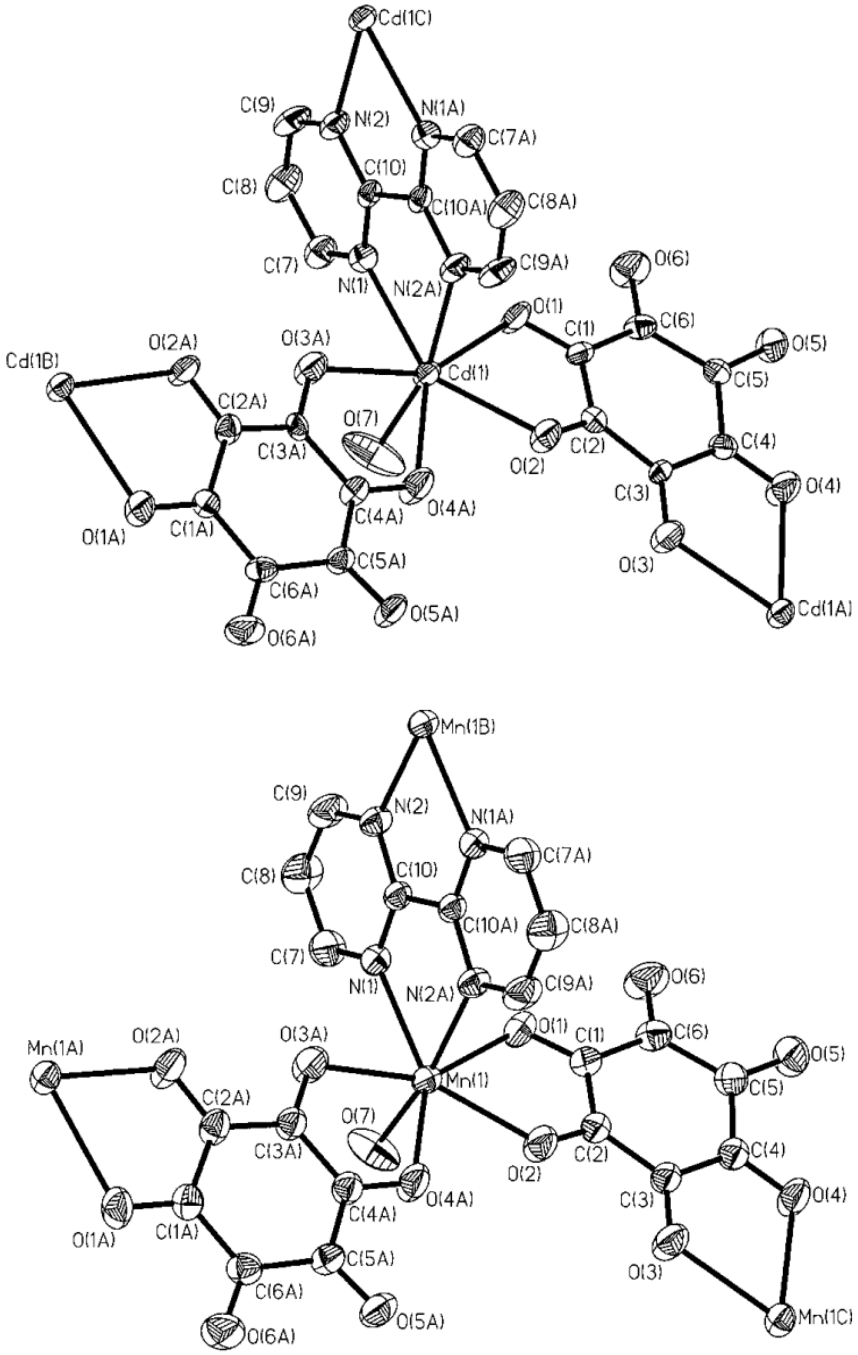

Figure 1.4: ORTEP representations of a Cd(II)-rhodizonate-2,2'-bipyrimidine complex (top) and of a Mn(II)-rhodizonate-2,2'-bipyrimidine complex (bottom). The thermal ellipsoids are set at 50% probability, and H and solvent molecules have been removed. Both drawings show both rhodizonate and 2,2'-bipyrimidine in bis-bridging binding modes. Drawings reprinted from [24].

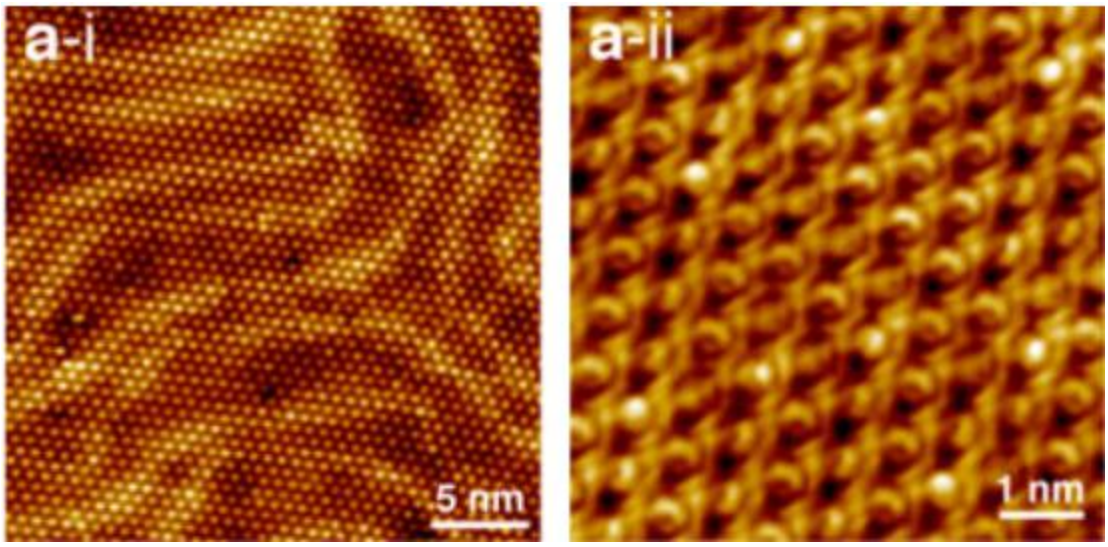

Figure 1.5: Scanning tunneling microscopy images of rhodizonic acid deposited on gold. Figure is reprinted from [49].

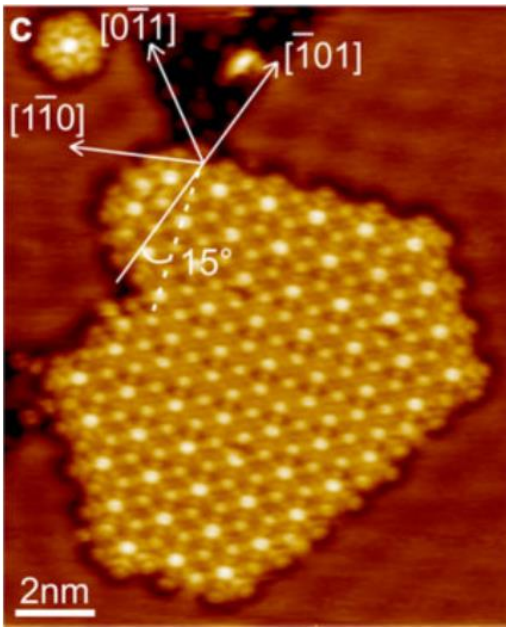

Figure 1.6: Scanning tunneling microscopy image of rhodizonic acid deposited on copper. Figure is reprinted from [49].

1.7 Experimental Methods and Analysis

A system in which a metal, M, and a ligand, L, bind in a 1:1 ratio can be described by the following equation:

$$M + L \leftrightarrows ML$$

The degree to which M and L combine to form ML can be described by the association (or binding) constant, K_a:

$$K_a = \frac{[ML]}{[M][L]}$$

where [M], [L], and [ML] are the molar concentrations of the metal, ligand, and complex, respectively.

The quantity [ML] is impractical to work with. Instead, it is much easier to work with the fraction of complex, $f_{ML,}$ described in the equation below [50]:

$$f_{ML} = \frac{K_a[L]}{1 + K_a[L]} = \frac{[L]_t - [L]}{[M]_t}$$

where the t subscript denotes the total amount in solution.

If one of the quantities is held constant throughout the titration, f_{ML} can be solved using a quadratic equation [50]. Since the measured quantity in a UV-Vis titration is the change in absorbance relative to a solution containing only the fixed reagent in the same concentration as the solution undergoing titration, the change in absorbance can be found with the following equation [51, 52].

$$\Delta A = \frac{-|\Delta A_{max}| \times ([L] + [M] + K_a^{-1} - \sqrt{([L] + [M] + K_a^{-1})^2 - 4 \times [L] \times [M]})}{2 \times [L]}$$

1.8 Dissertation Scope and Overall Summary

This dissertation will describe our progress in understanding the chemistry of croconate and rhodizonate oxocarbons and the implications to the Na-rho forensic test in six distinct chapters, which correspond to publications published, submitted, or in preparation. Chapter 2 describes work done to characterize the products of the sodium rhodizonate test. Chapter 3 details the work done on rhodizonate complexation with

lanthanides. Chapter 4 describes the work done on rhodizonate with toxic metals, mainly cadmium, mercury, and lead, also including mixed ligand coordination with N-donor co-ligands, such as 2,2'-bipyridine (bipy), 1,10-phenahtroline (phen) and imidazole (imid). Chapter 5 (Silverman, J. A., Mathivathanan, L., Govor, E. V., Raptis, R. G., Kavallieratos, K. *Acta Cryst. C,* **2019,** *75,* 935-940) describes two new Pb(II) croconate and Cd(II) croconate complexes. These were obtained in attempting to crystallize the rhodizonate complexes, but decomposition to croconate gave the described products. Chapter 6 describes two new crystal structures of 3D MOFs with oxalate formed from the decomposition of rhodizonate and later croconate, as well as research into the decomposition of rhodizonate. Finally, Chapter 7 serves as a conclusion, tying up the previous chapters together and summarizing the research outcomes of this dissertation.

1.9 References

[1] West, R., *Isr. J. Chem.,* **1979,** *20,* 300-307.

[2] Gmelin, L., *Ann. Physik. Chem.,* **1825,** *4,* 3.

[3] The Cambridge Crystallographic Data Centre, https://www.ccdc.cam.ac.uk/structures/Search?Compound=rhodiz&DatabaseToSearch=Published, Accessed May 7, 2021.

[4] The Cambridge Crystallographic Data Centre, https://www.ccdc.cam.ac.uk/structures/Search?Compound=crocon&DatabaseToSearch=Published, Accessed May 7, 2021.

[5] The Cambridge Crystallographic Data Centre, https://www.ccdc.cam.ac.uk/structures/Search?Compound=squar&DatabaseToSearch=Published, Accessed May 7, 2021.

[6] Seitz, G. and Imming, P., *Chem. Rev.,* **1992,** *92,* 1227-1260.

[7] Iraci, G. and Back, M. H., *Can. J. Chem.,* **1988,** *66,* 1293-1294.

[8] Dillon, J. H., *AFTA J.,* **1990,** *22,* 251-256.

[9] Lichtenberg, W., *Forensic Sci. Rev.,* **1990,** *2,* 38-62.

[10] Dillon, J. H., *AFTA J.,* **1990,** *22,* 257-268.

[11] Feigl, F. and Suter, H. A., *Ind. Eng. Chem.,* **1942,** *14,* 840-842.

[12] Feigl, F., Gentil, V., Libergott, E., *Isr. J. Chem.,* **1969,** *7,* 123-125.

[13] Fabbro, L. A. and Wentzel, C. S., Process for Detecting Trace Amounts of Lead in Unleaded Gasoline, US 19743806319, April 23, 1974.

[14] Cole, S. L., Chemical Spot Test for Lead in Paint and Other Media, US 20030203496 A1, October 30, 2003.

[15] Ronneau, C. J-M., Jacob, N. M., Apers, D. J., *Anal. Chem.,* **1973,** *45,* 2152.

[16] Morosanova, E. I., Kuz'min, N. M., Zolotov, Y. A., *J. Anal. Chem.,* **1997,** *357,* 853-859.

[17] Marshall, J., *Can. Soc. Forensic Sci. J.,* **2006,** *39,* 115-124.

[18] Andreola, S., Gentile, G., Battistini, A., Cattaneo, C., Zoja, R., *J. Forensic Sci.,* **2011,** *56,* 771-774.

[19] Glater, R. A. B. and Hernandez, L., *J. Air Waste Manage. Assoc.,* **1972,** *22,* 463-467.

[20] Seregin, I. V. and Kozhevnikova, A. D., *Russ. J. Plant Physiol.,* **2011,** *58,* 721-727.

[21] Fisher, M. G., Gale, P. A., Light, M. E., Quesada, R., *Cryst. Eng. Comm.,* **2008,** *10,* 1180-1190.

[22] Finger, L. H. and Sundermeyer, J., *J. Inorg. Gen. Chem.,* **2015,** *641,* 2565-2569.

[23] Eiji, A., Shoji, M., Haruka, T., Satoshi, T., Makoto, T., Yuji, M., Daisuke, Y., Masahiro, M., *Chem. Lett.,* **2009,** *38,* 1170-1171.

[24] Wang, C., Kuo, C., Chou, P., Lee, G., *Angew. Chem. Int. Ed.*, **2004,** *43*, 4507-4510.

[25] Gale, P. A., Light, M. E., Quesada, R., *Cryst. Eng. Comm.*, **2006,** *8*, 178-188.

[26] Dinnebier, R. E., Nuss, H., Jansen, M., *Acta Crystallogr., Sect. E: Struct. Rep. Online*, **2005,** *61*, 2148-2150.

[27] Braga, D., Cojazzi, G., Maini, L., Grepioni, F., *New J. Chem.*, **2001,** *25*, 1221-1223.

[28] Cowan, J. A. and Howard, J. A. K., *Acta Crystallogr., Sect. E: Struct. Rep. Online*, **2004,** *60*, 511-513.

[29] Lam, C. and Mak, T. C. W., *Angew. Chem. Int. Ed.*, **2001,** *40*, 3453-3455.

[30] Lam, C-K., and Mak, T. C. W., *Chem. Commun.*, **2001,** 1568-1569.

[31] Abrahams, B. F., Haywood, M. G., Robson, R., *Cryst. Eng. Comm.*, **2005,** *7*, 629-632.

[32] Murray, C. A., Zhu, Z., Cardin, C. J., Colquhoun, H. M., Greenland, B. W., *Supramolecular Chem.*, **2018,** *30*, 751-757.

[33] Chalmers, R. A. and Telling, G. M., *Microchim Acta*, **1966,** 1126-1135.

[34] Kovalchukova, O. and Strashnova, S., *Rev. Inorg. Chem.*, **2014,** *34*, 1-24.

[35] West, R., Downing, J. W., Inagaki, S., Michl, J., *J. Am. Chem. Soc.*, **1981,** *103*, 5073-5078.

[36] Aihara, J., *Bull. Chem. Soc. Jpn.*, **1974,** *11*, 2899-2900.

[37] Bailey, R. T., *J. Chem. Soc. (B)*, **1971,** 627-629.

[38] Gonçalves, N. S. and Santos, P. S., *J. Raman Spectrosc.*, **1995,** *26*, 363-372.

[39] de Oliveira, L. F. C. and Santos, P. S., *J. Mol. Struct.*, **1991,** *263*, 59-67.

[40] Schröder, D., Schwarz, H., Dua, S., Blanksby, S., J., Bowie, J., H., *Int. J. Mass Spectrom.*, **1999,** *188*, 17-25.

[41] Staedli, W., Hollenstein, R., von Phillipsborn, W., *Helv. Chim. Acta*, **1977,** *60*, 948.

[42] Quiñonero, D., Garau, C., Frontera, A., Ballester, P., Costa, A., Deyà, P., M., *Chem. Eur. J.*, **2002,** *8,* 433-438.

[43] I'Hara, Y. J. and Sakamoto, K., *J. Am. Chem. Soc.*, **1970**, *92,* 2636-2639.

[44] Ito, M., and West, R., *J. Am. Chem. Soc.,* **1963,** *85,* 2580.

[45] Junqueira, G. M. A., Rocha, W. R., de Almeida, W. B., Dos Santos, H. F., *J. Mol. Struct.,* **2004,** *684,* 141-147.

[46] Kolev, T., Koleva, B. B., Spiteller, M., *Cent. Eur. J. Chem.,* **2008,** *6,* 393-399.

[47] Neumann, M. A., PhD Thesis, University of Wisconsin, **1965.**

[48] von Ragué Schleyer, P., Najafian, K., Kiran, B., Jiao, H., *J. Org. Chem.*, **2000,** *65,* 426-431.

[49] Kunkel, D. A., Hooper, J., Simpson, S., Beniwal, S., Morrow, K. L., Smith, D. C., Cousins, K., Ducharme, S., Zurek, E., Enders, A., *J. Phys. Chem. Lett.,* **2013,** *4,* 3413-3419.

[50] Thordarson, P. *Chem. Soc. Rev.,* **2011,** *40,* 1305-1323.

[51] Kavallieratos, K., Rosenberg, J. M., Bryan, J. C., *Inorg. Chem.,* **2005,** *44,* 2573.

[52] Connors, K. A. (1987). *Binding Constants: The Measurement of Molecular Complex Stability*, Wiley-Interscience: New York.

CHAPTER II. COMPLEXATION OF Pb(II) AND RHODIZONATE: TOWARDS UNDERSTANDING THE SODIUM RHODIZONATE TEST

Joshua A. Silverman, Christopher J. Dares, Konstantinos Kavallieratos*

2.1 Abstract

Addition of HCl to a red product formed after the rhodizonate oxocarbon $C_6O_6^{2-}$ (rho) in the form of its disodium salt ($Na_2C_6O_6$) is mixed with Pb-containing residue in a pH 2.8 tartrate (tart) buffer gives a blue-purple product, which has been used for years as a confirmatory test for Pb presence in forensic applications. UV-Vis, FT-IR, and XPS measurements are all consistent with the hypothesis that this product is a Pb(II) complex containing $C_6O_6^{2-}$, tartrate, and Cl^- ligands. All the above methods show noticeable differences in the Pb(II) binding environment as the red Pb-rhodizonate-tartrate complex $Pb_2(C_6O_6)(C_4H_4O_6)(H_2O)_3$ (*catena*-[[μ_2-rhodizonato-$\kappa^4O^1,O^2:O^3,O^4$]-bis[diaqualead(II)]-[aqualead(II)-μ_2-tartrato-κ^2O^1,O^4]]) (Pb-Rho-Tart), which is initially formed during the first step of the test, is subsequently converted into the final Cl^--containing product $Pb_3(C_6O_6)_2Cl_2(H_2O)_6$ (*catena*-di-μ-chlorido-bis[diaqualead(II)-μ_2-rhodizonato-$\kappa^4O^1,O^2:O^3,O^4$] (Pb-Rho-Cl). Specifically, in XPS, the Pb 4f 7/2 binding energy increases from 138.6 eV to 139.0 eV, which is consistent with a Pb(II)-Cl bonding environment. Furthermore, the high resolution C 1s spectrum of the Cl^--containing blue-purple complex Pb-rho-Cl^- shows an intense peak at 284.7 eV, which corresponds to a C-C single bond environment and an intense peak at 288.7 eV which corresponds to a C=O, suggesting that the complexed rhodizonate in the final product has a structure closer to the resonance form containing distinct C=O and C-O^-, as opposed to the Pb-rho and the Pb-rho-tartrate complexes that show a uniform environment for C-O bonds. Addition of HCl to the red Pb-Rho-Tart complex in solution shows little change in the maximum absorbance

wavelength. However, the UV-Vis spectra of the purple Pb-Rho, red Pb-Rho-Tart, and purple Pb-Rho-Cl complexes show a loss of the shoulder at 446 nm found in the $Na_2C_6O_6$ UV-Vis spectrum. These measurements, as well UV-Vis titration experiments, were made possible by using a 50/50 v/v water-ethanol solvent that not only facilitates solubility in the μM concentration range, but also prevents the well-known decomposition pathway of rhodizonate to 5-member croconate, for the duration of these experiments. Non-linear regression analysis of the UV-Vis binding curves are consistent with 1:1 binding, with fitting to the 1:1 binding isotherm giving a binding constant $K_{11} = 1.2 (\pm 0.2) \times 10^6\ M^{-1}$ for the formation of Pb(II)-rho complex in solution. Comparison of the FT-IR spectra shows differences both in frequency and number of bands for the C=O stretching region. Most notably, the final product of the test (Pb-Rho-Cl) shows C=O stretches at the 1750-1600 cm^{-1} range, a higher frequency than any of the other complexes, which are indicative of C=O higher bond order. In contrast, the Pb-rho and Pb-rho-tart complexes show stretching bands in the 1500-1300 cm^{-1} range, suggesting resonance forms with $C\text{-}O^-$ bonding, intermediate between a single and double bond.

2.2 Introduction

One of the most well-known uses of rhodizonate oxocarbon (rho) is in the sodium rhodizonate test, a procedure used in the forensic sciences to detect lead in gunpowder residues, primarily for distance-to-target determination. This test can detect Pb in various forms including solids [1-4], solutions [5, 6], or gaseous [7] forms. The test's utility is not restricted to the forensic sciences, however. Home lead detection kits first hit the consumer market in 1988, ten years after the United States banned lead paint for use in residential buildings. These kits use a simplified form of the modern sodium rhodizonate test, are easy

to use, and give fast results while having well-known interferences that are conveniently listed on the box [8]. Despite its wide use, the underlying chemistry of the sodium rhodizonate test is not well understood, and studies have been hindered by the lack of rhodizonate stability in solution, as it decomposes to the 5-member croconate [9]. Research into the sodium rhodizonate test has focused on ease of use [6], applying the sodium rhodizonate test for Pb to different surfaces, such as several fabrics [10], skin [11], and plants [12,13], and transferring gunshot residues from dark-colored backgrounds onto lighter surfaces to make the test results easier to interpret [14]. The modern sodium rhodizonate test is performed using three solutions: a saturated aqueous sodium rhodizonate solution (typically 50 mg of sodium rhodizonate dissolved in 25 mL of deionized water), a pH 2.8 buffer of sodium bitartrate and tartaric acid (1.5 g of tartaric acid and 1.9 g of sodium tartrate in 100 mL of deionized water), and a 5% solution of HCl in deionized water [15,16]. In the presence of the tartrate buffer at pH 2.8, Pb reacts with rhodizonate to form a scarlet red complex. Unfortunately, it was soon discovered that other metals will also form a red complex. While they may not produce a precipitate of the exact same color, the colors are similar enough to make the test unreliable as a colorimetric test [2]. Furthermore, since bullet holes are frequently accompanied by large amounts of blood, finding the red-colored precipitate to prove that Pb is present is extremely difficult. A final step, the addition of 5% HCl, confirms the presence of Pb by turning the red complex into a blue-purple color, which is unique to Pb(II) presence [17].

Unfortunately, the instability of rhodizonate in aqueous solutions has led to very few studies of the solution chemistry of the test [18] and a dearth of characterized rhodizonate structures. As of September 2020, there are only 17 rhodizonate-containing

structures in the Cambridge Crystallographic Data Centre (compared with 158 croconate structures and 866 squarate structures) [19]. The few binary rhodizonate crystal structures that are known tend to feature alkali metals [20-22]. Oxocarbon dianions usually exist as two tautomers: a charge-localized form with C_{2v} symmetry and a charge-delocalized form with D_{nh} symmetry [20, 22-27]. The rhodizonate anion and sodium rhodizonate, however, have a twisted ring conformation giving those molecules a C_2 symmetry [22]. The structures of the compounds involved in the sodium rhodizonate test are also unknown to date, though a study recently presumed that compounds of formulas $Pb_3(C_6O_6)_2(OH)_2 \cdot 6H_2O$ for the scarlet complex and $Pb_2(C_6O_6)(Cl)_2 \cdot 2H_2O$ for the blue-violet complex are involved [28]. Attempts to simulate the sodium rhodizonate test in solution (in order to obtain spectroscopic and binding data) are hampered by the instability of the rhodizonate and because of the tendency for many metal rhodizonates to precipitate out of solution [1]. Herein, we demonstrate that by using a water/ethanol (50/50 by volume) solvent system, we can substantially increase the rho stability in solution, and thus study its interaction and coordination with Pb and the interconversion of products involved in the sodium rhodizonate test. While the literature contains studies on the degradation of aqueous rhodizonate anion over time [18, 24], to our knowledge, this is the first study to date that successfully simulates the Na-rho test in solution, having addressed the stability issues. UV-Vis titrations and Job Plots in solution, as well as FT-IR and XPS spectra in solid state provide important clues to the structures of these commonly made, yet poorly understood products and thus provide avenues for further improvement of the test and expansion of its application to potentially more complicated systems.

2.3 Experimental Section

2.3.1 Materials and Methods

3,4,5,6-Tetraoxocyclohexene-1,2-diol disodium salt (rhodizonic acid, disodium salt) was purchased from Sigma-Aldrich. Anhydrous $Pb(NO_3)_2$ was purchased from Fisher Scientific. All chemicals were reagent grade and were used without further purification. HCl was purchased from Fisher Scientific. All buffer compounds were purchased from Sigma-Aldrich. The water used in all experiments was nano-pure with a resistivity >17 MΩ cm^{-1} (Millipore by Barnstead Thermolyne Corporation, Dubuque, IA). Acetone (spectroscopic grade) was purchased from Fisher Scientific and was used without further purification. Ethanol (200 proof) was purchased by Pharmco-Aaper. FT-IR measurements were collected on an Agilent Technologies Cary 670 FT-IR with a diamond ATR attachment. X-ray photoelectron spectra (XPS) were collected on a Kratos Axis Ultra DLD X-ray photoelectron spectrometer using a monochromatic Al K-alpha source with a 20 eV analyzer pass energy for high resolution work. Energy correction using the lowest energy binding component of the C 1s peak to 284.6 eV. Peak fittings were achieved using pseudo-Voight functions adjusted to minimize the residual difference between modeled peaks and experimentally acquired data. UV-Vis spectra were collected on a Varian Cary-100 UV-Visible spectrophotometer or on a Shimadzu UV-2101PC UV-Visible spectrophotometer.

2.3.2 Synthesis

2.3.2.1 Pb(II)-Rhodizonate, $Pb_2(C_6O_6)(OH)_2(H_2O)_4 \bullet H_2O$ (**1**)

Lead (II) rhodizonate (isolated as a 1:1 coordination polymer of Pb(II) rhodizonate and Pb(II)-hydroxide) was formed by mixing a solution of 64.2 mg (0.3 mmol) of $Na_2C_6O_6$ in 100.0 mL of water with a solution of 99.3 mg (0.3 mmol) of $Pb(NO_3)_2$ in 100.0 mL of

water. Doing so causes a purple precipitate to immediately form. This precipitate was vacuum filtered, washed with water, acetone, and dichloromethane (DCM), and dried under vacuum overnight (92.8 mg, 0.135 mmol, 82.4% yield). Elemental analysis calculated for $Pb_2(C_6O_6)(OH)_2(H_2O)_4 \bullet H_2O$: C = 10.20%, H = 1.72%, N = 0.00%. Found: C = 10.43%, H = 1.78%, N = 0.00%. FT-IR (cm^{-1}): 3358 (w, br), 1604 (s), 1574 (s), 1456 (s), 1368 (s), 1304 (s), 1081 (w), 1057 (m), 779 (m).

2.3.2.2 Pb(II)-Tartrate-Rhodizonate, $Pb_2(C_6O_6)(C_4H_4O_6)(H_2O)_3$ **(2)**

A pH = 2.8 bitartrate/tartaric acid buffer was prepared by dissolving 1.5 g of tartaric acid and 1.9 g of sodium bitartrate in 100.0 mL of water as described in the AFTE guidelines [6]. After forming the buffer, 42.8 mg of $Na_2C_6O_6$ (0.2 mmol) and 66.2 mg of $Pb(NO_3)_2$ (0.2 mmol) were dissolved in the tartrate buffer solution. A red precipitate was immediately formed, which was vacuum filtered, washed with water, acetone, and DCM, and dried under vacuum overnight (83.6 mg. 0.107 mmol 53.5% yield). Elemental analysis calculated for $Pb_2(C_6O_6)(C_4H_4O_6)(H_2O)_3$: C = 15.29%, H = 1.41%, N = 0.00%. Found: C = 15.05%, H = 1.42%, N = 0.00%; FT-IR (cm^{-1}): 3182 (m, br), 1635 (m), 1582 (m), 1536 (m), 1454 (vs), 1420 (vs), 1361 (m), 1307 (m), 1266 (m), 1181 (w), 1115 (s, sh), 1069 (s, sh), 1049 (m), 997 (vw), 922 (vw), 896 (vw), 838 (w), 813 (w), 779 (vw), 714 (m), 664 (w).

2.3.2.3 Pb(II)-Tartrate-Rhodizonate-Cl, $Pb_3(C_6O_6)_2Cl_2(H_2O)_6$ **(3)**

10 mL of concentrated HCl was directly added to 40.2 mg (0.0515 mmol) of the red powder **2** in water (the red powder had already precipitated out of solution)**.** After briefly stirring, the powder's color changed from red into blue-purple. The blue-purple powder was filtered under vacuum, washed with water, acetone, and DCM, and dried

overnight under vacuum (25.0 mg, 0.0220 mmol, 42.7% yield). Elemental analysis calculated for $Pb_3(C_6O_6)_2Cl_2(H_2O)_6$: C = 12.68%, H = 1.07%, Cl = 6.24%. Found: C = 12.31%, H = 0.90%, Cl = 6.59%. FT-IR (cm^{-1}): 3404 (w, br), 1716 (m), 1592 (w, br), 1426 (s), 1362 (s), 1294 (s), 1114 (w), 1061 (m).

2.3.3 X-Ray Photoelectron Spectroscopy

XPS spectra were acquired using a Kratos Axis Ultra DLD X-ray photoelectron spectrometer using a base pressure of 6×10^{-9} Torr. A monochromatic Al K-alpha x-ray source was used with an analyzer pass energy of 80 eV and 20 eV were used for survey and high resolution scans respectively. Baselines were fit to polynomials using a least-squares regression. Features in baseline-subtracted data were fit to a minimal number of pseudo-voight functions. These peaks were fit to model the data using the Solver add-on to Microsoft Excel such that the residual difference between the model and experimental data was minimized.

2.3.4 Rhodizonate Stability Study in Water/EtOH (50/50 by volume)

To determine the stability of rhodizonate in solution over time, a 2.0×10^{-5} M aqueous solution of sodium rhodizonate was prepared. A cuvette was filled with 1.5 mL of this solution and 1.5 mL of a miscible organic solvent, then mixed. All spectra were collected with a Shimadzu UV-2101PC UV-Vis spectrophotometer. Cuvettes were left in the spectrophotometer for 2 hours, and the spectra were collected every 5 minutes. The same procedure was used with a cuvette filled with 3.0 mL of a 1.0×10^{-5} M aqueous solution of sodium rhodizonate to compare the change in absorbance over time in a purely aqueous solvent.

2.3.5 UV-Visible Titrations

All measurements were performed in triplicate using three independently prepared samples. In a typical UV-Vis titration experiment, solutions of sodium rhodizonate ($Na_2C_6O_6$, 1.0 x 10^{-5} M) in water/ethanol (50/50 v/v) (solution A) were titrated with water/ethanol (50/50 v/v) solutions of $Pb(NO_3)_2$ (1.0 x 10^{-3} M) at constant sodium rhodizonate concentration (1.0 x 10^{-5} M) (Solution B). For spectra collection, 3.00 mL of the $Na_2C_6O_6$ solution (solution A) were added to a cuvette and 5.00-25.0 μL sequential additions of solution B were added at 5 min intervals until a total of 200.0 μL had been added. All spectra were collected with a Shimadzu UV-2101PC UV-Visible spectrophotometer. Titrations at longer time intervals established that the complex formation reaction in solution reaches equilibrium in less than 5 min.

The above procedure was repeated for the tartrate buffer titration. Solution A contained **1** (3.0 x 10^{-5} M) in water/ethanol (50/50 v/v). Solution B contained **1** (3.0 x 10^{-5} M), 1.5 x 10^{-3} M of L-tartaric acid, and 1.5 x 10^{-3} M of sodium bitartrate in water/ethanol (50/50 v/v). A similar procedure was used to for the third step of the sodium rhodizonate test: Solution A contained **2** (5.0 x 10^{-5} M) in water/ethanol (50/50 v/v). Solution B contained **2** (5.0 x 10^{-5} M) and HCl (0.6 M) in water/ethanol (50/50 v/v). In order to verify the stoichiometric ratios between Pb(II), tartrate, rho, and Cl^-, the last two series of titration experiments were performed by adding Pb(II) to solutions of rho/tart and rho/tart/HCl respectively. Specifically, tartrate buffer titration was repeated with Solution A containing only 5.0 x 10^{-5} M $Na_2C_6O_6$ and 5.0 x 10^{-5} M of tartrate buffer (instead of **1**). Solution B contained 5.0 x 10^{-5} M $Na_2C_6O_6$, 5.0 x 10^{-5} M of tartrate buffer, and 5.0 x 10^{-3} M of $Pb(NO_3)_2$. The last step was repeated as well with Solution A containing 5.0 x 10^{-5} M

$Na_2C_6O_6$, 5.0 x 10^{-5} M of tartrate buffer, and 5.0 x 10^{-5} M HCl. Solution B contained 5.0 x 10^{-5} M $Na_2C_6O_6$, 5.0 x 10^{-5} M of tartrate buffer, 5.0 x 10^{-5} M HCl, and 5.0 x 10^{-3} M of $Pb(NO_3)_2$.

2.3.6 UV-Visible Job Plots

To determine the Pb-rhodizonate complexation ratio by Job's method, $Na_2C_6O_6$ (40.0 mg, 0.187 mmol) was dissolved in 1.00 L of deionized water, giving an orange solution. An amount of this solution (50.0 mL) was added to an equal amount of acetone. An equimolar amount of $Pb(NO_3)_2$ (61.9 mg, 0.187 mmol), was also dissolved in 1.00 L of deionized water. Some of this solution (50.0 mL) was mixed with acetone in the same manner as $Na_2C_6O_6$. Aliquots of both solutions (10.0 mL total) were added to 11 different vials in such a way that every integer ratio of each solution was represented (i.e. one vial with 0.0 mL $Na_2C_6O_6$ and 10.0 mL $Pb(NO_3)_2$, one vial with 1.0 mL $Na_2C_6O_6$ and 9.0 mL $Pb(NO_3)_2$, one vial with 2.0 mL $Na_2C_6O_6$ and 8.0 mL $Pb(NO_3)_2$, etc.). Each vial was shaken by hand for 5 minutes to achieve equilibrium. The UV-Vis spectra of each sample (3.00 mL total volume) were collected. The wavelength of interest is the absorbance maximum for $Na_2C_6O_6$, at 482 nm.

The Job plot experiments for formation of the red Pb(II)-rho-tart complex (**2S**) were performed in water/ethanol (50/50 v/v) by a modification of the procedure described above using the tartaric acid buffer (see titration section).

The Job plot experiments for the formation of the blue-violet Pb(II)-rhodizonate-Cl complex (**3S**) were performed in water/ethanol (50/50 v/v) by a modification of the procedure described above using 5% HCl (see titration section).

2.4 Results and Discussion

2.4.1 Synthesis

Compound **1**, was readily precipitated as a purple polymeric powder with formula $Pb_2(C_6O_6)(OH)_2(H_2O)_4 \bullet H_2O$ by mixing $Pb(NO_3)_2$ with $Na_2C_6O_6$ in an aqueous solution. This reaction is instantaneous. Unlike aqueous $Na_2C_6O_6$, which will decompose into croconate after a few days, the purple Pb(II)-rhodizonate powder is stable even after several months. This purple polymer resists attempts to dissolve it – the only common solvent that dissolved this complex was DMSO, which decomposed the complex, giving a purple-colored solution with a ^{13}C-NMR spectrum similar to the one for Na-rho (δ = 185 ppm compared to δ = 188 ppm).

Compound **2** was readily precipitated as a red polymeric powder with formula $Pb_2(C_6O_6)(C_4H_4O_6)(H_2O)_3$ by mixing $Pb(NO_3)_2$ into an aqueous 0.1 M pH 2.8 sodium bitartrate/tartaric acid buffer with dissolved $Na_2C_6O_6$. This reaction is instantaneous. Like the purple Pb(II)-rhodizonate complex, the red Pb(II)-rhodizonate-tartrate powder is stable even after several months. Also, this red polymer resists attempts to dissolve it – the only common solvent that dissolved this complex was DMSO, which decomposed the complex, giving a red-colored solution with a ^{13}C-NMR spectrum similar to the one for Na-rho (δ = 184 ppm compared to δ = 188 ppm).

Compound **3** was readily precipitated as a purple polymeric powder by mixing solid preformed compound **2** with aqueous 5% HCl. This reaction is instantaneous. Unlike complexes **1** and **2**, this complex loses its purple color if left in an acidic medium, as previously reported [28]. This purple polymer, like compounds **1** and **2**, resists many attempts to dissolve it – the only common solvent that dissolved this complex was DMSO,

which decomposed the complex, giving a colorless solution with a ^{13}C-NMR spectrum similar to the one for Na-rho (δ = 189 ppm compared to δ = 188 ppm).

2.4.2 FT-IR Spectroscopy

The FT-IR spectra of compounds **1, 2,** and **3** (Figure 2.1) provide important clues to their molecular structure and bonding. In agreement with the elemental analysis results, and despite the drying process, a broad absorption band indicative of hydrogen bonded O-H···H stretch at 3358 cm^{-1} suggests the presence of H-bonded water and/or OH^- in the complex. Unlike the $Na_2C_6O_6$ spectrum (Figure 2.1), with a broad C-O stretch at 1440 cm^{-1}, the spectrum of **1** features several carbon-oxygen stretches. However, while these stretches are quite strong and broad, like a typical C=O stretch, they occur below 1600 cm^{-1}, suggesting that these stretches have less of a double bond character for C-O. Additionally, the stretches at 1574 cm^{-1} and 1456 cm^{-1} suggest some aromatic character to the rhodizonate ring. The C-O stretches at 1081 cm^{-1} and 1057 cm^{-1} are on the lower end of known C-O stretches, but it is known in the literature that stretches for atoms that are bonded to heavy elements have IR stretching bands that are shifted to lower wavenumbers. [29,30]. A prior literature report on the structure of $Na_2C_6O_6$ shows that each O atom is coordinated with a Na atom in a distorted square antiprism [22]. However, the "sawtooth" pattern of the carbon-oxygen stretches suggest that **1** is bidentate with rhodizonate. Since symmetrical stretches in a six-membered ring would not be IR active but asymmetric ones would be, it is assumed that Pb(II) directly coordinates to adjacent O atoms in rhodizonate. The FT-IR spectrum of **2**, unsurprisingly, contains tartrate within its structure, as the spectrum of **2** is very distinct from the tartrate spectrum [31] and the spectrum of **1** (Fig. 2.1). As for **1**, there are no carbon-oxygen stretches above 1600 cm^{-1}, which is indicative

of carbon-oxygen bonds with bond order < 2. The bands at 1635 cm^{-1} and 1536 cm^{-1} suggest that the rhodizonate ring has some aromatic character, as for **1**. After addition of 5% HCl (Fig. 2.1, bottom) and formation of **3**, many of the tartrate bands that were found in **2** no longer appear. The aromatic carbon stretches present in **1** and **2** are absent in **3**. Instead, a broad (and rather weak) band at 1716 cm^{-1} suggests a C=O stretch with a double bond character. The low intensity of the band is indicative of symmetric C=O stretches on opposite sides of the rhodizonate ring.

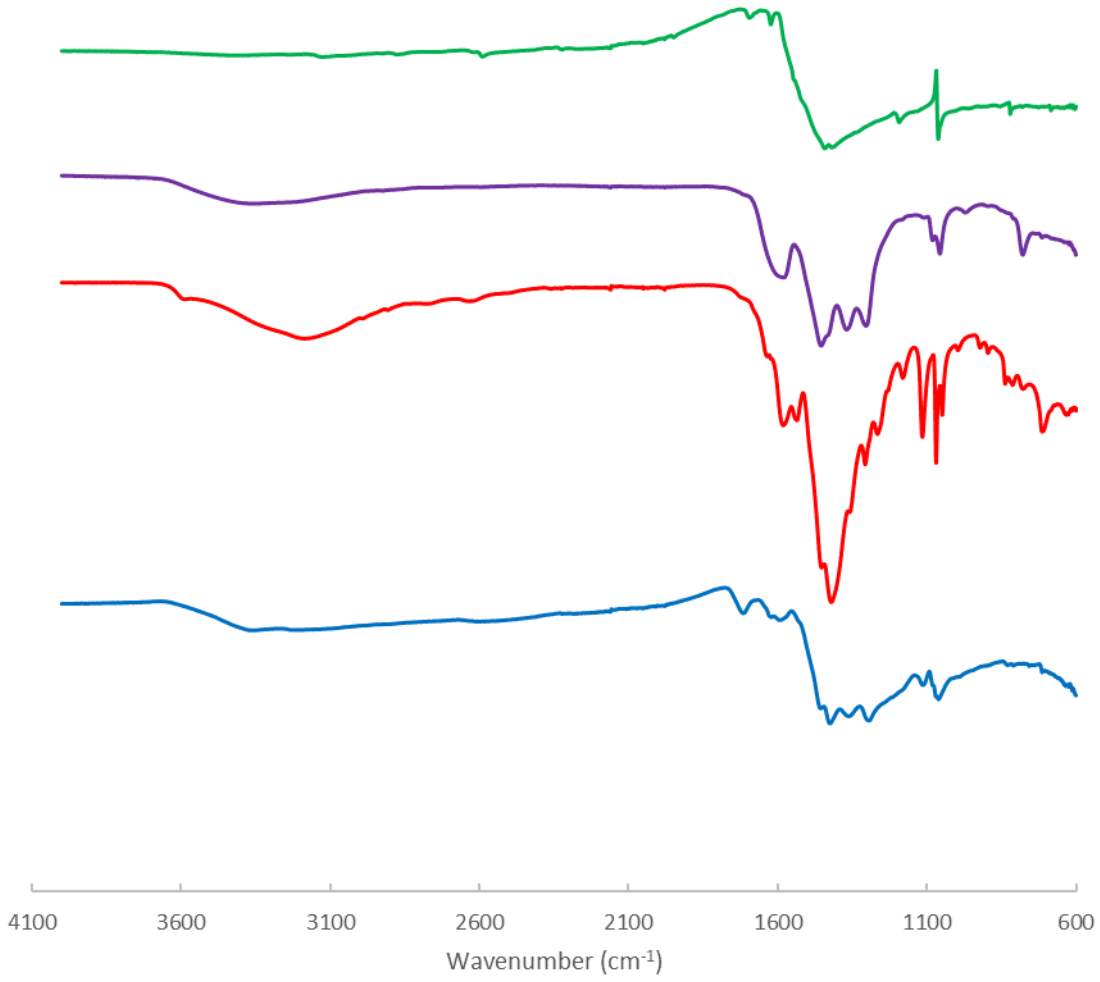

Figure 2.1: The FT-IR spectra of $Na_2C_6O_6$ (top, green), **1** (top-middle, purple), **2** (bottom-middle, red), and **3** (bottom, blue).

2.4.3 X-Ray Photoelectron Spectroscopy

Powder samples of **1**, **2**, and **3** underwent X-ray photoelectron spectroscopy. High-resolution scans for all three compounds were performed for the Pb 4f 7/2, Pb 4f 5/2, C 1s, and O 1s spectral lines. For **1** and **2**, the Pb 4f 7/2 spectral line is centered at 138.6 eV and 138.7 eV, respectively, which are consistent with Pb in a 2+ oxidation state that is coordinated with O. This is also borne out in the O 1s spectral lines, each of which have a deconvoluted peak at 531.2 eV and 531.6 eV, respectively, consistent with a Pb^{2+}-O interaction [32]. Deconvoluting the Pb 4f 7/2 spectral line for compound **3**, however, is best achieved using two peaks, indicating two different chemical environments for Pb. Compound **3** has its Pb 4f 7/2 peaks centered at 139.0 eV, consistent with a Pb^{2+}-Cl interaction and at 138.7 eV, which is similar to compounds **1** and **2**. The peak areas of these Pb 4f 7/2 peaks give a 2:1 ratio of Cl^--coordinated Pb to non-Cl^--coordinated Pb, consistent with the elemental analysis. All Pb(II) in compound **3** are still coordinated with O as well, as the O 1s spectra has a deconvoluted peak at 531.3 eV, consistent with Pb-O coordination.

In all three compounds (**1**, **2**, and **3**) the high-resolution C 1s spectra can be deconvoluted into three peaks: one at 284.9 eV, 284.9 eV, and 284.7 eV, respectively; one at 286.2 eV, 286.4 eV, and 286.6 eV, respectively; and one at 288.2 eV, 288.3 eV, and 288.7 eV, respectively. All three spectra are broadly consistent with rhodizonate XPS C 1s spectra as previously reported in the literature [33]. While the peak centers of the three C 1s peaks for each compound are similar, their relative intensities are not. Most notably, the 284.7 eV peak, which has been assigned to a C-C interaction, of **3** is a major component of the C 1s spectrum, while it is considerably smaller for **1** and **2**. This suggests that the addition of Cl^- has an effect on the rhodizonate ring itself, giving it more of a charge-

localized form as compared to **1** and **2**. This is also suggested in the FT-IR spectra of these compounds. The C 1s spectra for all three compounds are shown in Figure 2.2.

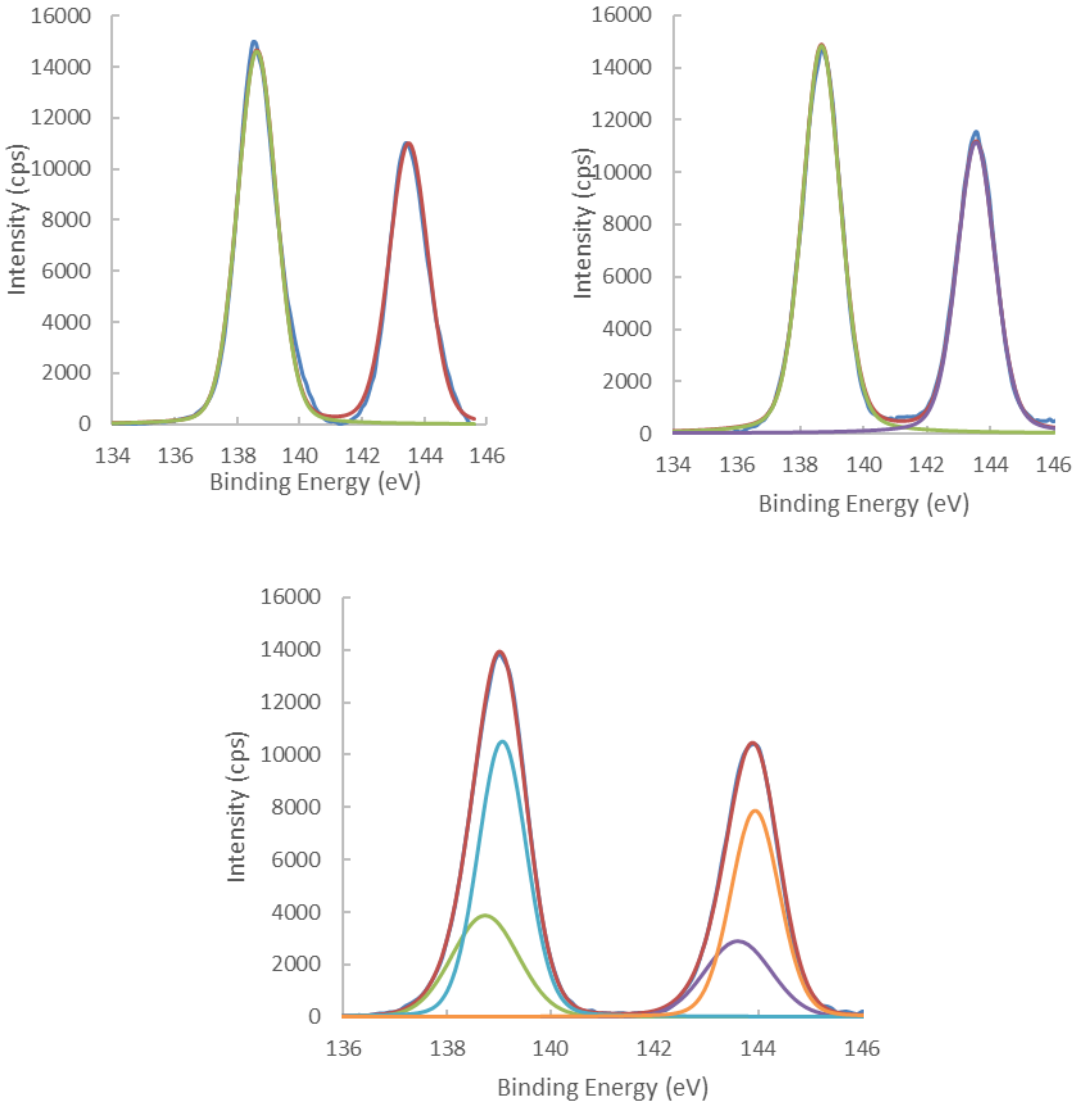

Figure 2.2: The high-resolution XPS spectra for the Pb 4f 7/2 (left curve) and 4f 5/2 (right curve) spectral lines for **1** (top left), **2** (top right), and **3** (bottom). While the Pb 4f 7/2 and Pb 4f 5/2 spectral lines for **1** and **2** can be adequately simulated with one curve, the Pb 4f 7/2 and Pb 4f 5/2 spectral lines for **3** need two curves to simulate each peak, suggesting two coordination environments in **3**

2.4.4 UV-Visible Titrations

UV-Vis titrations simulating all three steps of the sodium rhodizonate test in solution were performed in order to determine the binding constants for formation of the

rhodizonate complexes for each step of the test. The spectra of each step of the sodium rhodizonate test are shown in Figure 2.3.

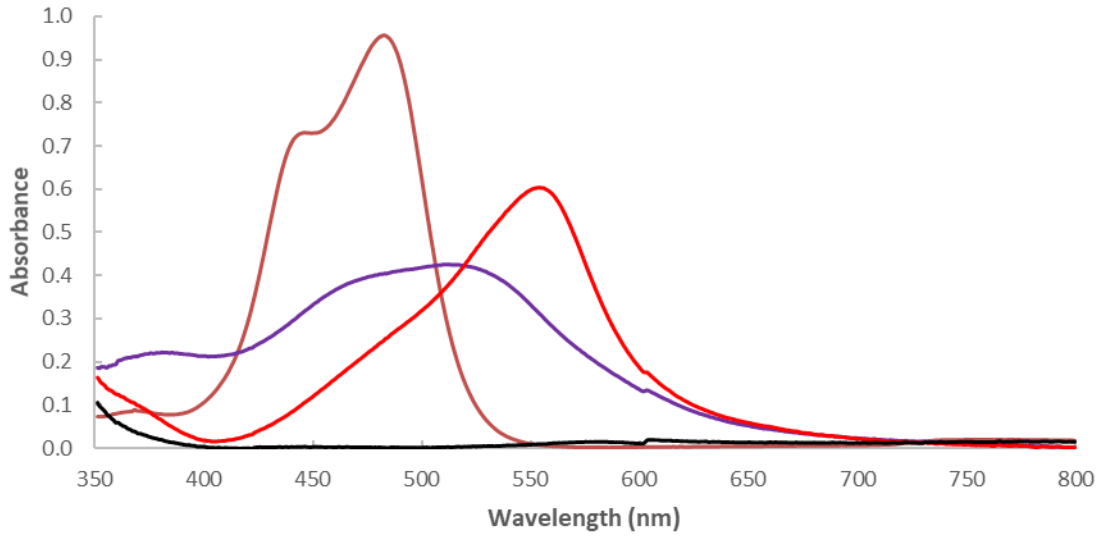

Figure 2.3: The UV-Vis spectra of $Na_2C_6O_6$ (orange), **1** (purple), **2** (red), and **3** (black). All solutions are 1.8 x 10^{-5} M rhodizonate.

Formation of **1** in solution **(1S)** results in a shift in wavelength from 482 nm to 525 nm. Adding the tartrate buffer to a solution of **1S** (under constant 1.8 x 10^{-5} M concentration of **1S**), producing **(2S)**, shifts the maximum absorbance wavelength from 525 nm to 554 nm. Addition of 5% HCl, resulting in **(3S)**, momentarily turns the solution the characteristic blue-purple color before rendering it colorless. For all complexes, the shoulder found in the plain $Na_2C_6O_6$ spectrum disappears. The shoulder is due to the Jahn-Teller effect of the LUMO for the first π-π^* transition, which in oxocarbons is doubly degenerate [9]. The loss of this shoulder suggests that this degeneracy is resolved upon complexation.

Upon addition of Pb(II) nitrate in water/ethanol (50/50 by volume) the band at 482 nm decreases in intensity (Figures 2.4 through 2.7), while there is a band shift to a higher

wavelength. Applying the decrease in absorption to the 1:1 binding isotherm [34], gives an excellent fit to the 1:1 binding model, indicating that, in solution, Pb(II) rhodizonates exist as 1:1 complexes. Non-linear regression analysis of the binding curve gives a binding constant of K_{11} = 1.2 (± 0.2) x 10^6 M^{-1} for Pb(II)-rhodizonate, leading to a free energy of complexation of ΔG = -34.7 (± 0.4) kJ/mol. Applying the standard deviation to slope ratio to the isotherm data gives a limit of detection of 1.43 x 10^{-6} M and a limit of quantification of 4.34 x 10^{-6} M [35].

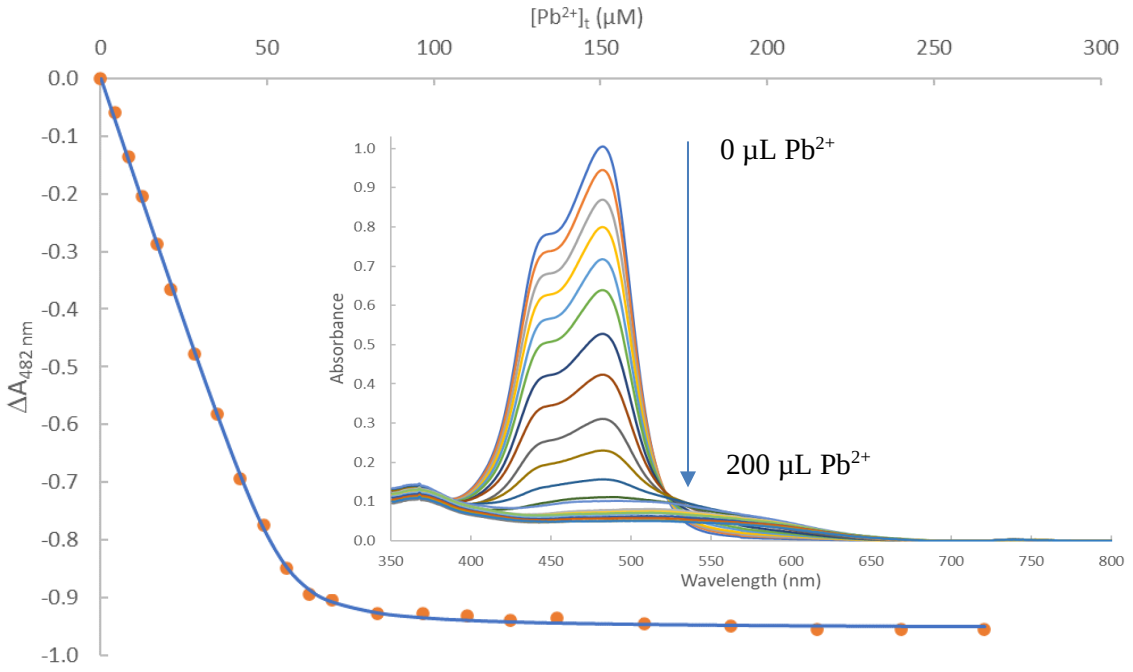

Figure 2.4: Binding curve for the titration of a solution of 5.29 x 10^{-5} M of $Na_2C_6O_6$ with a solution of 2.55 x 10^{-3} M of $Pb(NO_3)_2$ in 5.29 x 10^{-5} M of $Na_2C_6O_6$ in water/ethanol (50/50 v/v). K_{11} = 1.07 x 10^6 M^{-1}. **Cutaway:** UV-Visible absorption spectrum for the titration of a solution of 5.29 x 10^{-5} M of $Na_2C_6O_6$ with solution of 2.55 x 10^{-3} M of $Pb(NO_3)_2$ in 5.29 x 10^{-5} M of $Na_2C_6O_6$ in water/ethanol (50/50 v/v).

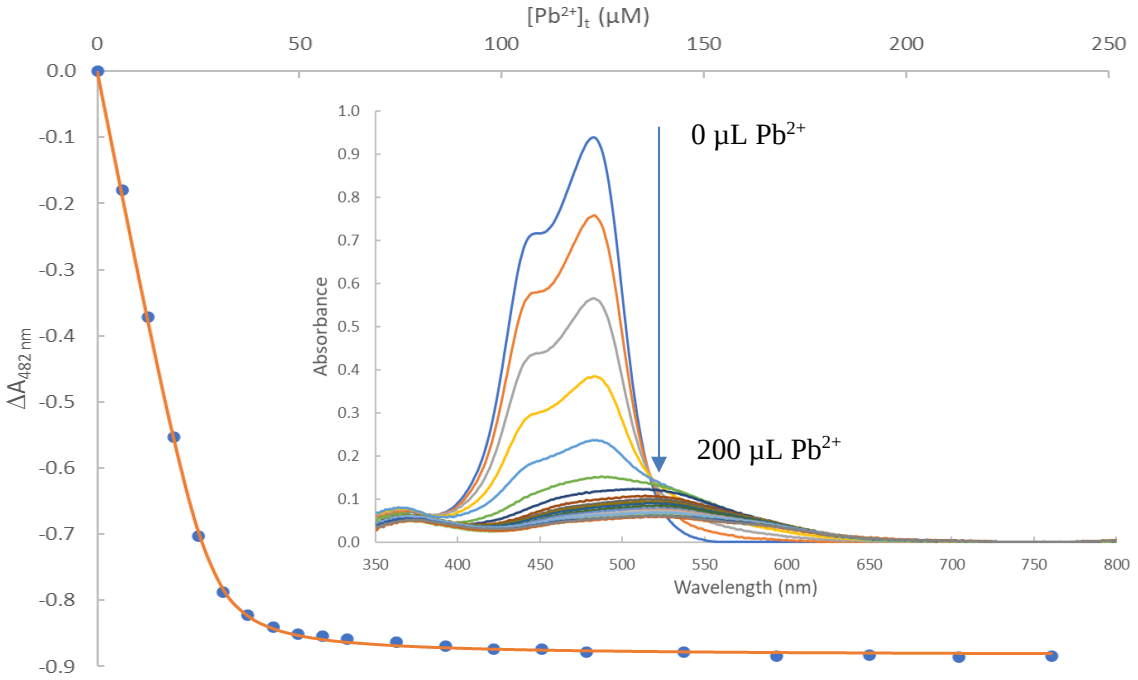

Figure 2.5: Binding curve for the titration of a solution of 3.05 x 10^{-5} M of $Na_2C_6O_6$ with a solution of 4.24 x 10^{-3} M of $Pb(NO_3)_2$ in 3.05 x 10^{-5} M of $Na_2C_6O_6$ in water/ethanol (50/50 v/v). K_{11} = 1.13 x 10^6 M^{-1}. **Cutaway:** UV-Visible absorption spectrum for the titration of a solution of 3.05 x 10^{-5} M of $Na_2C_6O_6$ with solution of 4.24 x 10^{-3} M of $Pb(NO_3)_2$ in 3.05 x 10^{-5} M of $Na_2C_6O_6$ in water/ethanol (50/50 v/v).

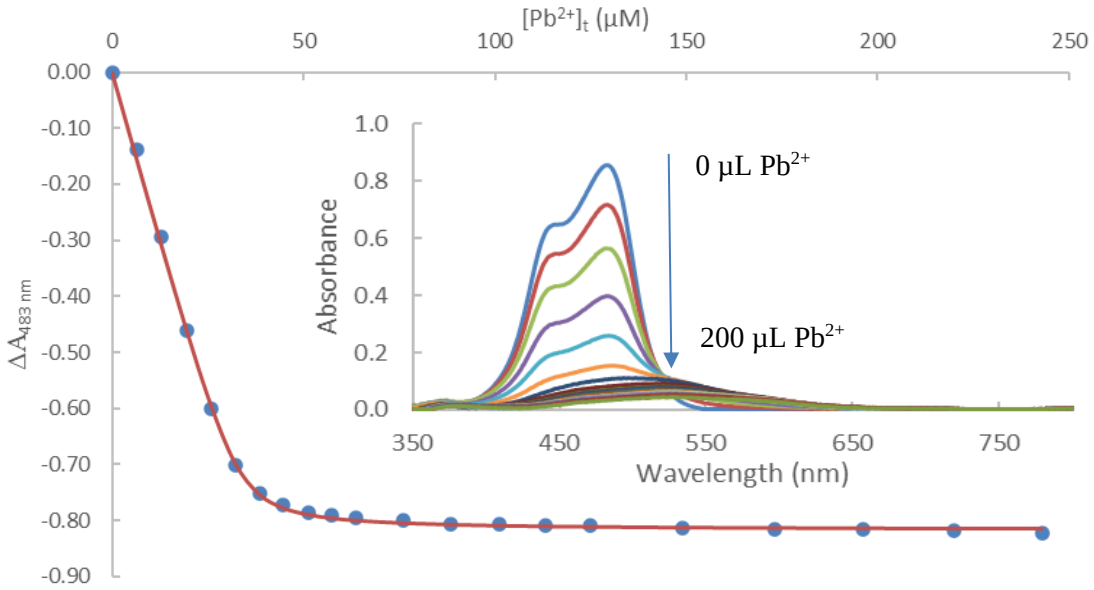

Figure 2.6: Binding curve for the titration of a solution of 3.30 x 10^{-5} M of $Na_2C_6O_6$ with a solution of 6.46 x 10^{-3} M of $Pb(NO_3)_2$ in 3.05 x 10^{-5} M of $Na_2C_6O_6$ in water/ethanol (50/50 v/v). K_{11} = 1.47 x 10^6 M^{-1}. **Cutaway:** UV-Visible absorption spectrum for the titration of a solution of 3.30 x 10^{-5} M of $Na_2C_6O_6$ with solution of 6.46 x 10^{-3} M of $Pb(NO_3)_2$ in 3.30 x 10^{-5} M of $Na_2C_6O_6$ in water/ethanol (50/50 v/v).

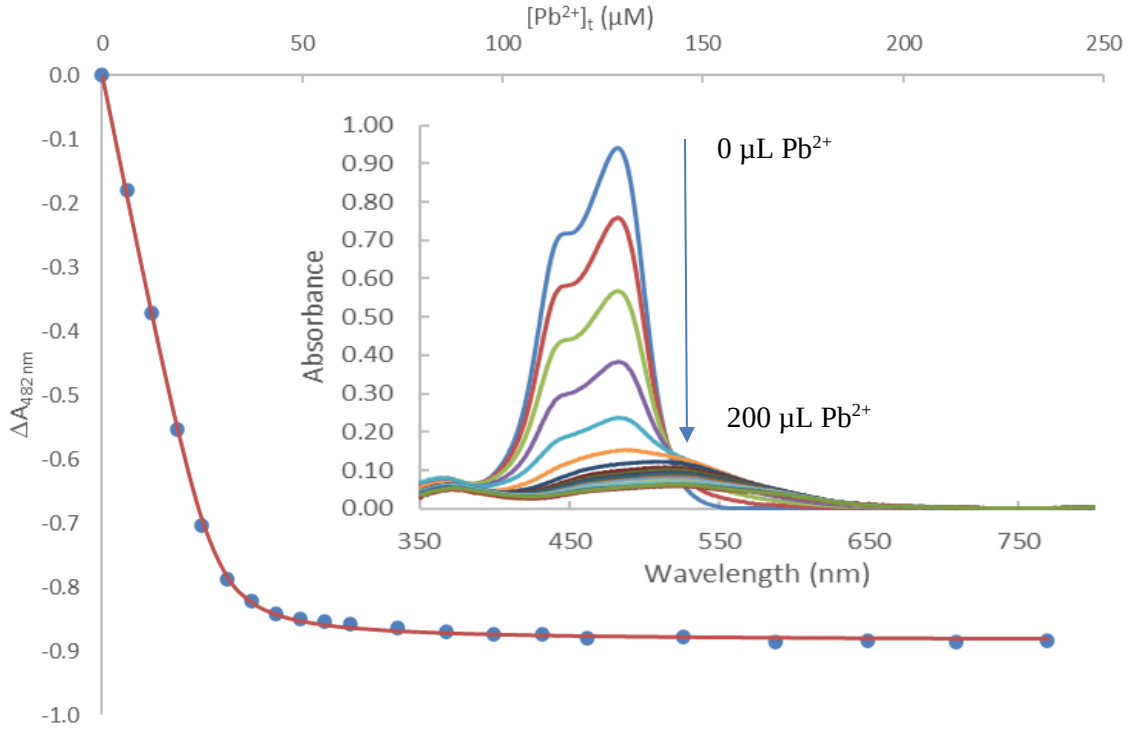

Figure 2.7: Binding curve for the titration of a solution of 2.79 x 10^{-5} M of $Na_2C_6O_6$ with a solution of 6.27 x 10^{-3} M of $Pb(NO_3)_2$ in 2.79 x 10^{-5} M of $Na_2C_6O_6$ in water/ethanol (50/50 v/v). K_{11} = 1.21 x 10^6 M^{-1}. **Cutaway:** UV-Visible absorption spectrum for the titration of a solution of 2.79 x 10^{-5} M of $Na_2C_6O_6$ with solution of 6.27 x 10^{-3} M of $Pb(NO_3)_2$ in 2.79 x 10^{-5} M of $Na_2C_6O_6$ in water/ethanol (50/50 v/v).

Pb(II)-rhodizonate has an absorption band at 506 nm. Upon addition of tartrate buffer in water/ethanol (50/50 v/v) the band at 506 nm decreases in intensity (Figures 2.8 through 2.12), while there is a red shift to a higher wavelength. Applying the decrease in absorption to the 1:1 binding isotherm [34], gives excellent fittings to the 1:1 binding model, indicating that in solution Pb(II)-rhodizonate-tartrate buffer exists as a 1:1 complex (between Pb(II)-rhodizonate and tartrate buffer). As with **1**, solid **2** has a 2:1 Pb(II)/rhodizonate ratio, suggesting that the ethanol in solution is preventing a second Pb(II) from complexing with the red complex in solution. Non-linear regression analysis of the spectrum of **2S** gives an apparent binding constant of K_{11} = 1.8 (± 0.7) x 10^4 M^{-1} for Pb(II)-rhodizonate-tartrate buffer, leading to a free energy of complexation of ΔG = -24.3

± 0.9 kJ/mol. Applying the standard deviation to slope ratio to the isotherm data gives a limit of detection of 6.17 x 10^{-6} M and a limit of quantification of 1.87 x 10^{-5} M [35].

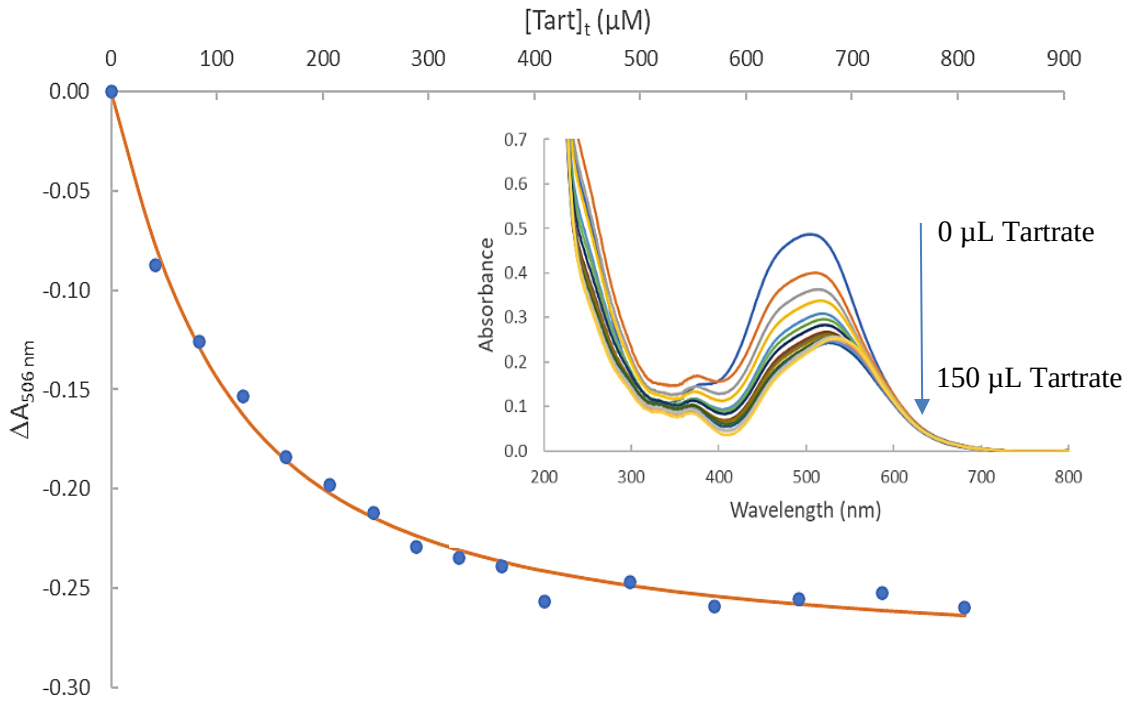

Figure 2.8: Binding curve for the titration of a solution of 1.43 x 10^{-4} M of **1S** with solution of 2.50 x 10^{-2} M of pH 2.8 tartrate buffer in 1.43 x 10^{-4} M of **1S** in water/ethanol (50/50 v/v). K_{11} = 2.23 x 10^{4} M^{-1}. **Cutaway:** UV-Visible absorption spectrum for the titration of a solution of 1.43 x 10^{-4} M of **1S** with a solution of 2.50 x 10^{-2} M of pH 2.8 tartrate buffer in 1.43 x 10^{-4} M of **1S** in water/ethanol (50/50 v/v).

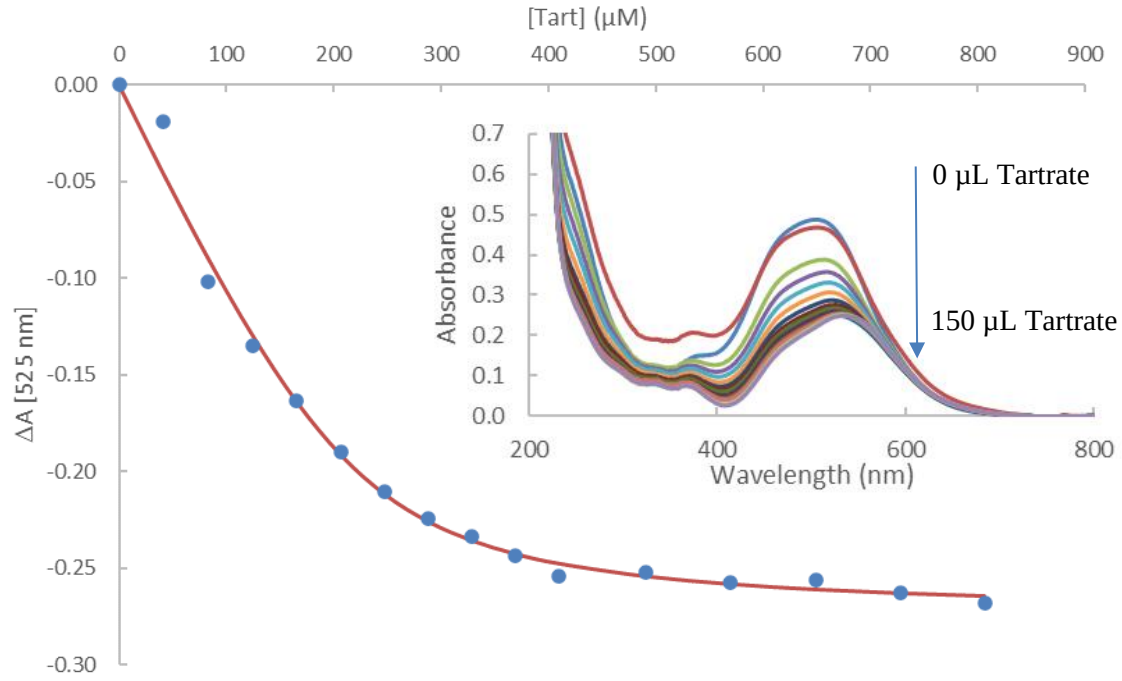

Figure 2.9: Binding curve for the titration of a solution of 2.20 x 10^{-4} M of **1S** with solution of 2.50 x 10^{-2} M of pH 2.8 tartrate buffer in 2.20 x 10^{-4} M of **1S** in water/ethanol (50/50 v/v). K_{11} = 4.31 x 10^{4} M^{-1}. **Cutaway:** UV-Visible absorption spectrum for the titration of a solution of 2.20 x 10^{-4} M of **1S** with a solution of 2.50 x 10^{-2} M of pH 2.8 tartrate buffer in 2.20 x 10^{-4} M of **1S** in water/ethanol (50/50 v/v).

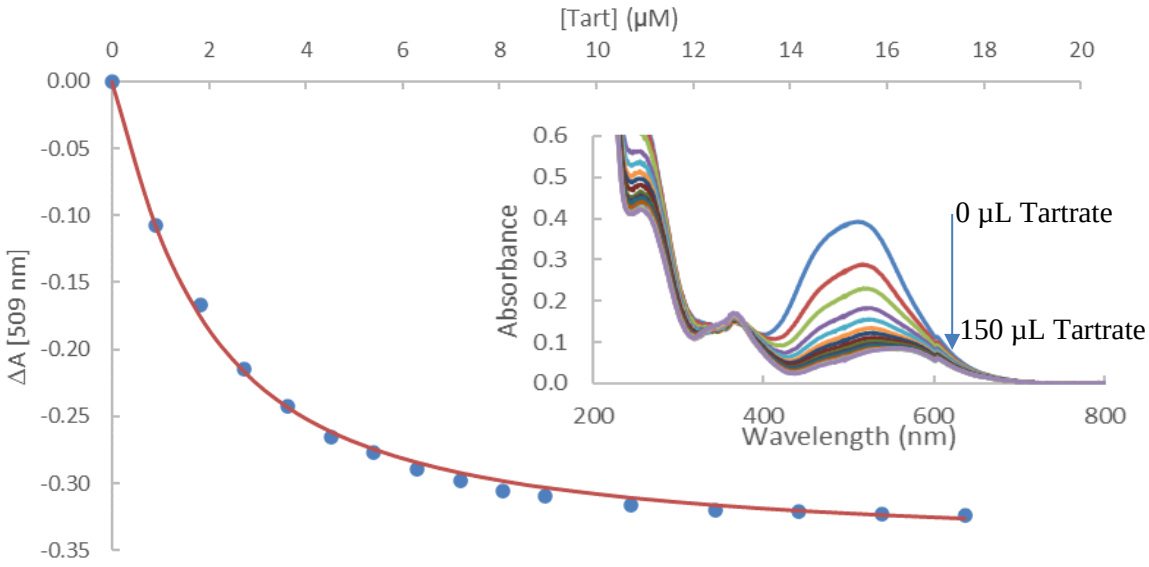

Figure 2.10: Binding curve for the titration of a solution of 1.13 x 10^{-6} M of **1S** with solution of 5.46 x 10^{-4} M of pH 2.8 tartrate buffer in 1.13 x 10^{-6} M of **1S** in water/ethanol (50/50 v/v). K_{11} = 7.90 x 10^{5} M^{-1}. **Cutaway:** UV-Visible absorption spectrum for the titration of a solution of 1.13 x 10^{-6} M of **1S** with a solution of 5.46 x 10^{-4} M of pH 2.8 tartrate buffer in 1.13 x 10^{-6} M of **1S** in water/ethanol (50/50 v/v).

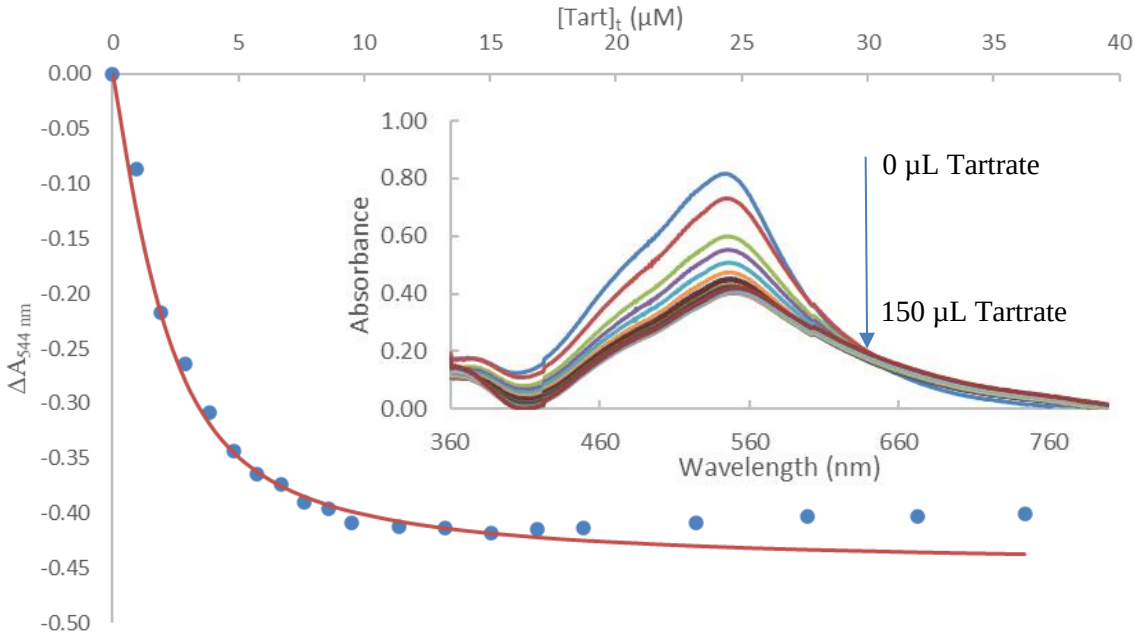

Figure 2.11: Binding curve for the titration of a solution of 2.00 x 10^{-6} M of **1S** with solution of 5.80 x 10^{-4} M of pH 2.8 tartrate buffer in 2.00 x 10^{-6} M of **1S** in water/ethanol (50/50 v/v). K_{11} = 1.00 x 10^{6} M^{-1}. **Cutaway:** UV-Visible absorption spectrum for the titration of a solution of 2.00 x 10^{-6} M of **1S** with a solution of 5.80 x 10^{-4} M of pH 2.8 tartrate buffer in 2.00 x 10^{-6} M of **1S** in water/ethanol (50/50 v/v).

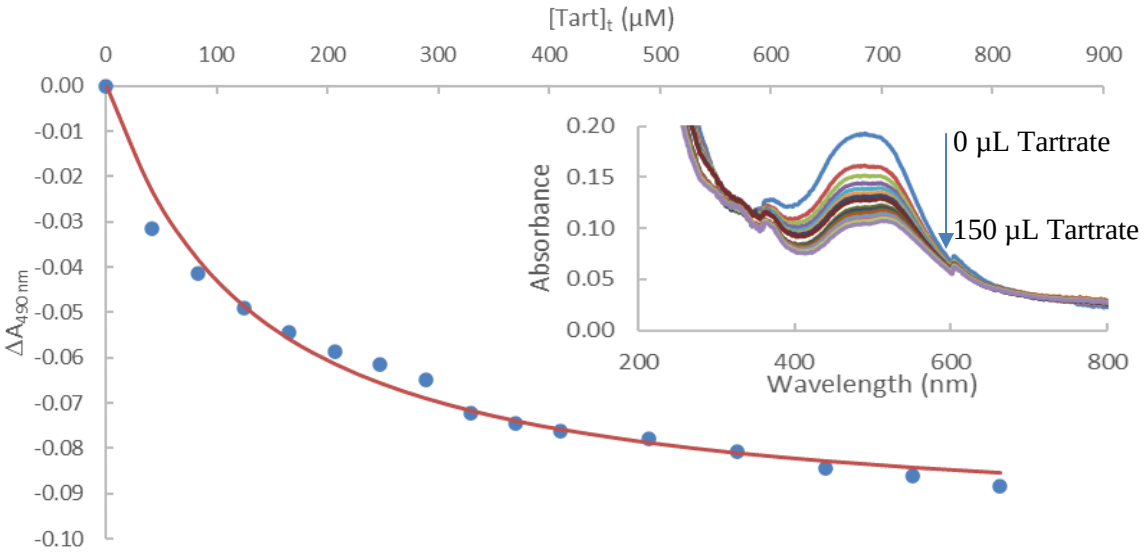

Figure 2.12: Binding curve for the titration of a solution of 2.59 x 10^{-5} M of **1S** with solution of 2.50 x 10^{-2} M of pH 2.8 tartrate buffer in 2.59 x 10^{-5} M of **1S** in water/ethanol (50/50 v/v). K_{11} = 8.93 x 10^{3} M^{-1}. **Cutaway:** UV-Visible absorption spectrum for the titration of a solution of 2.59 x 10^{-5} M of **1S** with a solution of 2.50 x 10^{-2} M of pH 2.8 tartrate buffer in 2.59 x 10^{-5} M of **1S** in water/ethanol (50/50 v/v).

Previous research into optimizing the Na-rho test suggests that results have greater reproducibility by dissolving the rhodizonate in the tartrate buffer prior to use [28]. As described in the literature, the low pH of the tartrate buffer solution protonates the rhodizonate dianion, leading to a loss of sodium rhodizonate's orange color in solution. Addition of Pb(II) still produces the characteristic scarlet complex with no apparent loss of visible color. A titration in water/ethanol (50/50 v/v) confirms this (Figures 2.13 through 2.15). Applying the increase in absorption to the 1:1 binding isotherm [34], still gives excellent fitting to the 1:1 binding model. Non-linear regression analysis of the spectrum of **2S** gives an apparent binding constant of K_{11} = 5.6 (± 2.8) x 10^5 M^{-1} for formation of Pb(II)-rhodizonate-tartrate by the reaction Pb^{2+} + $C_6O_6H^-$ + tartrate → $Pb(C_6O_6H)(C_4H_5O_6)$, leading to a free energy of complexation of ΔG = -32.8 (± 1.7) kJ/mol.

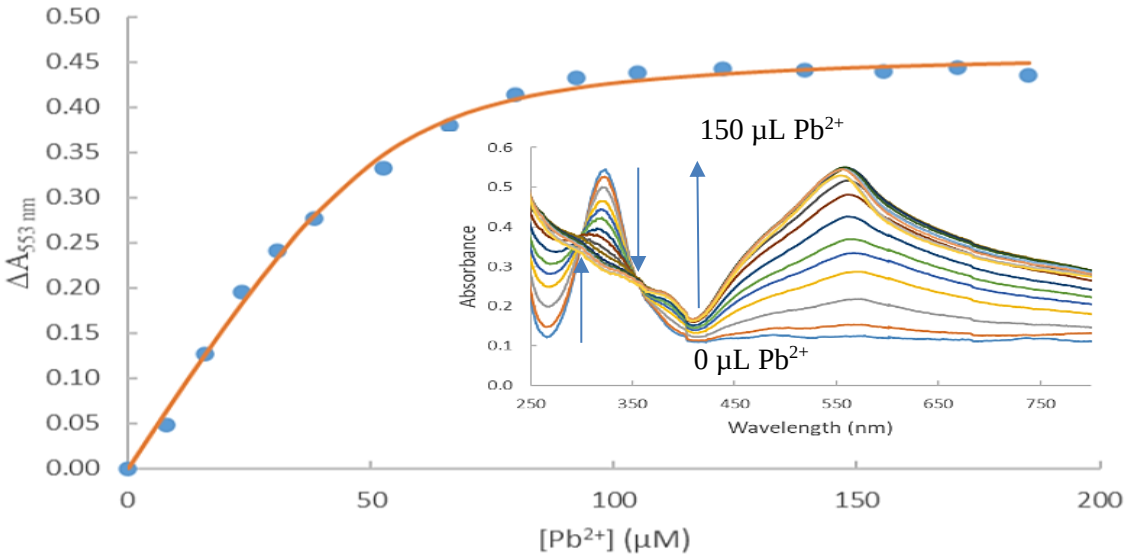

Figure 2.13: Binding curve for the titration of a solution of 0.01 M of pH 2.8 sodium bitartrate/L-tartaric acid buffer and 3.57 x 10^{-5} M of sodium rhodizonate with a solution of 1.98 x 10^{-3} M of $Pb(NO_3)_2$ and 0.01 M of pH 2.8 sodium bitartrate/L-tartaric acid buffer and 3.57 x 10^{-5} M of sodium rhodizonate in water/ethanol (50/50 v/v). K_{11} = 2.17 x 10^5 M^{-1}. **Cutaway:** UV-Visible absorption spectrum for the titration of a solution of 1.98 x 10^{-3} M of $Pb(NO_3)_2$ and 0.01 M of pH 2.8 sodium bitartrate/L-tartaric acid buffer and 3.57 x 10^{-5} M of sodium rhodizonate in water/ethanol (50/50 v/v).

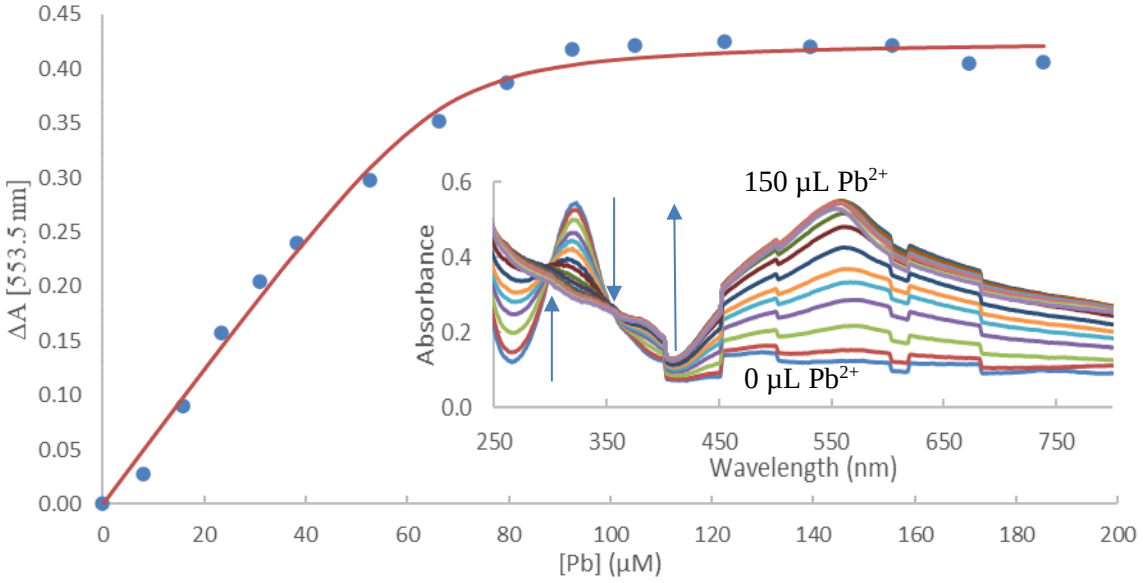

Figure 2.14: Binding curve for the titration of a solution of 0.01 M of pH 2.8 sodium bitartrate/L-tartaric acid buffer and 6.64 x 10^{-5} M of sodium rhodizonate with a solution of 8.03 x 10^{-4} M of $Pb(NO_3)_2$ and 0.01 M of pH 2.8 sodium bitartrate/L-tartaric acid buffer and 6.64 x 10^{-5} M of sodium rhodizonate in water/ethanol (50/50 v/v). K_{11} = 5.77 x 10^5 M^{-1}. **Cutaway:** UV-Visible absorption spectrum for the titration of a solution of 8.03 x 10^{-4} M of $Pb(NO_3)_2$ and 0.01 M of pH 2.8 sodium bitartrate/L-tartaric acid buffer and 6.64 x 10^{-5} M of sodium rhodizonate in water/ethanol (50/50 v/v).

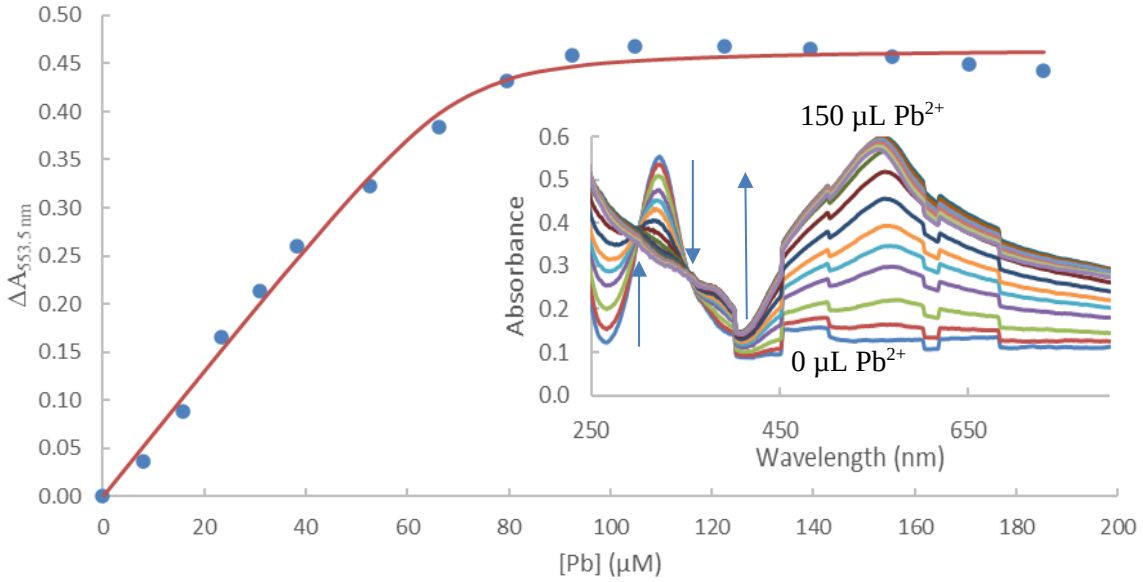

Figure 2.15: Binding curve for the titration of a solution of 0.01 M of pH 2.8 sodium bitartrate/L-tartaric acid buffer and 6.99 x 10^{-5} M of sodium rhodizonate with a solution of 8.03 x 10^{-4} M of $Pb(NO_3)_2$ and 0.01 M of pH 2.8 sodium bitartrate/L-tartaric acid buffer and 6.99 x 10^{-5} M of sodium rhodizonate in water/ethanol (50/50 v/v). K_{11} = 8.97 x 10^5 M^{-1}. **Cutaway:** UV-Visible absorption spectrum for the titration of a solution of 8.03 x 10^{-4} M of $Pb(NO_3)_2$ and 0.01 M of pH 2.8 sodium bitartrate/L-tartaric acid buffer and 6.99 x 10^{-5} M of sodium rhodizonate in water/ethanol (50/50 v/v).

The Pb(II)-rhodizonate-tartrate buffer has a broad absorption band at 553 nm. Upon addition of HCl in water/ethanol (50/50 v/v) the band at 554 nm decreases in intensity (Figures 2.16 through 2.18). Applying the decrease in absorption to the 1:1 binding isotherm [34], gives excellent fitting to the 1:1 binding model, indicating that in solution **3S** exists as a 1:1 complex between **2S** and HCl. Non-linear regression analysis gives an apparent binding constant of K_{11} = 2.0 (± 0.7) x 10^3 M^{-1} for formation of **3S** by the reaction $Pb(C_6O_6H)(C_4H_5O_6)$ + HCl → $Pb(C_6O_6H)Cl$ leading to a free energy of complexation of ΔG = -18.8 (± 0.9) kJ/mol. Applying the standard deviation to slope ratio to the isotherm data gives a limit of detection of 3.72 x 10^{-4} M and a limit of quantification of 1.13 x 10^{-3} M [35].

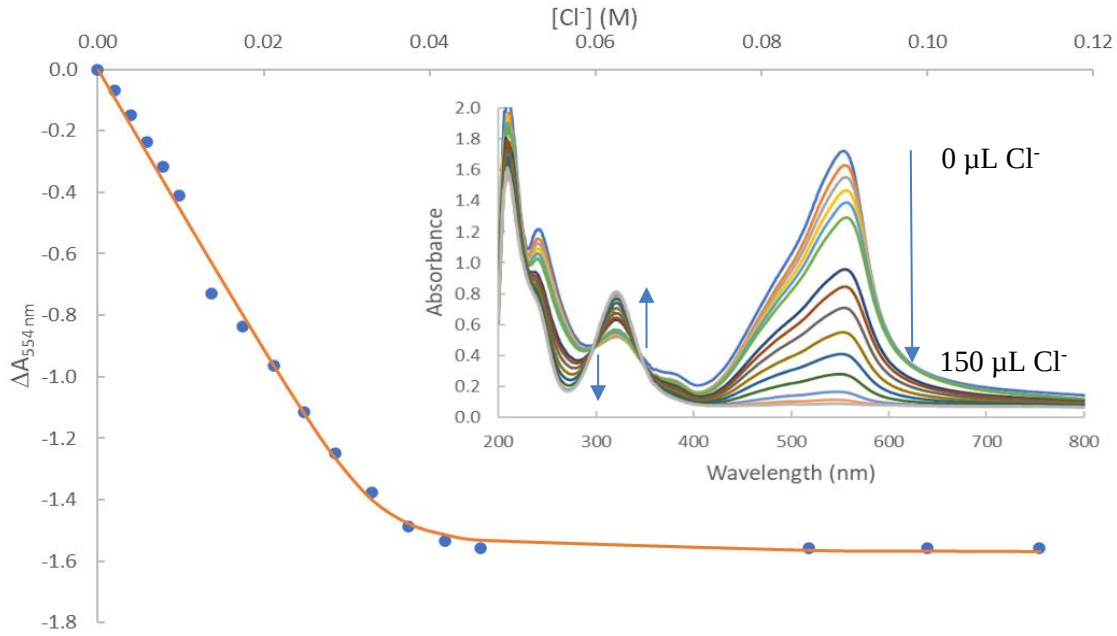

Figure 2.16: Binding curve for the titration of a solution of 3.40 x 10^{-2} M of **2S** with a solution of 0.6 M of HCl in 3.40 x 10^{-2} M of **2S** in water/ethanol (50/50 v/v). K_{11} = 2.54 x 10^{3} M^{-1}. **Cutaway:** UV-Visible absorption spectrum for the titration of a solution of 3.40 x 10^{-2} M of **2** with solution of 0.6 M of HCl in 3.40 x 10^{-2} M of **2S** in water/ethanol (50/50 v/v).

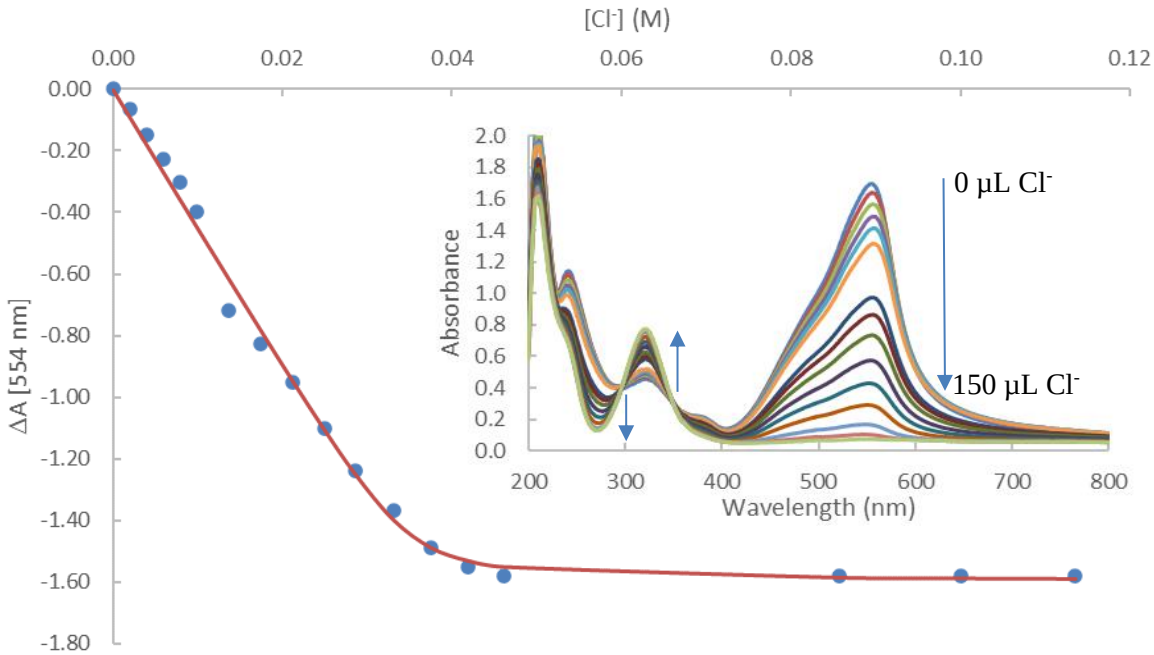

Figure 2.17: Binding curve for the titration of a solution of 3.49 x 10^{-2} M of **2S** with a solution of 0.6 M of HCl in 3.49 x 10^{-2} M of **2S** in water/ethanol (50/50 v/v). K_{11} = 2.73 x 10^{3} M^{-1}. **Cutaway:** UV-Visible absorption spectrum for the titration of a solution of 3.49 x 10^{-2} M of **2** with solution of 0.6 M of HCl in 3.49 x 10^{-2} M of **2S** in water/ethanol (50/50 v/v).

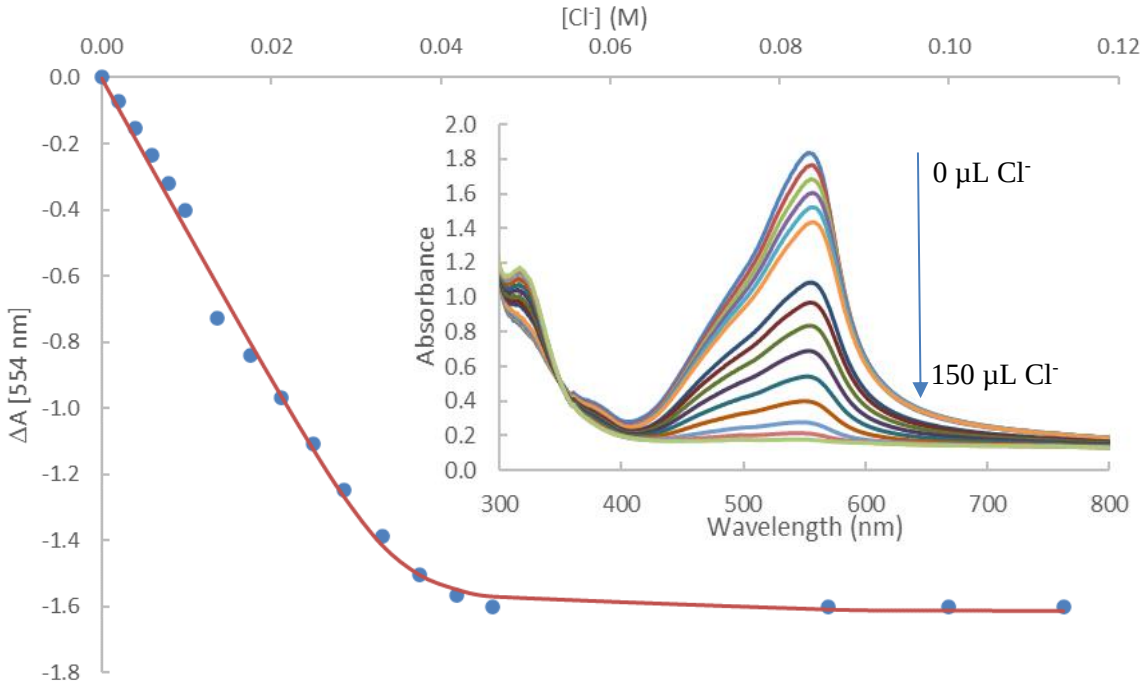

Figure 2.18: Binding curve for the titration of a solution of 3.47 x 10^{-2} M of **2S** with a solution of 0.6 M of HCl in 3.47 x 10^{-2} M of **2S** in water/ethanol (50/50 v/v). K_{11} = 2.37 x 10^{3} M^{-1}. **Cutaway:** UV-Visible absorption spectrum for the titration of a solution of 3.47 x 10^{-2} M of **2** with solution of 0.6 M of HCl in 3.47 x 10^{-2} M of **2S** in water/ethanol (50/50 v/v).

2.4.5 UV-Vis Job Plots

To determine the appropriate molar ratio of all three compounds in solution, Job plot experiments were performed. The UV-Visible spectra are shown in Figure 2.19.

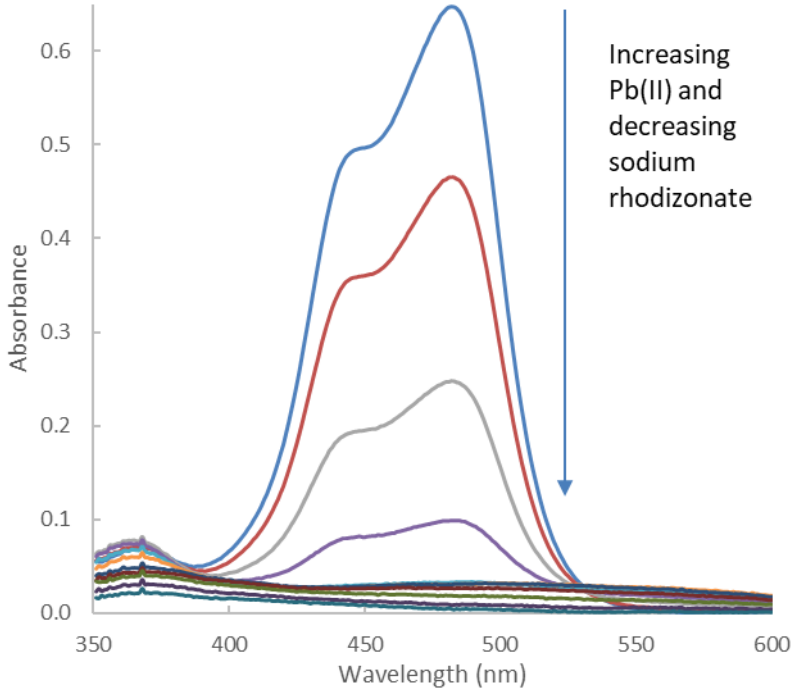

Figure 2.19: The UV-Visible spectra of all solutions for the method of continuous variation between Pb(II) and $Na_2C_6O_6$ in water/ethanol (50/50 v/v). All vials contain a total of 0.187 mmol of analyte.

The Job plot of Pb(II) with sodium rhodizonate is shown in Figure 2.20.

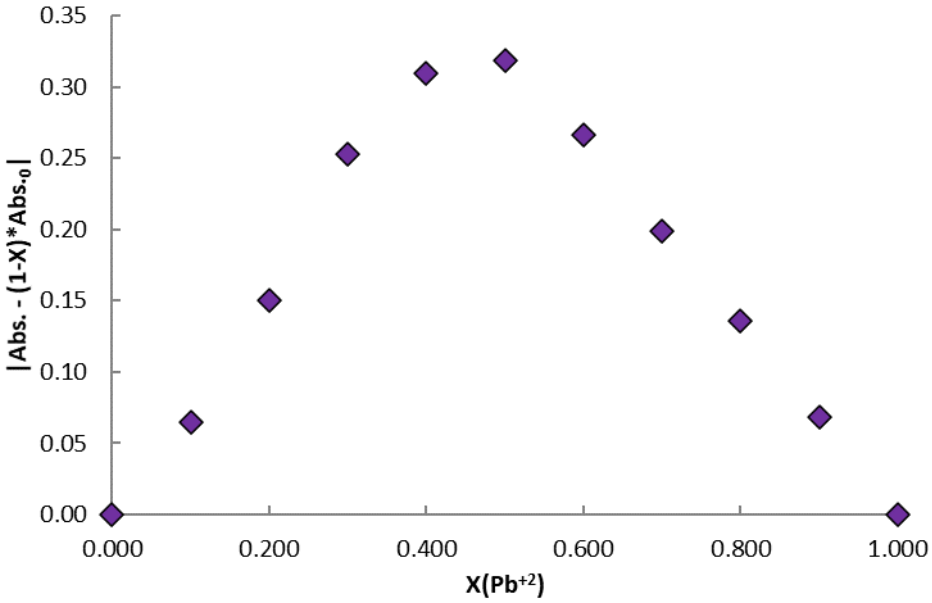

Figure 2.20: The Job plot from the data shown in Figure 2.19 of Pb(II) with sodium rhodizonate in water/ethanol (50/50 v/v).

As demonstrated by the Job plot (Fig. 2.20), Pb(II) and $C_6O_6^{2-}$ coordinate in a 1:1 ratio in water/ethanol (50/50 v/v). This 1:1 ratio of Pb(II) to $C_6O_6^{2-}$ is different from the 2:1 Pb(II)/rhodizonate ratio shown in the elemental analysis for the solid state. Since rapid polymerization occurs in a purely aqueous solution, it can be inferred that the miscible organic solvent (in this case ethanol) prevents polymerization and additional metal coordination. This is true regardless of solvent choice, as these results were replicated using methanol, acetone, and acetonitrile as the second solvent.

The UV-Visible data used in the Job plot of **1S** with equimolar pH 2.8 tartaric acid buffer is shown in Figure 2.21; the Job plot itself is shown in Figure 2.22.

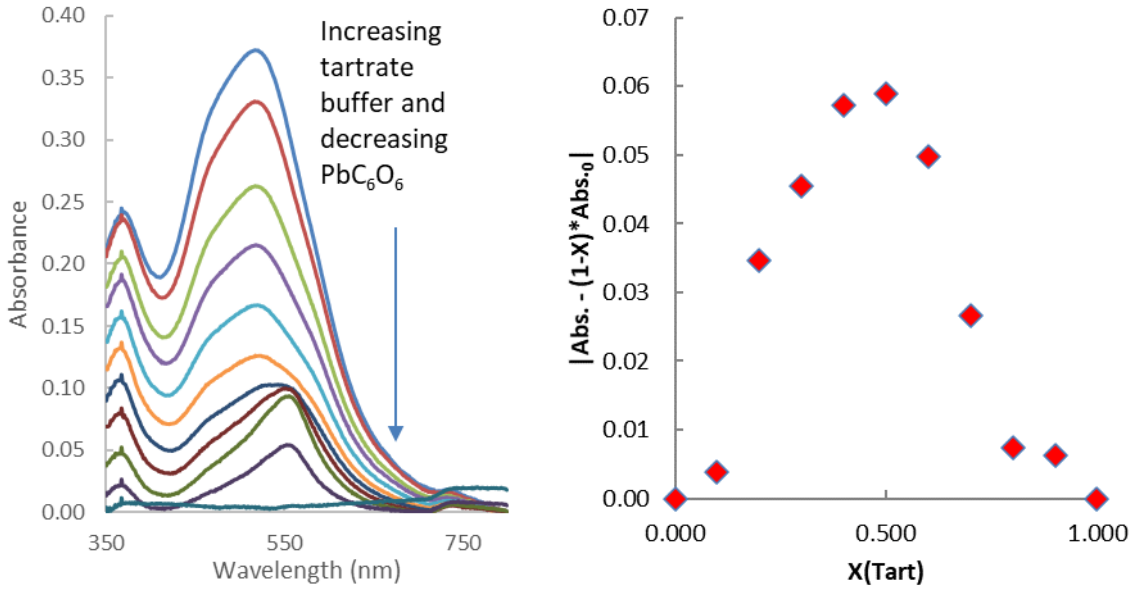

Figures 2.21 (left) and 2.22 (right): The UV-Visible spectra of **1S** with tartrate (left), and the Job plot of **1S** with tartrate (right) in water/ethanol (50/50 v/v). All vials contain a total of 0.187 mmol of analyte.

The Job plot suggests that Pb(II), rhodizonate, and tartrate bind in a 1:1:1 molar ratio in water/ethanol (50/50 v/v). As in the Job plot between Pb(II) and rhodizonate, these results are also replicated in methanol, ethanol, acetone, and acetonitrile.

2.4.6 Discussion of solid rhodizonate complexes

Without a single-crystal x-ray crystal structure, the exact arrangement of the bonds within these structures cannot be definitively determined. However, the data from the XPS and FT-IR experiments do permit a reasonable approximation of the structures of the three compounds. For **1**, The Pb 4f 7/2 peak at 138.6 eV indicates coordination of Pb with O. With several FT-IR stretching bands in the C-O to C=O range, all six O atoms in the rhodizonate are coordinated with Pb and have less than double bond character. The broad band centered at 1577 cm^{-1} has the highest double bond character, while the three bands at 1450 cm^{-1}, 1368 cm^{-1}, and 1300 cm^{-1} have stronger single bond character. Since stretches that in turn are coordinated with heavy atoms have lower absorbance wavenumbers than those coordinated with lighter elements [30], it is not surprising that these bands occur at lower wavenumbers than normal. While there are many possible structures that are consistent with the information obtained from the above experiments, they are all slight variations of the structure shown in Figure 2.23.

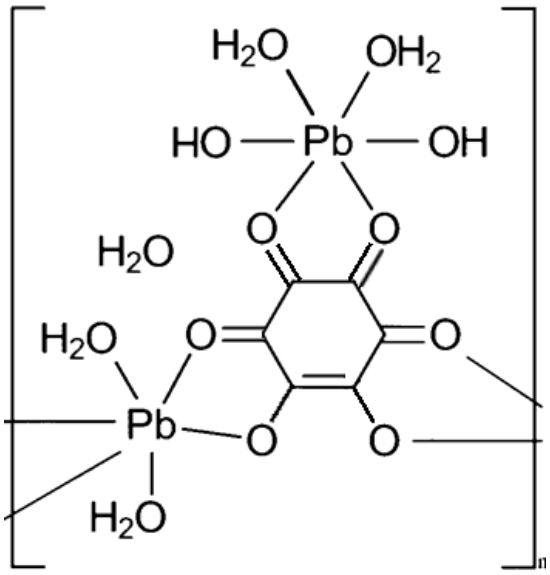

Figure 2.23: A projected structure of **1**, $Pb_2(C_6O_6)(OH)_2(H_2O)_4 \bullet H_2O$.

Mixing Pb(II) with rhodizonate in the presence of the pH 2.8 tartrate buffer results in the scarlet-red complex, **2**. With the XPS Pb 4f 7/2 peak largely unchanged, Pb is still coordinated to O atoms. The presence of more C=O and C-O FT-IR absorbance bands compared to **1** can be explained by a coordinating tartrate. Matching this information with the elemental analysis gives the structure in Figure 2.24.

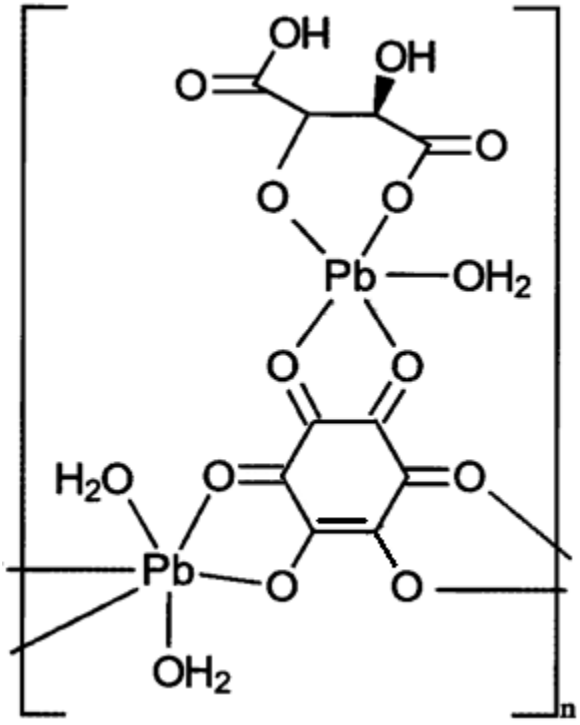

Figure 2.24: The projected structure of **2**, $Pb_2(C_6O_6)(C_4H_4O_6)(H_2O)_3$.

The addition of 5% HCl to the scarlet-red complex while the complex is still *in situ* produces the blue-purple complex, **3**. The XPS peak for Pb 4f 7/2 is best described by two curves: one centered at 138.7 eV, which corresponds to Pb(II)-O coordination as in **1** and **2**, and one centered at 139.0 eV, which corresponds to a Pb(II)-Cl bond. The XPS data for this peak is consistent with the elemental analysis: the area under the curve centered at 139.0 eV is twice as large as the area under the curve centered at 138.7 eV, meaning there are two Pb(II)-Cl environments for every one Pb(II)-O environment. The FT-IR spectrum

for **3** does not show the absorbance bands from tartrate, suggesting that the tartrate is displaced in the polymer due to the addition of Cl^- and because the tartrate gets protonated in the highly acidic environment. Since none of the FT-IR absorption bands are particularly strong, we suggest that this complex is largely symmetrical. A likely structure for **3** is shown in Figure 2.25.

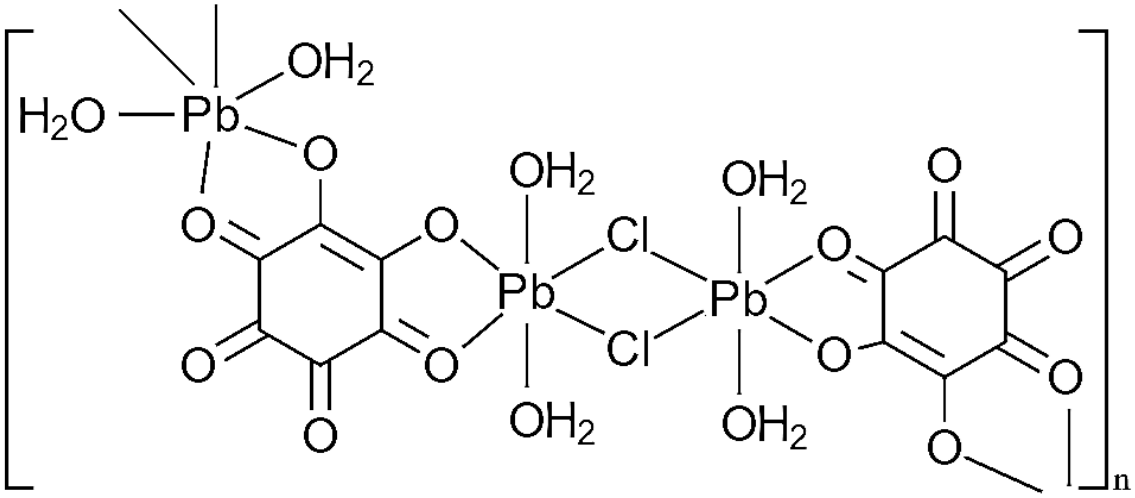

Figure 2.25: The projected structure of **3**, $Pb_3(C_6O_6)_2Cl_2(H_2O)_6$.

2.4.7 Discussion of rhodizonates in solution

In a mixed solvent system with water and a polar organic solvent, such as EtOH, soluble form of complexes **1S-3S** are formed, presumably with coordinated EtOH molecules breaking the coordination polymer structure. A proposed schematic drawing of the sodium rhodizonate test sequence in solution is shown in Figure 2.26.

All three compounds in solution exist in 1:1 molar ratios, which suggests that the organic solvent mixture prevents the second Pb from coordinating with the compound, at low enough concentrations. At higher concentrations and in the absence of the polar organic solvent, multiple Pb(II) atoms are able to coordinate to a single rhodizonate ring,

leading to formation of insoluble precipitates. While there are studies that attempted to measure the UV-Vis spectra of **1S**, **2S**, and **3S** [28], to our knowledge, no other study has tried to mimic the sodium rhodizonate test for Pb in solution and to measure the changes as the test progresses.

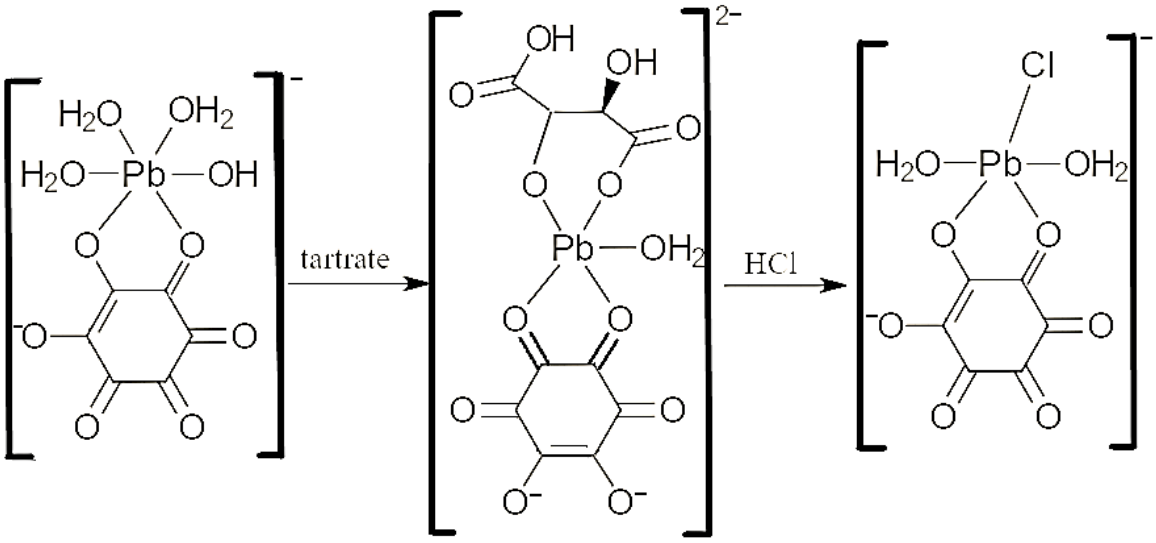

Figure 2-26: The projected schematic of the sodium rhodizonate test in solution. Given the 1:1 binding isotherms, the general formula for **1S** would be $PbC_6O_6(H_2O)_4$, for **2S** would be $Pb(C_6O_6)(C_4H_4O_6)H_2O$, and for **3S** would be $Pb(C_6O_6)(H_2O)_2Cl$. The EtOH is omitted from these structures. The estimated structure of **3** is formed from the dimerization of **3S**.

2.5 Conclusion

The compounds involved in the widely used and little understood sodium rhodizonate test for detection of Pb(II) have now been characterized in the solid state by elemental analysis, XPS, FT-IR, and in solution by UV-Vis spectroscopy. The XPS data show that addition of 5% HCl in the last step of the sodium rhodizonate test displaces the tartrate from **2** and replaces it with a Cl^- to form **3**. This is borne out in the FT-IR spectra of all three compounds. We have now--for the first time--addressed the problem of performing spectroscopic measurements in solution with metal rhodizonate complexes by using a EtOH/H_2O (50/50 v/v) solvent mixture that maintains stability of rhodizonate for

over 2 h. Unsurprisingly, the first step of the sodium rhodizonate test (interaction of Pb(II) with rhodizonate), shows the strongest binding affinity. All complexation in solution occurs in a 1:1 molar ratio, suggesting that EtOH is critical for keeping the compounds in solution, as it may coordinate to Pb(II) or rho, thus breaking the bonds forming the coordination polymers. Understanding the reactions involved in the sodium rhodizonate test not only confirms its chemical validity, but also presents potential for future improvements.

2.6 Acknowledgements

JS was supported by a U.S. Nuclear Regulatory Commission Fellowship (NRC-HQ-84-14-G-0040/NRC-HQ-84-15-G-0038 and 0038B). XPS work was performed by the Chapel Hill Analytical and Nanofabrication Laboratory (CHANL), a member of the North Carolina Research Triangle Nanotechnology Network, which is supported by the NSF, Grant ECCS-1542015, as part of the National Nanotechnology Coordinated Infrastructure.

2.7 References

[1] Chalmers, R. A. and Telling, G. M., *Mikrochim. Acta*, **1967,** *6*, 1126-1135.

[2] Feigl, F. and Suter, H. A., *Ind. Eng. Chem.*, **1942,** *14*, 840-842.

[3] Feigl, F., Gentil, V., Libergott, E., *Isr. J. Chem.*, **1969,** *7*, 123-125.

[4] Cole, S. L., Chemical Spot Test for Lead in Paint and Other Media, US 20030203496 A1, October 30, 2003.

[5] Fabbro, L. A. and Wentzel, C. S., Process for Detecting Trace Amounts of Lead in Unleaded Gasoline, US 19743806319, April 23, 1974.

[6] Morosanova, E. I., Kuz'min, N. M., Zolotov, Y. A., *J. Anal. Chem.*, **1997,** *357*, 853-859.

[7] Ronneau, C. J-M., Jacob, N. M., Apers, D. J., *Anal. Chem.*, **1973,** *45*, 2152.

[8] Lead Test Kit Buying Guide, https://www.consumerreports.org/cro/lead-test-kits/buying-guide/index.htm

[9] West, R., *Isr. J. Chem.,* **1980,** *20,* 300-307.

[10] Marshall, J., *Can. Soc. Forensic Sci. J.,* **2006,** *39,* 115-124.

[11] Andreola, S., Gentile, G., Battistini, A., Cattaneo, C., Zoja, R., *J. Forensic Sci.,* **2011,** *56,* 771-774.

[12] Glater, R. A. B. and Hernandez, L., *J. Air Waste Manage. Assoc.,* **1972,** *22,* 463-467.

[13] Seregin, I. V. and Kozhevnikova, A. D., *Russ. J. Plant Physiol.,* **2011,** *58,* 721-727.

[14] Geusens, N., Nys, B., Charles, S., *J. Forensic Sci.,* **2019,** *64,* 1169-1172.

[15] Reagents and Test Media for the Sodium Rhodizonate Test, http://projects.nfstc.org/firearms/module12/fir_m12_t05_03_l.htm.

[16] Firearm Examiner Training Reagents and Test Media, http://projects.nfstc.org/firearms/module12/fir_m12_t05_03_l.htm

[17] Dillon, J. H., *AFTA J.,* **1990,** *22,* 251-256.

[18] Iraci, G. and Back, M. H., *Can. J. Chem.,* **1988,** *66,* 1293-1294.

[19] Cambridge Crystallographic Data Centre https://www.ccdc.cam.ac.uk/.

[20] Cowan, J. A., and Howard J. A. K., *Acta Cryst.***, 2004,** *E60,* m511-m513.

[21] Neumann, M. A. (1965). PhD thesis, University of Wisconsin, USA.

[22] Dinnebier, R. E., Nuss, H., Jansen, M., *Acta Cryst.,* **2005,** *E61,* m2148-m2150.

[23] Kolev, T., Koleva, B. B., Spiteller, M., *Cent. Eur. J. Chem.,* **2008,** *6,* 393-399.

[24] Bettermann, H., Dasting, I., Wolff, U., *Spectrochim. Acta Part A,* **1997,** *53,* 233-245.

[25] Lam, C-K., and Mak, T. C. W., *Angew. Chem. Int. Ed.,* **2001,** *40,* 3453-3455.

[26] Lam, C-K., and Mak, T. C. W., *Chem. Commun.,* **2001,** 1568-1569.

[27] Cheng, M-F., Li, C-L., Li, W-K., *Chem. Phys. Lett.,* **2004,** *391,* 157-164.

[28] Bartsch, M. R., Kobus, H. J., and Wainwright, K. P., *J. Forensic Sci.,* **1996,** *41,* 1046-1051.

[29] Portillo-Moreno, O., Gutierrez-Perez, R., Chavez Portillo, M., Marquez Specia, M. N., Hernandez-Tellez, G., Lazcano Hernandez, M., Moreno Rodriguez, A., Palomino-Merino, R., Rubio Rosas, E., *Revista Mexicana de Fisica*, **2016**, *62*, 456-460.

[30] Kavallieratos, K., Rosenberg, J. M., Bryan, J. C., *Inorg. Chem.,* **2005,** *44,* 2573.

[31] Mathivanan, V. and Haris M., *Optik,* **2013,** *124,* 4614-4617.

[32] NIST X-ray Photoelectron Spectroscopy Database, https://srdata.nist.gov/xps/Default.aspx.

[33] Wu, D., Li, H., Li, R., Hu, Y., and Hu, X., *Chem. Commun.,* **2018,** *54,* 11415-11418.

[34] Connors, K. A., In *Binding Constants: The Measurement of Molecular Complex Stability,* New York: Wiley-Interscience, **1987**.

[35] Araujo, P., *J Chromatogr. B,* **2009,** *877,* 2224-2234.

CHAPTER III. RHODIZONATE COORDINATION WITH LANTHANIDES(III): A SPECTROSCOPIC STUDY

Joshua A. Silverman, Cristian Nodarse, Christopher J. Dares, Konstantinos Kavallieratos*

3.1 Abstract

Rhodizonate readily forms complexes with a variety of Ln(III). FT-IR and XPS data show that several lanthanides have similar structures when complexed with rhodizonate. All formed Ln(III) complexes showed broad IR absorption bands at ~3300 cm^{-1}, corresponding to a hydroxide stretch; three strong bands in the 1600 – 1300 cm^{-1} region, corresponding to C=O stretches; and a strong band in the 1090 – 1030 cm^{-1} range, corresponding to a C-C stretch. The high resolution C 1s and O 1s XPS spectra for two different Ln(III) (La and Gd) are nearly identical, suggesting that C and O within those complexes have a very similar coordination environment. Elemental analysis, UV-Vis Job Plots, and UV-Vis titrations all indicate formation of Ln(III)-rhodizonate complexes in 1:1 ratios. Some differences between coordination with several Ln(III) is indicated by their binding affinities to rhodizonate. Binding constants, K_{11}, for formation of several lanthanide-rhodizonate complexes range between ~10^5 M^{-1} for Gd(III) to almost 10^7 M^{-1} for Nd(III).

3.2 Introduction

Rhodizonate ($C_6O_6^{2-}$) is the six-carbon member of a group of compounds known as oxocarbons. First synthesized by Leopold Gmelin in 1825, the anion's superficial resemblance to benzene led many chemists at the time to believe that the two compounds had similar properties [1]. This, however, is not the case, and while benzene and phenyl-ring-containing compounds are well known and understood, there are much fewer studies with rhodizonate-containing compounds. As of September 2020, just 17 structures are

recorded in the Cambridge Crystallographic Data Center (CCDC) [2]. What few rhodizonate structures that are in the CCDC tend to contain alkali metals [3-5], other +1 cations [6], or contain more elaborate organic frameworks [7-9]. With regard to f-elements, this rarity of rhodizonate structures is especially striking. Specifically, we found no crystal structures of lanthanides complexed with rhodizonate reported in the literature. The dearth of rhodizonate structures is explained by the instability of the rhodizonate anion in water. In aqueous solution and in the presence of oxygen, rhodizonate anion rapidly undergoes oxidative ring contraction giving the 5-membered analog croconate [10] (Figure 1.1). Mixing a miscible organic solvent with water extends the useful lifetime of rhodizonate as a colorimetric analytical reagent. The analytical uses of rhodizonate have been known since the mid-20th century [11, 12]. Rhodizonate readily forms brightly-colored precipitates with a variety of metals. The color of the precipitate is dependent on the metal cation and the pH of the solution in which they were mixed. Rhodizonate also forms colored solutions with metal cations, in mixed solvents, such as water/ethanol or water/acetone [10]. We have recently found that a water/ethanol (50/50 v/v) solvent system is very effective in stabilizing rhodizonate solutions for a period of 3h, allowing collection of reliable spectroscopic data [13].

Understanding the coordination of rhodizonate with f-elements is critical, as rhodizonate has been used in radiological work, yet the published literature on f-element-rhodizonate coordination is very limited [10, 14]. Uranyl (UO_2^{2+}) cations complex with rhodizonate to form brown precipitates at neutral pH [10]. There are several reported radiological applications of rhodizonate: rhodizonate has been used to co-crystalize potassium and plutonium for alpha spectroscopy [14]. Pb(II) rhodizonate prepared in basic

solution and adhered to activated carbon can adsorb and concentrate radium for alpha spectroscopy [15-17]. In this work we have studied the complexation of rhodizonate with several Ln(III) by XPS and FT-IR in solid state, and by UV-Visible and fluorescence spectroscopy in solution. Our findings show that rhodizonate has strong affinity to trivalent lanthanide cations and that Ln^{3+}-rhodizonate binary compounds differ substantially across the Ln(III) series.

3.3 Experimental Section

3.3.1 Materials and Methods

3,4,5,6-Tetraoxocyclohexene-1,2-diol disodium salt (rhodizonic acid, disodium salt) was purchased from Sigma-Aldrich. Hydrated lanthanide nitrates were purchased from Fisher Scientific. All chemicals were reagent grade and were used without further purification. The water used in all experiments was nano-pure with a resistivity >17 MΩ cm^{-1} (Millipore by Barnstead Thermolyne Corporation, Dubuque, IA). Ethanol (200 proof) was purchased by Pharmco-Aaper. FT-IR measurements were collected on an Agilent Technologies Cary 670 FT-IR with a diamond ATR attachment. X-ray photoelectron spectra (XPS) were collected on a Kratos Axis Ultra DLD X-ray photoelectron spectrometer using a monochromatic Al K-alpha source for high resolution work. Energy correction using the lowest energy binding component of the C 1s peak to 284.6 eV. Peak fittings were achieved using pseudo-Voight peaks to minimize the residual difference between modeled peaks and experimentally acquired data. UV-Vis spectra were collected on a Varian Cary-100 UV-Visible spectrophotometer or on a Shimadzu UV-2101PC UV-Visible spectrophotometer. Elemental analysis was performed by Atlantic Microlab Inc.

3.3.2 Synthesis

3.3.2.1 General Synthesis

Ln^{3+}-rhodizonate binary complexes were formed by mixing a solutions of 0.3 mmol of $Na_2C_6O_6$ in 100.0 mL of water with a solution of 0.3 mmol of $Ln(NO_3)_3 \cdot xH_2O$ (x = 5 or 6) in 100.0 mL of water. Doing so causes precipitates to immediately form, with colors ranging from pink to red to purple. The precipitates were vacuum filtered, washed with water, acetone, and dichloromethane (DCM), and dried under vacuum overnight.

3.3.2.2 Lanthanum Rhodizonate

Mixing $Na_2C_6O_6$ (64.2 mg, 0.3 mmol) in 100.0 mL of water with a solution of $La(NO_3)_3 \cdot 6H_2O$ (101.0 mg, 0.3 mmol) results in a purple, flaky precipitate. Elemental analysis calculated for $La_3(C_6O_6)_2(H_2O)_9(OH)_5$: C = 14.42%, H = 2.32%. Found: C = 14.41%, H = 2.30%. FT-IR (cm^{-1}): 3389 (vs, br), 3251 (s), 1634 (s), 1435 (vs), 1294 (vs), 1040 (s, sh), 816 (m, sh), 738 (m, sh).

3.3.2.3 Europium Rhodizonate

Mixing $Na_2C_6O_6$ (64.2 mg, 0.3 mmol) in 100.0 mL of water with a solution of $Eu(NO_3)_3 \cdot 6H_2O$ (103.4 mg, 0.3 mmol) results in a red, powdery precipitate. Elemental analysis calculated for $Eu_4(C_6O_6)_3(H_2O)_{12}(OH)_6$: C = 15.02%, H = 2.11%. Found: C = 15.10%, H = 2.49%. FT-IR (cm^{-1}): 3524 (s), 3452 (s), 3190 (s, br), 1651 (s), 1620 (s), 1445 (vs), 1312 (vs), 1288 (vs), 1043 (s, sh), 1034 (s, sh), 877 (w), 812 (s, sh), 737 (m), 634 (m, br).

3.3.2.4 Gadolinium Rhodizonate

Mixing $Na_2C_6O_6$ (64.2 mg, 0.3 mmol) in 100.0 mL of water with a solution of $Gd(NO_3)_3 \cdot 6H_2O$ (105.6 mg, 0.3 mmol) results in a red, powdery precipitate. Elemental

analysis calculated for $GdC_6O_6(H_2O)_6OH$: C = 15.76%, H = 2.87%. Found: C = 15.60%, H = 2.75%. FT-IR (cm^{-1}): 3527 (s), 3452 (s), 3192 (s, br), 1653 (s), 1619 (s), 1446 (vs), 1315 (vs), 1290 (vs), 1044 (s, sh), 1035 (s, sh), 812 (s, sh), 738 (m), 631 (m, br).

3.3.2.5 Ytterbium Rhodizonate

Mixing $Na_2C_6O_6$ (64.2 mg, 0.3 mmol) in 100.0 mL of water with a solution of $Yb(NO_3)_3•5H_2O$ (104.3 mg, 0.3 mmol) results in a pink, powdery precipitate. Elemental analysis calculated for $Yb_5(C_6O_6)_4(H_2O)_{19}(OH)_7$: C = 14.21%, H = 2.24%. Found: C = 14.22%, H = 2.38%. FT-IR (cm^{-1}): 3211 (s, br), 1605 (vs), 1506 (vs), 1368 (vs), 1318 (vs), 1147 (w), 1082 (s, sh), 944 (w).

3.3.3 X-Ray Photoelectron Spectroscopy

XPS spectra were acquired using a Kratos Axis Ultra DLD X-ray photoelectron spectrometer using a monochromatic Al K_α X-ray source. The base pressure for sample acquisition was 6×10^{-9} Torr. The analyzer pass energy was 80 eV for survey scans and 20 eV for high resolution scans. Data fittings of high resolution spectra were fitted to the minimum number of pseudo-voigt functions possible to accurately model baseline subtracted data. Baseline subtraction were completed using a polynomial least squares regression, while peak fittings were performed using the solver in Microsoft Excel to minimize the difference between the model and experimental data.

3.3.4 UV-Visible Titrations

In a typical UV-Vis titration experiment, solutions of sodium rhodizonate ($Na_2C_6O_6$, 3.0 x 10^{-5} M) in water/ethanol (50/50 v/v) (solution A) were titrated with water/ethanol (50/50 v/v) solutions of $Ln(NO_3)_3$ (1.0 x 10^{-3} M) at constant sodium rhodizonate concentration (3.0 x 10^{-5} M) (Solution B). For spectra collection, 3.00 mL of

the $Na_2C_6O_6$ solution (solution A) were added to a cuvette and 5.00 - 25.0 μL sequential additions of solution B were added at 5 min intervals until a total of 200.0 μL had been added. All spectra were collected with a Shimadzu UV-2101PC UV-Visible spectrophotometer. Titrations at longer time intervals established that the complex formation reaction in solution reaches equilibrium in less than 5 min. Binding constants were determined using the method described in Section 1.7.

3.3.5 UV-Visible Job Plots

To determine the Ln-rhodizonate complexation ratio by Job's method, 40.0 mg of $Na_2C_6O_6$ (0.187 mmol) was dissolved in 1.00 L of deionized water, giving an orange solution. An amount of this solution (50.0 mL) was added to an equal amount of ethanol. An equimolar amount of $Ln(NO_3)_3$ (0.187 mmol), was also dissolved in 1.00 L of deionized water. Some of this solution (50.0 mL) was mixed with ethanol in the same manner as $Na_2C_6O_6$. Aliquots of both solutions (10.0 mL total) were added to 11 different vials in such a way that every integer ratio of each solution was represented (i.e. one vial with 0.0 mL $Na_2C_6O_6$ and 10.0 mL $Ln(NO_3)_3$, one vial with 1.0 mL $Na_2C_6O_6$ and 9.0 mL $Ln(NO_3)_3$, one vial with 2.0 mL $Na_2C_6O_6$ and 8.0 mL $Ln(NO_3)_3$, etc.). Each vial was shaken by hand for 5 minutes to achieve equilibrium. The UV-Vis spectra of each sample (3.00 mL total volume) were collected. The wavelength of interest is the absorbance maximum for $Na_2C_6O_6$, which is 482 nm.

3.4 Results

3.4.1 FT-IR Spectroscopy

The FT-IR spectra of several Ln(III) rhodizonate complexes are remarkably similar. The spectra of several lanthanide rhodizonates are shown in Figure 3.1.

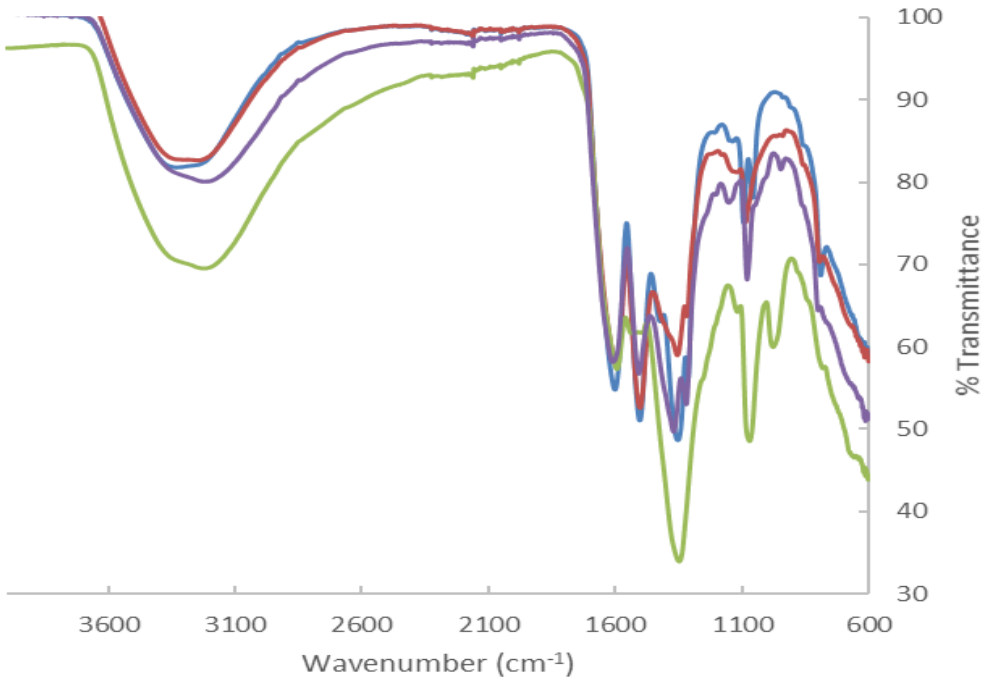

Figure 3.1: The FT-IR spectra of $Eu_4(C_6O_6)_3(H_2O)_{12}(OH)_6$ (red), $GdC_6O_6(H_2O)_6OH$ (green), $La_3(C_6O_6)_2(H_2O)_9(OH)_5$ (blue), and $Yb_5(C_6O_6)_4(H_2O)_{19}(OH)_7$ (purple).

All the Ln(III) rhodizonate complexes showed three common features in their FT-IR spectra: First, all complexes showed a broad band around 3300 cm^{-1}, indicative of O-H···H stretching. All Ln(III)-rho complexes tested had some stronger, somewhat sharper bands between 3500 cm^{-1} to 3100 cm^{-1}, which indicate coordinated hydroxide. Second, all Ln(III)-rho complexes showed three sets of very strong stretching bands in the C-O region from 1650 cm^{-1} to 1300 cm^{-1}. The highest wavenumber stretch corresponds to C=O stretches that are very close to bond order 2. The middle and lowest wavenumber stretches are assigned to C-O stretches that indicate coordination to the Ln(III). The stretches with higher energies correspond to an intermediate bond order between 1 and 2, while the lower energy stretches correspond to bond orders closer to 1. Finally, all Ln(III)-rho complexes showed a sharp band between 1090 cm^{-1} and 1030 cm^{-1} which corresponds to C-C stretching.

3.4.2 X-Ray Photoelectron Spectroscopy

Samples of $GdC_6O_6(H_2O)_6OH$ and $La_3(C_6O_6)_2(H_2O)_9(OH)_5$ powders underwent X-ray photoelectron spectroscopy (XPS). High-resolution scans for both compounds were performed for the C 1s and O 1s spectral lines. These are shown in Figures 3.2 and 3.3.

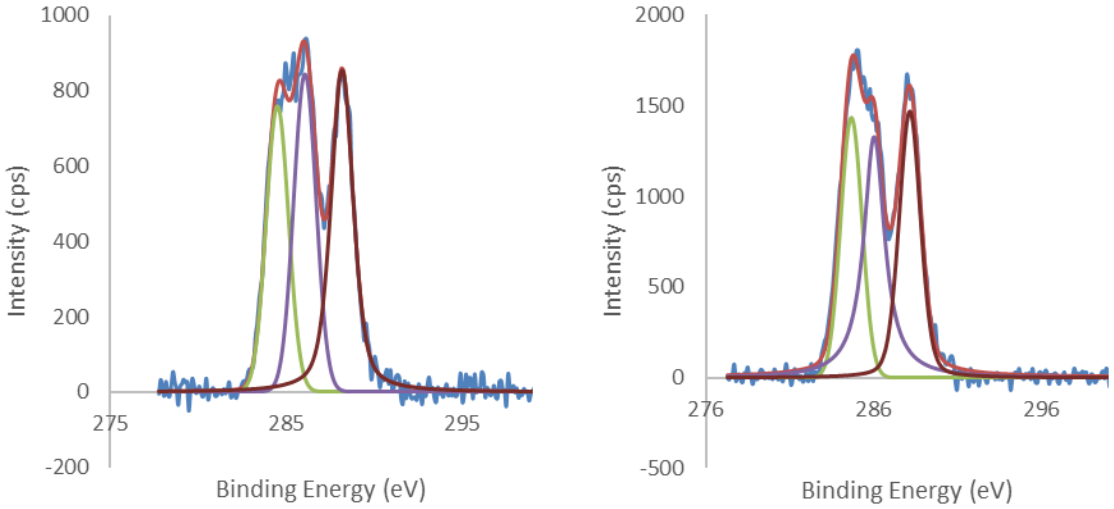

Figure 3.2: The high-resolution XPS spectra for the C 1s spectra lines for $GdC_6O_6(H_2O)_6OH$ (left) and $La_3(C_6O_6)_2(H_2O)_9(OH)_5$ (right). Both compounds' C 1s spectra required three peaks to adequately deconvolute the data, which is suggestive of three different C coordination spheres.

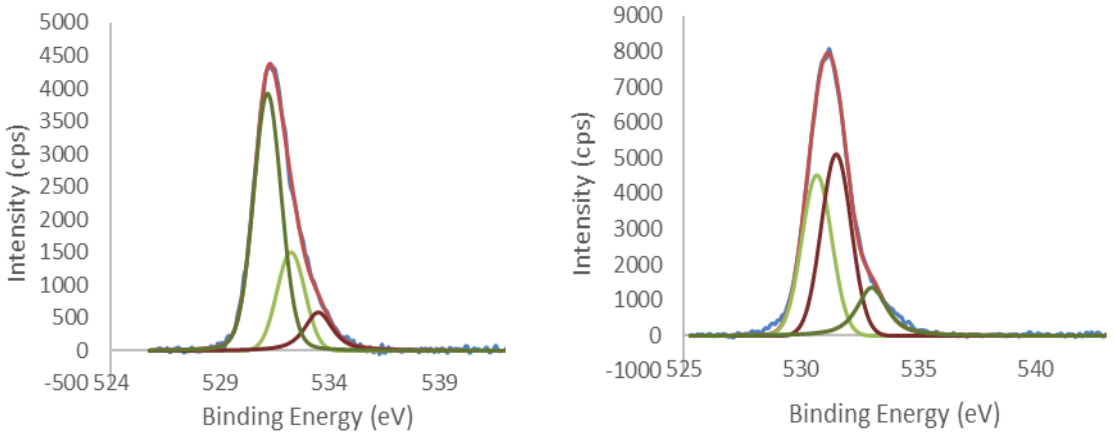

Figure 3.3: The high-resolution XPS spectra for the O 1s spectra lines for $GdC_6O_6(H_2O)_6OH$ (left) and $La_3(C_6O_6)_2(H_2O)_9(OH)_5$ (right). Both compounds' O 1s spectra required three peaks to adequately deconvolute the data, which is suggestive of three different O coordination spheres.

For $GdC_6O_6(H_2O)_6OH$, carbon is shown to have three XPS peaks: one at 284.5 eV, one at 286.1 eV, and one at 288.2 eV. $La_3(C_6O_6)_2(H_2O)_9(OH)_5$ has carbons with similar XPS peaks: one at 284.7 eV, one at 286.0 eV, and one at 288.2 eV. In both compounds, the deconvoluted peaks are of similar intensities, suggesting an equal presence of all three types. The lowest binding energy peak corresponds to a C-C coordination sphere, the middle binding energy peak corresponds to a C-O coordination sphere, and the highest binding energy peak corresponds to a C=O coordination sphere. It is important to note that for both compounds, the C=O binding energy is substantially lower than the typical 289.0 eV C=O environment, suggesting that neither of these compounds have true double bonds between carbon and oxygen, but instead have bonds that have a bond order between 1 and 2 (but closer to 2 than 1).

For $GdC_6O_6(H_2O)_6OH$, oxygen is shown to have three XPS peaks: one at 531.2 eV, one at 532.2 eV, and one at 533.5 eV. $La_3(C_6O_6)_2(H_2O)_9(OH)_5$ has oxygens with similar XPS peaks: one at 530.7 eV, one at 531.5 eV, and one at 533.0 eV. In the Gd(III) compound, the lowest binding energy peak, which corresponds to metal-oxide coordination, is by far the largest peak, while in the La(III) compound, the metal-oxide band and the organic C=O band were of roughly equal intensity. Both compounds had a small organic C-O band (the highest binding energy band).

3.4.3 UV-Visible Titrations

Upon addition of a lanthanide nitrate in water/ethanol (50/50 v/v), the band at 482 nm decreases in intensity and shifts slightly to 491 nm, turning the solution from orange to red. Unlike with other metals [10], the shoulder at lower wavelength does not disappear. The shoulder comes from the Jahn-Teller effect from the LUMO for the first π-π*

transition. In rhodizonate, this orbital is doubly degenerate [1]. The shoulder's continued existence after complexation means that this degeneracy is not resolved through complexation with these metals, indicating a non-planar geometry of the rhodizonate ring, as a planar configuration would have resolved the degeneracy [5].

The complexation of Ln(III) with rhodizonate in solution is consistent with a 1:1 binding ratio, as indicated by fitting of the UV-Vis titration spectral changes to the 1:1 binding isotherm [19]. The results are shown in Figures 3.4 through 3.15.

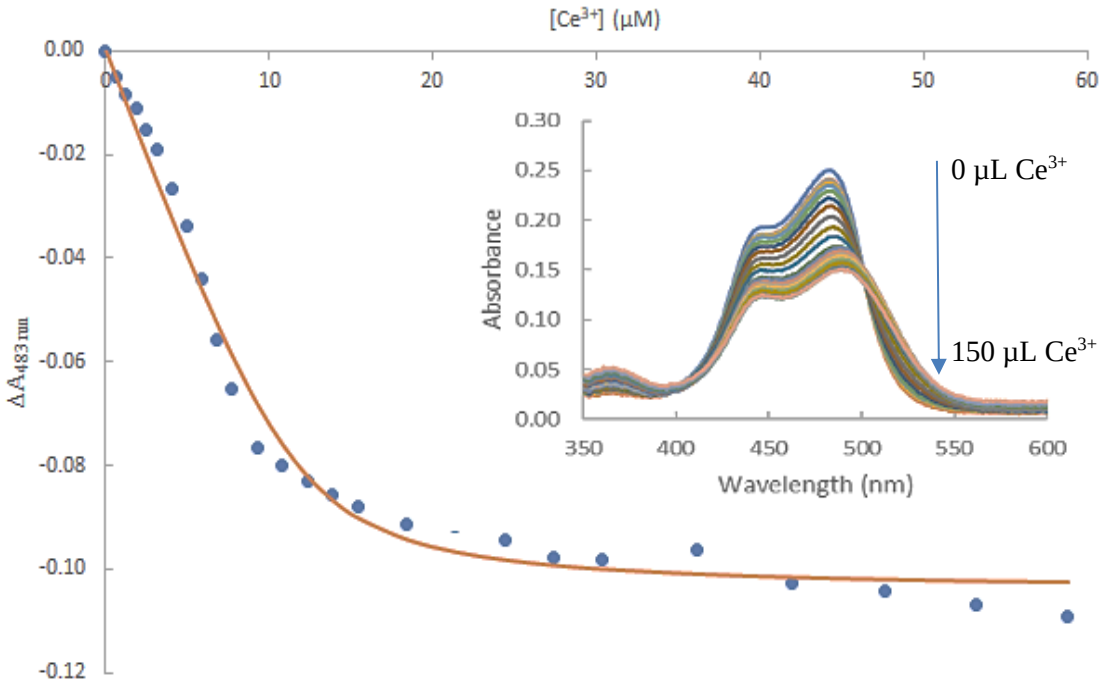

Figure 3.4: Binding curve for the titration of a solution of 9.72 x 10^{-6} M of $Na_2C_6O_6$ with a solution of 2.04 x 10^{-4} M of $Ce(NO_3)_3$•$6H_2O$ in 9.72 x 10^{-6} M of $Na_2C_6O_6$ in water/ethanol (50/50 v/v). K_{11} = 1.22 x 10^6 M^{-1}. **Cutaway:** UV-Visible absorption spectrum for the titration of a solution of 9.72 x 10^{-6} M of $Na_2C_6O_6$ with a solution of 2.04 x 10^{-4} M of $Ce(NO_3)_3$•$6H_2O$ in 9.72 x 10^{-6} M of $Na_2C_6O_6$ in water/ethanol (50/50 v/v).

Non-linear regression analysis of the spectrum of Ce(III)-Rho gives an apparent binding constant of K_{11} = 1.22 x 10^6 M^{-1}, leading to a free energy of complexation of ΔG = -34.7 kJ/mol.

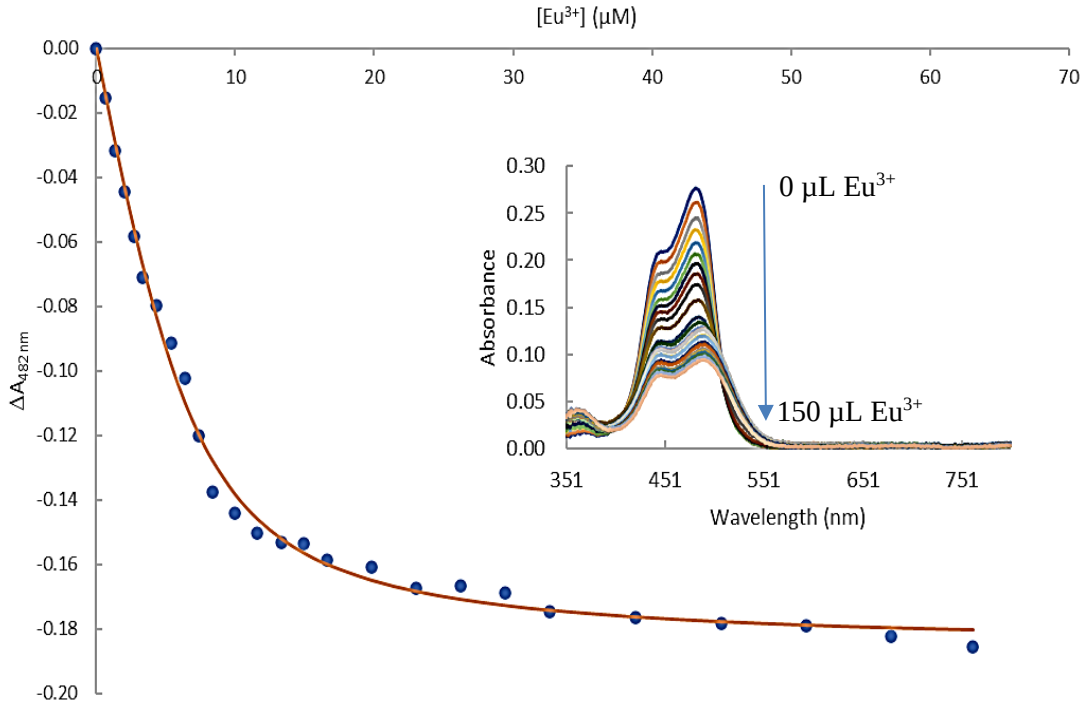

Figure 3.5: Binding curve for the titration of a solution of 9.80 x 10^{-6} M of $Na_2C_6O_6$ with a solution of 2.24 x 10^{-4} M of $Eu(NO_3)_3$•$6H_2O$ in 9.80 x 10^{-6} M of $Na_2C_6O_6$ in water/ethanol (50/50 v/v). K_{11} = 5.53 x 10^5 M^{-1}. **Cutaway:** UV-Visible absorption spectrum for the titration of a solution of 9.80 x 10^{-6} M of $Na_2C_6O_6$ with a solution of 2.24 x 10^{-4} M of $Eu(NO_3)_3$ • $6H_2O$ in 9.80 x 10^{-6} M of $Na_2C_6O_6$ in water/ethanol (50/50 v/v).

Non-linear regression analysis of the spectrum of Eu(III)-Rho gives an apparent binding constant of K_{11} = 5.53 x 10^5 M^{-1}, leading to a free energy of complexation of ΔG = -32.8 kJ/mol.

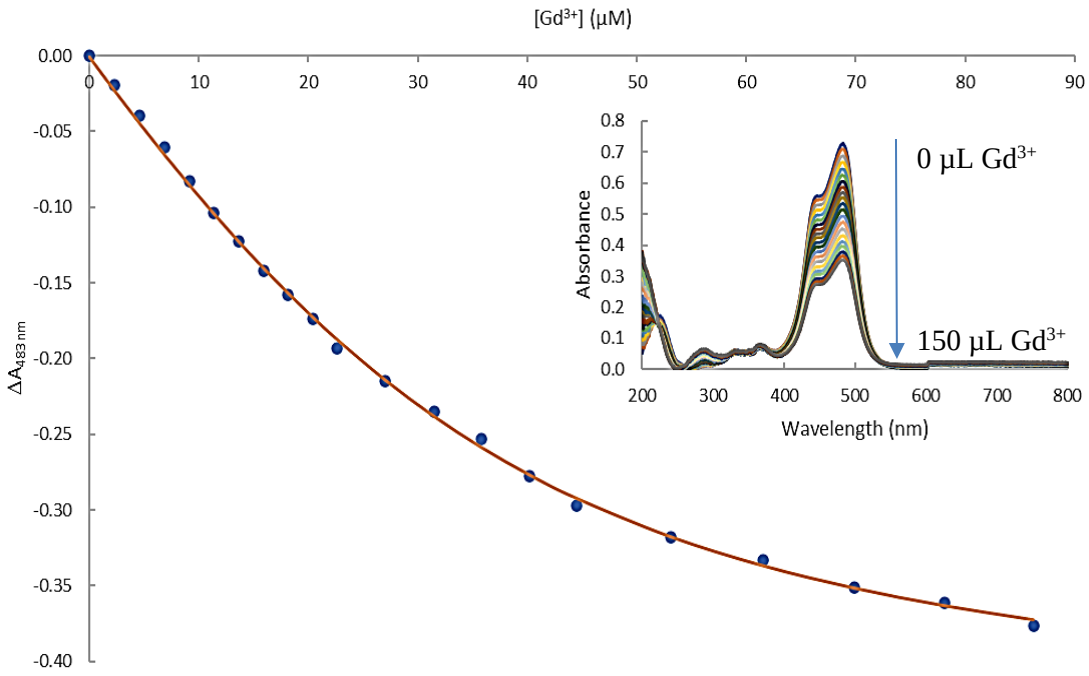

Figure 3.6: Binding curve for the titration of a solution of 2.64 x 10^{-5} M of $Na_2C_6O_6$ with a solution of 7.65 x 10^{-4} M of $Gd(NO_3)_3 \cdot 6H_2O$ in 2.64 x 10^{-5} M of $Na_2C_6O_6$ in water/ethanol (50/50 v/v). K_{11} = 7.86 x 10^4 M^{-1}. **Cutaway:** UV-Visible absorption spectrum for the titration of a solution of 2.64 x 10^{-5} M of $Na_2C_6O_6$ with a solution of 7.65 x 10^{-4} M of $Gd(NO_3)_3 \cdot 6H_2O$ in 2.64 x 10^{-5} M of $Na_2C_6O_6$ in water/ethanol (50/50 v/v).

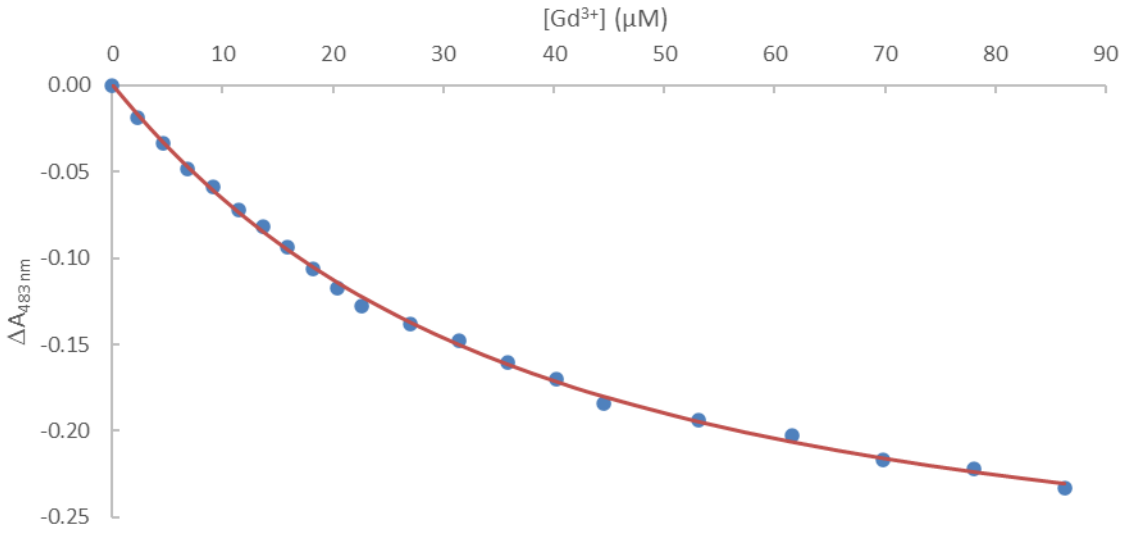

Figure 3.7: Binding curve for the titration of a solution of 2.54 x 10^{-5} M of $Na_2C_6O_6$ with a solution of 1.38 x 10^{-4} M of $Gd(NO_3)_3 \cdot 6H_2O$ in 2.54 x 10^{-5} M of $Na_2C_6O_6$ in water/ethanol (50/50 v/v). K_{11} = 3.68 x 10^4 M^{-1}.

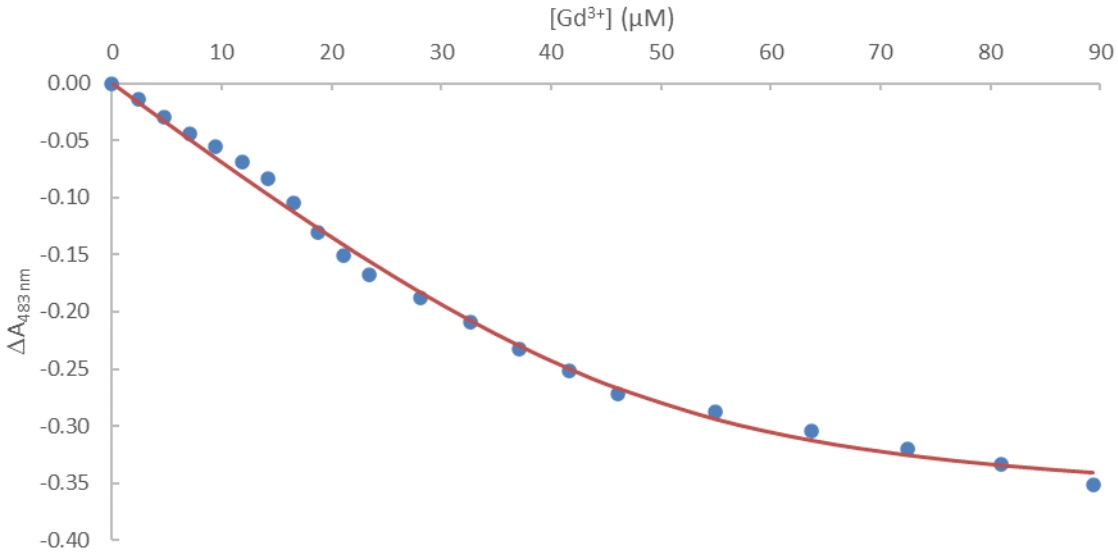

Figure 3.8: Binding curve for the titration of a solution of 2.87 x 10^{-5} M of $Na_2C_6O_6$ with a solution of 1.43 x 10^{-4} M of $Gd(NO_3)_3 \cdot 6H_2O$ in 2.87 x 10^{-5} M of $Na_2C_6O_6$ in water/ethanol (50/50 v/v). K_{11} = 2.04 x 10^5 M^{-1}.

Non-linear regression analysis of the spectrum of Gd(III)-Rho gives an apparent binding constant of K_{11} = 1.1 (± 0.9) x 10^5 M^{-1}, leading to a free energy of complexation of ΔG = -28.7 (± 1.5) kJ/mol. Applying the standard deviation to slope ratio to the isotherm data gives a limit of detection of 2.6 x 10^{-6} M and a limit of quantification of 7.8 x 10^{-6} M [20].

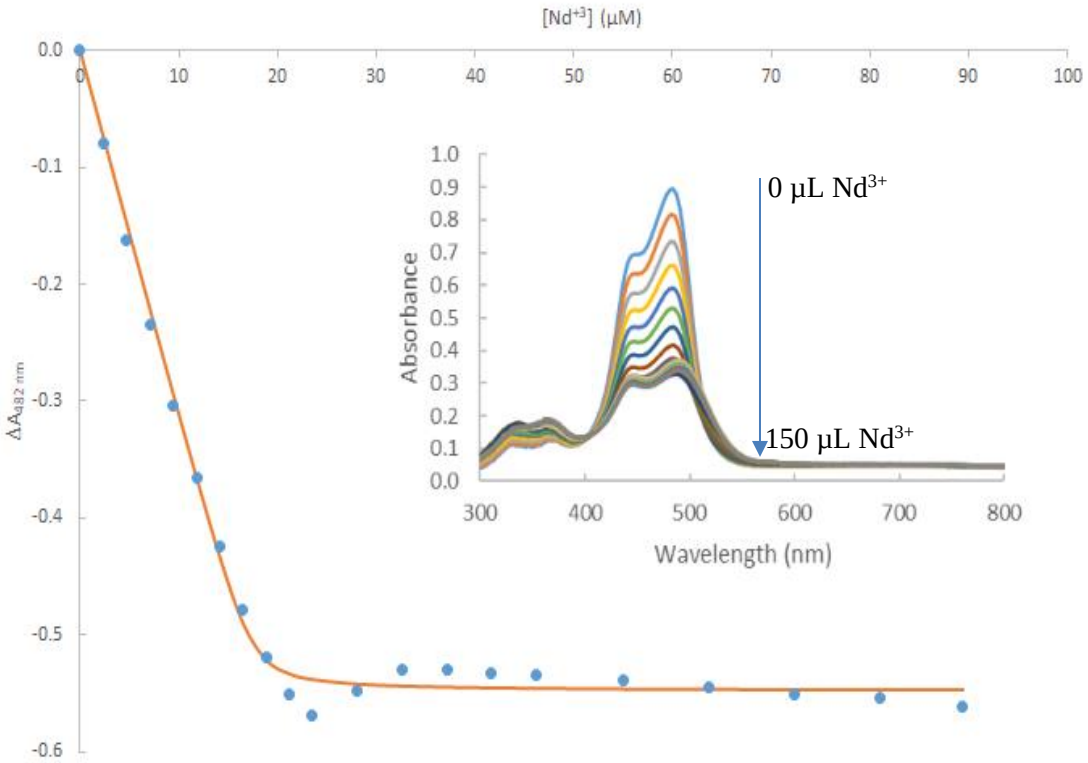

Figure 3.9: Binding curve for the titration of a solution of 3.25 x 10^{-5} M of $Na_2C_6O_6$ with a solution of 7.92 x 10^{-4} M of $Nd(NO_3)_3$•$6H_2O$ in 3.25 x 10^{-5} M of $Na_2C_6O_6$ in water/ethanol (50/50 v/v). K_{11} = 8.34 x 10^6 M^{-1}. **Cutaway:** UV-Visible absorption spectrum for the titration of a solution of 3.25 x 10^{-5} M of $Na_2C_6O_6$ with a solution of 7.92 x 10^{-4} M of $Nd(NO_3)_3$•$6H_2O$ in 3.25 x 10^{-5} M of $Na_2C_6O_6$ in water/ethanol (50/50 v/v).

Non-linear regression analysis of the spectrum of Nd(III)-Rho gives an apparent binding constant of K_{11} = 8.34 x 10^6 M^{-1}, leading to a free energy of complexation of ΔG = -39.5 kJ/mol.

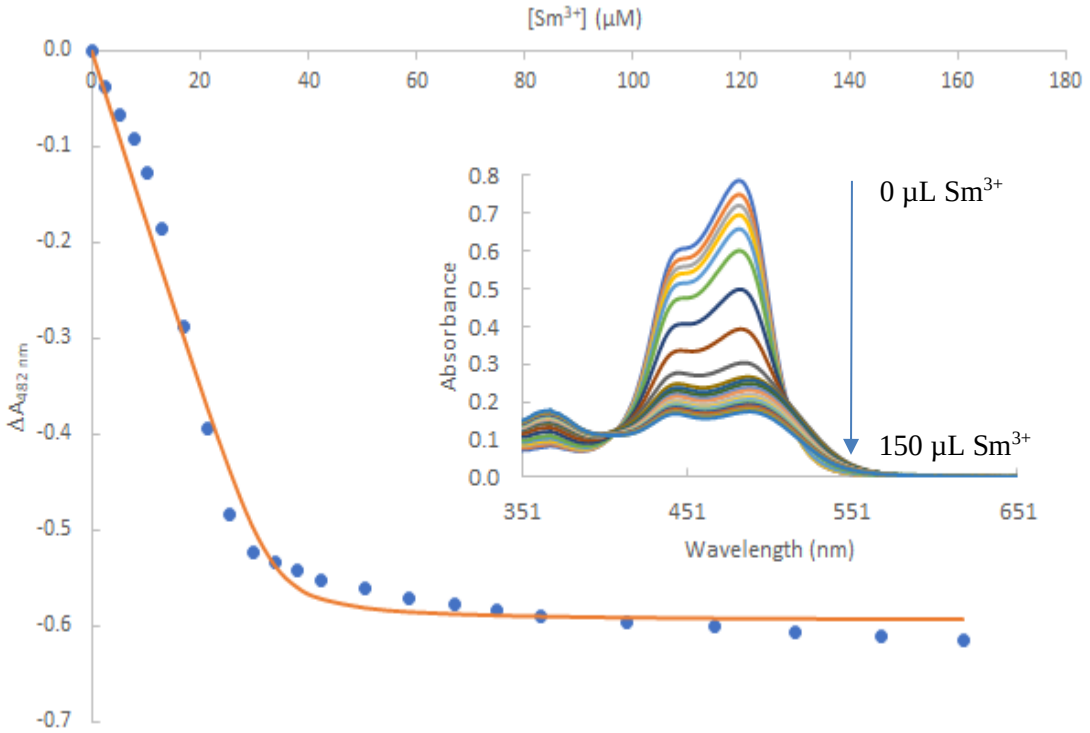

Figure 3.10: Binding curve for the titration of a solution of 3.18 x 10^{-5} M of $Na_2C_6O_6$ with a solution of 8.56 x 10^{-4} M of $Sm(NO_3)_3 \cdot 6H_2O$ in 3.18 x 10^{-5} M of $Na_2C_6O_6$ in water/ethanol (50/50 v/v). K_{11} = 2.27 x 10^6 M^{-1}. **Cutaway:** UV-Visible absorption spectrum for the titration of a solution of 3.18 x 10^{-5} M of $Na_2C_6O_6$ with a solution of 8.56 x 10^{-4} M of $Sm(NO_3)_3 \cdot 6H_2O$ in 3.18 x 10^{-5} M of $Na_2C_6O_6$ in water/ethanol (50/50 v/v).

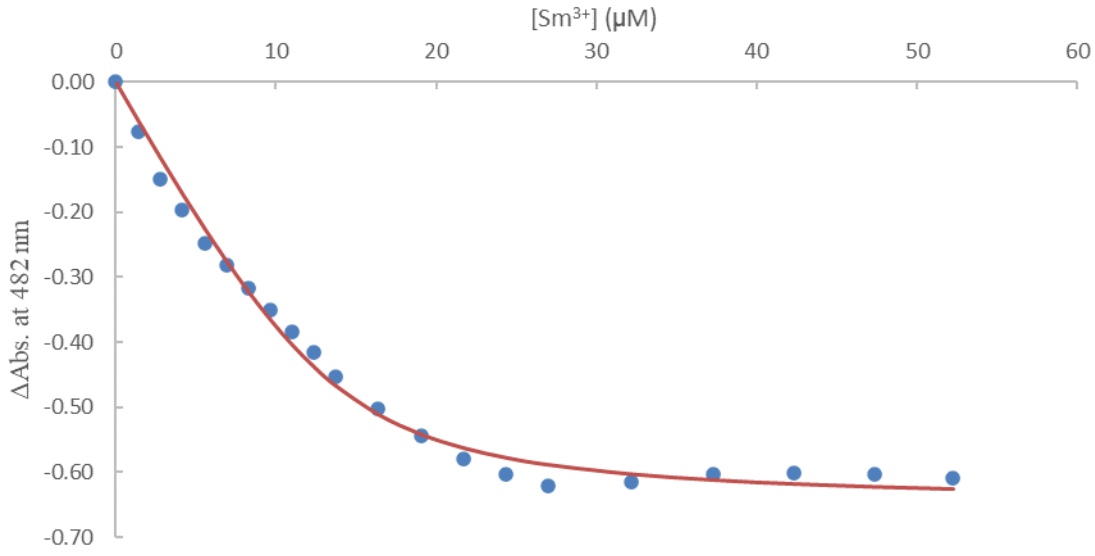

Figure 3.11: Binding curve for the titration of a solution of 3.69 x 10^{-5} M of $Na_2C_6O_6$ with a solution of 8.36 x 10^{-4} M of $Sm(NO_3)_3 \cdot 6H_2O$ in 3.18 x 10^{-5} M of $Na_2C_6O_6$ in water/EtOH (50/50 v/v). K_{11} = 6.47 x 10^5 M^{-1}.

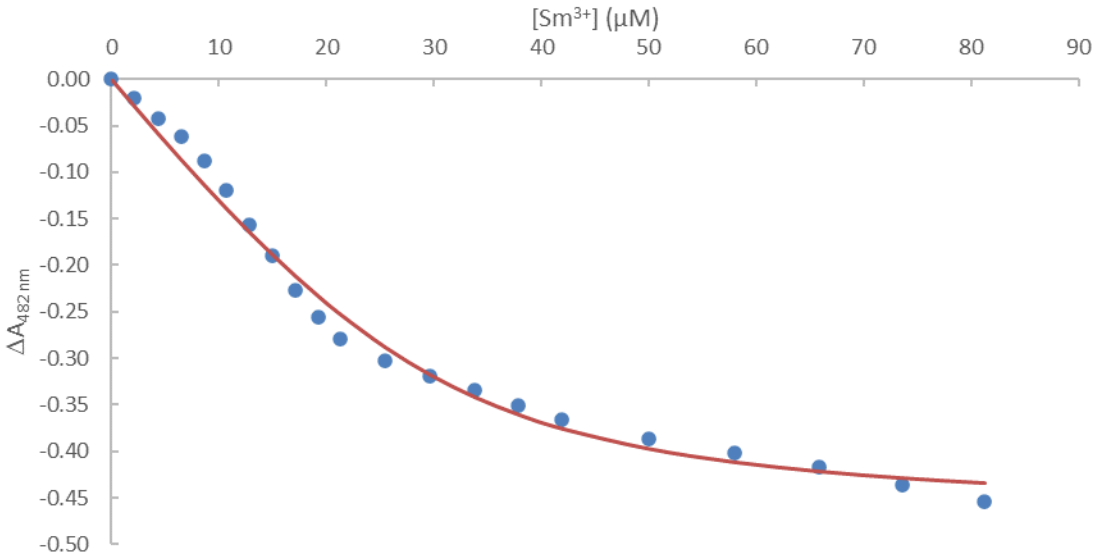

Figure 3.12: Binding curve for the titration of a solution of 2.84 x 10^{-5} M of $Na_2C_6O_6$ with a solution of 1.30 x 10^{-3} M of $Sm(NO_3)_3 \cdot 6H_2O$ in 2.84 x 10^{-5} M of $Na_2C_6O_6$ in water/EtOH (50/50 v/v). K_{11} = 2.13 x 10^5 M^{-1}.

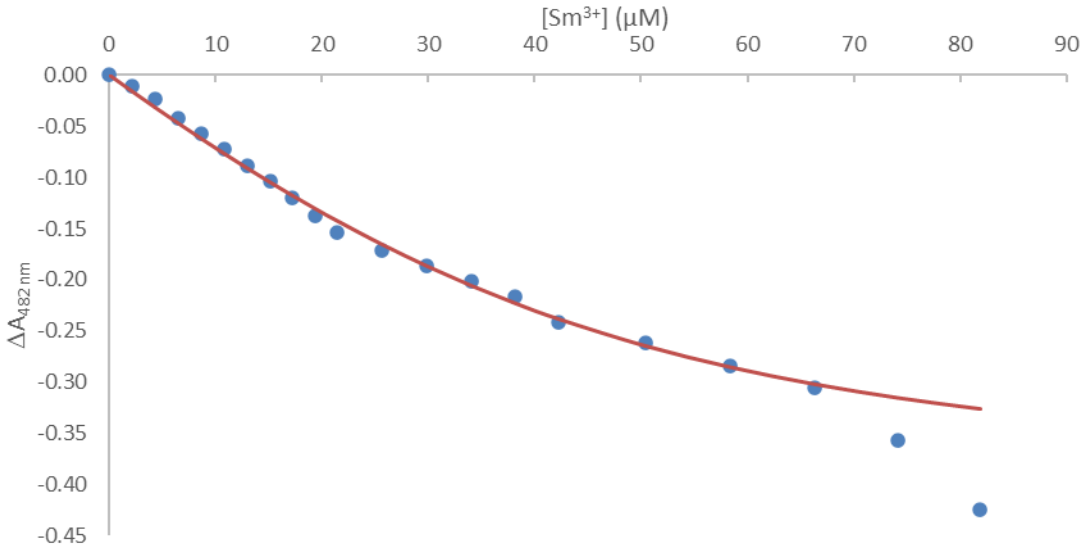

Figure 3.13: Binding curve for the titration of a solution of 2.49 x 10^{-5} M of $Na_2C_6O_6$ with a solution of 1.31 x 10^{-4} M of $Sm(NO_3)_3 \cdot 6H_2O$ in 2.49 x 10^{-5} M of $Na_2C_6O_6$ in water/EtOH (50/50 v/v). K_{11} = 7.21 x 10^4 M^{-1}.

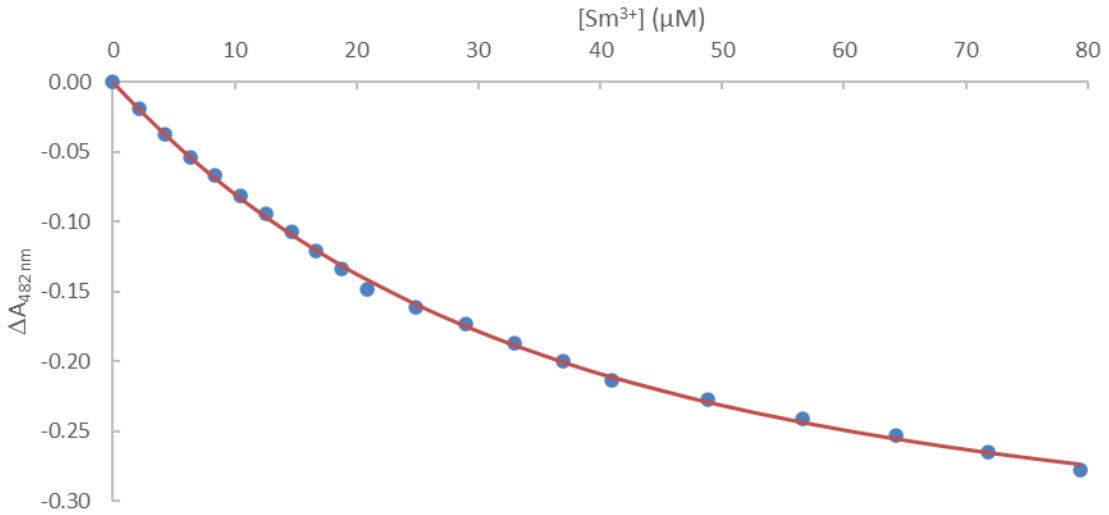

Figure 3.14: Binding curve for the titration of a solution of 2.33 x 10^{-5} M of $Na_2C_6O_6$ with a solution of 1.27 x 10^{-4} M of $Sm(NO_3)_3 \cdot 6H_2O$ in 2.33 x 10^{-5} M of $Na_2C_6O_6$ in water/EtOH (50/50 v/v). K_{11} = 3.95 x 10^4 M^{-1}.

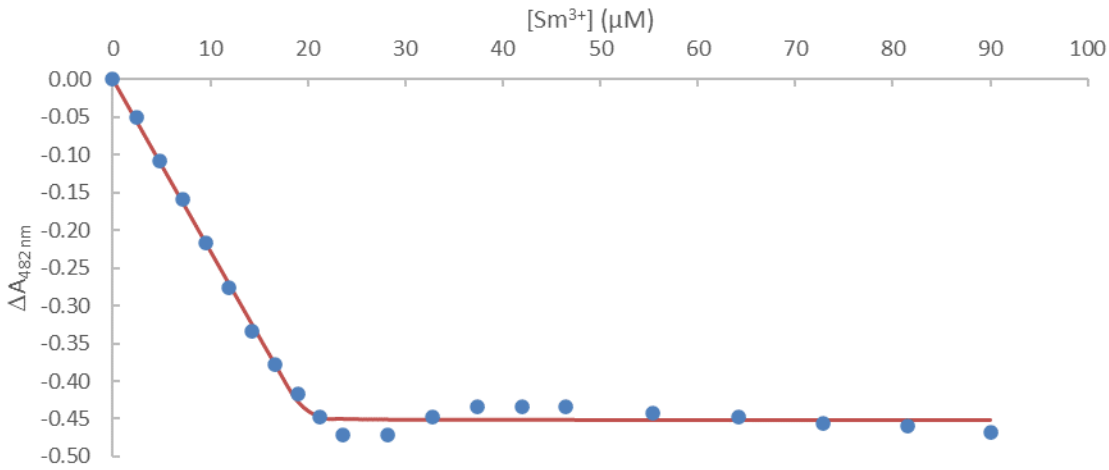

Figure 3.15: Binding curve for the titration of a solution of 2.29 x 10^{-5} M of $Na_2C_6O_6$ with a solution of 1.44 x 10^{-4} M of $Sm(NO_3)_3 \cdot 6H_2O$ in 2.29 x 10^{-5} M of $Na_2C_6O_6$ in water/EtOH (50/50 v/v). K_{11} = 7.46 x 10^7 M^{-1}.

Non-linear regression analysis of the spectrum of Sm(III)-Rho gives an apparent binding constant of K_{11} = 1.0 (± 1.0) x 10^6 M^{-1}, leading to a free energy of complexation of ΔG = -34.3 (± 1.7) kJ/mol. Applying the standard deviation to slope ratio to the isotherm data gives a limit of detection of 3.0 x 10^{-6} M and a limit of quantification of 9.0 x 10^{-6} M [20].

3.4.4 Job Plots

The Method of Continuous Variation (a.k.a. Job's method) was performed for complexation of several Ln(III), as well as Y(III) with rhodizonate. The results are shown on Figures 3.16 through 3.22.

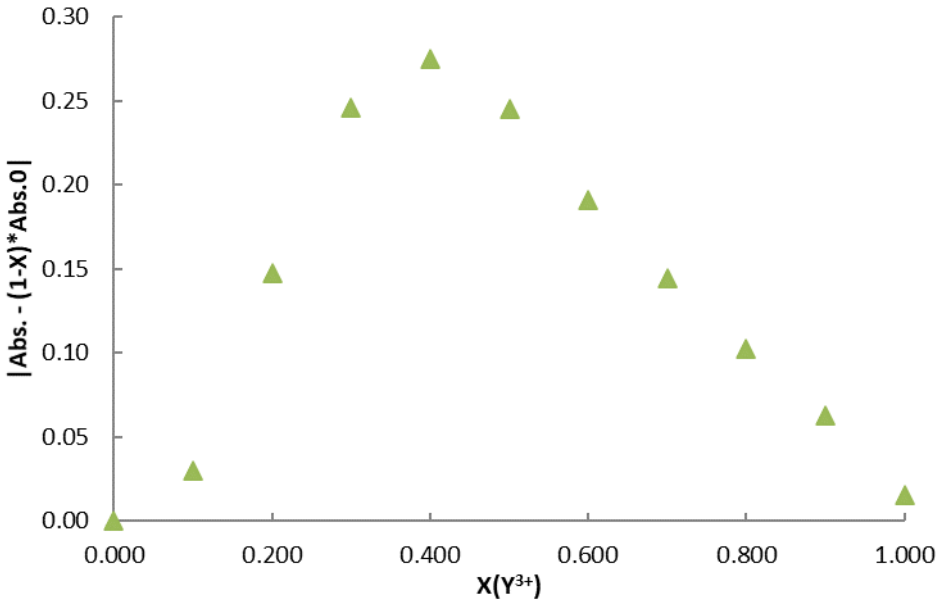

Figure 3.16: Job plot for Na-Rho and $Y(NO_3)_3 \cdot 6H_2O$. The binding is suggestive of a 3:2 complexation ratio of rhodizonate to Y(III).

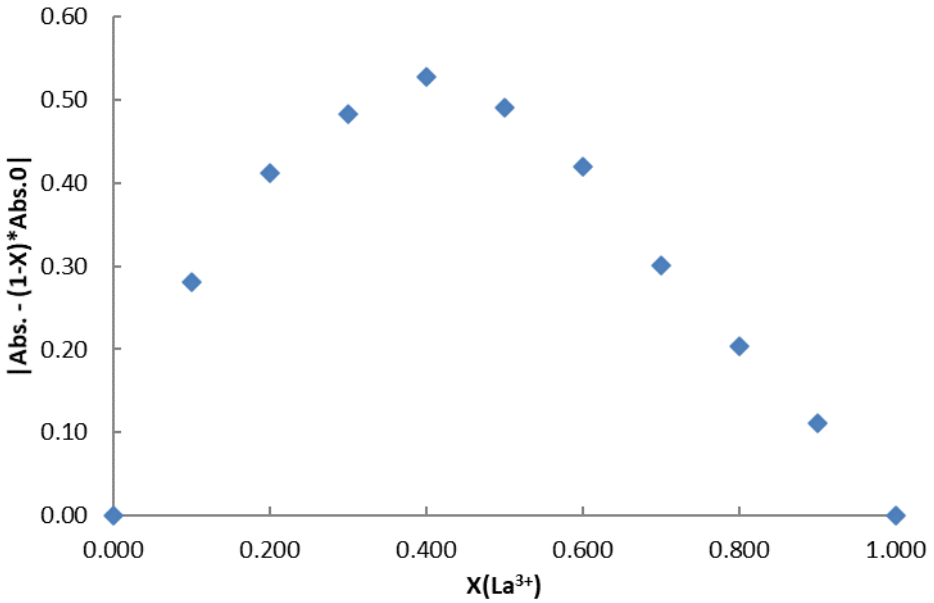

Figure 3.17: Job plot for Na-Rho and $La(NO_3)_3 \bullet 6H_2O$. The binding is suggestive of a 3:2 complexation ratio of rhodizonate to La(III).

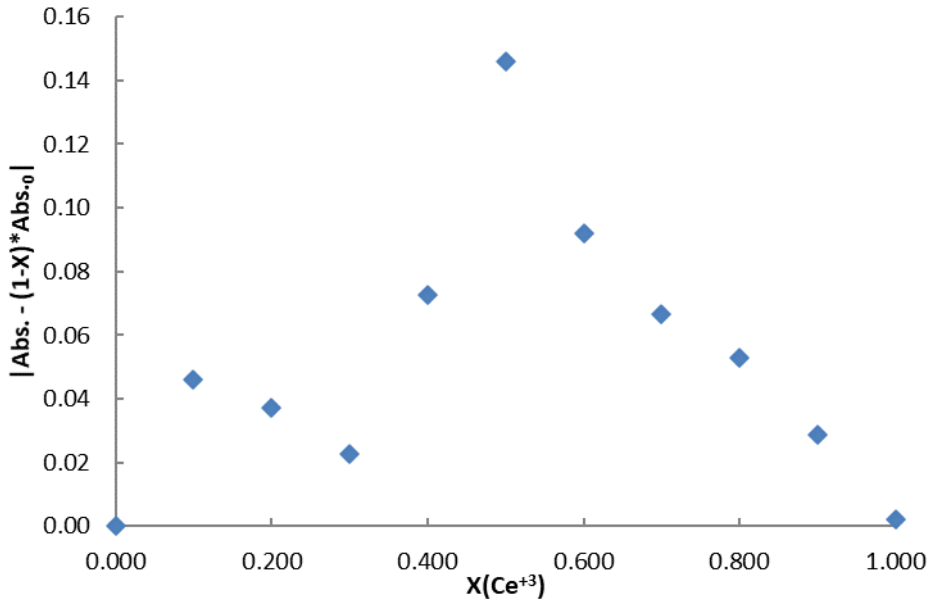

Figure 3.18: Job plot for Na-Rho and $Ce(NO_3)_3 \bullet 6H_2O$. The binding is suggestive of a 1:1 complexation ratio of rhodizonate to Ce(III).

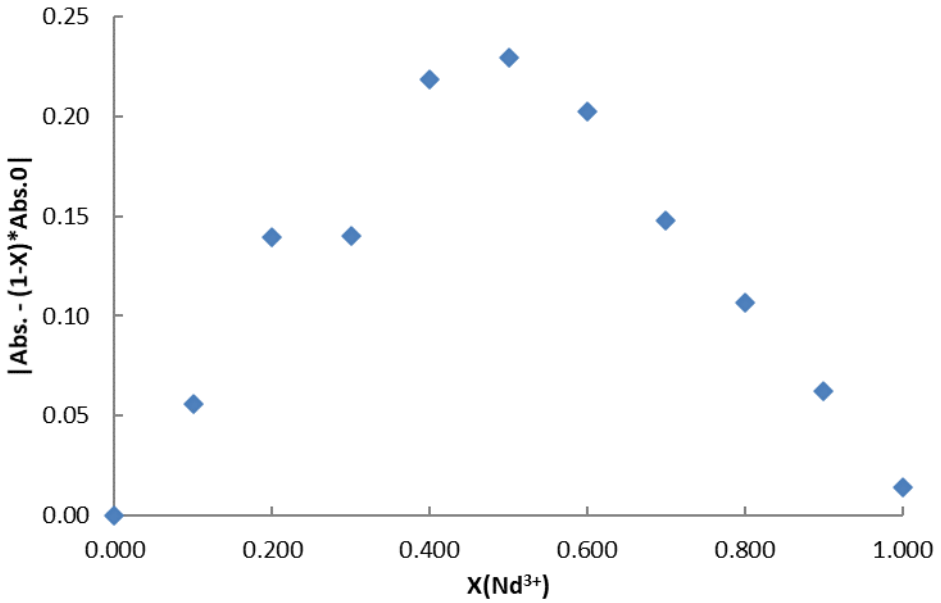

Figure 3.19: Job plot for Na-Rho and $Nd(NO_3)_3 \bullet 6H_2O$. The binding is suggestive of a 1:1 complexation ratio of rhodizonate to Nd(III).

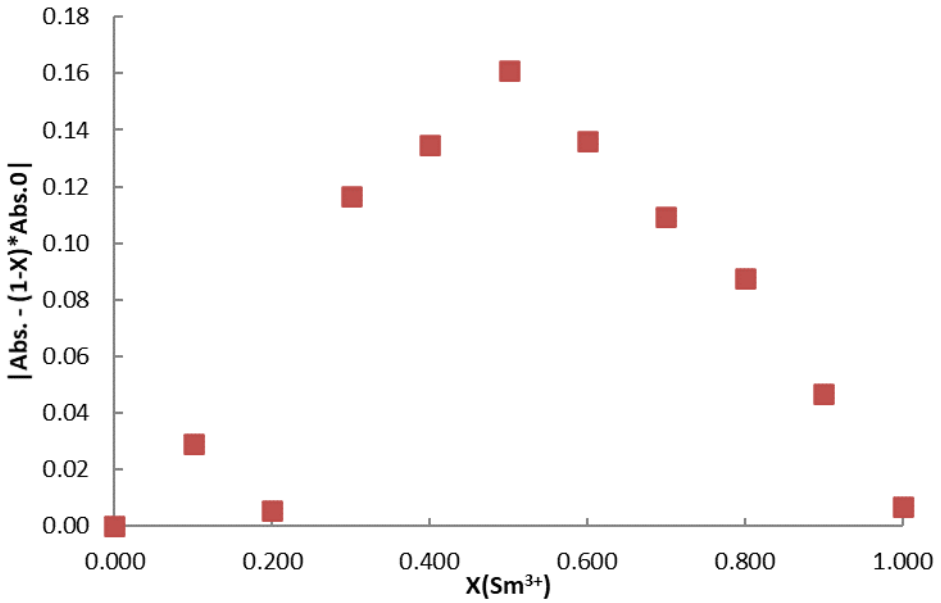

Figure 3.20: Job plot for Na-Rho and $Sm(NO_3)_3 \bullet 6H_2O$. The binding is suggestive of a 1:1 complexation ratio of rhodizonate to Sm(III).

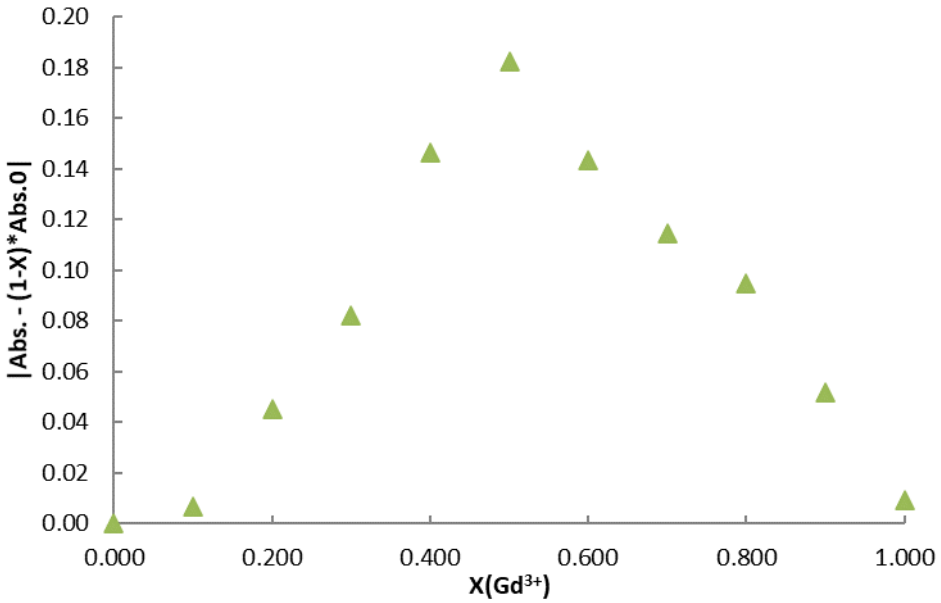

Figure 3.21: Job plot for Na-Rho and $Gd(NO_3)_3 \bullet 6H_2O$. The binding is suggestive of a 1:1 complexation ratio of rhodizonate to Gd(III).

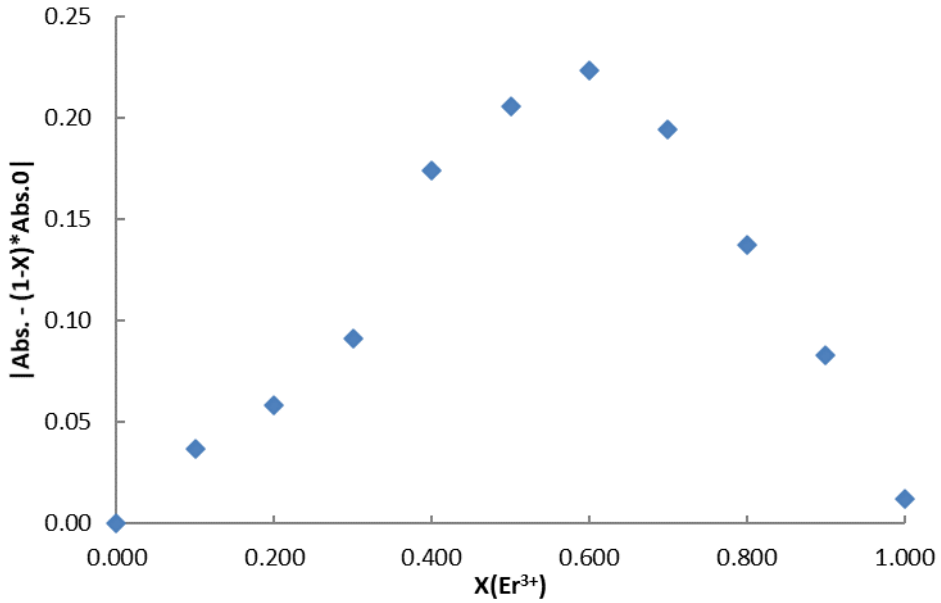

Figure 3.22: Job plot for Na-Rho and $Er(NO_3)_3 \bullet 5H_2O$. The binding is suggestive of a 3:2 complexation ratio of rhodizonate to Er(III).

3.5 Discussion

All lanthanides tested show approximately a 1:1 complexation ratio between Ln(III) and rhodizonate. This is consistent with the UV-Vis titration work, which, for all Ln(III)-rhodizonates tested, conforms to the 1:1 binding isotherm. Since the water/ethanol

(50/50 v/v) solvent keeps the Ln(III)-Rho complex in solution, Job Plots are a good method of determining molecular binding ratios [21]. The similarity in binding ratios is further reinforced by the similarity of FT-IR spectra, for the variety of Ln(III)-rhodizonate complexes. As we did not use Job Plots to determine binding constants, we were able to avoid some of the pitfalls of Job's method [22, 23].

The binding constants for complexation of several Ln(III) with rhodizonate are summarized in Table 3.1.

Table 3.1: A summary of the binding constants for complexation of several Ln(III) with rhodizonate

Ln(III)	K_{11} (M^{-1})
Ce	1.2×10^6
Nd	8.3×10^6
Sm	$1.0 (\pm 1.0) \times 10^6$
Eu	5.5×10^5
Gd	$1.1 (\pm 0.9) \times 10^5$

Overall, rhodizonate was shown to bind quite strongly to all Ln(III) tested. However, the degree of association is highly variant, with binding constants spanning from ~10^5 M^{-1} to almost 10^7 M^{-1}. This great span of binding constants is suggestive of some selectivity for binding of different lanthanides and rhodizonate that does not follow any known periodic trend along the Ln(III) series. Such peak selectivity could potentially be used for lanthanide separations through selective precipitation.

Future research will involve obtaining X-ray structures and powder diffraction patterns for Ln(III)-rhodizonate complexes in order to fully elucidate coordination patterns for all species involved. Completing the UV-Vis titration work would allow for a better understanding of binding between Ln(III) and rhodizonate.

3.6 Acknowledgements

The XPS work was performed by the Chapel Hill Analytical and Nanofabrication Laboratory (CHANL), a member of the North Carolina Research Triangle Nanotechnology Network, which is supported by the NSF, Grant ECCS-1542015, as part of the National Nanotechnology Coordinated Infrastructure. JS was supported by a U.S. Nuclear Regulatory Commission Fellowship (NRC-HQ-84-14-G-0040/NRC-HQ-84-15-G-0038 and 0038B).

3.7 References

[1] West, R., *Isr. J. Chem.,* **1979,** *20,* 300-307.

[2] Cambridge Crystallographic Data Centre https://www.ccdc.cam.ac.uk/.

[3] Cowan, J. A., and Howard J. A. K., *Acta Cryst.***, 2004,** *E60,* m511-m513.

[4] Neumann, M. A. (1965). PhD thesis, University of Wisconsin, USA.

[5] Dinnebier, R. E., Nuss, H., Jansen, M., *Acta Cryst.,* **2005,** *E61,* m2148-m2150.

[6] Finger, L. H., and Sundermeyer, J., *J. Inorg. Gen. Chem.,* **2015,** *641,* 2565-2569.

[7] Abrahams, B. F., Haywood, M. G., Robson, R., *Cryst. Eng. Comm.,* **2005,** *7,* 629-632.

[8] Lam, C-K., and Mak, T. C. W., *Angew. Chem. Int. Ed.,* **2001,** *40,* 3453-3455.

[9] Lam, C-K., and Mak, T. C. W., *Chem. Commun.,* **2001,** 1568-1569.

[10] Chalmers, R. A. and Telling, G. M., *Mikrochim. Acta,* **1967,** *6,* 1126-1135.

[11] Iraci, G. and Back, M. H., *Can. J. Chem.,* **1988,** *66,* 1293-1294.

[12] Feigl, F., Gentil, V., Libergott, E., *Isr. J. Chem.,* **1969,** *7,* 123-125.

[13] Silverman, J. A., Dares, C. J., Kavallieratos, K., Chapter 2 of this document.

[14] Coleman, G. H.; *The Radiochemistry of Plutonium*; NAS-NS 3058; National Academy of Sciences—National Research Council: Springfield, VA, 164-165.

[15] Ganzerli, M. T. V., Maggi, L., Caramella, V. C., *Anal. Chem.,* **1999,** *71,* 162-166.

[16] Ganzerli, M. T. V., Maggi, L., Caramella, V. C., *J. Radioanal. Nucl. Chem.,* **1997,** *221,* 105-108.

[17] Ganzerli, M. T. V., Maggi, L., Caramella, V. C., Premoli, G., *J. Radioanal. Nucl. Chem.,* **1997,** *221,* 109-113.

[18] Saxena, O. C., *Microchem. J.,* **1968,** *13,* 222-226.

[19] Connors, K. A., In *Binding Constants: The Measurement of Molecular Complex Stability,* New York: Wiley-Interscience, **1987**.

[20] Araujo, P., *J. Chromatogr. B,* **2009,** *877,* 2224-2234.

[21] Renny, J. S., Tomasevich, L. L., Tallmadge, E. H., Collum, D. B., *Angew Chem. Int. Ed. Engl.,* **2013,** *52,* 11998-12013.

[22] Hibbert, D. B., Thordarson, P., *Chem. Commun.,* **2016,** *52,* 12792-12805.

[23] Ulatowski, F., Dabrowa, K., Bałakier, T., Jurczak, J., *J. Org. Chem.,* **2016,** *81,* 1746-1756.

CHAPTER IV. COMPLEXATION OF Pb(II), Cd(II), AND Hg(II) WITH RHODIZONATE AND N-DONATING CO-LIGANDS

Joshua A. Silverman, Shannon J. Saluga, Konstantinos Kavallieratos*

4.1 Abstract

Toxic metals such as Pb(II), Cd(II), and Hg(II) form both binary complexes with rhodizonate and ternary complexes with rhodizonate (**1**, **2**, and **3**, respectively) and N-donating co-ligands such as 1,10-phenanthroline (**1P**, **2P**, and **3P**), 2,2'-bipyridine (**1B**, **2B**, and **3B**), and imidazole (**1I**, **2I**, and **3I**). FT-IR data show that Cd(II)-rho and Hg(II)-rho have nearly identical structures when complexed with rhodizonate. Both Cd(II)-rho and Hg(II)-rho showed weak, yet broad, FT-IR bands at ~1380 cm^{-1}, corresponding to a symmetrical C=O stretch of intermediate bond order; and a stronger band at 1090 cm^{-1}, corresponding to a C-C stretch. UV-Vis titrations indicate that all three metals complex to rhodizonate in a 1:1 ratio, and that the ternary complexes with imidazole are formed in a 1:1:1 complexation ratio. Binding constants, K_{11}, between Cd(II)-rhodizonate and Hg(II)-rhodizonate are in the order of 10^4 M^{-1}, while imidazole binds to pre-formed binary complexes M(II)-rho with binding constants in the order of 10^5 M^{-1}.

4.2 Introduction

The rhodizonate anion, $C_6O_6^{2-}$, is the six-carbon member of a class of cyclical oxocarbons [1, 2] with the general formula $C_nO_n^{2-}$ (n = 3-6). Numerous reviews and books have documented the historical importance and chemical properties of these compounds [3, 4]. Within the oxocarbon family, spectroscopic and x-ray single crystal diffraction data are most prevalent for squarate (n = 4) and croconate (n = 5) [5]. Owing to its instability, there is very little in the way of spectroscopic or x-ray data for deltate (n = 3) and also for rhodizonate (n = 6). Most known X-ray structures for binary metal-rhodizonate complexes

involve alkali metal-rhodizonate complexes [6-8]. That is not to say that the properties of rhodizonate are a complete mystery. By the mid-20th century, it was known that rhodizonate coordinates with a variety of metals at different pHs to provide colored solids [9, 10]. Rhodizonate has been used in simple colorimetric tests to detect certain metals, most notably Pb [11-17]. Research into other uses for binary metal-rhodizonate complexes show that they may be feasible as a new class of semiconductors [18, 19].

Rhodizonate can also form lattices with other N-containing organic molecules, both in the presence of metals [20, 21] and without [22]. These purely organic compounds form hydrogen bonds between the rhodizonate oxygens and nitrogen-bound hydrogens on other organic molecules [20, 21]. If there is a metal present, the metal forms the center of the complex, bound to the rhodizonate and the nitrogen atoms on other organic molecules, forming a type of metal-organic framework (MOF) [22]. Metal-organic framework compounds have a variety of uses, including as electrocatalysts [23, 24], in actinide sequestration and separation [25], and for carbon capture technology [26].

In this paper, we report spectroscopic data for complexation of rhodizonate with three toxic metals: Pb(II), Cd(II), and Hg(II). We also form and characterize ternary complexes involving these metals, rhodizonate, and three different N-donor co-ligands: 1,10-phenanthroline (phen); 2,2'-bipyridine (bipy); and imidazole (imid). We emphasize the results with the imid-containing complexes as they showed different colors from the binary rho complexes and phen and bipy counterparts, which may find application in toxic metal sensing. Finally, we collected reliable UV-Vis spectroscopic data for formation of these complexes in solution using a water/ethanol (50/50 v/v) solvent system. Further research can provide applications in optical sensing and in sequestering these toxic metals.

4.3 Experimental Section

4.3.1 Materials and Methods

Pb(II)-Rhodizonate (isolated as $Pb_2(C_6O_6)(OH)_2 \bullet 4H_2O$) (**1**) was prepared as reported previously (See Chapter 2). 3,4,5,6-Tetraoxocyclohexene-1,2-diol disodium salt (rhodizonic acid, disodium salt) was purchased from Sigma-Aldrich. Anhydrous $Pb(NO_3)_2$, $Cd(NO_3)_2 \bullet 4H_2O$, and $Hg(OAc)_2$ were purchased from Fisher Scientific. All chemicals were reagent grade and were used without further purification. 1,10-phenanthroline, 2,2'-bipyridine, and imidazole were purchased from Fisher Scientific. The water used in all experiments was nano-pure water with a resistivity >17 MΩ cm^{-1} (Millipore by Barnstead Thermolyne Corporation, Dubuque, IA). Ethanol (200 proof) was purchased by Pharmco-Aaper. FT-IR measurements were collected on an Agilent Technologies Cary 670 FT-IR with a diamond ATR attachment. UV-Vis spectra were collected on a Varian Cary-100 UV-Vis spectrophotometer or on a Shimadzu UV-2101PC UV-Vis spectrophotometer.

4.3.2 Synthesis

4.3.2.1 Cd(II)-Rhodizonate, $Cd_3(C_6O_6)_2(OH)_2 \bullet 7H_2O$ (**2**)

Cadmium (II) rhodizonate was formed by mixing a solution $Na_2C_6O_6$ (64.2 mg, 0.3 mmol) in 100.0 mL of water with a solution of $Cd(NO_3)_2 \bullet 4H_2O$ (92.5 mg, 0.3 mmol) in 100.0 mL of water. A red precipitate forms immediately. This precipitate was vacuum filtered, washed with water, acetone, and dichloromethane (DCM), and dried under vacuum overnight (54.7 mg, 0.195 mmol, 65.1% yield). Elemental analysis calculated for $Cd_3(C_6O_6)_2(OH)_2 \bullet 7H_2O$: C = 17.30%, H = 1.94%, N = 0.00%. Found: C = 17.25%, H = 1.76%, N = 0.00%. FT-IR (cm^{-1}): 1396 (s, br), 1023 (vs, br), 795 (m), 670 (m).

4.3.2.2 Hg(II)-Rhodizonate, (**3**)

Mercury (II) rhodizonate was formed by mixing an aqueous solution of $Na_2C_6O_6$ with an aqueous solution of $Hg(OAc)_2$. Doing so causes a white precipitate to immediately form. This precipitate was vacuum filtered, washed with water, acetone, and dichloromethane (DCM), and dried under vacuum overnight. FT-IR (cm^{-1}): 1375 (m, br), 1033 (vs, br), 795 (m), 670 (m).

4.3.2.3 Pb(II)-Rhodizonate-Phenanthroline, **(1P)**

Lead (II) rhodizonate-phenanthroline was formed by mixing an aqueous solution of $Na_2C_6O_6$, $Pb(NO_3)_2$, and $C_{12}H_8N_2$. A purple-colored precipitate was immediately formed, which was vacuum filtered, washed with water, acetone, and DCM, and dried under vacuum overnight. FT-IR (cm^{-1}): 1625 (vw), 1615 (vw), 1590 (vw), 1502 (m), 1478 (m), 1459 (s), 1410 (s), 1386 (s), 1361 (s, br), 1343 (m), 1310 (m), 1310 (m), 1287 (m), 1251 (w), 1221 (w), 1185 (w), 1162 (w), 1127 (w), 1099 (m), 1063 (s), 1035 (w), 1024 (w), 996 (vw), 892 (vw), 884 (vw), 849 (s), 819 (w), 782 (s), 776 (s), 719 (s), 694 (m, br), 665 (w), 636 (vw).

4.3.2.4 Cd(II)-Rhodizonate-Phenanthroline, **(2P)**

Cadmium (II) rhodizonate-phenanthroline was formed by mixing an aqueous solution of $Na_2C_6O_6$, $Cd(NO_3)_2 \bullet 4H_2O$, and $C_{12}H_8N_2$. A peach-colored precipitate was immediately formed, which was vacuum filtered, washed with water, acetone, and DCM, and dried under vacuum overnight. FT-IR (cm^{-1}): 1622 (m, sh), 1592 (vw), 1563 (m), 1548 (m), 1472 (vs, br), 1405 (vs, br), 1345 (m), 1101 (m), 1052 (s, br), 865 (w), 845 (s, sh), 770 (m, sh), 724 (vs, sh), 673 (vw), 642 (m).

4.3.2.5 Hg(II)-Rhodizonate-Phenanthroline, **(3P)**

Mercury (II) rhodizonate-phenanthroline was formed by mixing an aqueous solution of $Na_2C_6O_6$, $Hg(OAc)_2$, and $C_{12}H_8N_2$. A gray-colored precipitate was immediately formed, which was vacuum filtered, washed with water, acetone, and DCM, and dried under vacuum overnight. FT-IR (cm^{-1}): 3057 (vw), 1619 (vw), 1575 (vw), 1517 (m, sh), 1491 (w), 1429 (s, sh), 1417 (w, sh), 1346 (m, sh), 1223 (w), 1099 (m), 1033 (s, br), 994 (m, sh), 861 (w, sh), 843 (vs, sh), 770 (m, sh), 722 (vs, sh), 672 (vw), 638 (m).

4.3.2.6 Pb(II)-Rhodizonate-Bipyridine, **(1B)**

Lead (II) rhodizonate-bipyridine was formed by mixing a solution of $Na_2C_6O_6$, $Pb(NO_3)_2$, and $C_{10}H_8N_2$. A purple-colored precipitate was immediately formed, which was vacuum filtered, washed with water, acetone, and DCM, and dried under vacuum overnight. FT-IR (cm^{-1}): 3386 (vw, br), 2988 (vw), 1589 (s), 1503 (m), 1489 (m), 1459 (m), 1415 (s), 1372 (vs), 1338 (vs), 1300 (s, sh), 1247 (w), 1173 (w), 1160 (w), 1127 (w), 1098 (m), 1063 (s, sh), 1036 (w), 1003 (s), 880 (m, br), 819 (w), 784 (m), 763 (vs, sh), 734 (s, sh), 719 (s, sh), 665 (w), 645 (s, sh), 626 (s), 611 (s), 560 (s).

4.3.2.7 Cd(II)-Rhodizonate-Bipyridine, **(2B)**

Cadmium (II) rhodizonate-bipyridine was formed by mixing a solution of $Na_2C_6O_6$, $Cd(NO_3)_2 \bullet 4H_2O$, and $C_{10}H_8N_2$. A peach-colored precipitate was immediately formed, which was vacuum filtered, washed with water, acetone, and DCM, and dried under vacuum overnight.

4.3.2.8 Hg(II)-Rhodizonate-Bipyridine, **(3B)**

Mercury (II) rhodizonate-bipyridine was formed by mixing a solution of $Na_2C_6O_6$, $Hg(C_2H_3O_2)_2$, and $C_{10}H_8N_2$. A gray-colored precipitate was immediately formed, which

was vacuum filtered, washed with water, acetone, and DCM, and dried under vacuum overnight.

4.3.2.9 Pb(II)-Rhodizonate-Imidazole, **(1I)**

Lead (II) rhodizonate-imidazole was formed by mixing an aqueous solution of $Na_2C_6O_6$, $Pb(NO_3)_2$, and $C_3H_4N_2$. A blue-colored precipitate was immediately formed, which was vacuum filtered, washed with water, acetone, and DCM, and dried under vacuum overnight. FT-IR (cm^{-1}): 3130 (vw), 2973 (vw), 1591 (s), 1463 (s), 1349 (vs, br), 1305 (vs, br), 1082 (m), 1066 (m), 1044 (w), 939 (vw), 896 (vw), 835 (s), 771 (s), 727 (vw), 624 (w).

4.3.2.10 Cd(II)-Rhodizonate-Imidazole, **(2I)**

Cadmium (II) rhodizonate-imidazole was formed by mixing an aqueous solution of $Na_2C_6O_6$, $Cd(NO_3)_2 \bullet 4H_2O$, and $C_3H_4N_2$. A red-colored precipitate was immediately formed, which was vacuum filtered, washed with water, acetone, and DCM, and dried under vacuum overnight. FT-IR (cm^{-1}): 3267 (w, br), 1596 (m, br), 1496 (s, br), 1373 (vs, br), 1084 (s), 1010 (w, br), 949 (m), 787 (m), 610 (m).

4.3.2.11 Hg(II)-Rhodizonate-Imidazole, **(3I)**

Mercury (II) rhodizonate-imidazole was formed by mixing an aqueous solution of $Na_2C_6O_6$, $Hg(OAc)_2$, and $C_3H_4N_2$. An orange-colored precipitate was immediately formed, which was vacuum filtered, washed with water, acetone, and DCM, and dried under vacuum overnight. FT-IR (cm^{-1}): 3141 (w), 1651 (vw), 1599 (w), 1474 (vs, br), 1326 (m), 1092 (vs, br), 1048 (m), 901 (m, br), 834 (m), 765 (m), 670 (vw), 641 (s, sh), 628 (w).

4.3.3 UV-Visible Titrations

In a typical UV-Visible titration experiment, solutions of sodium rhodizonate ($Na_2C_6O_6$, 2.0 x 10^{-5} M) in water/ethanol (50/50 v/v) (solution A) were titrated with water/ethanol (50/50 v/v) solutions of either $Pb(NO_3)_2$, $Cd(NO_3)_2 \bullet 4H_2O$, or $Hg(OAc)_2$ (2.0 x 10^{-3} M) at constant sodium rhodizonate concentration (2.0 x 10^{-5} M) (Solution B). For spectra collection, 3.00 mL of the $Na_2C_6O_6$ solution (solution A) were added to a cuvette and 5.00 - 25.0 μL sequential additions of solution B were added at 5 min intervals until a total of 200.0 μL had been added. All spectra were collected with a Shimadzu UV-2101PC UV-Visible spectrophotometer. Titrations at longer time intervals established that the complex formation reaction in solution reaches equilibrium in less than 5 min.

The above procedure was repeated for the ternary complexes **1P, 1B, 1I, 2P, 2B, 2I, 3P, 3B, and 3I**. Solution A contained either **1, 2, or 3** (2.0 x 10^{-5} M) in water/ethanol (50/50 v/v). Solution B contained either **1, 2 or 3** (2.0 x 10^{-5} M) and 2.0 x 10^{-3} M of either phen, bipy, or imid in water/ethanol (50/50 v/v). In order to verify the stoichiometric ratios from these titrations, the last ternary series of titration experiments were performed by adding either Pb(II), Cd(II), or Hg(II) to solutions of rho/(phen, bipy, or imid). Specifically, these titrations were repeated with Solution A containing only 3.0 x 10^{-5} M $Na_2C_6O_6$ and 3.0 x 10^{-5} M of either phen, bipy, or imid (instead of **1, 2, or 3**). Solution B contained 3.0 x 10^{-5} M $Na_2C_6O_6$, 3.0 x 10^{-5} M of either phen, bipy, or imid, and 3.0 x 10^{-3} M of either $Pb(NO_3)_2$, $Cd(NO_3)_2 \bullet 4H_2O$, or $Hg(OAc)_2$.

4.4 Results

4.4.1 Synthesis

Compounds **1** and **2** were readily precipitated as polymeric powders with formulas $Pb_2(C_6O_6)(OH)_2 \bullet 4H_2O$ and $Cd_3(C_6O_6)_2(OH)_2 \bullet 7H_2O$, respectively by mixing either $Pb(NO_3)_2$ or $Cd(NO_3)_2 \bullet 4H_2O$, with $Na_2C_6O_6$ in an aqueous solution. The reactions with the Pb(II) or Cd(II) salts were instantaneous, while the reaction with Hg(II) took about 2 minutes to complete. Unlike aqueous $Na_2C_6O_6$, which will decompose into croconate after a few days, all three M(II)-rhodizonate powders were stable even after several weeks. These polymers resist attempts to dissolve them – the only common solvent that dissolved these complexes was DMSO, which decomposed the complexes.

4.4.2 FT-IR Spectroscopy

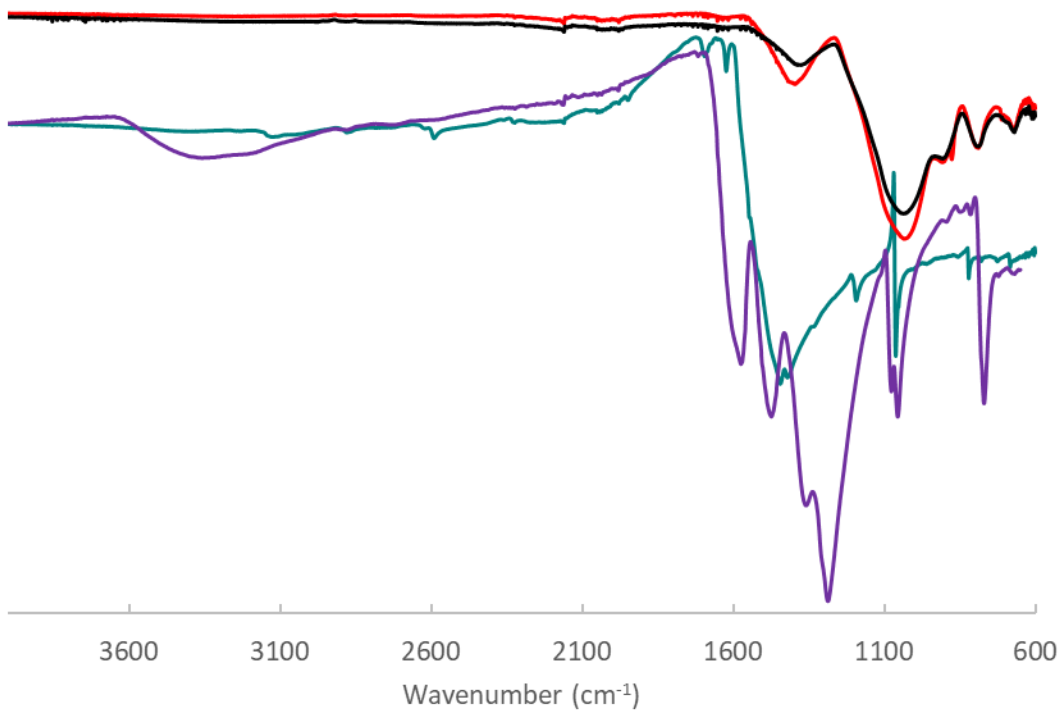

Figure 4.1: The FT-IR spectra of $Na_2C_6O_6$ (green), **1** (purple), **2** (red), and **3** (black).

The FT-IR spectra of binary compounds **1, 2,** and **3** (Figure 4.1) give important structural clues of the rhodizonate ring conformation. In its planar form, the rhodizonate ring exhibits D_{6h} symmetry; however, $Na_2C_6O_6$ features a twisted rhodizonate ring, placing it in the C_{2v} point group [8, 20, 27, 28]. The large number of absorption bands in the C-C stretching region for **1** is consistent with a twisted ring conformation. Compounds **2** and **3**, in addition to being almost identical, have very few FT-IR absorption bands, indicative of highly symmetrical structures. These stand in stark contrast to their corresponding ternary complexes shown below, reported in the literature for those metals [20], or reported in the literature for other transition metals [29].

The FT-IR spectra of ternary complexes **1P, 2P,** and **3P; 1B;** and **1I, 2I,** and **3I** are shown in Figures 4.2, 4.3, and 4.4 respectively.

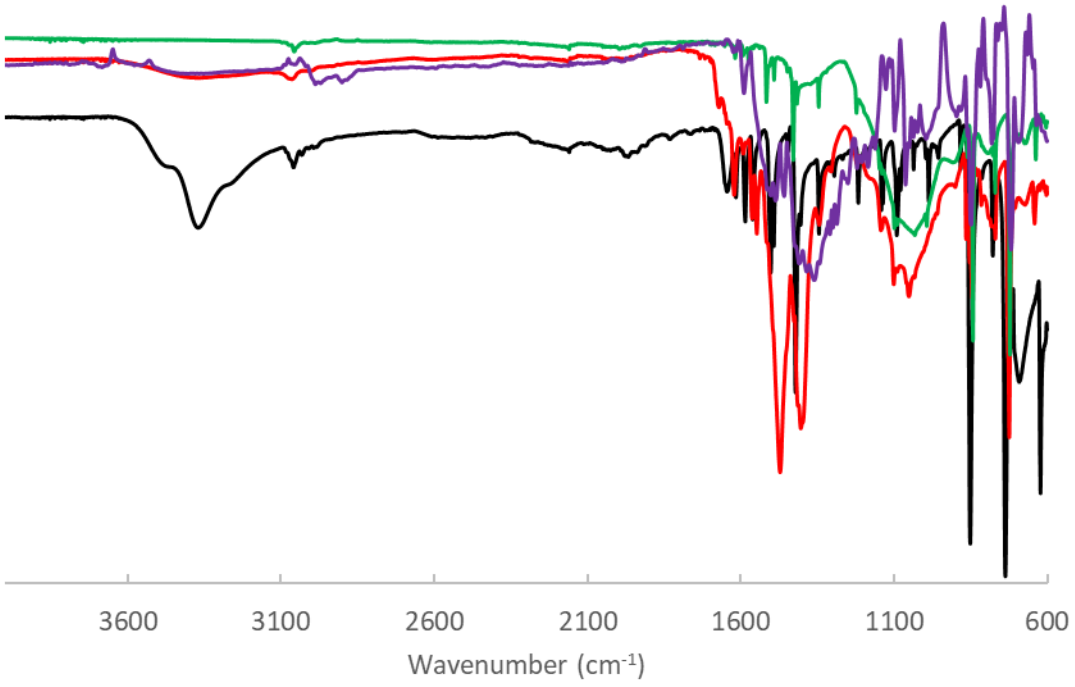

Figure 4.2: The FT-IR spectra of 1,10-phenanthroline (black), **1P** (purple), **2P** (red), and **3P** (green).

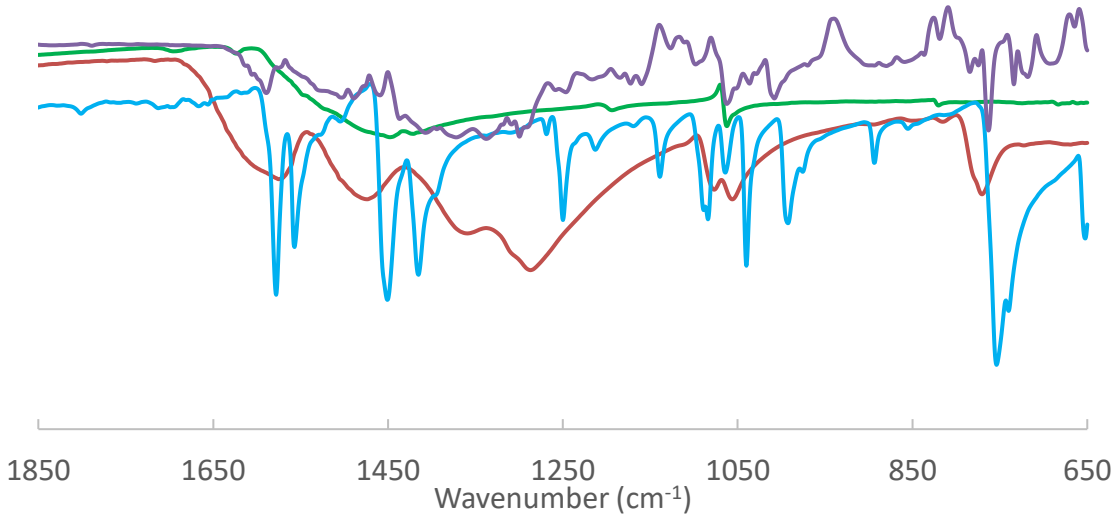

Figure 4.3: The FT-IR spectra of $Na_2C_6O_6$ (green), 2,2'-bipyridine (blue), **1** (red), and **1B** (purple).

Unlike the binary complexes **2** and **3**, ternary complexes **2P** and **3P** have markedly different FT-IR absorbance patterns. All three phen-containing complexes show strong carbon-oxygen stretches, though none above 1600 cm^{-1}. This indicates that these carbon-oxygen bonds have a bond order less than 2. Since complexes **2** and **3** had just one of these bands, and a weak one at that, the additional and more intense carbon-oxygen absorption bands are indicative of a less symmetrical structure. This would be consistent with the literature that shows ternary transitional metal rhodizonates have twisted conformations [20, 29]. All three complexes, **1P, 2P,** and **3P**, unsurprisingly have a number of absorption bands from the 1,10-phenanthroline, yet many of these bands vary in both wavenumber and intensity. As the complete assignment of these bands is known, noting which bands are absent can present further clues as to the coordination of complex constituent parts in lieu of a crystal structure [30]. Notably, the bands that are absent in **2P** and **3P** are assigned to C-N stretches and C-H bends. The Pb(II)-containing complex, **1P**, has almost all of these bands, though at slightly different wavenumbers.

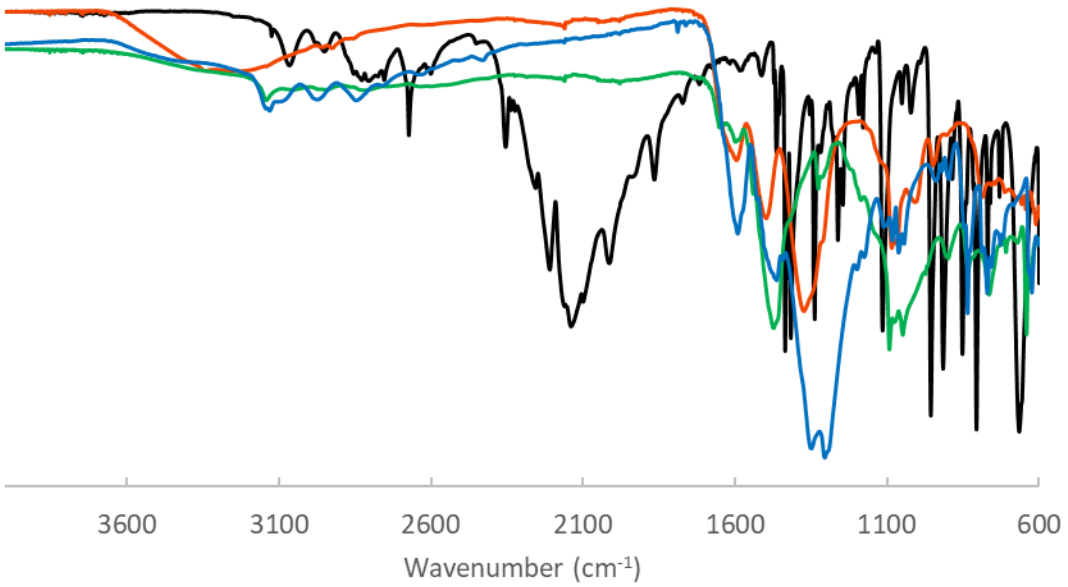

Figure 4.4: The FT-IR spectra of imidazole (black), **1I** (blue), **2I** (red), and **3I** (green).

All three imidazole-containing compounds', **1I, 2I,** and **3I**, FT-IR spectra show an even greater deviation from imidazole than **1P, 2P,** and **3P** did from 1,10-phenanthroline. Like the phen complexes, **1I, 2I,** and **3I** have strong, broad absorbances indicative of carbon-oxygen stretching; also, like the phen complexes, none of these bands are above 1600 cm^{-1}, suggesting a lower bond order. Since the FT-IR absorption band assignments for imidazole are known, the absence of certain bands can give clues as to the orientation and coordination for the complex [31]. For all three complexes, their FT-IR spectra lack the N-H stretches, suggestive of coordination between metal and imidazole at its deprotonated nitrogen. None of the three complexes featured any of the cluster of absorption bands centered at 2100 cm^{-1}, but these are assigned as overtone and combination bands, so their absence is unsurprising [31].

4.4.3 UV-Visible Titrations

Upon addition of Pb(II) nitrate in water/ethanol (50/50 v/v) the band at 482 nm decreases in intensity, while there is a red shift to higher wavelength (See Figs. 2.4-2.7 and Chapter 2 for details). Applying the decrease in absorption to the 1:1 binding isotherm [32], gives an excellent fit to the 1:1 binding model, indicating that, in solution, Pb(II) rhodizonates exist as 1:1 complexes. Non-linear regression analysis of the binding curve gives a binding constant of K_{11} = 1.2 (± 0.2) x 10^6 M^{-1} for Pb(II)-rhodizonate, leading to a free energy of complexation of ΔG = -34.7 (± 0.4) kJ/mol (Chapter 2). Applying the standard deviation to slope ratio to the isotherm data gives a limit of detection of 1.43 x 10^{-6} M and a limit of quantification of 4.34 x 10^{-6} M [33].

Upon addition of Cd(II) nitrate tetrahydrate in water/ethanol (50/50 v/v) the band at 482 nm decreases in intensity (Figure 4.5), with no chromic shift. Applying the decrease in absorption to the 1:1 binding isotherm [32], gives an excellent fit to the 1:1 binding model, indicating that, in solution, Cd(II) rhodizonate exist in solution as a 1:1 complex. Non-linear regression analysis of the binding curve gives a binding constant of K_{11} = 4.11 x 10^4 M^{-1} for Cd(II)-rhodizonate, corresponding to a free energy of complexation of ΔG = -26.3 kJ/mol.

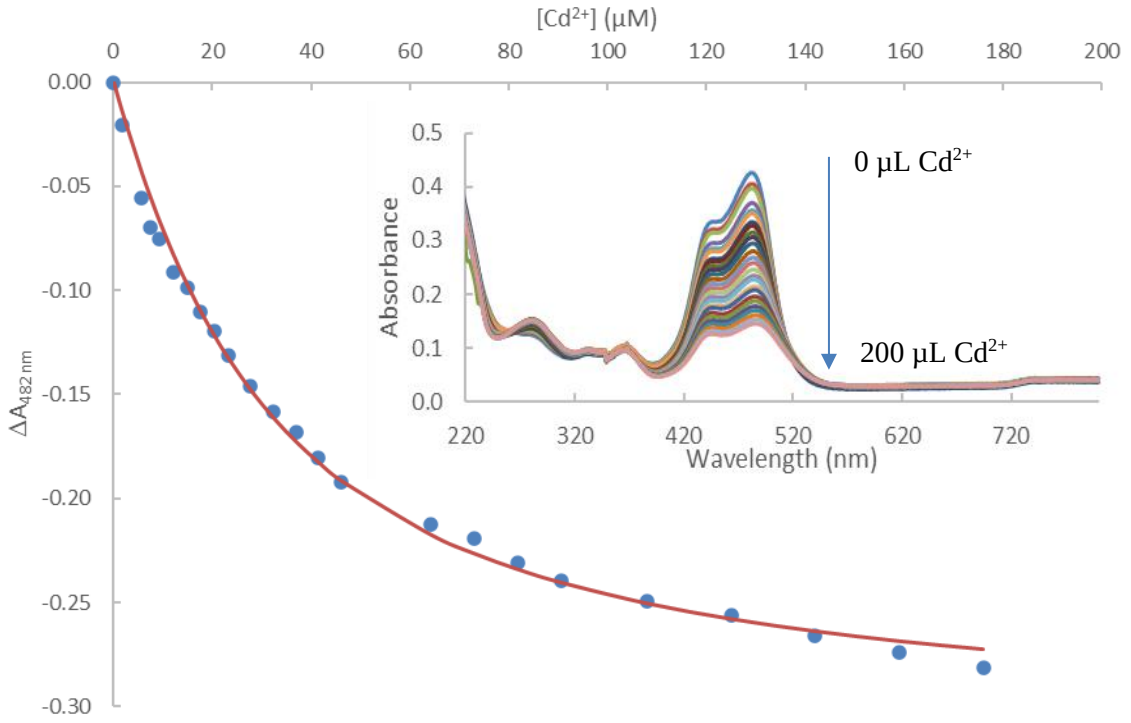

Figure 4.5: Binding curve for the titration of a solution of 1.51 x 10^{-5} M of $Na_2C_6O_6$ with a solution of 2.81 x 10^{-3} M of $Cd(NO_3)_2 \cdot 4H_2O$ in 1.51 x 10^{-5} M of $Na_2C_6O_6$ in water/ethanol (50/50 v/v). K_{11} = 4.11 x 10^4 M^{-1}. **Cutaway:** UV-Visible absorption spectrum for the titration of a solution of 1.51 x 10^{-5} M of $Na_2C_6O_6$ with solution of 2.81 x 10^{-3} M of $Cd(NO_3)_2 \cdot 4H_2O$ in 1.51 x 10^{-5} M of $Na_2C_6O_6$ in water/ethanol (50/50 v/v).

Upon addition of Hg(II) acetate in water/ethanol (50/50 v/v) the band at 482 nm decreases in intensity (Figures 4.6 through 4.8), with no chromic shift. Applying the decrease in absorption to the 1:1 binding isotherm [32], gives an excellent fit to the 1:1 binding model, indicating that, in solution, Hg(II) rhodizonate exist in solution as a 1:1 complex. Non-linear regression analysis of the binding curve gives a binding constant of K_{11} = 4.0 (± 0.2) x 10^4 M^{-1} for Hg(II)-rhodizonate formation, corresponding to a free energy of complexation of ΔG = -26.2 (± 0.1) kJ/mol.

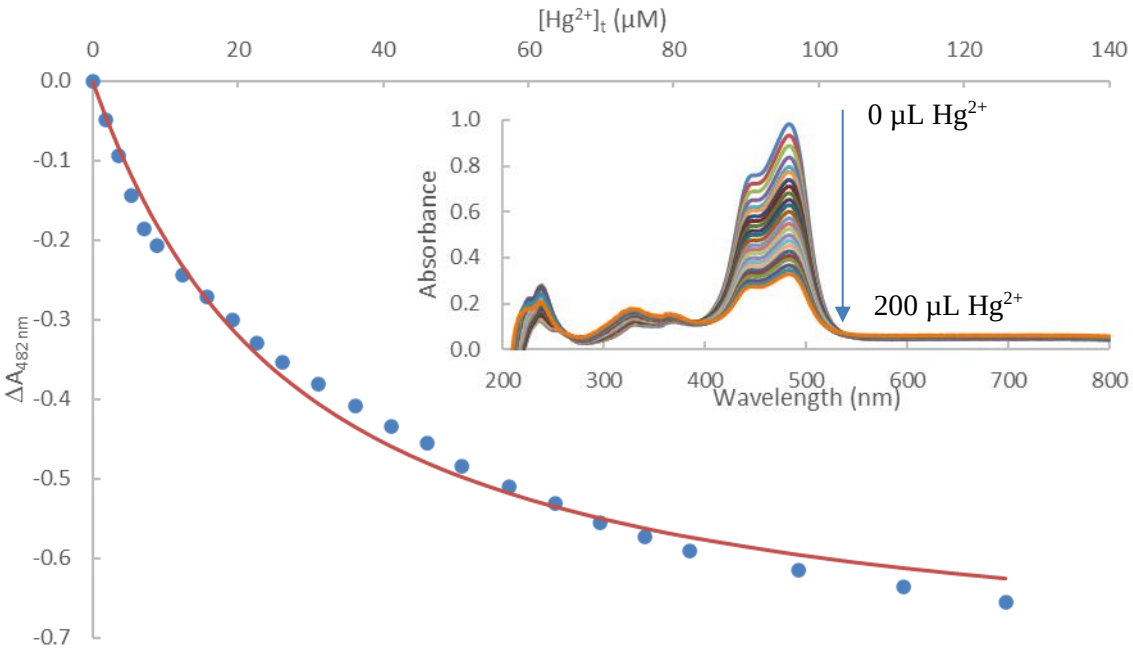

Figure 4.6: Binding curve for the titration of a solution of 5.18 x 10^{-6} M of $Na_2C_6O_6$ with a solution of 1.07 x 10^{-3} M of $Hg(OAc)_2$ in 5.18 x 10^{-6} M of $Na_2C_6O_6$ in water/ethanol (50/50 v/v). K_{11} = 4.19 x 10^4 M^{-1}. **Cutaway:** UV-Visible absorption spectrum for the titration of a solution of 5.18 x 10^{-6} M of $Na_2C_6O_6$ with solution of 1.07 x 10^{-3} M of $Hg(OAc)_2$ in 5.18 x 10^{-6} M of $Na_2C_6O_6$ in water/ethanol (50/50 v/v).

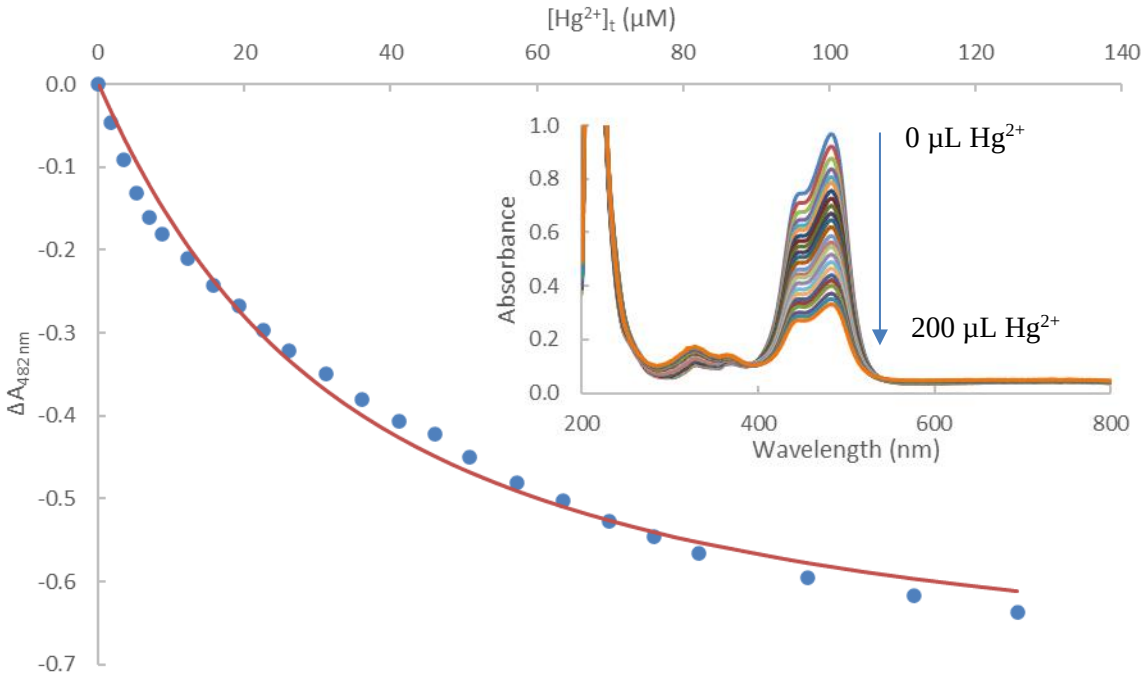

Figure 4.7: Binding curve for the titration of a solution of 1.14 x 10^{-5} M of $Na_2C_6O_6$ with a solution of 1.07 x 10^{-3} M of $Hg(OAc)_2$ in 1.14 x 10^{-5} M of $Na_2C_6O_6$ in water/ethanol (50/50 v/v). K_{11} = 3.80 x 10^4 M^{-1}. **Cutaway:** UV-Visible absorption spectrum for the titration of a solution of 3.31 x 10^{-5} M of $Na_2C_6O_6$ with solution of 1.07 x 10^{-3} M of $Hg(OAc)_2$ in 1.14 x 10^{-5} M of $Na_2C_6O_6$ in water/ethanol (50/50 v/v).

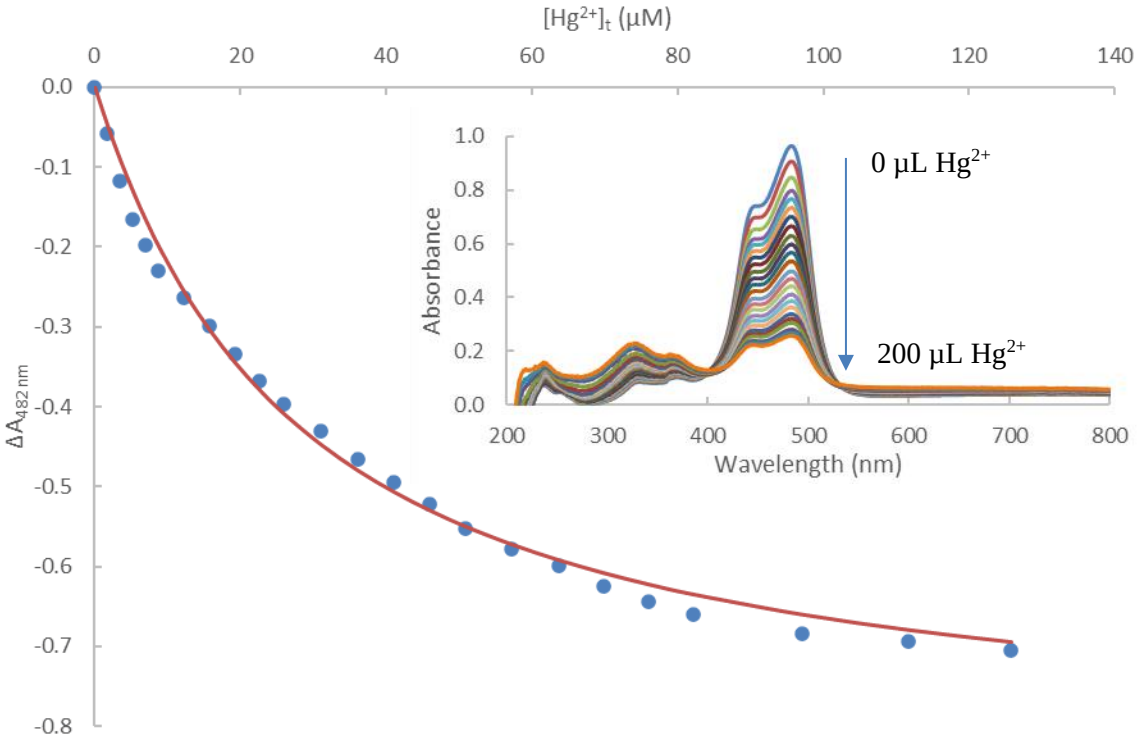

Figure 4.8: Binding curve for the titration of a solution of 3.31 x 10^{-5} M of $Na_2C_6O_6$ with a solution of 1.07 x 10^{-3} M of $Hg(OAc)_2$ in 3.31 x 10^{-5} M of $Na_2C_6O_6$ in water/ethanol (50/50 v/v). K_{11} = 3.91 x 10^4 M^{-1}. **Cutaway:** UV-Visible absorption spectrum for the titration of a solution of 3.31 x 10^{-5} M of $Na_2C_6O_6$ with solution of 1.07 x 10^{-3} M of $Hg(OAc)_2$ in 3.31 x 10^{-5} M of $Na_2C_6O_6$ in water/ethanol (50/50 v/v).

Upon addition of Cd(II) to a solution of rhodizonate and 1,10-phenanthroline in water/ethanol (50/50 v/v), the band at 482 nm decreases in intensity (Figure 4.9), with no chromic shift. Applying the decrease in absorption to the 1:1 binding isotherm [32], does not give a good fit to the 1:1 binding model, though whether this is because the ternary complex is not formed under these conditions, or because of some other experimental error is not known.

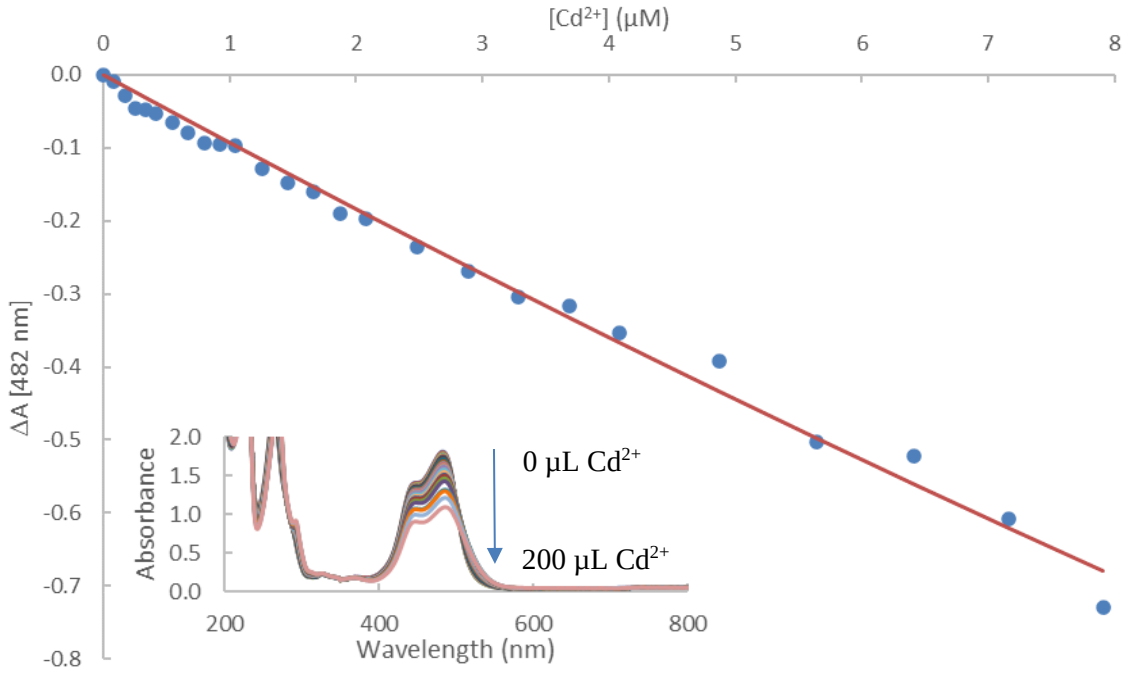

Figure 4.9: Binding curve for the titration of a solution of 2.25 x 10^{-5} M of $Na_2C_6O_6$ and 1.38 x 10^{-4} M 1,10-phenanthroline with a solution of 1.27 x 10^{-4} M of $CdCl_2$ in 2.25 x 10^{-5} M of $Na_2C_6O_6$ and 1.38 x 10^{-4} M 1,10-phenanthroline in water/ethanol (50/50 v/v). No binding constant could be found. **Cutaway:** UV-Visible absorption spectrum for the titration of a solution of 2.25 x 10^{-5} M of $Na_2C_6O_6$ and 1.38 x 10^{-4} M 1,10-phenanthroline with solution of 1.27 x 10^{-3} M of $CdCl_2$ in 2.25 x 10^{-5} M of $Na_2C_6O_6$ and 1.38 x 10^{-4} M 1,10-phenanthroline in water/ethanol (50/50 v/v).

To clarify the results of the previous experiment, the titration was performed in reverse by adding 1,10-phenanthroline to a solution of Cd(II)-rhodizonate in water/ethanol (50/50 v/v). Like the previous experiment, the band at 484 nm decreases in intensity (Figure 4.10), with no chromic shift. Applying the decrease in absorption to the 1:1 binding isotherm [32], gives a reasonably good fit to the 1:1 binding model, which is indicative that, in solution, Cd(II)-rho-phen exists as an 1:1:1 complex. Non-linear regression analysis of the binding curve gives a binding constant of K_{11} = 2.93 x 10^5 M^{-1} for formation of Cd(II)-rho-phen, from Cd(II)-rho and phen leading to a free energy of complexation of ΔG = -31.2 kJ/mol.

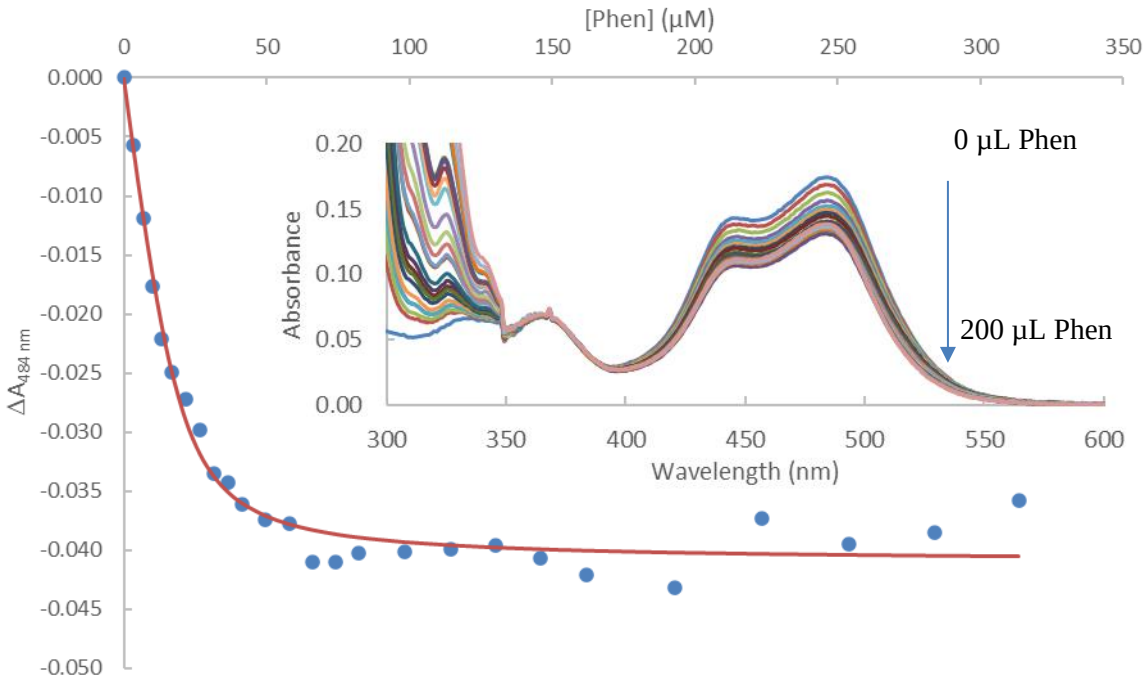

Figure 4.10: Binding curve for the titration of a solution of 1.26 x 10^{-4} M of $Na_2C_6O_6$ and 1.55 x 10^{-4} M $CdCl_2$ with a solution of 1.25 x 10^{-4} M of 1,10-phenanthroline in 1.26 x 10^{-4} M of $Na_2C_6O_6$ and 1.55 x 10^{-4} M $CdCl_2$ in water/ethanol (50/50 v/v). K_{11} = 2.93 x 10^5 M^{-1}. **Cutaway:** UV-Visible absorption spectrum for the titration of a solution of 1.26 x 10^{-4} M of $Na_2C_6O_6$ and 1.55 x 10^{-4} M $CdCl_2$ with a solution of 1.25 x 10^{-4} M of 1,10-phenanthroline in 1.26 x 10^{-4} M of $Na_2C_6O_6$ and 1.55 x 10^{-4} M $CdCl_2$ in water/ethanol (50/50 v/v).

Upon addition of Hg(II) to a solution of rhodizonate and 1,10-phenanthroline in water/ethanol (50/50 v/v), the band at 482 nm decreases in intensity (Figure 4.11), with no chromic shift. Applying the decrease in absorption to the 1:1 binding isotherm [32], gives an excellent fit to the 1:1 binding model, confirming that, in solution, Hg(II)-rho-phen exists as an 1:1:1 complex. Non-linear regression analysis of the binding curve gives a binding constant of K_{11} = 1.28 x 10^6 M^{-1} for formation of Hg(II)-rho-phen from Hg(II) and rho+phen leading to a free energy of complexation of ΔG = -34.8 kJ/mol.

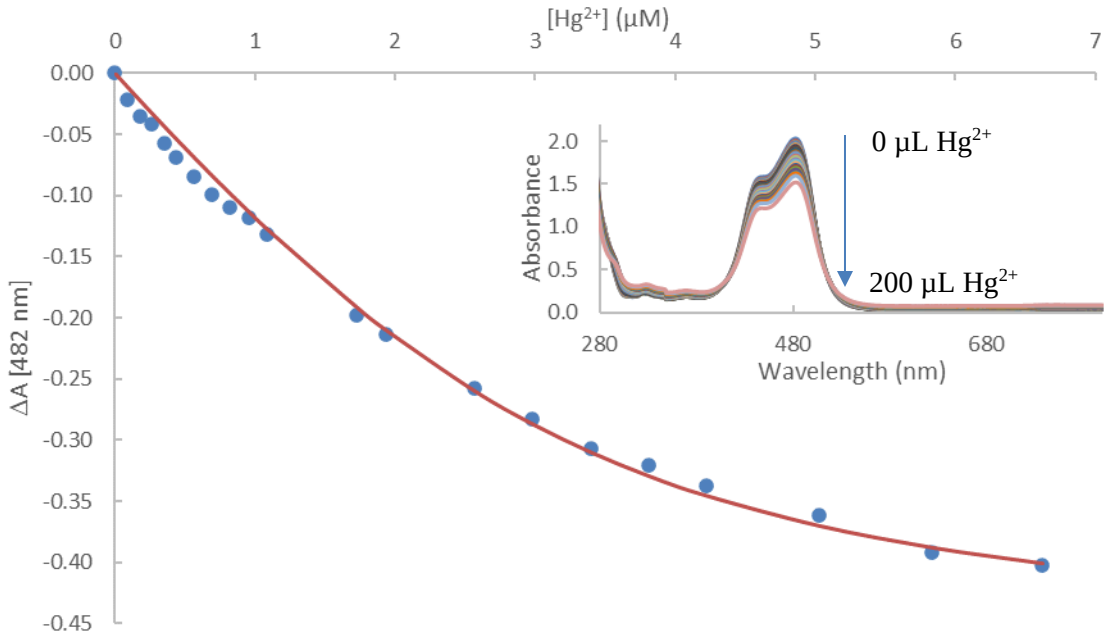

Figure 4.11: Binding curve for the titration of a solution of 1.30 x 10^{-4} M of $Na_2C_6O_6$ and 1.38 x 10^{-4} M 1,10-phenanthroline with a solution of 1.29 x 10^{-4} M of $HgCl_2$ in 1.30 x 10^{-4} M of $Na_2C_6O_6$ and 1.38 x 10^{-4} M 1,10-phenanthroline in water/ethanol (50/50 v/v). K_{11} = 1.28 x 10^6 M^{-1}. **Cutaway:** UV-Visible absorption spectrum for the titration of a solution of 1.30 x 10^{-4} M of $Na_2C_6O_6$ and 1.38 x 10^{-4} M 1,10-phenanthroline with solution of 1.29 x 10^{-3} M of $HgCl_2$ in 1.30 x 10^{-4} M of $Na_2C_6O_6$ and 1.38 x 10^{-4} M 1,10-phenanthroline in water/ethanol (50/50 v/v).

To clarify the results of the previous experiment, the titration was performed in reverse by adding 1,10-phenanthroline to a solution of Hg(II)-rhodizonate in water/ethanol (50/50 v/v) (Figure 4.12). Unfortunately, adding 1,10-phenanthroline to a pre-existing Hg(II)-rhodizonate solution has no appreciable effect on the absorbance of the complex. The 1:1 binding isotherm [32] could not a match the data and no binding constant could be obtained. This indicates that the formation of ternary Hg(II)-rho-phen from Hg(II)-rho and phen is not a straightforward process.

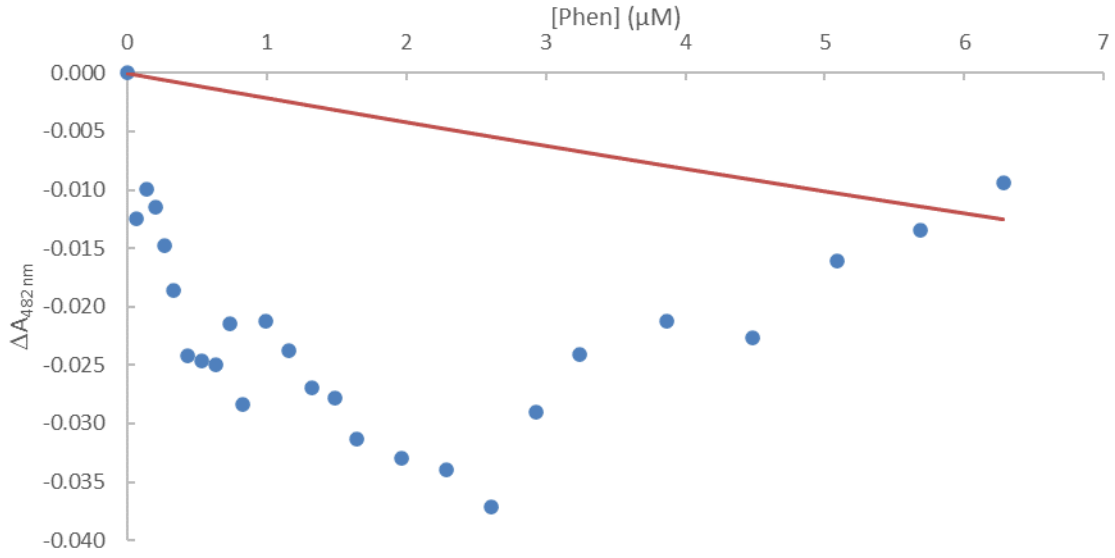

Figure 4.12: Binding curve for the titration of a solution of 1.35 x 10^{-4} M of $Na_2C_6O_6$ and 1.27 x 10^{-4} M $HgCl_2$ with a solution of 1.00 x 10^{-4} M of 1,10-phenanthroline in 1.35 x 10^{-4} M of $Na_2C_6O_6$ and 1.00 x 10^{-4} M $HgCl_2$ in water/ethanol (50/50 v/v). No binding constant could be determined.

Upon addition of Cd(II) to a solution of rhodizonate and 2,2'-bipyridine in water/ethanol (50/50 v/v), the band at 482 nm decreases in intensity (Figure 4.13), with no chromic shift. Applying the decrease in absorption to the 1:1 binding isotherm [32], gives an excellent fit to the 1:1 binding model, confirming that, in solution, Cd(II)-rho-bipy exists as an 1:1:1 complex. Non-linear regression analysis of the binding curve gives a binding constant of K_{11} = 4.41 x 10^4 M^{-1} for formation of Cd(II)-rho-bipy, from rho+bipy leading to a free energy of complexation of ΔG = -26.5 kJ/mol.

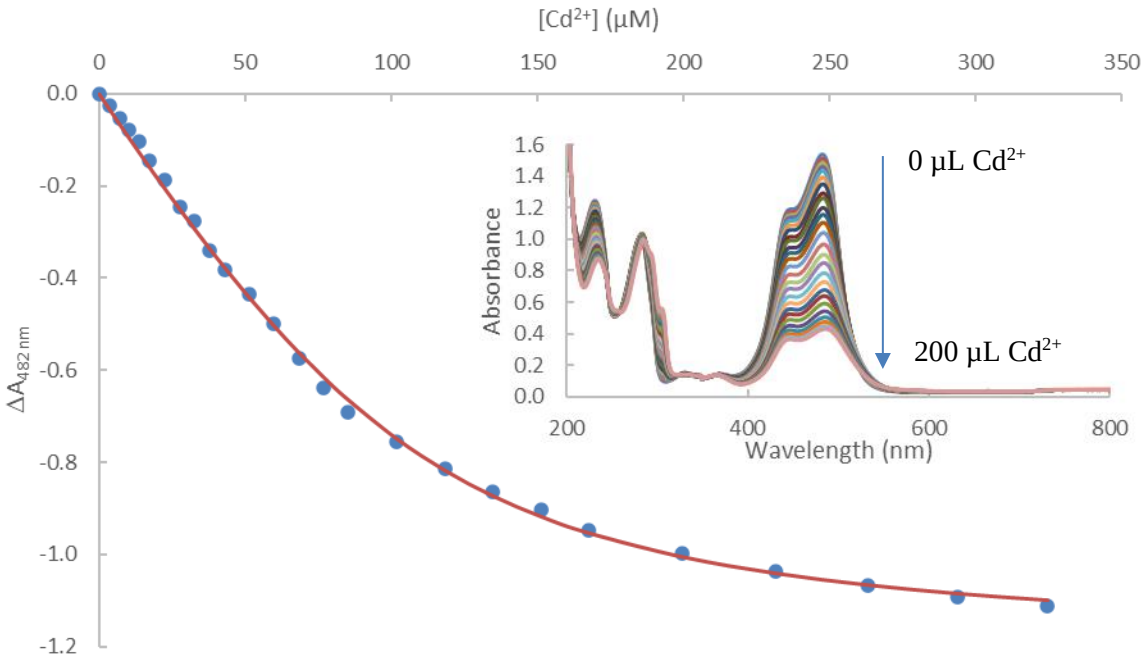

Figure 4.13: Binding curve for the titration of a solution of 1.30 x 10^{-4} M of $Na_2C_6O_6$ and 1.38 x 10^{-4} M 2,2'-bipyridine with a solution of 1.30 x 10^{-4} M of $CdCl_2$ in 1.30 x 10^{-4} M of $Na_2C_6O_6$ and 1.38 x 10^{-4} M 2,2'-bipyridine in water/ethanol (50/50 v/v). K_{11} = 4.41 x 10^4 M^{-1}. **Cutaway:** UV-Visible absorption spectrum for the titration of a solution of 1.30 x 10^{-4} M of $Na_2C_6O_6$ and 1.38 x 10^{-4} M 2,2'-bipyridine with solution of 1.30 x 10^{-3} M of $CdCl_2$ in 1.30 x 10^{-4} M of $Na_2C_6O_6$ and 1.38 x 10^{-4} M 2,2'-bipyridine in water/ethanol (50/50 v/v).

To clarify the results of the previous experiment, the titration was performed in reverse by adding 2,2'-bipyridine to a solution of Cd(II)-rhodizonate in water/ethanol (50/50 v/v). Like the previous experiment, the band at 484 nm decreases in intensity (Figure 4.14), with no chromic shift. Applying the decrease in absorption to the 1:1 binding isotherm [32], gives an excellent fit to the 1:1 binding model, confirming that, in solution, Cd(II)-rho-bipy exists as an 1:1:1 complex. Non-linear regression analysis of the binding curve gives a binding constant of K_{11} = 5.84 x 10^4 M^{-1} for formation of Cd(II)-rho-bipy, from Cd(II)-rho leading to a free energy of complexation of ΔG = -27.2 kJ/mol.

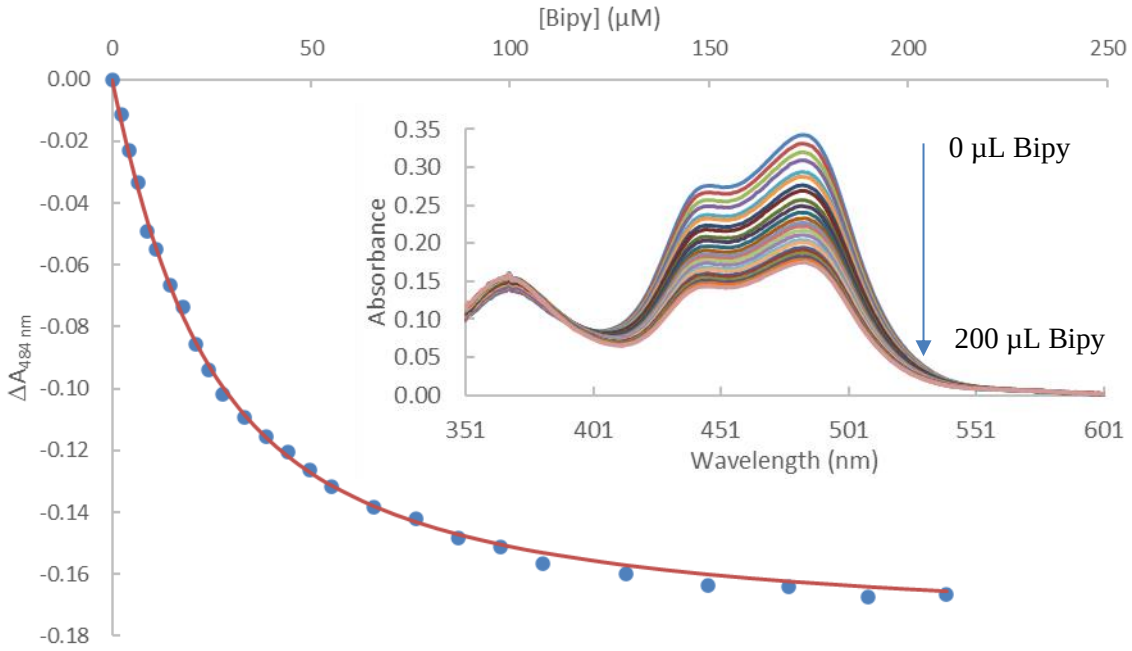

Figure 4.14: Binding curve for the titration of a solution of 1.27 x 10^{-4} M of $Na_2C_6O_6$ and 1.55 x 10^{-4} M $CdCl_2$ with a solution of 8.59 x 10^{-5} M of 2,2'-bipyridine in 1.27 x 10^{-4} M of $Na_2C_6O_6$ and 1.55 x 10^{-4} M $CdCl_2$ in water/ethanol (50/50 v/v). K_{11} = 2.93 x 10^5 M^{-1}. **Cutaway:** UV-Visible absorption spectrum for the titration of a solution of 1.27 x 10^{-4} M of $Na_2C_6O_6$ and 1.55 x 10^{-4} M $CdCl_2$ with a solution of 8.59 x 10^{-5} M of 2,2'-bipyridine in 1.27 x 10^{-4} M of $Na_2C_6O_6$ and 1.55 x 10^{-4} M $CdCl_2$ in water/ethanol (50/50 v/v).

Upon addition of Hg(II) to a solution of rhodizonate and 2,2'-bipyridine in water/ethanol (50/50 v/v), the band at 482 nm decreases in intensity (Figure 4.15), with no chromic shift. Applying the decrease in absorption to the 1:1 binding isotherm [32], gives an excellent fit to the 1:1 binding model, confirming that, in solution, Hg(II)-rho-bipy exists as an 1:1:1 complex. Non-linear regression analysis of the binding curve gives a binding constant of K_{11} = 3.00 x 10^5 M^{-1} for formation of Hg(II)-rho-bipy, from Hg(II) and rho+bipy leading to a free energy of complexation of ΔG = -31.2 kJ/mol.

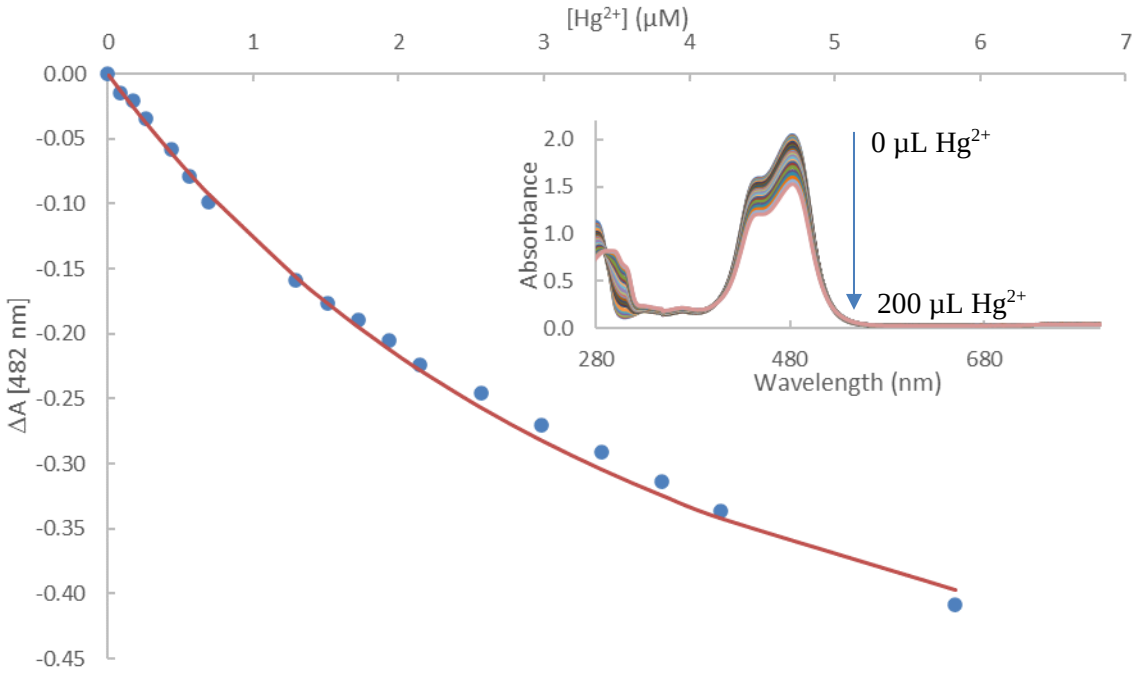

Figure 4.15: Binding curve for the titration of a solution of 1.35 x 10^{-4} M of $Na_2C_6O_6$ and 1.31 x 10^{-4} M 2,2'-bipyridine with a solution of 1.30 x 10^{-4} M of $HgCl_2$ in 1.35 x 10^{-4} M of $Na_2C_6O_6$ and 1.31 x 10^{-4} M 2,2'-bipyridine in water/ethanol (50/50 v/v). K_{11} = 4.41 x 10^4 M^{-1}. **Cutaway:** UV-Visible absorption spectrum for the titration of a solution of 1.35 x 10^{-4} M of $Na_2C_6O_6$ and 1.31 x 10^{-4} M 2,2'-bipyridine with solution of 1.30 x 10^{-3} M of $HgCl_2$ in 1.35 x 10^{-4} M of $Na_2C_6O_6$ and 1.31 x 10^{-4} M 2,2'-bipyridine in water/ethanol (50/50 v/v).

To clarify the results of the previous experiment, the titration was performed in reverse by adding 2,2'-bipyridine to a solution of Hg(II)-rhodizonate in water/ethanol (50/50 v/v). Like in the previous experiment, the band at 482 nm decreases in intensity (Figure 4.16), with no chromic shift. Applying the decrease in absorption to the 1:1 binding isotherm [32], gives an excellent fit to the 1:1 binding model, confirming that, in solution, Hg(II)-rho-bipy exists as an 1:1:1 complex. Non-linear regression analysis of the binding curve gives a binding constant of K_{11} = 2.33 x 10^5 M^{-1} for formation of Hg(II)-rho-bipy, from Hg(II)-rho and bipy leading to a free energy of complexation of ΔG = -30.6 kJ/mol.

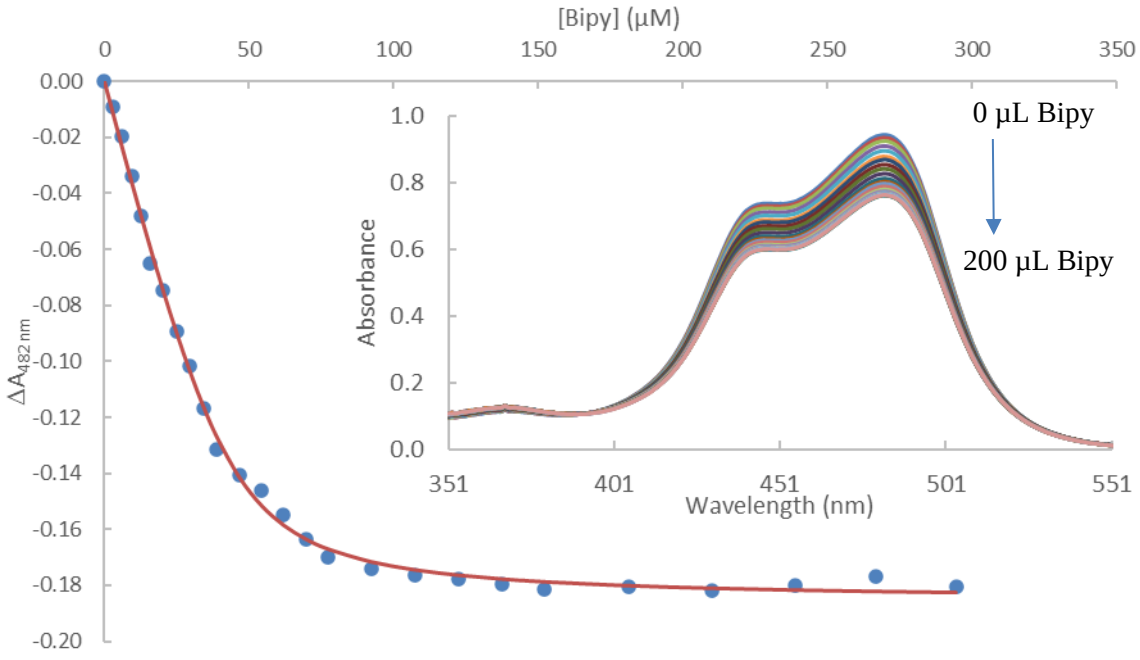

Figure 4.16: Binding curve for the titration of a solution of 1.28 x 10^{-4} M of $Na_2C_6O_6$ and 1.36 x 10^{-4} M $HgCl_2$ with a solution of 1.18 x 10^{-4} M of 2,2'-bipyridine in 1.28 x 10^{-4} M of $Na_2C_6O_6$ and 1.36 x 10^{-4} M $HgCl_2$ in water/ethanol (50/50 v/v). K_{11} = 2.33 x 10^5 M^{-1}. **Cutaway:** UV-Visible absorption spectrum for the titration of a solution of 1.28 x 10^{-4} M of $Na_2C_6O_6$ and 1.36 x 10^{-4} M $HgCl_2$ with a solution of 1.18 x 10^{-4} M of 2,2'-bipyridine in 1.28 x 10^{-4} M of $Na_2C_6O_6$ and 1.36 x 10^{-4} M $HgCl_2$ in water/ethanol (50/50 v/v).

Upon addition of Pb(II) to a solution of rhodizonate and imidazole in water/ethanol (50/50 v/v), the band at 482 nm decreases in intensity (Figures 4.17 through 4.19), with no chromic shift. Applying the decrease in absorption to the 1:1 binding isotherm [32], gives an excellent fit to the 1:1 binding model, indicating that, in solution, Pb(II)-rho-imid exists as an 1:1:1 complex. Non-linear regression analysis of the binding curve gives a binding constant of K_{11} = 9.1 (± 7.8) x 10^6 M^{-1} for formation of Pb(II)-rho-imid, from Pb(II) and rho+imid, corresponding to a free energy of complexation of ΔG = -39.7 (± 3.2) kJ/mol.

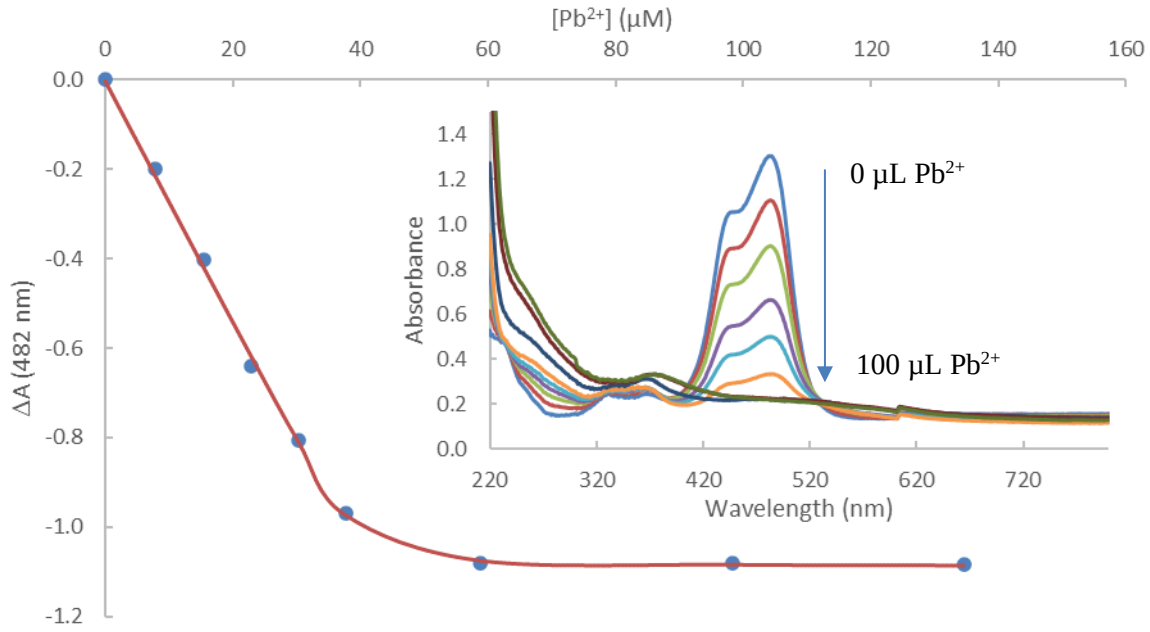

Figure 4.17: Binding curve for the titration of a solution of 3.99 x 10^{-5} M of $Na_2C_6O_6$ and 4.33 x 10^{-5} M imidazole with a solution of 9.42 x 10^{-4} M of $Pb(NO_3)_2$ in 3.99 x 10^{-5} M of $Na_2C_6O_6$ and 4.33 x 10^{-5} M imidazole in water/ethanol (50/50 v/v). K_{11} = 4.08 x 10^6 M^{-1}. **Cutaway:** UV-Visible absorption spectrum for the titration of a solution of 3.99 x 10^{-5} M of $Na_2C_6O_6$ and 4.33 x 10^{-5} M imidazole with solution of 9.42 x 10^{-3} M of $Pb(NO_3)_2$ in 3.99 x 10^{-5} M of $Na_2C_6O_6$ and 4.33 x 10^{-5} M imidazole in water/ethanol (50/50 v/v).

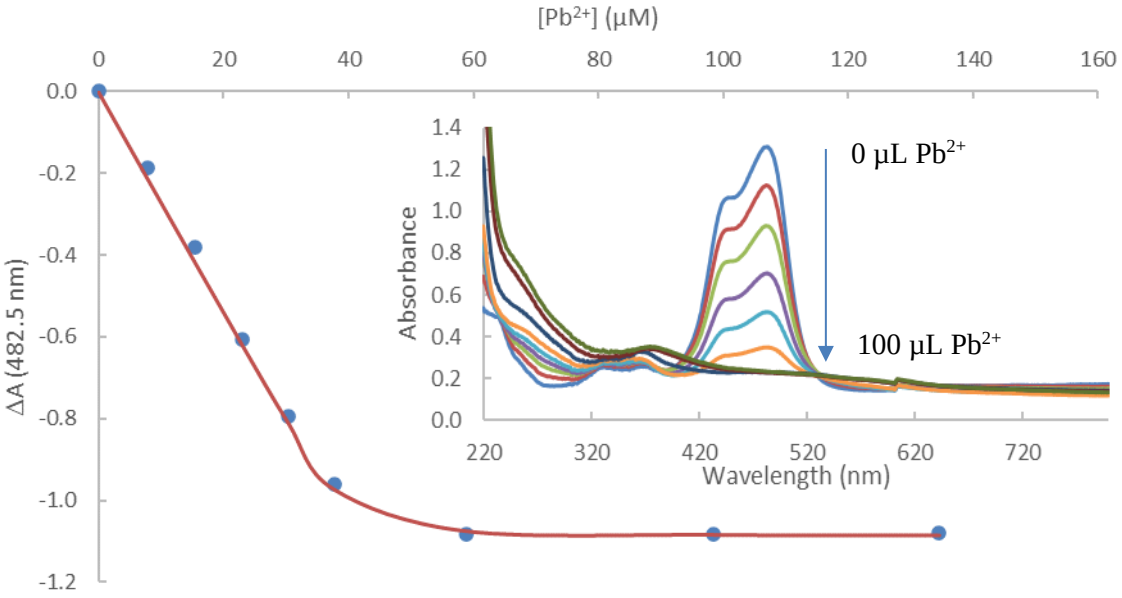

Figure 4.18: Binding curve for the titration of a solution of 4.17 x 10^{-5} M of $Na_2C_6O_6$ and 4.71 x 10^{-5} M imidazole with a solution of 9.42 x 10^{-4} M of $Pb(NO_3)_2$ in 4.17 x 10^{-5} M of $Na_2C_6O_6$ and 4.71 x 10^{-5} M imidazole in water/ethanol (50/50 v/v). K_{11} = 1.81 x 10^7 M^{-1}. **Cutaway:** UV-Visible absorption spectrum for the titration of a solution of 4.17 x 10^{-5} M of $Na_2C_6O_6$ and 4.71 x 10^{-5} M imidazole with solution of 9.42 x 10^{-3} M of $Pb(NO_3)_2$ in 4.17 x 10^{-5} M of $Na_2C_6O_6$ and 4.71 x 10^{-5} M imidazole in water/ethanol (50/50 v/v).

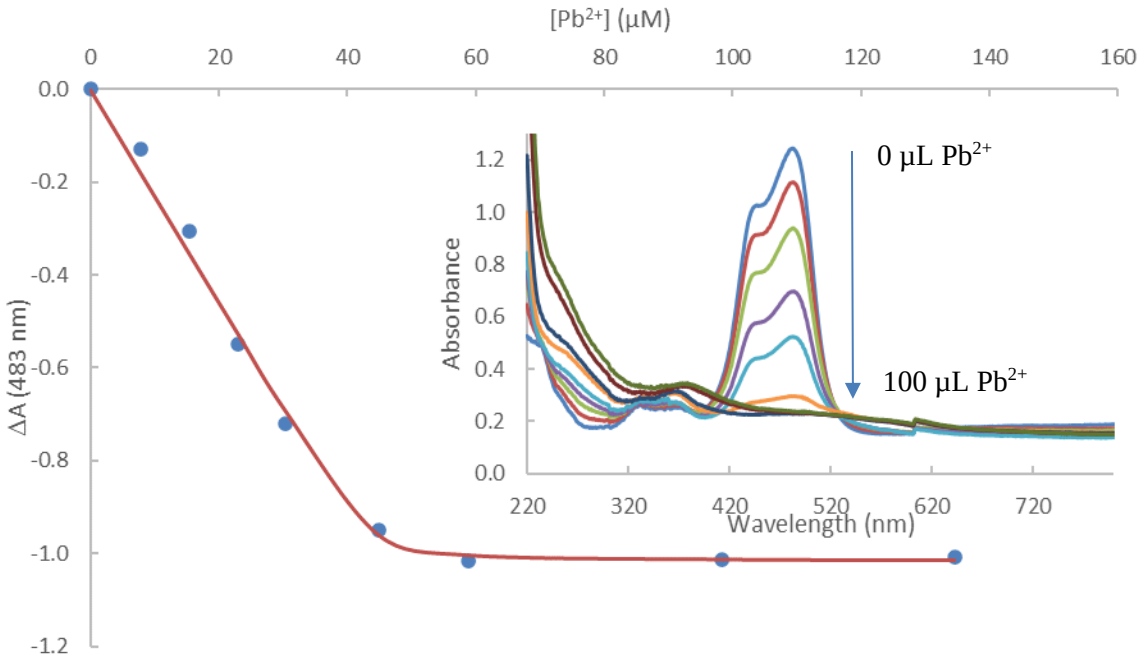

Figure 4.19: Binding curve for the titration of a solution of 4.40 x 10^{-5} M of $Na_2C_6O_6$ and 4.46 x 10^{-5} M imidazole with a solution of 9.42 x 10^{-4} M of $Pb(NO_3)_2$ in 4.40 x 10^{-5} M of $Na_2C_6O_6$ and 4.46 x 10^{-5} M imidazole in water/ethanol (50/50 v/v). K_{11} = 5.04 x 10^6 M^{-1}. **Cutaway:** UV-Visible absorption spectrum for the titration of a solution of 4.40 x 10^{-5} M of $Na_2C_6O_6$ and 4.46 x 10^{-5} M imidazole with solution of 9.42 x 10^{-3} M of $Pb(NO_3)_2$ in 4.40 x 10^{-5} M of $Na_2C_6O_6$ and 4.46 x 10^{-5} M imidazole in water/ethanol (50/50 v/v).

Upon addition of Cd(II) to a solution of rhodizonate and imidazole in water/ethanol (50/50 v/v), the band at 482 nm decreases in intensity (Figure 4.20), with no chromic shift. Applying the decrease in absorption to the 1:1 binding isotherm [32], gives an excellent fit to the 1:1 binding model, indicating that, in solution, Cd(II)-rho-imid exists as an 1:1:1 complex. Non-linear regression analysis of the binding curve gives a binding constant of K_{11} = 9.48 x 10^4 M^{-1} for formation of Cd(II)-rho-imid from Cd(II) and rho+imid, leading to a free energy of complexation of ΔG = -28.4 kJ/mol.

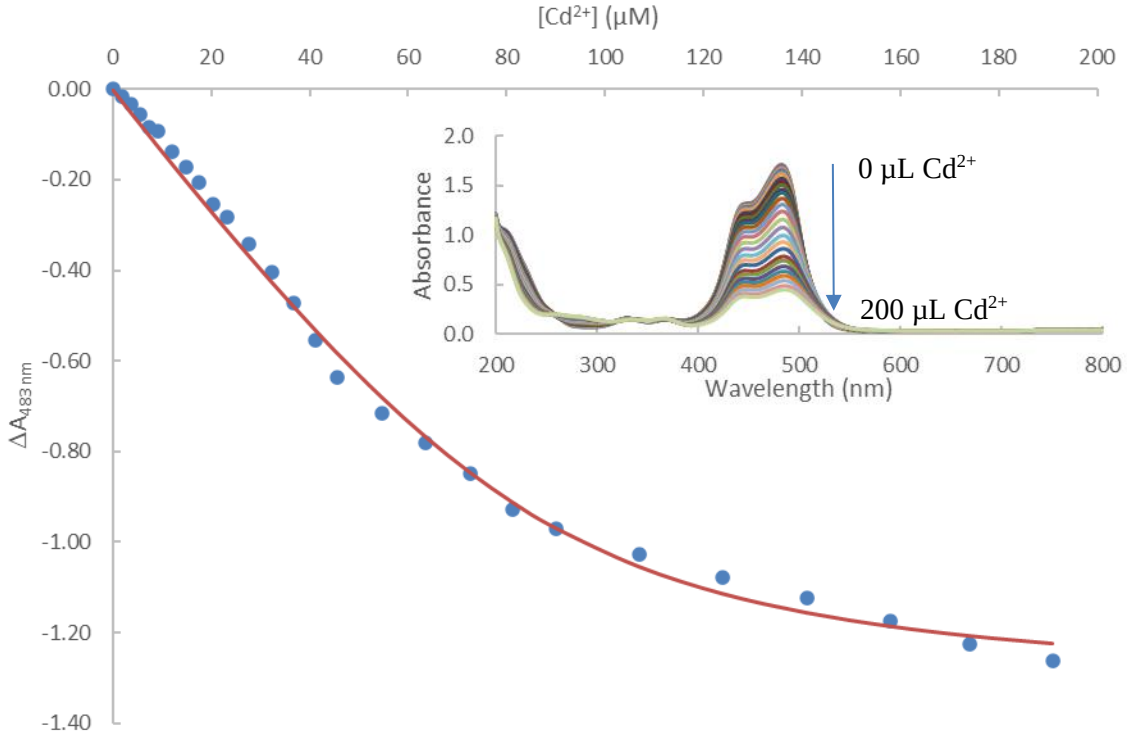

Figure 4.20: Binding curve for the titration of a solution of 6.66 x 10^{-5} M of $Na_2C_6O_6$ and 8.63 x 10^{-5} M of imidazole with a solution of 6.66 x 10^{-5} M of $Na_2C_6O_6$, 8.63 x 10^{-5} M of imidazole, and 5.58 x 10^{-3} M of $Cd(NO_3)_2 \cdot 4H_2O$ in water/ethanol (50/50 v/v). K_{11} = 9.48 x 10^4 M^{-1}. **Cutaway:** UV-Visible absorption spectrum for the titration of 6.66 x 10^{-5} M of $Na_2C_6O_6$ and 8.63 x 10^{-5} M of imidazole with a solution of 6.66 x 10^{-5} M of $Na_2C_6O_6$, 8.63 x 10^{-5} M of imidazole, and 5.58 x 10^{-3} M of $Cd(NO_3)_2 \cdot 4H_2O$ in water/ethanol (50/50 v/v).

To confirm the results of the previous experiment, the titration was performed in reverse by adding imidazole to a solution of Cd(II) rhodizonate in water/ethanol (50/50 v/v). Like the previous experiment, the band at 482 nm decreases in intensity (Figure 4.21), with no chromic shift. Applying the decrease in absorption to the 1:1 binding isotherm [32], gives an excellent fit to the 1:1 binding model, confirming that, in solution, Cd(II)-rho-imid exists as an 1:1:1 complex. Non-linear regression analysis of the binding curve gives a binding constant of K_{11} = 2.81 x 10^5 M^{-1} for formation of Cd(II)-rho-imid from Cd(II)-rho and imid, leading to a free energy of complexation of ΔG = -31.1 kJ/mol.

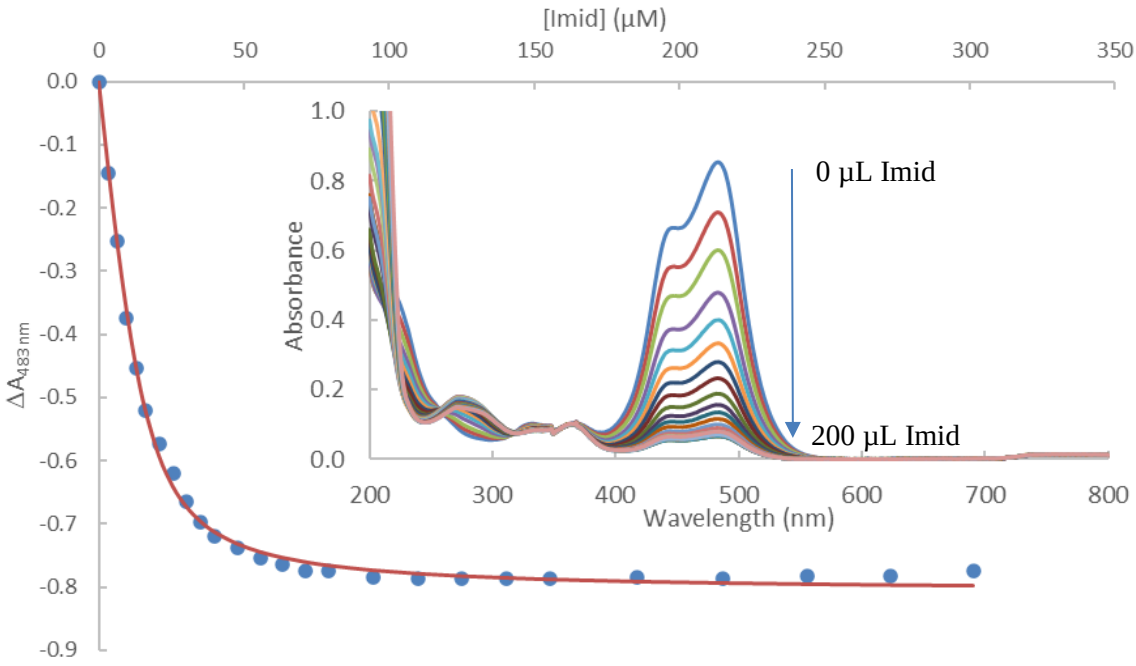

Figure 4.21: Binding curve for the titration of a solution of 6.35 x 10^{-5} M of $Na_2C_6O_6$ and 4.82 x 10^{-3} M of $Cd(NO_3)_2$•$4H_2O$ with a solution of 6.35 x 10^{-5} M of $Na_2C_6O_6$, 4.82 x 10^{-3} M of $Cd(NO_3)_2$•$4H_2O$, and 1.55 x 10^{-4} M of imidazole in water/ethanol (50/50 v/v). K_{11} = 2.81 x 10^5 M^{-1}. **Cutaway:** UV-Visible absorption spectrum for the titration of 6.35 x 10^{-5} M of $Na_2C_6O_6$ and 4.82 x 10^{-3} M of $Cd(NO_3)_2$ • $4H_2O$ with a solution of 6.35 x 10^{-5} M of $Na_2C_6O_6$, 4.82 x 10^{-3} M of $Cd(NO_3)_2$ • $4H_2O$, and 1.55 x 10^{-4} M of imidazole in water/ethanol (50/50 v/v).

Upon addition of Hg(II) to a solution of rhodizonate and imidazole in water/ethanol (50/50 v/v), the band at 482 nm decreases in intensity (Figure 4.22), with no chromic shift. Applying the decrease in absorption to the 1:1 binding isotherm [32], does not give a fit to the 1:1 binding model, indicating that, in solution, Hg(II)-rho-imid either cannot form from Hg(II) and a mixture of rho+imid or experimental error has led to inconclusive results. No binding constant could be determined.

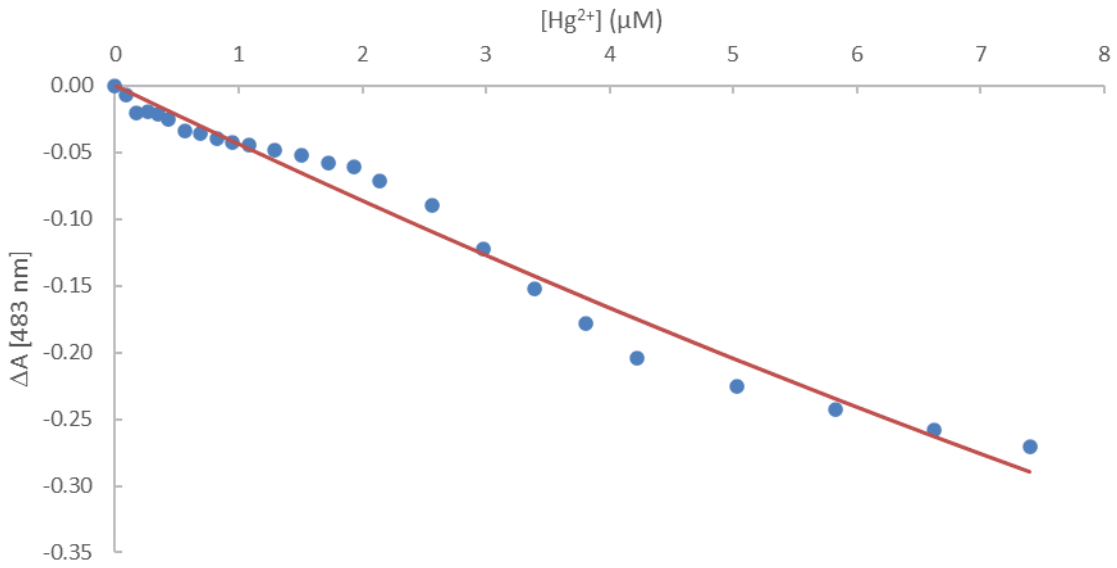

Figure 4.22: Binding curve for the titration of a solution of 1.35 x 10^{-4} M of $Na_2C_6O_6$ and 1.47 x 10^{-4} M of imidazole with a solution of 1.35 x 10^{-4} M of $Na_2C_6O_6$, 1.47 x 10^{-4} M of imidazole, and 1.31 x 10^{-4} M of $HgCl_2$ in water/ethanol (50/50 v/v). No binding constant could be determined.

To clarify the results of the previous experiment, the titration was performed in reverse by adding imidazole to a solution of Hg(II) rhodizonate in water/ethanol (50/50 v/v). Like the previous experiment, the band at 483 nm decreases in intensity (Figure 4.23), with no chromic shift. Applying the decrease in absorption to the 1:1 binding isotherm [32], gives an excellent fit to the 1:1 binding model, confirming that, in solution, Hg(II)-rho-imid exists as an 1:1:1 complex. Non-linear regression analysis of the binding curve gives a binding constant of K_{11} = 1.22 x 10^4 M^{-1} for formation of Hg(II)-rho-imid from Hg(II)-rho and imidazole, leading to a free energy of complexation of ΔG = -23.3 kJ/mol.

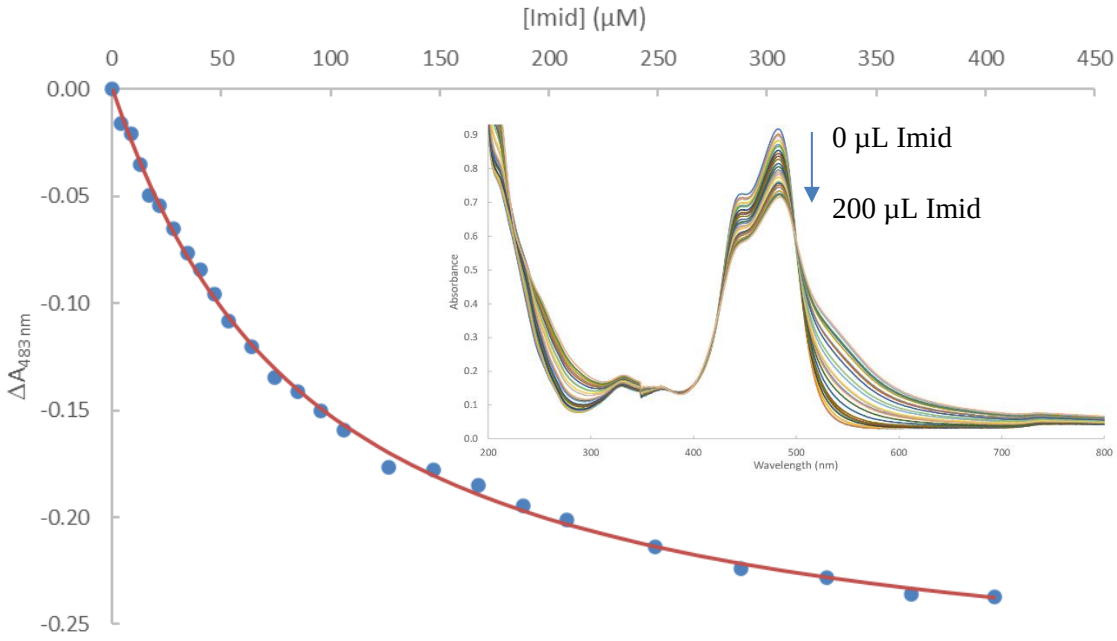

Figure 4.23: Binding curve for the titration of a solution of 1.35 x 10^{-4} M of $Na_2C_6O_6$ and 1.27 x 10^{-4} M of $HgCl_2$ with a solution of 1.35 x 10^{-4} M of $Na_2C_6O_6$, 1.27 x 10^{-4} M of $HgCl_2$, and 1.62 x 10^{-4} M of imidazole in water/ethanol (50/50 v/v). K_{11} = 1.22 x 10^4 M^{-1}. **Cutaway:** UV-Visible absorption spectrum for the titration of 1.35 x 10^{-4} M of $Na_2C_6O_6$ and 1.27 x 10^{-4} M of $HgCl_2$ with a solution of 1.35 x 10^{-4} M of $Na_2C_6O_6$, 1.27 x 10^{-4} M of $HgCl_2$, and 1.62 x 10^{-4} M of imidazole in water/ethanol (50/50 v/v).

4.4.4 UV-Vis Job Plots

To determine the appropriate molar ratio of the binary compounds in solution, Job plots were performed. The Job plot of Cd(II) with sodium rhodizonate is shown in Figure 4.24, and the Job plot of Hg(II) with sodium rhodizonate is shown in Figure 4.25. The Job plot of Pb(II) with sodium rhodizonate is shown in Chapter 2.

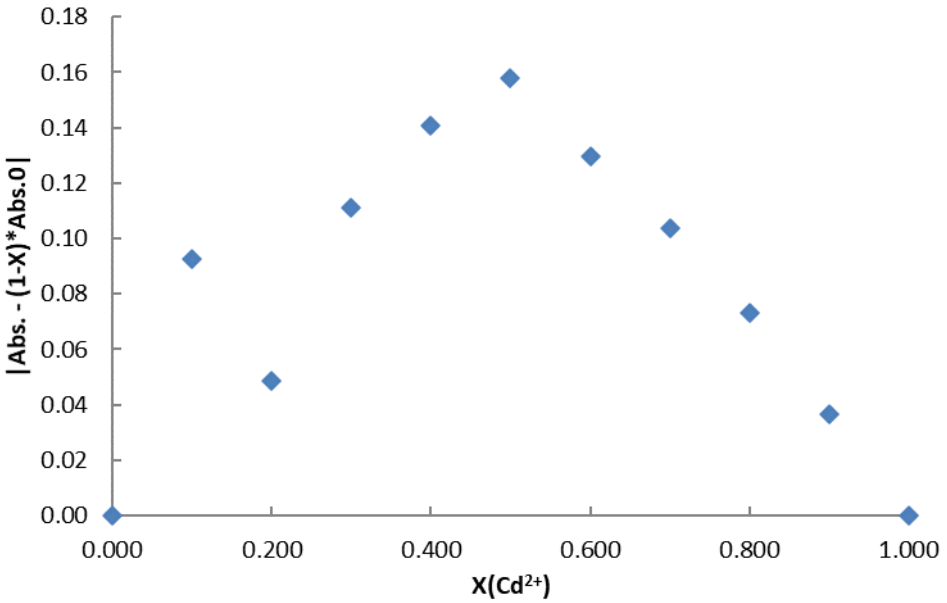

Figure 4.24: The Job plot of Cd(II) with sodium rhodizonate in water/ethanol (50/50 v/v). The Job Plot shows that Cd(II) and rhodizonate complex in solution in a 1:1 mole ratio.

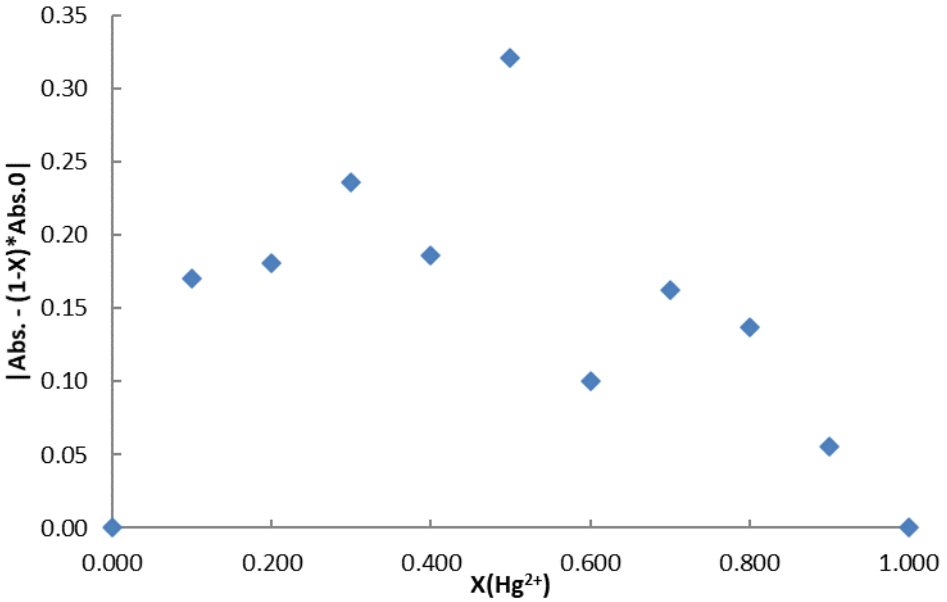

Figure 4.25: The Job plot of Hg(II) with sodium rhodizonate in water/ethanol (50/50 v/v). The Job Plot shows that Hg(II) and rhodizonate complex in solution in a 1:1 mole ratio.

As demonstrated by the Job plot, both Cd(II) and Hg(II) coordinate in a 1:1 ratio with $Na_2C_6O_6$ in water/ethanol (50/50 v/v).

4.5 Discussion

The UV-Vis titrations show a consistent pattern: Addition an N-donor co-ligand gives ternary complexes with higher binding affinity than the corresponding binary metal complexes with rhodizonate. This pattern holds true even when the metal-rhodizonate complex is pre-formed and the co-ligand is added later. This is in contrast to the ternary complex with tartaric acid (see Chapter 2). All the co-ligands tested are organic bases, it is possible that the difference in pH (as compared to the work in Chapter 2 when the solutions are acidic) may be responsible for stronger ternary complex formation with N-donor ligands.

The FT-IR spectra and the UV-Vis data also preclude the possibility that two separate complexes are formed: a metal-rhodizonate binary complex and a metal-co-ligand binary complex. The FT-IR spectra for both the phen and imid complexes show marked differences from the binary metal-rhodizonate compounds and from the spectra of the plain co-ligand. These differences also manifest in the colors of the powdered complexes. Binary Pb(II)-rhodizonate, Pb(II)-rho-phen, and Pb(II)-rho-bipy are purple, while Pb(II)-rho-phen is blue. Binary Cd(II)-rhodizonate, Cd(II)-rho-phen, and Cd(II)-rho-bipy are red, while Cd(II)-rho-phen is orange. Binary Hg(II)-rhodizonate, Hg(II)-rho-phen, and Hg(II)-rho-bipy are grey, while Hg(II)-rho-phen is peach colored.

4.6 Acknowledgements

JS was supported by a U.S. Nuclear Regulatory Commission Fellowship (NRC-HQ-84-14-G-0040/NRC-HQ-84-15-G-0038 and 0038B).

4.7 References

[1] Quiñonero, D., Frontera, A., Ballester, P., Deya, P. M., *Tetrahedron Lett.*, **2000,** *41*, 2001-2005.

[2] von Ragué Schleyer, P., Najafian, K., Kiran, B., Jiao, H., *J. Org. Chem.*, **2000,** *65*, 426-431.

[3] West, R., *Isr. J. Chem.*, **1980,** *20*, 300-307.

[4] Kovalchukova, O. and Strashnova, S., *Rev. Inorg. Chem.*, **2014,** *34*, 1-24.

[5] Cambridge Crystallographic Data Centre https://www.ccdc.cam.ac.uk/.

[6] Cowan, J. A., and Howard J. A. K., *Acta Cryst.***, 2004,** *E60*, m511-m513.

[7] Neumann, M. A. (1965). PhD thesis, University of Wisconsin, USA.

[8] Dinnebier, R. E., Nuss, H., Jansen, M., *Acta Cryst.*, **2005,** *E61*, m2148-m2150.

[9] Chalmers, R. A. and Telling, G. M., *Mikrochim. Acta*, **1967,** *6*, 1126-1135.

[10] Feigl, F. and Suter, H. A., *Ind. Eng. Chem.*, **1942,** *14*, 840-842.

[11] Feigl, F., Gentil, V., Libergott, E., *Isr. J. Chem.*, **1969,** *7*, 123-125.

[12] Cole, S. L., Chemical Spot Test for Lead in Paint and Other Media, US 20030203496 A1, October 30, 2003.

[13] Fabbro, L. A. and Wentzel, C. S., Process for Detecting Trace Amounts of Lead in Unleaded Gasoline, US 19743806319, April 23, 1974.

[14] Morosanova, E. I., Kuz'min, N. M., Zolotov, Y. A., *J. Anal. Chem.*, **1997,** *357*, 853-859.

[15] Ronneau, C. J-M., Jacob, N. M., Apers, D. J., *Anal. Chem.*, **1973,** *45*, 2152.

[16] Glater, R. A. B. and Hernandez, L., *J. Air Waste Manage. Assoc.*, **1972,** *22*, 463-467.

[17] Seregin, I. V. and Kozhevnikova, A. D., *Russ. J. Plant Physiol.*, **2011,** *58*, 721-727.

[18] Stott, A. C., Vaid, T. P., Bylaska, E. J., Dixon, D. A., *J. Phys. Chem. C*, **2012,** *116*, 8370-8378.

[19] Hendon, C. H., Tiana, D., Vaid, T. P., Walsh, A., *J. Mater. Chem. C,* **2013,** *1,* 95-100.

[20] Lam, C-K., and Mak, T. C. W., *Angew. Chem. Int. Ed.,* **2001,** *40,* 3453-3455.

[21] Abrahams, B. F., Haywood, M. G., Robson, R., *Cryst. Eng. Comm.,* **2005,** *7,* 629-632.

[22] Wang, C.-C., Kuo, C.-T., Chou, P.-T., Lee, G.-H., *Angew. Chem. Int. Ed.,* **2004,** *43,* 4507-4510.

[23] Cheng, W., Zhao, X., Su, H., Tang, F., Che, W., Zhang, H., Liu, Q., *Nat. Energy,* **2019,** *4,* 115-122.

[24] Liu, M., Zheng, W., Ran, S., Boles, S. T., Lee, L. Y. S., *Adv. Mater. Interfaces,* **2018,** *5.*

[25] Dolgopolova, E. A., Ejegbavwo, O. A., Martin, C. R., Smith, M. D., Setyawan W., Karakalos, S. G., Henager, C. H., Zur Loye, H. C., Shustova, N. B., *J. Am. Chem. Soc.,* **2017,** *139,* 16852-16861.

[26] Choi, S., Drese, J. H., Jones, C. W., *Chem. Sus. Chem.,* **2009,** *2,* 796-854.

[27] Kolev, T., Koleva, B. B., Spiteller, M., *Cent. Eur. J. Chem.,* **2008,** *6,* 393-399.

[28] Bettermann, H., Dasting, I., Wolff, U., *Spectrochim. Acta Part A,* **1997,** *53,* 233-245.

[29] Finger, L. H. and Sundermeyer, J., *J. Inorg. Gen. Chem.,* **2015,** *641,* 2565-2569.

[30] Thornton, D. A. and Watkins, G. M., *Spectrochim. Acta,* **1991,** *47A,* 1085-1096.

[31] Ramasamy, R., *Arm. J. Phys.,* **2015,** *8,* 51-55.

[32] Connors, K. A., In *Binding Constants: The Measurement of Molecular Complex Stability,* New York: Wiley-Interscience, **1987**.

[33] Araujo, P., *J. Chromatogr. B,* **2009,** *877,* 2224-2234.

CHAPTER V. COORDINATION POLYMERS OF Cd(II) AND Pb(II) WITH CROCONATE SHOW REMARKABLE DIFFERENCES IN COORDINATION PATTERNS: A STRUCTURAL AND SPECTROSCOPIC STUDY

Joshua A. Silverman,[a] Logesh Mathivathanan,[a] Evgen V. Govor,[a,b] Raphael G. Raptis[a] and Konstantinos Kavallieratos[a]*

[a]Department of Chemistry and Biochemistry and Biomolecular Sciences Institute, Florida International University, 11200 SW 8th St., Miami, FL 33199, USA,

[b]Applied Research Center, Florida International University, 10555 W. Flagler St., Miami, FL 33174, USA.

*Correspondence e-mail: kavallie@fiu.edu

This chapter was reproduced and adapted from Silverman, J. A., Mathivathanan, L., Govor, E. V., Raptis, R. G., Kavallieratos, K., *Acta Cryst C*, **2019,** *75*, 935-940. https://doi.org/10.1107/S2053229619007277.

5.1 Abstract

The croconate dianion is a highly versatile ligand with two tautomeric forms making it useful for building large superstructures in the solid state. The single crystal X-ray structures of Pb(II)– and Cd(II)–croconate coordination polymers, namely *catena*-poly[[[diaqualead(II)]-μ-croconato-$\kappa^4O^1,O^2:O^3,O^4$] monohydrate], $\{[Pb(C_5O_5)(H_2O)_2]H_2O\}_n$, **1**, and *catena*-poly[[triaquacadmium(II)]-μ-croconato-$\kappa^4O^1,O^2:O^3,O^4$], $[Cd(C_5O_5)(H_2O)_3]_n$, **2**, have been determined. Both polymers form one-dimensional (1D) structures; **1** is a nonplanar 1D zigzag coordination polymer extended along the crystallographic b axis, whereas **2** is a planar 1D ribbon parallel to the [101] direction. In **2**, three H_2O molecules are coordinated directly to the metal atom, while in **1**, only two H_2O molecules are directly coordinated to the metal atom. A third interstitial H_2O molecule is involved in hydrogen bonding with O atoms of the croconate ligands of an

adjacent layer and other H_2O molecules, resulting in stacked double layers parallel to the [105] plane. Solid-state FT–IR and solution UV–Vis spectra also substantiate the croconate coordination.

5.2 Introduction

Croconate ($C_5O_5^{2-}$) is the five-carbon member of a class of cyclic compounds known as oxocarbons. First isolated by Gmelin in 1825 [1], croconate has been of interest to researchers for its ability to form supramolecular polymeric structures [2-12]. Oxocarbons are of interest because of their catalytic [13], optical [14], electrical [15], and magnetic [16] properties. Computational [17, 18] and synthetic studies show that Pb–rhodizonate (the oxocarbons with n = 6) complexes exhibit semiconductor electrical properties [19]. Croconate, like rhodizonate, contains charge-delocalized electrons that are delocalized throughout the oxocarbon ring, suggesting that metal–croconate complexes and their analogs might also exhibit such properties.

The croconate dianion is a highly versatile ligand, as it adopts a variety of coordination modes [20]. Croconate has two tautomers, the charge-localized C_{2v} and the charge-delocalized D_{5h} mode, which have been shown to be stabilized within a crystal structure [21]. The O atoms of croconate can engage in chemical reactions, whether through addition, creating croconate ethers [22], or through substitution reactions [23]. While this makes croconate quite useful in building large crystal superstructures, the difficulty in synthesizing croconate on a large scale has limited the volume of croconate research [23]. The bulk of the research into metal–croconate coordination involves either alkali metals [24-26] or first-row transition metals [2, 4, 5, 8, 11, 12, 27-30]. Several of these structures contain other bridging ligands, such as 4,4’-bipyridine [4, 6, 11], 2,2’-

bipyrimidine [7], imidazole [31], or histidine [32]. There is a total of six Cd–croconate structures in the Cambridge Structural Database [33], namely Cd-croconate mixed-ligand MOFs with 4,4'-bipyridine [6], 2,2'-bipyrimidine linkers [7], or 1,2-bis(pyridin-4-yl)ethylene [8, 34], and using exclusively croconate anions as the building blocks for making MOFs [9]. Recently, croconate was used as a receptor for Cd in a hybrid system containing other auxiliary ligands [35].

We present herein the crystal structure of a Pb(II)–croconate coordination polymer, namely *catena*-poly[[[diaqualead(II)]-μ-croconato-$\kappa^4O^1,O^2:O^3,O^4$] monohydrate], $\{[Pb(C_5O_5)\text{-}(H_2O)_2]H_2O\}_n$. To the best of our knowledge, it is the first reported structure containing both Pb and croconate, in which Pb adopts a distorted nine-coordinate geometry. There are six strong Pb-O interactions and three longer, weaker Pb-O interactions on the apparent open face of the Pb coordination sphere. We also report the analogous Cd(II)–croconate coordination polymer, *catena*-poly[[triaquacadmium(II)]-μ-croconato-$\kappa^4O^1,O^2:O^3,O^4$], $[Cd(C_5O_5)(H_2O)_3]_n$, **2**, which is also the first Cd–croconate structure reported that does not contain any other non-water ligands.

5.3 Experimental

5.3.1. Materials and Methods

3,4,5,6-Tetraoxocyclohexene-1,2-diol disodium salt (rhodizonic acid disodium salt) and $Cd(NO_3)_2 \bullet 4H_2O$ were purchased from Sigma–Aldrich. $Pb(NO_3)_2$ and sodium croconate (croconic acid disodium salt) were purchased from Fisher Scientific. All chemicals were of reagent grade and were used without further purification. For all the experiments, nanopure water, with a resistivity > 17 M cm^{-1}, was used (Millipore by Barnstead Thermolyne Corporation, Dubuque, IA). The ethanol used for UV–Vis

spectroscopy was obtained from Pharmaco-Aaper (200 proof, absolute). FT–IR spectra for both complexes (bulk powder samples) were collected on an Agilent Technologies Cary 670 FT–IR with a diamond ATR attachment.

5.3.2. Formation of the Pb–croconate coordination polymer, ***1***

Aqueous solutions of lead(II) nitrate [$Pb(NO_3)_2$; 33.1 mg, 0.1 mmol] and sodium rhodizonate ($Na_2C_6O_6$; 21.4 mg, 0.1 mmol) were mixed in a test vial, immediately forming a purple precipitate, which was removed by filtration. After four weeks, small yellow-white crystals were collected from the vial near the surface of the aqueous solution.

The lead(II) croconate salt was prepared in powder form by mixing sodium croconate ($Na_2C_5O_5$; 140.2 mg, 0.754 mmol) and lead(II) nitrate [$Pb(NO_3)_2$; 343.7 mg, 1.038 mmol] in deionized water (250 ml). A yellow precipitate formed immediately, and an additional amount of the same precipitate formed upon chilling to 5 ºC for 1 h. The yellow precipitate was filtered off and washed sequentially with deionized water, acetone, and dichloromethane. It was then dried under vacuum for 1 h (278.1 mg recovered, 0.69 mmol, 91.9% yield). FT–IR (cm^{-1}): 3168 (w, br, H_2O stretch), 1729 (vw, C=O stretch), 1686 (w, C=O stretch), 1642 (vw, C=O stretch), 1594 (w, C=O stretch), 1483 (vs, C=O stretch), 1251 (vw), 1083 (s, C=C stretch), 886 (m), 770 (s), 723 (s), 671 (s, ring breathing).

5.3.3. Formation of the Cd–croconate coordination polymer, ***2***

Crystals of $[Cd(C_5O_5)(H_2O)_3]_n$, **2**, were obtained through the layering of a methanolic solution of $Cd(NO_3)_2 \bullet 4H_2O$ over an intermediate layer of 1:1 (v/v) water–methanol, in turn, over an aqueous sodium rhodizonate solution. After allowing the layers to diffuse slowly over a period of one month, pale yellow crystals were found at the layer boundary.

Cadmium croconate powder was formed by mixing sodium croconate ($Na_2C_5O_5$; 135.7 mg, 0.729 mmol) and cadmium nitrate tetrahydrate [$Cd(NO_3)_2 \bullet 4H_2O$; 321.9 mg, 1.044 mmol] in deionized water (300 ml). A yellow precipitate formed immediately, and an additional amount of the same precipitate formed upon chilling to 5 ºC for 1 h. The yellow precipitate was filtered off and washed sequentially with deionized water, acetone, and dichloromethane. It was then dried under vacuum for 1 h (136.4 mg recovered, 0.45 mmol, 61.0% yield). FT–IR (cm^{-1}): 3209 (m, br, H_2O stretch), 1671 (m, C=O stretch), 1625 (w, C=O stretch), 1585 (m, C=O stretch), 1555 (m, C=O stretch), 1458 (vs, C=O stretch), 1333 (w), 1222 (m, C=C stretch), 1107 (w), 744 (w), 639 (s, ring breathing).

5.3.4. X-ray crystallography

Details of the X-ray crystallographic data collection, solution, and refinement can be found in Table 5.1. H atoms bonded to O6 were refined in geometrically constrained positions, with $U_{iso}(H) = 1.5U_{eq}(O6)$. H atoms on O7 and O8 were restrained to have O-H = 0.88(2) Å and freely refined displacement parameters. In **2**, H atoms were initially included in geometrically calculated positions, but were allowed to refine freely.

All esds (except the esd in the dihedral angle between two l.s. planes) are estimated using the full covariance matrix. The cell esds are taken into account individually in the estimation of esds in distances, angles and torsion angles; correlations between esds in cell parameters are only used when they are defined by crystal symmetry. An approximate (isotropic) treatment of cell esds is used for estimating esds involving l.s. planes.

Data were collected on a Bruker D8 Quest diffractometer with graphite monochromated Mo Kα radiation using the APEX3 suite [36]. Structures were solved by

intrinsic phasing method using SHELXT [37] and were refined using SHELXL [38] with the Olex2 program [39]. Graphics were prepared using CrystalMaker [40].

5.3.5. UV–Visible (UV–Vis) titrations

In a typical UV–Vis titration experiment, solutions of sodium croconate ($Na_2C_5O_5$, 1.0 x 10^{-5} M) in 1:1 (v/v) water-ethanol solvent (solution A) were titrated with 1:1 (v/v) water-ethanol solutions of $Pb(NO_3)_2$ (1.0 x 10^{-3} M) or $Cd(NO_3)_2 \cdot H_2O$ (1.0 x 10^{-3} M) at a constant sodium croconate concentration (1.0 x 10^{-5} M) (solution B). For the collection of spectral data, the $Na_2C_5O_5$ solution (solution A) (3 ml) was added to a cuvette and 5.00–20.0 ml sequential additions of solution B were made at 5 min intervals until a total of 200 ml had been added. Titrations at longer time intervals established that the complex formation reaction in solution reaches equilibrium in less than 5 min.

5.4. Results and Discussion

5.4.1. Synthesis

The title Pb(II)- and Cd(II)-croconate complexes are readily precipitated as yellow powders by reacting Cd(II) or Pb(II) nitrate salts with Na-croconate in aqueous solutions. They can also be formed from sodium rhodizonate ($Na_2C_6O_6$) instead of Na-croconate, as rhodizonate is known to decompose slowly to croconate with time [20]. Indeed, we successfully obtained crystals suitable for single crystal X-ray analysis by utilizing this latter method.

Table 5.1: Experimental crystallographic details of Pb(II) and Cd(II) croconates. Experiments were carried out with Mo *Kα* radiation using a Bruker D8 diffractometer with a PHOTON 100 detector. Absorption was corrected for by multi-scan methods [41]. Computer programs: SAINT [36], APEX2 [36], SHELXT2014 [37], SHELXL2018 [38], OLEX2 [39] and CrystalMaker [40].

Crystal data	**1**	**2**
Chemical formula	$[Pb(C_5O_5)(H_2O)_2]\bullet H_2O$	$[Cd(C_5O_5)(H_2O)_3]$
M_r	401.29	306.50
Crystal system, space group	Triclinic, $P\bar{1}$	Monoclinic, $P2_1/n$
Temperature (K)	296	298
a, *b*, *c* (Å)	6.4360(4), 7.9058(4), 8.3495(5)	6.5123(3), 8.8174(4), 13.8763(6)
α, *β*, *γ* (º)	104.055(1), 90.956(2), 96.200(2)	90, 96.053(1), 90
V (Å^3)	409.30(4)	792.36(6)
Z	2	4
μ (mm^{-1})	20.63	2.78
Crystal size (mm)	0.13 x 0.04 x 0.03	0.18 x 0.14 x 0.09
F(000)	364	592
D_x (Mg m^{-3})	3.256	2.569
Mo *Kα* radiation, λ (Å)	0.71073	0.71073
Cell parameter reflections	6853	9903
θ range (º)	3.2-28.3	3.0-28.3
Shape and color	Needle, yellow	Block, red
Data collection		
T_{min}, T_{max}	0.415, 0.746	0.688, 0.746
No. of measured, Independent and observed [$I > 2\sigma(I)$] reflections	8040, 2026, 1928	22305, 1970, 1843
R_{int}	0.027	0.023
$(\sin\theta/\lambda)_{max}$ (Å^{-1})	0.666	0.667
h	-8 → 8	-8 → 8
k	-10 → 10	-11 → 11
l	-11 → 10	-18 → 18
Refinement		
$R[F^2 > 2\sigma(F^2)]$, $wR(F^2)$, *S*	0.017, 0.042, 1.22	0.015, 0.038, 1.13
No. of reflections	2026	1970
No. of parameters	144	151
No. of restraints	4	0
H-atom treatment	H atoms treated by a mixture of independent and constrained refinement	All H-atom parameters refined
$\Delta\rho_{max}$, $\Delta\rho_{min}$, (e Å^{-3})	0.49, -1.37	0.48, -0.52

5.4.2. X-ray crystallography

Crystals of $\{[Pb(C_5O_5)(H_2O)_2]\bullet H_2O\}_n$, **1**, and $[Cd(C_5O_5)(H_2O)_3]_n$, **2**, suitable for X-ray diffraction analysis were formed by mixing sodium rhodizonate with Pb(II) or Cd(II) nitrate salts in water. As rhodizonate slowly decomposes to croconate over a period of 15 d, small yellow crystals were formed. The crystallographic data for both compounds are shown in Table 5.1.

5.4.3. Crystal structure descriptions

*5.4.3.1. $\{[Pb(C_5O_5)(H_2O)_2]\bullet H_2O\}_n$, **1***

Compound **1** crystallizes in the triclinic space group $P\bar{1}$ with one Pb(II) center, one croconate anion, and three water molecules per asymmetric unit. The Pb atom shows a distorted square-pyramidal coordination geometry, bonding to three croconate O atoms and two water molecules in its coordination sphere (Table 5.5). The coordination can also be considered as being a puckered pentagonal pyramidal one if the fourth croconate O atom (at 2.960(4) Å from the Pb atom, which is shorter than the sum of the van der Waals radii of Pb and O) is included in the coordination sphere (Fig. 5.1). In fact, the coordination of the Pb atom has been described in various geometries depending on the coordination sphere radii [42]. Along those lines, the Pb atom in **1** may be regarded as the link between two adjacent croconate sheets, considering a coordination sphere with a radius of 3.5 Å. The Pb center is located 1.07 Å from the mean O_4 plane, resulting in a puckered structure due to the active $6s^2$ lone-pair electrons found on the Pb atom. These electrons have a distorting effect on the coordination geometry around the metal, which is consistent with other Pb(II)-containing structures [17, 18, 43-45]. Four of the five O atoms of the croconate anion are involved in bonding with Pb(II) and, at the same time, the croconate O atoms form

hydrogen-bonding interactions with water molecules (Table 5.5 and Fig. 5.2). The axially bound and the interstitial water molecules bind the two chains via hydrogen bonds with croconate O atoms forming a ribbon (Fig. 5.2). The O atoms bound to Pb, i.e. O6 and O7, form two hydrogen bonds each, one with the interstitial water molecule and the other with a croconate O atom. The interstitial water molecule forms three hydrogen bonds, with both bound water molecules and with a croconate O atom. It forms the strongest interaction with O7, at an O…O distance of 2.691(4) Å. To the best of our knowledge, this is the first reported example of an X-ray structure that contains a Pb(II)-croconate coordination complex.

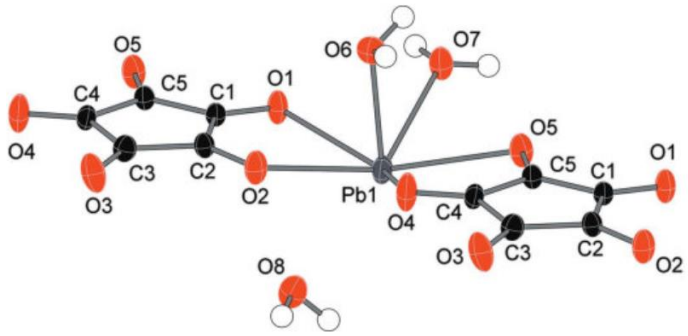

Figure 5.1: The molecular structure of the repeat unit of **1**, showing the atom-labeling scheme. Displacement ellipsoids are drawn at 50% probability level. Color coding: Pb gray, C black, O red, and H white.

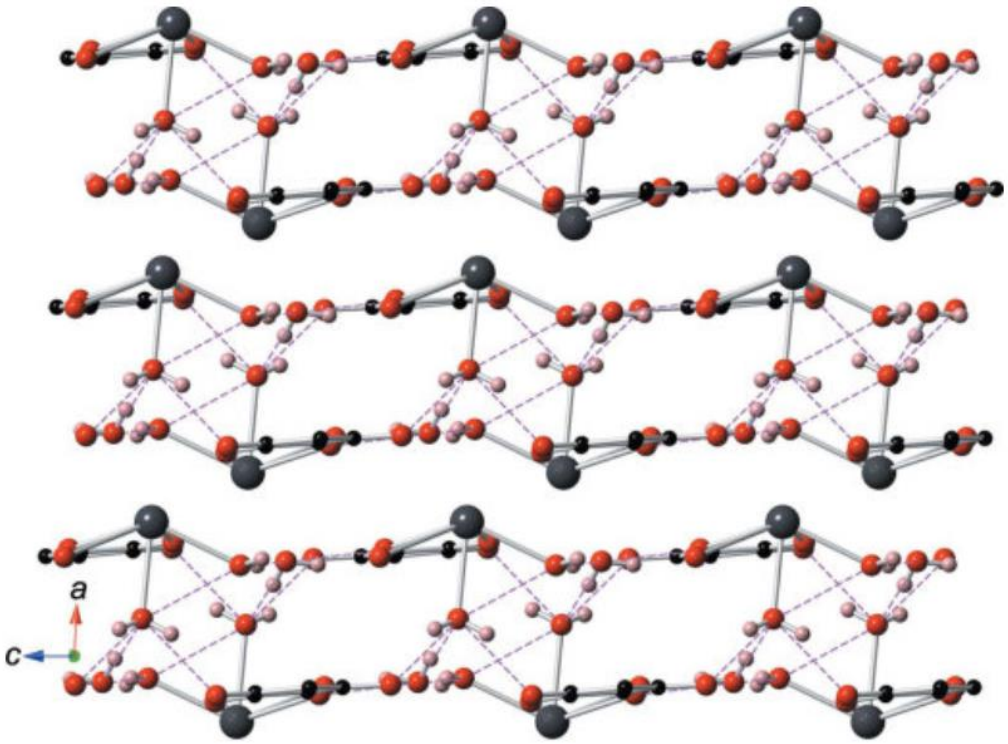

Figure 5.2: Crystal-packing diagram of **1**, viewed parallel to the crystallographic b axis. O—H…O interactions are shown as magenta dashed lines. Color coding: Pb grey, C black, O red, and H pink.

Table 5.2: Data collection details for **1**: *SAINT* [36]; cell refinement: *APEX2* [36]; data reduction: *SAINT* [36]; program(s) used to solve structure: SHELXT2014 [37]; program(s) used to refine structure: *SHELXL2018* [38]. Molecular graphics: OLEX2 [39] and *CrystalMaker* [40] for rgr545_a_pl; OLEX2 [39] and *CrystalMaker* [40].

catena-Poly[[[diaqualead(II)]-μ-croconato-$\kappa^4O^1,O^2:O^3,O^4$] monohydrate] (rgr545_a_pl)

Data collection

Bruker D8 with PHOTON 100 detector diffractometer
Detector resolution: 10.42 pixels mm^{-1} φ and ω shutterless scans
Absorption correction: multi-scan [41]
T_{min} = 0.415, T_{max} = 0.746
8040 measured reflections, 2026 independent reflections, 1928 reflections with $I > 2\sigma(I)$
R_{int} = 0.027
θ_{max} = 28.3°, θ_{min} = 3.2°
h = -8→8
k = -10→10
l = -11→10

Refinement

Refinement on F^2
Least-squares matrix: full
$R[F^2 > 2\sigma(F^2)]$ = 0.017
$wR(F^2)$ = 0.042
S = 1.22
2026 reflections
144 parameters
4 restraints
Hydrogen site location: difference Fourier map
H atoms treated by a mixture of independent and constrained refinement
$w = 1/[\sigma^2(F_o^2) + (0.0217P)^2 + 0.0167P]$, where $P = (F_o^2 + 2F_c^2)/3$
$(\Delta/\sigma)_{max}$ = 0.001
$\Delta\rho_{max}$ = 0.49 e Å^{-3}
$\Delta\rho_{min}$ = -1.37 e Å^{-3}

Table 5.3: Fractional atomic coordinates and isotropic or equivalent isotropic displacement parameters (Å^2)

Atom	*x*	*y*	*z*	U_{iso}*/U_{eq}
Pb1	0.09912(2)	0.70968(2)	0.35063(2)	0.02400(6)
O1	0.1805(4)	0.4301(3)	0.4220(3)	0.0249(5)
O2	0.2089(4)	0.4717(3)	0.0930(3)	0.0265(5)
O3	0.2472(5)	0.1217(3)	-0.1318(3)	0.0318(6)
O4	0.2391(5)	-0.1311(3)	0.0789(3)	0.0352(6)
O5	0.2032(4)	0.0626(3)	0.4195(3)	0.0267(5)
O6	0.4883(4)	0.7389(3)	0.3353(3)	0.0262(5)
H6A	0.548854	0.801583	0.429182	0.039*
H6B	0.528764	0.800381	0.264501	0.039*
O7	0.2731(4)	0.8030(3)	0.6382(3)	0.0288(5)
O8	-0.2576(5)	0.4678(4)	0.2181(3)	0.0307(6)
C1	0.2054(5)	0.3091(4)	0.2983(4)	0.0171(6)
C2	0.2195(5)	0.3295(4)	0.1308(4)	0.0178(6)
C3	0.2370(5)	0.1582(4)	0.0204(4)	0.0215(7)
C4	0.2352(5)	0.0287(4)	0.1255(4)	0.0196(6)
C5	0.2143(5)	0.1274(4)	0.2964(4)	0.0181(6)
H7A	0.248(9)	0.902(5)	0.706(6)	0.060(16)*
H7B	0.274(7)	0.721(5)	0.692(5)	0.043(13)*
H8A	-0.351(6)	0.537(6)	0.254(6)	0.046(15)*
H8B	-0.270(9)	0.467(8)	0.116(3)	0.072(19)*

Table 5.4: Atomic displacement parameters (Å^2)

Atom	U^{11}	U^{22}	U^{33}	U^{12}	U^{13}	U^{23}
Pb1	0.02980(8)	0.01489(8)	0.02673(8)	0.00468(5)	0.00083(5)	0.00310(5)
O1	0.0435(15)	0.0158(11)	0.0156(11)	0.0059(10)	0.0042(10)	0.0030(9)
O2	0.0445(15)	0.0166(12)	0.0203(12)	0.0050(10)	0.0031(11)	0.0077(9)
O3	0.0536(17)	0.0246(13)	0.0134(11)	-0.0008(12)	0.0083(11)	-0.0005(10)
O4	0.0583(19)	0.0171(13)	0.0294(14)	0.0106(12)	0.0021(13)	0.0013(10)
O5	0.0456(16)	0.0163(12)	0.0200(12)	0.0018(10)	0.0004(10)	0.0088(9)
O6	0.0277(13)	0.0318(14)	0.0190(12)	0.0030(10)	0.0020(9)	0.0060(10)
O7	0.0427(15)	0.0198(13)	0.0233(13)	0.0043(11)	0.0006(11)	0.0042(10)
O8	0.0431(16)	0.0321(15)	0.0192(13)	0.0121(12)	0.0035(11)	0.0072(11)
C1	0.0207(15)	0.0147(15)	0.0157(14)	0.0028(11)	0.0012(11)	0.0030(11)
C2	0.0232(15)	0.0147(15)	0.0153(14)	0.0014(11)	0.0018(11)	0.0039(11)
C3	0.0253(16)	0.0207(17)	0.0187(15)	0.0043(13)	0.0033(12)	0.0047(13)
C4	0.0238(16)	0.0153(15)	0.0192(15)	0.0058(12)	0.0010(12)	0.0016(12)
C5	0.0218(15)	0.0148(14)	0.0174(15)	0.0019(11)	0.0009(12)	0.0033(12)

Table 5.5: Geometric parameters (Å, º) Symmetry codes: (i) *x*, *y*+1, *z*; (ii) *x*, *y*-1, *z*.

Pb1—O1	2.529(2)	O6—H6B	0.8779
Pb1—O2	2.653(2)	O7—H7A	0.88(2)
Pb1—O5^{i}	2.714(2)	O7—H7B	0.876(19)
Pb1—O6	2.499(2)	O8—H8A	0.864(19)
Pb1—O7	2.537(3)	O8—H8B	0.85(2)
O1—C1	1.251(4)	C1—C2	1.449(4)
O2—C2	1.248(4)	C1—C5	1.440(4)
O3—C3	1.238(4)	C2—C3	1.458(4)
O4—C4	1.231(4)	C3—C4	1.501(5)
O5—C5	1.255(4)	C4—C5	1.467(4)
O6—H6A	0.8782		

O1—Pb1—O2	66.73(7)	H7A—O7—H7B	110(5)
O1—Pb1—O5^{i}	144.36(8)	H8A—O8—H8B	98(5)
O1—Pb1—O7	74.06(8)	O1—C1—C2	124.7(3)
O2—Pb1—O5^{i}	127.18(7)	O1—C1—C5	126.3(3)
O6—Pb1—O1	79.20(8)	C5—C1—C2	108.9(3)
O6—Pb1—O2	70.11(8)	O2—C2—C1	123.6(3)
O6—Pb1—O5^{i}	77.15(8)	O2—C2—C3	127.8(3)
O6—Pb1—O7	69.40(8)	C1—C2—C3	108.6(3)
O7—Pb1—O2	127.50(9)	O3—C3—C2	127.7(3)
O7—Pb1—O5^{i}	72.84(8)	O3—C3—C4	125.2(3)
C1—O1—Pb1	113.6(2)	C2—C3—C4	107.1(3)
C2—O2—Pb1	110.12(19)	O4—C4—C3	127.5(3)
C5—O5—Pb1^{ii}	115.4(2)	O4—C4—C5	125.7(3)
Pb1—O6—H6A	111.0	C5—C4—C3	106.7(3)
Pb1—O6—H6B	110.7	O5—C5—C1	126.0(3)
H6A—O6—H6B	103.2	O5—C5—C4	125.2(3)
Pb1—O7—H7A	120(4)	C1—C5—C4	108.7(3)
Pb1—O7—H7B	116(3)		

Pb1—O1—C1—C2	9.0(4)	O3—C3—C4—C5	-178.0(3)
Pb1—O1—C1—C5	-167.6(3)	O4—C4—C5—O5	2.0
Pb1—O2—C2—C1	-8.9(4)	O4—C4—C5—C1	-177.0(3)
Pb1—O2—C2—C3	168.0(3)	C1—C2—C3—O3	178.1(3)
Pb1^{ii}—O5—C5—C1	160.7(2)	C1—C2—C3—C4	-0.4(4)
Pb1^{ii}—O5—C5—C4	-18.3(4)	C2—C1—C5—O5	-178.8(3)
O1—C1—C2—O2	0.4(5)	C2—C1—C5—C4	0.2
O1—C1—C2—C3	-177.0(3)	C2—C3—C4—O4	177.0(3)
O1—C1—C5—O5	-1.7(6)	C2—C3—C4—C5	0.6(4)
O1—C1—C5—C4	177.3(3)	C3—C4—C5—O5	178.6(3)
O2—C2—C3—O3	0.9(6)	C3—C4—C5—C1	-0.5(4)
O2—C2—C3—C4	-177.7(3)	C5—C1—C2—O2	177.5(3)
O3—C3—C4—O4	-1.6(6)	C5—C1—C2—C3	0.1(4)

*5.4.3.2. $[Cd(C_5O_5)(H_2O)_3]_n$, **2***

Compound **2** crystallizes with the repeat motif in the asymmetric unit of a monoclinic $P2_1/n$ cell (Fig. 5-3). Four of the five O atoms of the croconate ligand bridge two Cd(II) metal centers along a 1D chain (Table 5.9). The separation of the Cd(II) atoms along the chain is 7.7107(3) Å, and between the chains is 6.5123(3) Å. In contrast to Pb(II)-croconate complex **1**, inter-chain interactions are due to hydrogen bonding between coordinated water molecules (Fig. 5.4 and Table 5.9). The Cd(II) center has a pentagonal bipyramidal geometry, with four croconate O atoms and one water molecule completing the equatorial plane, and two trans water molecules at the axial sites. Consecutive layers of the crystal structure are connected through hydrogen-bonding interactions with axial water molecules: O8 forms three intermolecular hydrogen-bonding interactions, whereas O6 forms two (Table 5.9). An equatorial water molecule is hydrogen bonded to an axial water molecule from an adjacent unit [O…O = 2.820(3) Å] and to a croconate O atom from another unit [O…O = 2.813(2) Å], forming an extended structure. The croconate ring is planar (average deviation = 0.005 Å from the median) and nearly fivefold symmetrical, with C—C bonds of 1.440(4)–1.501(5) Å and C—C—C angles ranging from 106.30(11) to 109.53(12). In contrast, Zn(II)-croconate complexes have a wider range of C—C bond lengths (1.415–1.501 Å). Unlike for Cd(II)-croconate **2**, and despite the similarities of Zn(II) and Cd(II) in their 2+ oxidation state, Zn(II)-croconate exhibits monodentate coordination [30]. To the best of our knowledge, this is the first reported example of an X-ray structure that contains both Cd and the croconate ligand, and no additional ligands (other than H_2O). Of the published Cd-croconate structures, the closest related structure is

a 1D chain containing $[Cd(C_5O_5)(NH_3)_5]_n$ repeat units, with NH_3 ligands in the axial positions and the Cd(II) atom in an octahedral coordination geometry [9].

Table 5.6: Data collection details for **2**: *SAINT* [36]; cell refinement: *APEX2* [36]; data reduction: *SAINT* [36]; program(s) used to solve structure: SHELXT2014 [37]; program(s) used to refine structure: *SHELXL2018* [38]. Molecular graphics: OLEX2 [39] and *CrystalMaker* [40] for rgr560_a. Software used to prepare material for publication: OLEX2 [39].

catena-Poly[[triaquacadmium(II)]-μ-croconato-$\kappa_4O_1,O_2:O_3,O_4$] (rgr560_a)

Data collection

Bruker D8 with PHOTON 100 detector diffractometer
φ and ω scans
Absorption correction: multi-scan [41]
T_{min} = 0.688, T_{max} = 0.746
22305 measured reflections, 1970 independent reflections, 1843 reflections with $I > 2\sigma(I)$
R_{int} = 0.023
θ_{max} = 28.3°, θ_{min} = 3.0°
h = -8→8
k = -11→11
l = -18→18

Refinement

Refinement on F^2
Least-squares matrix: full
$R[F^2 > 2\sigma(F^2)]$ = 0.015
$wR(F^2)$ = 0.038
S = 1.13
1970 reflections
151 parameters
0 restraints
Hydrogen site location: difference Fourier map
All H-atom parameters refined
$w = 1/[\sigma^2(F_o^2) + (0.0216P)^2 + 0.2417P]$, where $P = (F_o^2 + 2F_c^2)/3$
$(\Delta/\sigma)_{max}$ = 0.001
$\Delta\rho_{max}$ = 0.48 e Å^{-3}
$\Delta\rho_{min}$ = -0.52 e Å^{-3}

Table 5.7: Fractional atomic coordinates and isotropic or equivalent isotropic displacement parameters (Å^2)

Atom	*x*	*y*	*z*	U_{iso}*/U_{eq}
Cd1	0.43724(2)	0.88271(2)	0.68614(2)	0.02022(5)
O1	0.2558(2)	0.89361(12)	0.51854(9)	0.0268(3)
O2	0.37243(18)	0.63493(12)	0.62976(8)	0.0226(2)
O3	0.26637(19)	0.35768(12)	0.51165(9)	0.0248(2)
O4	0.08427(18)	0.46592(14)	0.32039(7)	0.0284(3)
O5	0.06505(17)	0.78557(14)	0.31997(7)	0.0290(3)
O6	0.7487(2)	0.87789(12)	0.61835(10)	0.0239(2)
O7	0.4245(2)	1.13414(13)	0.64388(10)	0.0317(3)
O8	0.1165(2)	0.89464(13)	0.74291(10)	0.0251(2)
C1	0.2310(2)	0.76145(16)	0.48626(10)	0.0182(3)
C2	0.2908(2)	0.62790(14)	0.54359(10)	0.0166(3)
C3	0.2409(2)	0.49220(15)	0.48598(10)	0.0166(3)
C4	0.1502(2)	0.54480(16)	0.39068(10)	0.0179(3)
C5	0.1411(2)	0.71068(16)	0.39055(10)	0.0190(3)
H6A	0.751(3)	0.798(3)	0.5861(16)	0.039(6)*
H8B	0.114(3)	0.970(3)	0.7824(18)	0.047(6)*
H6B	0.745(3)	0.944(3)	0.5841(16)	0.035(6)*
H8B	0.025(4)	0.896(2)	0.7057(19)	0.040(7)*
H7A	0.426(4)	1.198(4)	0.6907(19)	0.070(9)*
H7B	0.353(4)	1.182(4)	0.601(2)	0.076(9)*

Table 5.8: Atomic displacement parameters (Å^2)

Atom	U^{11}	U^{22}	U^{33}	U^{12}	U^{13}	U^{23}
Cd1	0.02547(7)	0.01806(7)	0.01602(7)	-0.00052(4)	-0.00309(4)	-0.00174(3)
O1	0.0415(7)	0.0179(5)	0.0192(6)	-0.0015(4)	-0.0054(5)	-0.0019(4)
O2	0.0318(6)	0.0213(5)	0.0132(5)	-0.0028(4)	-0.0054(4)	-0.0001(4)
O3	0.0334(6)	0.0182(5)	0.0217(6)	0.0032(4)	-0.0027(5)	0.0024(4)
O4	0.0419(7)	0.0225(6)	0.0178(5)	0.0003(5)	-0.0102(5)	-0.0043(4)
O5	0.0425(7)	0.0218(6)	0.0194(5)	0.0009(5)	-0.0119(5)	0.0034(4)
O6	0.0298(6)	0.0156(5)	0.0256(6)	0.0008(4)	0.0006(5)	0.0006(4)
O7	0.0514(8)	0.0207(6)	0.0207(6)	0.0074(5)	-0.0073(5)	0.0010(4)
O8	0.0279(6)	0.0239(6)	0.0226(6)	0.0021(4)	-0.0019(5)	-0.0032(4)
C1	0.0216(7)	0.0175(6)	0.0149(6)	-0.0013(5)	-0.0014(5)	-0.0004(5)
C2	0.0167(6)	0.0186(6)	0.0140(6)	-0.0004(5)	-0.0005(5)	0.0006(5)
C3	0.0173(6)	0.0175(6)	0.0146(6)	0.0001(5)	0.0000(5)	-0.0002(5)
C4	0.0195(6)	0.0183(7)	0.0152(6)	-0.0006(5)	-0.0015(5)	-0.0008(5)
C5	0.0219(7)	0.0189(7)	0.0154(6)	-0.0009(5)	-0.0022(5)	0.0003(5)

Table 5.9: Geometric parameters (Å, º) Symmetry codes: (i) *x*+½ , -*y*+3/2, *z*+½; (ii) *x*-½ , -*y*-3/2, *z*-½.

Cd1—O1	2.4971(12)	O6—H6A	0.83(2)
Cd1—O2	2.3439(11)	O6—H6B	0.75(2)
Cd1—O4^{i}	2.4067(11)	O7—H7A	0.86(3)
Cd1—O5^{i}	2.4529(11)	O7—H7B	0.83(3)
Cd1—O6	2.3244(13)	O8—H8A	0.86(3)
Cd1—O7	2.2924(12)	O8—H8B	0.74(3)
Cd1—O8	2.3112(13)	C1—C2	1.4512(19)
O1—C1	1.2528(18)	C1—C5	1.464(2)
O2—C2	1.2578(18)	C2—C3	1.4565(18)
O3—C3	1.2445(17)	C3—C4	1.4657(18)
O4—C4	1.2373(17)	O4—C5	1.464(2)
O5—C5	1.2402(17)		

O2—Cd1—O1	70.98(4)	Cd1—O6—H6A	107.5(15)
O2—Cd1—O4^{i}	144.91(4)	Cd1—O6—H6B	105.6(17)
O2—Cd1—O5^{i}	73.96(4)	H6A—O6—H6B	109(2)
O4^{i}—Cd1—O1	144.11(4)	Cd1—O7—H7A	116(2)
O4^{i}—Cd1—O5^{i}	70.97(4)	Cd1—O7—H7B	132(2)
O5^{i}—Cd1—O1	144.87(3)	H7A—O7—H7B	100(3)
O6—Cd1—O1	88.35(5)	Cd1—O8—H8A	109.4(15)
O6—Cd1—O2	88.96(4)	Cd1—O8—H8B	116.6(19)
O6—Cd1—O4^{i}	91.75(4)	H8A—O8—H8B	111(2)
O6—Cd1—O5^{i}	93.12(4)	O1—C1—C2	122.81(13)
O7—Cd1—O1	73.96(4)	O1—C1—C5	129.26(14)
O7—Cd1—O2	144.65(4)	C2—C1—C5	107.92(12)
O7—Cd1—O4^{i}	70.27(4)	O2—C2—C1	122.90(12)
O7—Cd1—O5^{i}	141.16(4)	O2—C2—C3	127.57(12)
O7—Cd1—O6	85.63(4)	C1—C2—C3	109.53(12)
O7—Cd1—O8	91.92(4)	O3—C3—C2	127.63(13)
O8—Cd1—O1	87.69(4)	O3—C3—C4	126.06(13)
O8—Cd1—O2	91.08(4)	C2—C3—C4	106.30(11)
O8—Cd1—O4^{i}	90.63(4)	O4—C4—C3	127.35(13)
O8—Cd1—O5^{i}	90.93(4)	O4—C4—C5	123.37(13)
O8—Cd1—O6	175.80(4)	C5—C4—C3	109.25(11)
C1—O1—Cd1	109.12(9)	O5—C5—C1	129.92(14)
C2—O2—Cd1	113.98(9)	O5—C5—C4	123.08(13)
C4—O4—Cd1^{ii}	112.03(10)	C4—C5—C1	106.98(12)
C5—O5—Cd1^{ii}	110.55(10)		

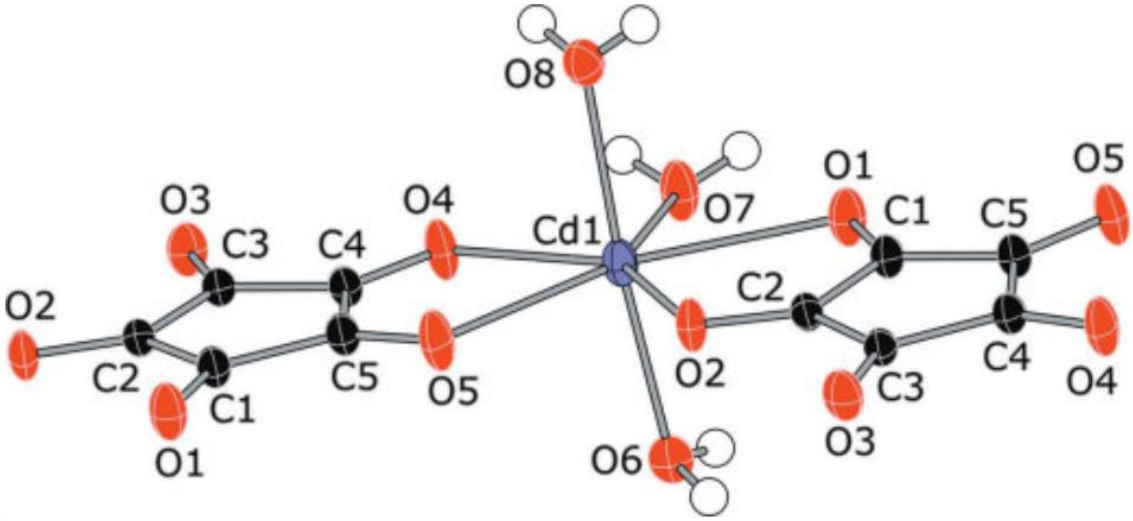

Figure 5.3: The structure of the repeat unit of **2**, showing the atom-labeling scheme. Displacement ellipsoids are drawn at the 50% probability level. Color coding: Cd purple, C black, O red, and H white.

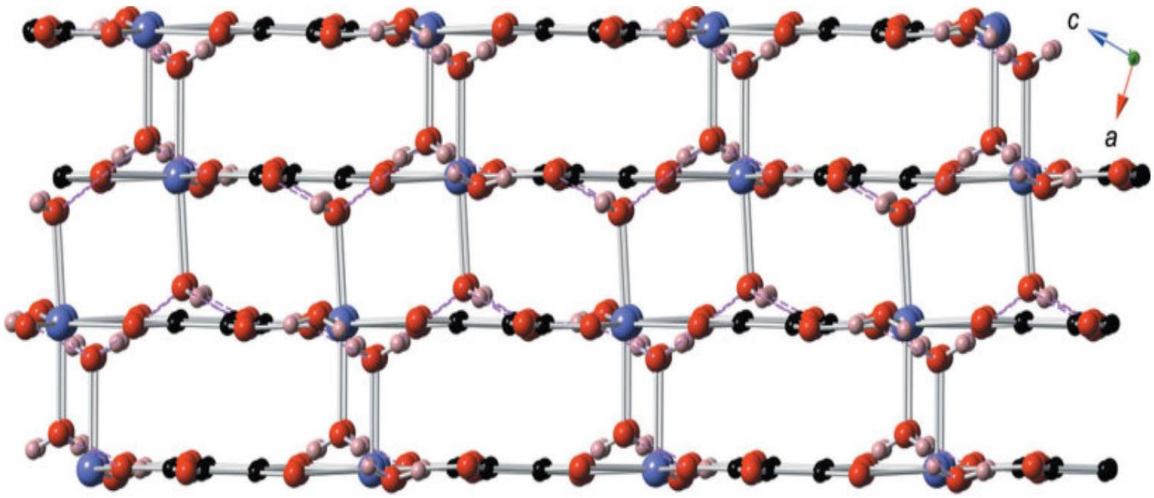

Figure 5.4: Crystal-packing diagram of **2**, viewed along the b axis. Hydrogen-bonding interactions are shown as magenta dashed lines. Color coding: Cd purple, C black, O red, and H pink.

5.4.4. FT–IR spectroscopy

Investigation into the FT-IR spectra for both compounds supports features of the X-ray analysis (Figures 5.5 and 5.6). Even after thorough drying under vacuum, both compounds show a broad absorption band indicative of a hydrogen-bonded water O—H

stretch (3209 cm^{-1} for the Pb(II) complex and 3168 cm^{-1} for the Cd(II) complex). The most prominent C=O stretching band shifts to lower energy relative to Na-croconate, with the heavier metal predictably causing a larger shift. For the Cd(II)-croconate and Pb(II)-croconate complexes, the most intense C=O band is at 1483 and 1458 cm^{-1}, respectively, while for Na-croconate it is at 1504 cm^{-1} (literature reports this band for the croconate anion at 1506 cm^{-1} [46]). This is suggestive of C=O—M binding to the metal cation. The number of C=O stretching bands is also in general agreement with the coordination modes as shown in the X-ray crystal structure. The Cd(II)-croconate complex features one additional asymmetric C=O stretch at 1594 cm^{-1}, while the Pb(II)-croconate complex has two such bands, at 1555 and 1585 cm^{-1}. Since the Pb(II)-croconate structure has lower overall symmetry than the Cd(II)-croconate structure, the higher number of FT-IR active bands of the former is expected.

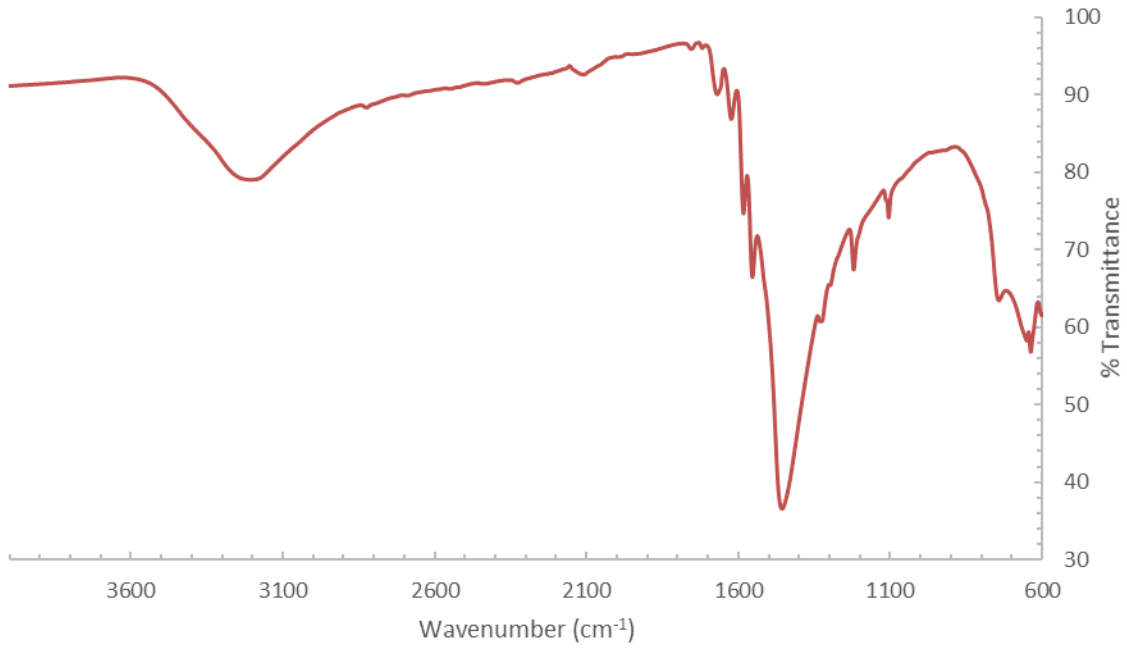

Figure 5.5: The FT-IR spectra of Pb(II)-croconate, **1**.

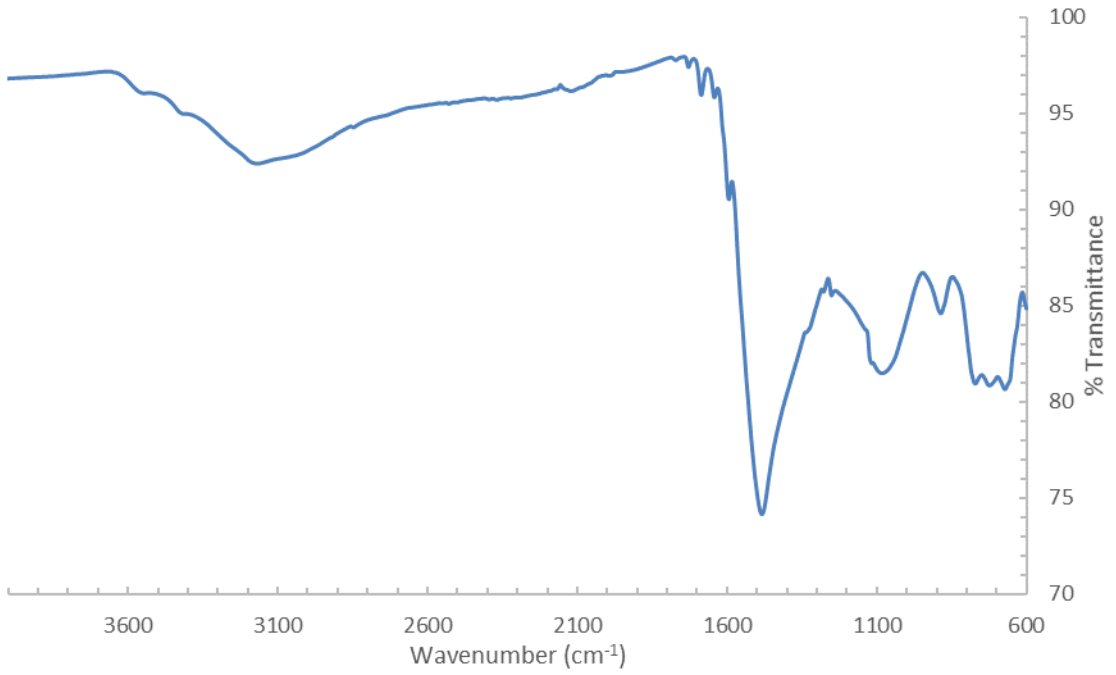

Figure 5.6: The FT-IR spectra of Cd(II)-croconate, **2**.

5.4.5. UV–Visible (UV–Vis) spectroscopy

UV–Vis titrations of Na-croconate solutions with Cd(II) or Pb(II) nitrate solutions were performed in order to determine the binding constants for formation of croconate complexes in solutions with Pb(II) (Figure 5.7) or Cd(II) (Figure 5.8). Croconate has a characteristic absorption band at 365 nm. Upon addition of Pb(II) or Cd(II) nitrate in 1:1 (v/v) water-ethanol, the band at 365 nm decreases in intensity. Applying the decrease in absorption to the 1:1 binding isotherm [47] gives excellent fittings to the 1:1 binding model, indicating that in solution, the Cd(II) and Pb(II) croconates exist as 1:1 complexes. Nonlinear regression analysis gives binding constants of K_{11} = 1.3 (± 0.3) x 10^5 M^{-1} for Cd(II)-croconate, leading to a free energy of complexation of ΔG = -29.2 (± 0.6) kJ mol^{-1}. The binding constant for Pb(II)-croconate is K_{11} = 1.6 (± 0.4) x 10^6 M^{-1}, leading to a free energy of complexation of ΔG = -35.3 (± 0.6) kJ mol^{-1}.

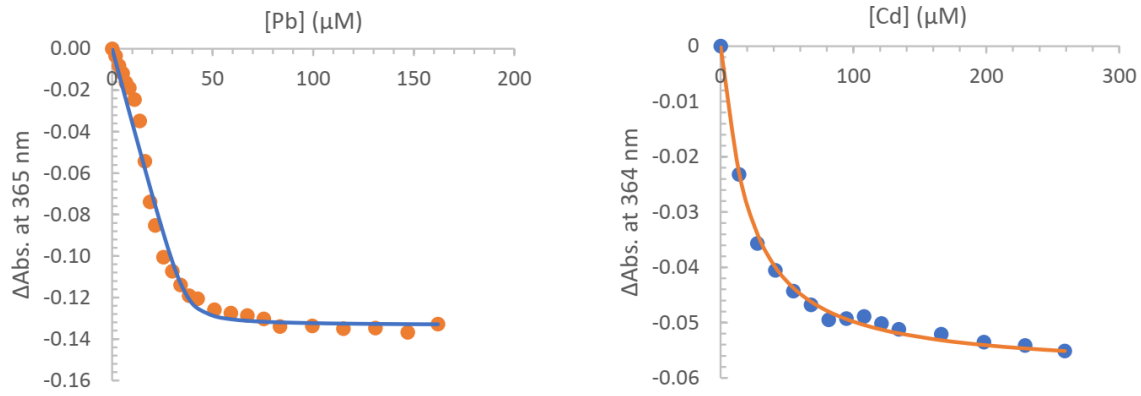

Figure 5.7 (left): Binding curve for the titration of a solution of 3.66 x 10^{-5} M of $Na_2C_5O_5$ with solution of 2.50 x 10^{-3} M of $Pb(NO_3)_2$ in 3.66 x 10^{-5} M of $Na_2C_5O_5$ in water/ethanol (50/50 v/v). K_{11} = 1.85 x 10^6 M^{-1}.

Figure 5.8 (right): Binding curve for the titration of a solution of 3.12 x 10^{-5} M of $Na_2C_5O_5$ with 8.29 x 10^{-3} M of $Cd(NO_3)_2 \cdot 4H_2O$ in 3.12 x 10^{-5} M of $Na_2C_5O_5$ in water/ethanol (50/50 v/v). K_{11} = 1.30 x 10^5 M^{-1}.

5.5. Conclusions

Two coordination polymer crystal structures for $\{[Pb(C_5O_5)(H_2O)_2] \cdot H_2O\}_n$ and $[Cd(C_5O_5)(H_2O)_3]_n$, are presented. Both complexes form 1D structures that are held together through hydrogen bonding between water molecules and the free O atom of coordinating croconate. While the Cd(II) chains are planar, the $6s^2$ lone-electron pair on the Pb atoms forces the Pb(II) atom into a distorted geometry with a nonplanar layer configuration. Hydrogen-bond interactions between adjacent zigzag chains of the Pb polymer form a ribbon-like structure. The complexation of Pb(II) is thermodynamically favored over that of Cd(II).

5.6. Acknowledgements

We would like to thank Dr. Indranil Chakraborty for useful discussions and suggestions.

5.7. Funding Information

Funding for this research was provided by: US Nuclear Regulatory Commission (NRC) fellowship grants (NRC-HQ-84-14-G-0040 and NRC-HQ-84-15-G-0038) to FIU, which supported JAS.

5.8. References

[1] Gmelin, L., *Ann. Phys. Chem.*, **1825**, *79*, 474–475.

[2] Dumestre, F., Soula, B., Galibert, A. M., Fabre, P. L., Bernardinelli, G., Donnadieu, B. & Castan, P., *J. Chem. Soc. Dalton Trans.*, **1998**, 4131–4137.

[3] Lam, C. K. & Mak, T. C. W., *Chem. Commun.*, **2001**, 1568–1569.

[4] Sain, S., Maji, T. K., Chaudhuri, N. R. & Zangrando, E., *Transition Met. Chem.*, **2002**, *27*, 716–719.

[5] Wang, C., Yang, C. H. & Lee, G. H., *Inorg. Chem.*, **2002**, *41*, 1015–1018.

[6] Wang, C., Yang, C. H., Tseng, S. M., Lee, G. H., Chiang, Y. P. & Sheu, H. S., *Inorg. Chem.*, **2003**, *42*, 8294–8299.

[7] Wang, C., Kuo, C. T., Yang, J. C., Lee, G. H., Shih, W. J. & Sheu, H. S., *Cryst. Growth Des.*, **2007**, *7*, 1476–1482.

[8] Wang, C., Tseng, S. M., Lin, S. Y., Liu, F. C., Dai, S. C., Lee, G. H., Shih, W. J. & Sheu, H. S., *Cryst. Growth Des.*, **2007**, *7*, 1783–1790.

[9] Maji, T. K., Konar, S., Mostafa, G., Zangrando, E., Lu, T. H. & Ray Chaudhuri, N., *Dalton Trans.*, **2003**, 171–175.

[10] Gale, P. A., Light, M. E. & Quesada, R., *Chem. Commun.*, **2005**, 5864–5866.

[11] Manna, S. C., Ghosh, A. K., Zangrando, E. & Chaudhuri, N. R., *Polyhedron*, **2007**, *26*, 1105–1112.

[12] Massoud, S. S., Williams, G. F., Louka, F. R., Henary, M. M., Herchel, R., Trávníček, Z., Fischer, R. C. & Mautner, F. A., *New J. Chem.*, **2017**, *41*, 3846–3856.

[13] Maruoka, K., Murase, N. & Yamamoto, H., *J. Org. Chem.*, **1993**, *58*, 2938–2939.

[14] Chen, C. & Suslick, K. S., *Coord. Chem. Rev.*, **1993**, *128*, 293–322.

[15] Hoskins, B. F. & Robson, R., *J. Am. Chem. Soc.*, **1990**, *112*, 1546–1554.

[16] Horiuchi, S. & Tokura, Y., *Nat. Mater.*, **2008**, *7*, 357–366.

[17] Stott, A. C., Vaid, T. P., Bylaska, E. J. & Dixon, D. A., *J. Phys. Chem. C*, **2012**, *116*, 8370–8378.

[18] Hendon, C. H., Tiana, D., Vaid, T. P. & Walsh, A., *J. Mater. Chem. C*, **2013**, *1*, 95–100.

[19] Turner, D. L., Vaid, T. P., Stephens, P. W., Stone, K. H., DiPasquale, A. G. & Rheingold, A. L., *J. Am. Chem. Soc.*, **2008**, *130*, 14–15.

[20] Kovalchukova, O. & Strashnova, S., *Rev. Inorg. Chem.*, **2014**, *34*, 1–24.

[21] Lam, C. K., Cheng, M. F., Li, C. L., Zhang, J. P., Chen, X. M., Li, W. K. & Mak, T. C. W., *Chem. Commun.*, **2004**, 448–449.

[22] Chen, H.-Y., Fang, Q., Xue, G. & Yu, W.-T., *Acta Cryst.*, **2005**, *E61*, o2696–o2698.

[23] Seitz, G. & Imming, P., *Chem. Rev.*, **1992**, *92*, 1227–1260.

[24] Baenziger, N. C. & Williams, D. G., *J. Am. Chem. Soc.*, **1966**, *88*, 689–692.

[25] Ranganathan, A. & Kulkarni, G. U., *J. Phys. Chem. A*, **2002**, *106*, 7813–7819.

[26] Braga, D., Maini, L. & Grepioni, F., *Chem. Eur. J.*, **2002**, *8*, 1804–1812.

[27] West, R. & Niu, H. Y., *J. Am. Chem. Soc.*, **1963**, *85*, 2586–2588.

[28] Bottei, R. S., Chang, H. S. & Lusardi, D. A., *J. Therm. Anal.*, **1979**, *16*, 389–397.

[29] Speier, G., Speier, E., Noll, B. & Pierpont, C. G., *Inorg. Chem.*, **1997**, *36*, 1520–1521.

[30] Ferreira, D. E. C., Dos Santos, H. F., Almeida, W. B. & Junqueira, G. M. A., *J. Braz. Chem. Soc.*, **2007**, *18*, 1379–1387.

[31] Deguenon, D., Bernardinelli, G., Tuchagues, J. P. & Castan, P., *Inorg. Chem.*, **1990**, *29*, 3031–3037.

[32] Deguenon, D., Castan, P. & Dahan, F., *Acta Cryst.*, **1991**, *C47*, 433–435.

[33] Groom, C. R., Bruno, I. J., Lightfoot, M. P. & Ward, S. C., *Acta Cryst.*, **2016**, *B72*, 171–179.

[34] Wang, C., Lin, H., Yang, C., Liao, C., Lan, I. & Lee, G., *New J. Chem.*, **2004**, *28*, 180–182.

[35] Gan, Q., Ronson, T. K., Vosburg, D. A., Thoburn, J. D. & Nitschke, J. R., *J. Am. Chem. Soc.*, **2015**, *137*, 1770–1773.

[36] Bruker, *APEX2* and *SAINT*, Bruker AXS Inc., Wisconsin, Madison, USA, **2015**.

[37] Sheldrick, G. M., *Acta Cryst.*, **2015**, *A71*, 3–8.

[38] Sheldrick, G. M., *Acta Cryst.*, **2015**, *C71*, 3–8.

[39] Dolomanov, O. V., Bourhis, L. J., Gildea, R. J., Howard, J. A. K. & Puschmann, H., *J. Appl. Cryst.*, **2009**, *42*, 339–341.

[40] Palmer, D. C., *CrystalMaker*, CrystalMaker Software Ltd, Begbroke, Oxfordshire, England, **2014**.

[41] Bruker, *SADABS*, Bruker AXS Inc., Madison, Wisconsin, USA, **2016**.

[42] Saunders, C. D. L., Longobardi, L. E., Burford, N., Lumsden, M. D., Werner-Zwanziger, U., Chen, B. & McDonald, R., *Inorg. Chem.*, **2011**, *50*, 2799–2810.

[43] Dale, S. H., Elsegood, M. R. J. & Kainth, S., *Acta Cryst.*, **2004**, *C60*, m76–m78.

[44] Kavallieratos, K., Rosenberg, J. M. & Bryan, J. C., *Inorg. Chem.*, **2005**, *44*, 2573–2575.

[45] Katz, M. J., Aguiar, P. M., Batchelor, R. J., Bokov, A. A., Ye, Z., Kroeker, S. & Leznoff, D. B., *J. Am. Chem. Soc.*, **2006**, *128*, 3669–3676.

[46] Santos, P. S., Sala, O., Noda, L. K. & Goncalves, N. S., *Spectrochim. Acta A Mol. Biomol. Spectrosc.*, **2000**, *56*, 1553–1562.

[47] Connors, K. A., In *Binding Constants: The Measurement of Molecular Complex Stability*, New York: Wiley-Interscience, **1987**.

CHAPTER VI. FORMATION OF 3D OXALATE MOFs THROUGH THE DECOMPOSITION OF RHODIZONATE

Joshua A. Silverman, Indranil Chakraborty, Raphael G. Raptis, Konstantinos Kavallieratos*

6.1 Abstract

Two novel MOFs, $Cd(ox)(H_2O)_2 \cdot H_2O$ (**1**) and $Yb(ox)_{1.5}(H_2O)_2 \cdot H_2O$ (**2**), were synthesized via prolonged decomposition of rhodizonate. UV-Vis experiments show that a 10^{-5} M aqueous solution of rhodizonate will decompose in 2 h, with the full transformation into croconate occurring after about one week. Mixed solvents, such as 50/50 v/v H_2O/CH_3OH, are shown to decrease substantially the decomposition rate of rhodizonate to croconate. After further time, some metal-croconates in aqueous solution will further decompose to metal-oxalate complexes. The oxalates of Cd(II) and Yb(III) have been isolated as 3D MOF structures. Cd(II)-ox has dual metal corners on its rectangular pore MOF. Yb(III)-ox has single Yb atoms on the vertices of its hexagonal pore MOF. Both form colorless block crystals that belong to the triclinic $P\bar{1}$ space group.

6.2 Introduction

Metal-organic frameworks (MOFs) have been the subject of much research over the last few decades owing to their potential application in gas separation, catalysis, near-infrared to ultraviolet optics, and medicine [1-22]. Special attention has been paid to proton-conducting materials based on MOFs [3, 7, 23-38]. Three-dimensional MOFs form pores, which allow for tunable architectures that can be configured for a variety of applications [7]. The choice of metal in the MOF plays a large role in the MOF properties and potential applications. MOFs containing transition metals, such as Cd(II), Cu(II),

Mn(II), and Zn(II), have been reported to have a catalytic effect in decarboxylation reactions [39-49]. MOFs containing lanthanides have unique properties and emission spectra, making them suitable for white LEDs, detection of ions and small molecules, and pH and temperature sensing [1, 50-57].

Oxalate has been shown to be a useful ligand in the construction of MOFs. Unlike the oxalate-containing MOFs reported in the literature [1, 3, 7, 13-15, 23, 39, 58-63], we did not use oxalate directly to make our MOFs. Instead, we reacted the metal salt with sodium rhodizonate in aqueous solution. The instability of rhodizonate in solution yields first croconate, then oxalate. An aqueous solution of 0.01 M sodium rhodizonate will completely decompose to the carboxy intermediate after about 36 hours. The transition to the five-membered croconate anion takes about one week. After several months, the croconate will decompose to oxalate and dihydroxymalonate [64].

While Ln(III)-oxalate structures are widely reported in the literature [59, 65-70], these structures are either 1D or 2D. Three dimensional Ln(III)-oxalate MOFs are quite rare [59, 66, 71]. We believe that our unique process of introducing oxalate into the metal chemical environment is responsible for the formation of these unique 3D structures. We present two such compounds, $Cd(ox)(H_2O)_2 \cdot H_2O$ (**1**) and $Yb(ox)_{1.5}(H_2O)_2 \cdot H_2O$ (**2**).

6.3 Experimental

6.3.1. Materials and Methods

3,4,5,6-Tetraoxocyclohexene-1,2-diol disodium salt (rhodizonic acid disodium salt) and $Cd(NO_3)_2 \cdot H_2O$, and $Yb(NO_3)_3 \cdot 6H_2O$ were purchased from Sigma–Aldrich. All chemicals were of reagent grade and were used without further purification. For all the

experiments, nanopure water, with a resistivity >17 M cm^{-1}, was used (Millipore by Barnstead Thermolyne Corporation, Dubuque, IA).

*6.3.2. Formation of the Cd–oxalate MOF, **1***

Cadmium oxalate crystals were formed by mixing sodium rhodizonate ($Na_2C_6O_6$; 45.2 mg, 0.243 mmol) and cadmium nitrate tetrahydrate [$Cd(NO_3)_2 \bullet 4H_2O$; 107.1 mg, 0.348 mmol] in deionized water (30 mL). After several months, colorless crystals formed.

*6.3.3. Formation of the Yb–oxalate MOF, **2***

Ytterbium oxalate crystals were formed by mixing sodium rhodizonate ($Na_2C_6O_6$; 44.9 mg, 0.242 mmol) and ytterbium nitrate hexahydrate [$Yb(NO_3)_3 \bullet 6H_2O$; 164.4 mg, 0.352 mmol] in deionized water (30 mL). After several months, colorless crystals formed.

6.3.3. Rhodizonate Decay Experiments

Solutions of 1.75 x 10^{-5} M $Na_2C_6O_6$ in water and water-miscible organic-solvent systems were placed in a cuvette and scanned in a Varian Cary 100 UV-Vis Spectrophotometer. Using water as a baseline, the solutions were scanned once every 5 min for 2 h (after 2 h, the water only sample had decomposed to the point in which its absorbance was 0).

6.3.4. X-ray Crystallography

Details of the X-ray crystallographic data collection, solution, and refinement are found on Table 1. All e.s.d.s (except the e.s.d. in the dihedral angle between two l.s. planes) are estimated using the full covariance matrix. The cell e.s.d.s are considered individually in the estimation of e.s.d.s in distances, angles and torsion angles; correlations between e.s.d.s in cell parameters are only used when they are defined by crystal symmetry. An approximate treatment of cell e.s.d.s is used for estimating e.s.d.s involving l.s. planes.

Table 6.1: Experimental crystallographic details of Yb(III) and Cd(II) oxalates. Experiments were carried out with Mo *Kα* radiation using a Bruker D8 Quest diffractometer with a PHOTON II detector. Computer programs: SAINT V8.40B [72], APEX3 [72], SHELXT [73], SHELXL [74], OLEX2 [75].

Crystal data	**1**	**2**
Chemical formula	$Cd(ox)(H_2O)_2 \bullet H_2O$	$Yb(ox)_{1.5}(H_2O)_2 \bullet H_2O$
M_r	254.47	359.12
Crystal system, space group	Triclinic, $P\bar{1}$	Triclinic, $P\bar{1}$
Temperature (K)	170	298
a, *b*, *c* (Å)	5.9926(7), 6.5986(8), 8.4598(11)	6.2630(7), 6.6376(7), 9.5866(10)
α, *β*, *γ* (º)	74.660(2), 74.323(2), 81.157(2)	75.074(2), 80.722(2), 81.783(2)
V (Å^3)	309.38(7)	377.89(7)
Z	2	2
μ (mm^{-1})	3.51	12.40
Crystal size (mm)	0.21 x 0.18 x 0.15	0.20 x 0.15 x 0.10
F(000)	244	332
D_x (Mg m^{-3})	2.732	3.156
Mo *Kα* radiation, λ (Å)	0.71076	0.71076
Cell parameter reflections	3074	7627
θ range (º)	2.6-25.3	2.5-24.9
Shape and color	Block, colorless	Block, colorless
Data collection		
T_{min}, T_{max}	0.589, 0.745	0.587, 0.746
No. of measured, Independent and observed [$I > 2\sigma(I)$] reflections	3068, 1025, 1024	5030, 1734, 1729
R_{int}	0.024	0.021
(sin θ/λ) (Å^{-1})	0.601	0.671
h	-7 → 7	-8 → 8
k	-7 → 7	-8 → 8
l	-9 → 10	-12 → 12
Refinement		
$R[F^2 > 2\sigma(F^2)]$, $wR(F^2)$, *S*	0.020, 0.052, 1.10	0.021, 0.052, 1.20
No. of reflections	1025	1734
No. of parameters	96	123
No. of restraints	0	0
H-atom treatment	H-atoms parameters constrained	H-atom parameters constrained
$\Delta\rho_{max}$, $\Delta\rho_{min}$, (e Å^{-3})	0.68, -0.58	1.21, -2.16

6.4 Results and Discussion

6.4.1. Synthesis

Cd(II)-rhodizonate complexes are readily precipitated as a thick layer of red powder by reacting $Cd(NO_3)_2 \cdot 4H_2O$ with $Na_2C_6O_6$ in aqueous solutions. After several months, the red powder remained, but on top of the red powder layer colorless rectangular crystals suitable for single-crystal X-ray analysis were formed. Yb(III)-rhodizonate complexes precipitate as a very thin layer of pink powder by reacting $Yb(NO_3)_3 \cdot 6H_2O$ with $Na_2C_6O_6$ in aqueous solutions. Unlike the Cd(II) complex, after several months, the pink powder disappeared, and in its place were blocks of colorless crystals suitable for single-crystal X-ray analysis.

6.4.2. Rhodizonate Decay Experiments

UV-Vis studies showed that rho immediately begins to decompose in aqueous solutions [76]. After 2 h, an amount of Na-rho suitable for UV-Vis spectroscopy ($\sim 10^{-5}$ M) in water solvent will lose its absorbance at 482 nm after 2 h. Several water-miscible organic solvent systems in 1:1 (v/v) concentrations were tested in an attempt to extend the useful UV-Vis spectroscopic lifetime of rhodizonate (Figure 6.1). These studies showed that Na-rho is stable for over 2 h in a 1:1 water/ethanol (v/v) solution allowing for titration experiments to be performed that can reliably investigate the system. Specifically, a 1:1 $EtOH/H_2O$ (v/v) mixture maintains stability of rhodizonate with 89.9% of initial absorbance maintained for over 120 min.

Figure 6.2 shows that there is a relationship between the dielectric constant of the solvent and how well rhodizonate resists decomposition in solution. The dielectric constant of a solvent is a measure of how polar the solvent is. As shown in Figures 6.1 and 6.2, the

less polar the solvent (i.e., the lower its dielectric constant), the longer rhodizonate remains in solution as rhodizonate dianion. Rhodizonate is a large molecule with a relatively low ionic charge. It is also no coincidence that the solvents tested which performed the best for preserving rhodizonate in solution are also the bulkiest molecules. Cd(II), Pb(II), and Hg(II) form 1:1 metal/rhodizonate complexes in solution, but show higher ratios of metal/rhodizonate in the solid state. Meanwhile, many of the lanthanides, Ln(III)-rhodizonate complexes exist in a 1:1 Ln(III)/rhodizonate ratio both in the solid state and in solution. We hypothesize that the organic portion of the mixed solvent system interacts with either the rhodizonate or the metal coordination sphere, preventing polymerization and keeping the complexes in solution, also preventing the decomposition reaction. Rhodizonate is not stable in perpetuity even in H_2O/organic solvent mixtures (Fig. 6.1 and 6.2), and, indeed, if a titration experiment lasts too long (> 2h), precipitates start to form in the cuvette, eventually bringing the titration experiment to a premature end.

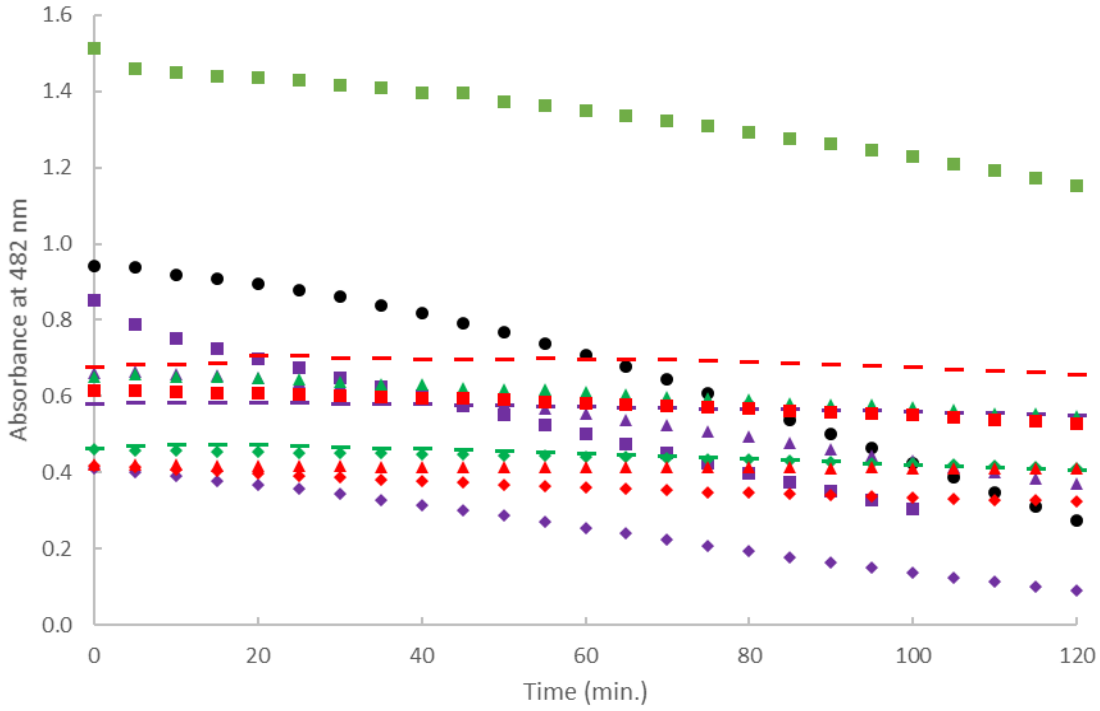

Figure 6.1: The absorbance at 482 nm of a 1.75 x 10^{-5} M solution of sodium rhodizonate in various solvent mixtures. Pure water is shown in black circles. 75% water mixtures are shown in red; 50% water mixtures are shown in green; 25% water mixtures are shown in purple. Methanol mixes are squares; ethanol mixes are diamonds; acetone mixtures are triangles; acetonitrile mixes are dashes.

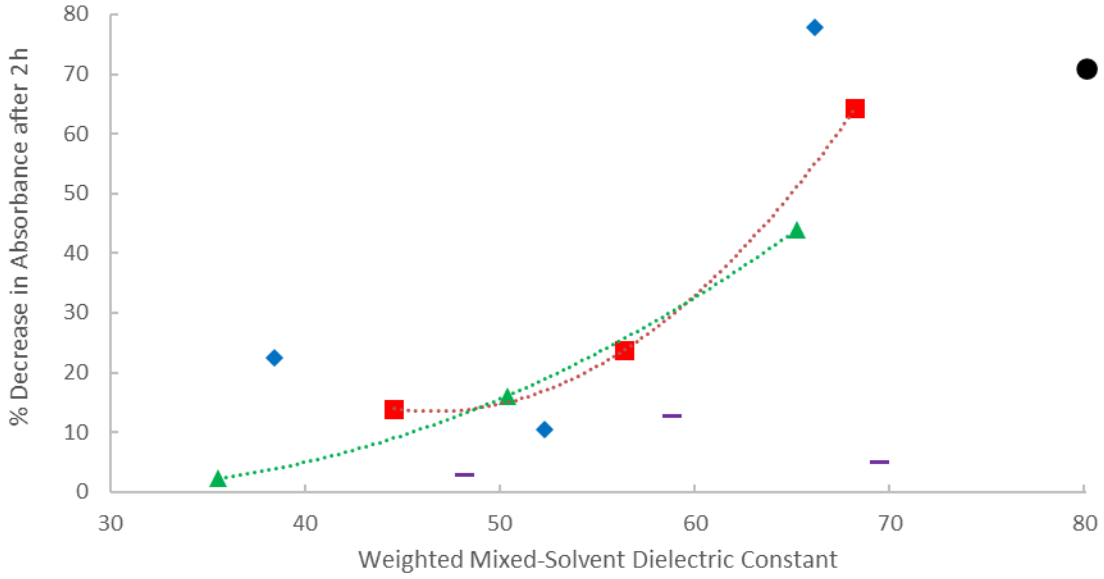

Figure 6.2: The relationship between solvent dielectric constant and the decrease in absorbance at 482 nm reflected in Figure 6.1. Pure water is shown as a black circle. Methanol mixes are red squares; ethanol mixes are blue diamonds; acetone mixtures are green triangles; acetonitrile mixes are purple dashes.

6.4.3. Crystal Structure Descriptions

*6.4.3.1. Cd-oxalate MOF, **1***

Compound **1** crystalizes in the triclinic space group $P\bar{1}$ with one Cd(II) center, two oxalate anions, two water molecules, and an extra interstitial water molecule per asymmetric unit. All of compound **1**'s geometric parameters are shown in Tables 6.2 through 6.4.

Table 6.2: Fractional atomic coordinates and isotropic or equivalent isotropic displacement parameters (Å^2)

Atom	*x*	*y*	*z*	U_{iso}*/U_{eq}
Cd01	0.54935(3)	0.80934(3)	0.70592	0.00649(14)
O002	0.3791(4)	1.2512(3)	1.0249(3)	0.0109(4)
O003	0.4153(4)	1.1064(4)	0.8094(3)	0.0114(5)
O004	0.2247(4)	0.6433(3)	0.8870(3)	0.0123(5)
H00A	0.259015	0.507483	0.917879	0.019*
H00B	0.116279	0.652751	0.833509	0.019*
O005	1.0427(4)	1.2226(3)	0.3339(3)	0.0121(5)
O006	0.7213(4)	1.0562(3)	0.4637(3)	0.0105(4)
O007	0.6531(4)	0.5031(4)	0.6156(3)	0.0168(5)
H00C	0.699505	0.531085	0.507045	0.025*
H00D	0.532657	0.434839	0.636878	0.025*
C008	0.4403(5)	1.1023(4)	0.9517(4)	0.0079(6)
O009	0.9365(4)	0.2393(5)	0.7976(3)	0.0240(6)
H00E	1.082028	0.207223	0.786078	0.036*
H00F	0.885975	0.247740	0.899909	0.036*
C00A	0.9333(5)	1.0807(5)	0.4409(4)	0.0075(6)

Table 6.3: Atomic displacement parameters (Å^2)

Atom	U^{11}	U^{22}	U^{33}	U^{12}	U^{13}	U^{23}
Cd01	0.00547(17)	0.00743(17)	0.00642(17)	-0.00043(9)	-0.00197(10)	-0.00090(9)
O002	0.0146(11)	0.0093(10)	0.0094(10)	0.0024(8)	-0.0053(8)	-0.0030(8)
O003	0.0140(11)	0.0112(11)	0.0098(11)	0.0025(9)	-0.0063(9)	-0.0024(8)
O004	0.0084(11)	0.0114(11)	0.0160(11)	-0.0012(8)	-0.0062(9)	0.0026(9)
O005	0.0092(11)	0.0131(11)	0.0126(11)	-0.0034(8)	-0.0044(8)	0.0027(8)
O006	0.0057(10)	0.0144(11)	0.0101(10)	-0.0024(8)	-0.0031(8)	0.0016(8)
O007	0.0168(12)	0.0149(12)	0.0207(12)	-0.0006(9)	-0.0048(10)	-0.0081(10)
C008	0.0047(13)	0.0093(14)	0.0087(13)	-0.0013(11)	-0.0012(11)	-0.0007(11)
O009	0.0173(13)	0.0295(13)	0.0284(15)	0.0064(10)	-0.0107(11)	-0.0117(11)
C00A	0.0076(14)	0.0109(14)	0.0057(13)	-0.0002(11)	-0.0034(11)	-0.0032(11)

Table 6.4: Geometric parameters (Å, º) Symmetry codes: (i) -*x*+1 , -*y*+2, -*z*+2; (ii) -*x*+2 , -*y*+2, -*z*+1; (iii) -*x*+1, -*y*+2, -*z*+1.

Cd01-O002^{i}	2.350(2)	O002-C008	1.253(4)
Cd01-O003	2.302(2)	O003-C008	1.246(4)
Cd01-O004	2.343(2)	O005-C00A	1.243(4)
Cd01-O005^{ii}	2.360(2)	O006-C00A	1.261(4)
Cd01-O006	2.350(2)	C008-C008^{i}	1.561(6)
Cd01-O006^{iii}	2.371(2)	C00A-C00A^{ii}	1.543(6)
Cd01-O007	2.287(2)		

O002^{i}-Cd01-O005^{ii}	73.51(8)	O007-Cd01-O004	85.76(9)
O002^{i}-Cd01-O006^{iii}	146.36(7)	O007-Cd01-O005^{ii}	78.39(8)
O002^{i}-Cd01-O006	125.86(8)	O007-Cd01-O006	101.17(9)
O003-Cd01-O002^{i}	71.23(8)	O007-Cd01-O006^{iii}	94.59(8)
O003-Cd01-O004	89.45(8)	C008-O002-Cd01^{i}	116.62(18)
O003-Cd01-O005^{ii}	105.84(8)	C008-O003-Cd01	117.43(19)
O003-Cd01-O006	82.72(8)	C00A-O005-Cd01^{ii}	117.41(19)
O003-Cd01-O006^{iii}	83.94(8)	Cd01-O006-Cd01^{iii}	109.36(8)
O004-Cd01-O002^{i}	76.38(8)	C00A-O006-Cd01^{iii}	132.55(19)
O004-Cd01-O005^{ii}	139.26(8)	C00A-O006-Cd01	117.82(19)
O004-Cd01-O006	151.34(7)	O002-C008-C008^{i}	116.4(3)
O004-Cd01-O006^{iii}	81.17(7)	O003-C008-O002	125.3(3)
O005^{ii}-Cd01-O006^{iii}	136.86(7)	O003-C008-C008^{i}	118.3(3)
O006-Cd01-O005^{ii}	69.22(7)	O005-C00A-O006	126.2(3)
O006-Cd01-O006^{iii}	70.64(8)	O005-C00A-C00A^{ii}	117.5(3)
O007-Cd01-O002^{i}	108.23(8)	O006-C00A-C00A^{ii}	116.3(3)
O007-Cd01-O003	175.15(8)		

The Cd atom is seven coordinate, bonding with each of two O atoms on two different oxalates, one O on a third oxalate, and two water molecules within its coordination sphere. Another interstitial water molecule lies within the Cd atom's coordination sphere. Another Cd atom, with an identical coordination sphere (bonding to the other O atom on the third oxalate), forms the corners of the greater MOF structure (Figures 6.3 through 6.5). Hydrogen bonding further binds the Cd center to oxalate.

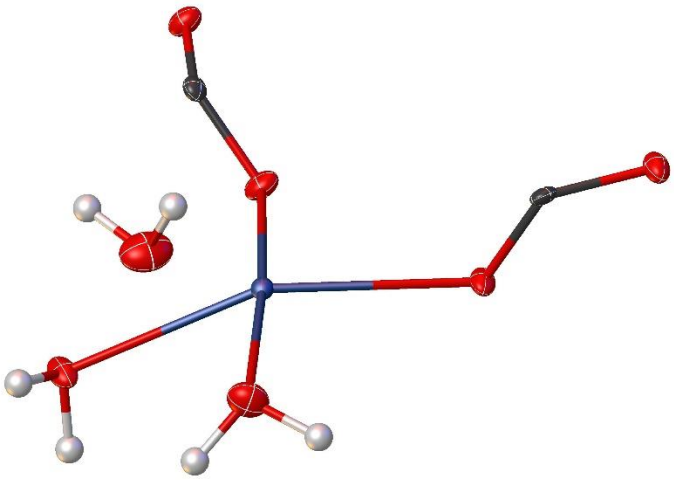

Figure 6.3: The asymmetric unit of **1**. Displacement ellipsoids calculated at the 50% probability level. Color coding: Cd purple, C black, O red, H white.

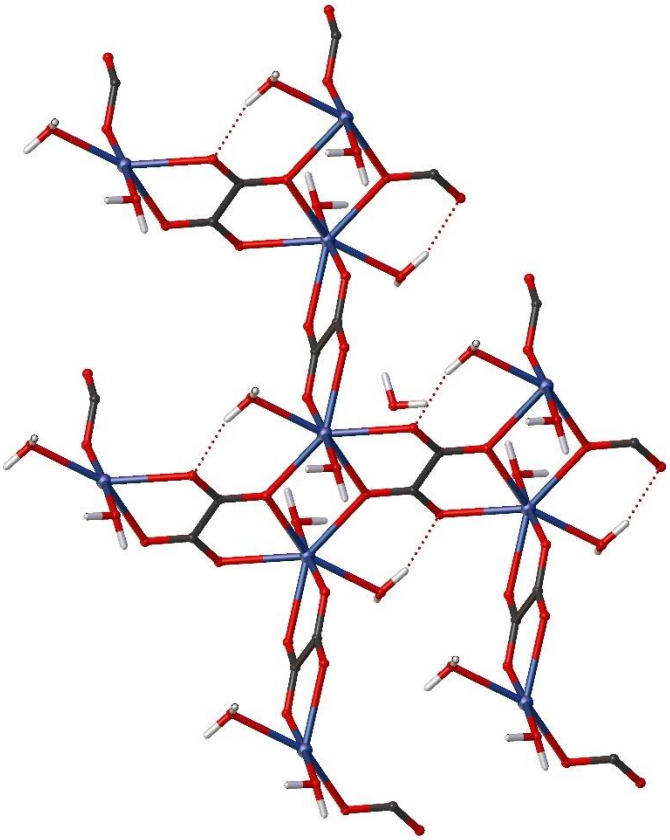

Figure 6.4: A closeup of the corners of the **1** MOF. Color coding: Cd purple, C black, O red, H white.

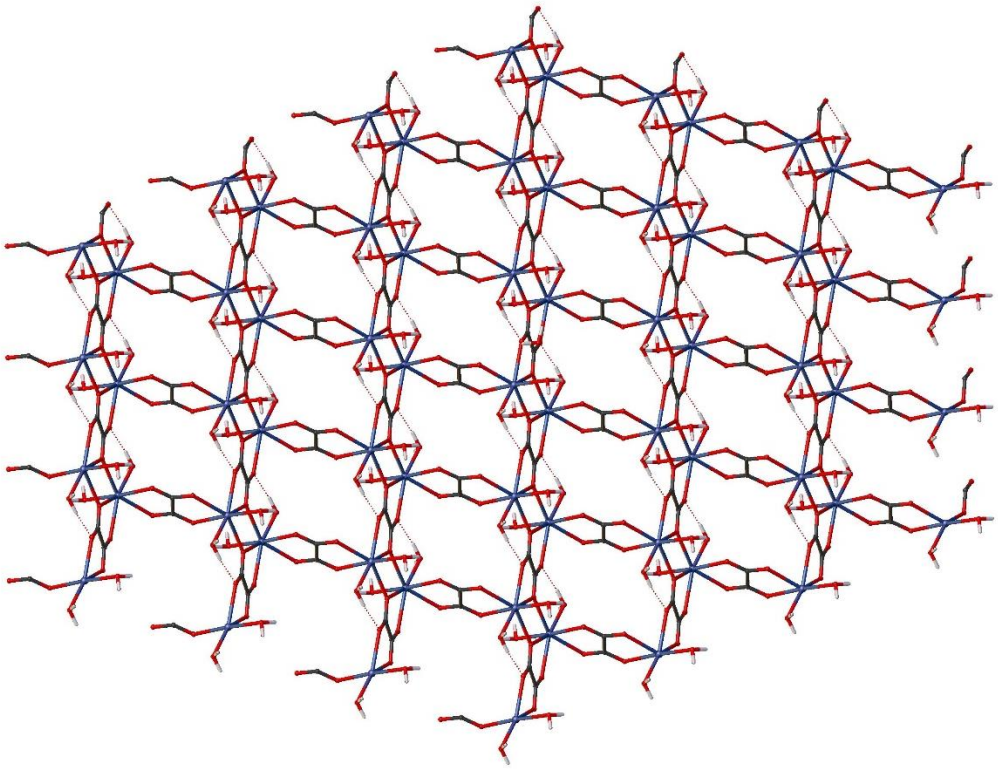

Figure 6.5: Crystal-packing diagram of **1**. Hydrogen-bonding interactions are shown as red dashed lines. Color coding: Cd purple, C black, O red, and H pink.

*6.4.3.2. Yb-oxalate MOF, **2***

Compound **2** crystalizes in the triclinic space group $P\overline{1}$ with one Yb(III) center, three oxalate anions, two water molecules, and an extra interstitial water molecule per asymmetric unit. All of compound **2**'s geometric parameters are shown in Tables 6.5 through 6.7.

Table 6.5: Fractional atomic coordinates and isotropic or equivalent isotropic displacement parameters (Å^2)

Atom	*x*	*y*	*z*	*Uiso*/Ueq*
Yb1	0.19805(2)	0.69096(2)	0.19296(2)	0.01083(8)
O1	0.2198(5)	0.4081(5)	0.0955(4)	0.0193(6)
O2	0.0735(5)	0.2594(5)	-0.0446(3)	0.0161(5)
O3	0.2202(5)	0.6467(5)	0.4367(3)	0.0197(6)
O4	0.0853(5)	0.4974(5)	0.6637(3)	0.0207(6)
O5	0.4379(5)	0.9294(5)	0.1884(3)	0.0181(6)
O6	0.6514(5)	1.1659(5)	0.0482(3)	0.0152(5)
O7	0.5170(6)	0.4654(6)	0.2344(4)	0.0263(7)
H7A	0.635598	0.534375	0.207807	0.039*
H7B	0.541828	0.374925	0.177157	0.039*
O8	-0.0424(6)	0.9655(5)	0.2536(4)	0.0233(6)
H8A	-0.117555	1.032681	0.180436	0.035*
H8B	0.027444	1.066670	0.265757	0.035*
C1	0.0846(6)	0.4033(6)	0.0147(4)	0.0136(7)
C2	0.0883(7)	0.5415(6)	0.5285(5)	0.0156(7)
C3	0.5247(6)	1.0265(6)	0.0681(4)	0.0132(7)
O9	-0.2724(14)	0.9122(13)	0.5244(7)	0.075(2)
H9A	-0.249009	1.031086	0.533175	0.112*
H9B	-0.401202	0.887819	0.562590	0.112*

Table 6.6: Atomic displacement parameters (Å^2)

Atom	U^{11}	U^{22}	U^{33}	U^{12}	U^{13}	U^{23}
Yb1	0.01159(11)	0.01276(11)	0.00875(10)	-0.00496(6)	-0.00068(6)	-0.00205(6)
O1	0.0184(14)	0.0177(13)	0.0266(15)	0.0024(11)	-0.0134(12)	-0.0102(12)
O2	0.0170(14)	0.0155(13)	0.0182(13)	-0.0009(10)	-0.0039(11)	-0.0074(11)
O3	0.0198(14)	0.0286(16)	0.0121(13)	-0.0126(12)	-0.0026(11)	-0.0018(11)
O4	0.0219(15)	0.0296(16)	0.0117(13)	-0.0133(12)	-0.0025(11)	-0.0012(11)
O5	0.0213(15)	0.0210(14)	0.0127(13)	-0.0104(12)	-0.0014(11)	-0.0015(11)
O6	0.0165(13)	0.0158(13)	0.0136(12)	-0.0069(10)	-0.0002(10)	-0.0025(10)
O7	0.0181(15)	0.0327(17)	0.0346(18)	0.0032(13)	-0.0098(13)	-0.0192(15)
O8	0.0261(16)	0.0210(15)	0.0230(15)	0.0020(12)	-0.0053(13)	-0.0067(12)
C1	0.0116(16)	0.0132(16)	0.0151(17)	-0.0037(13)	0.0021(13)	-0.0027(13)
C2	0.0167(18)	0.0158(17)	0.0155(18)	-0.0036(14)	-0.0041(14)	-0.0039(14)
C3	0.0124(16)	0.0116(16)	0.0152(17)	0.0008(13)	-0.0022(14)	-0.0035(13)
O9	0.096(5)	0.093(5)	0.045(3)	-0.040(4)	0.014(3)	-0.031(3)

Table 6.7: Geometric parameters (Å, º) Symmetry codes: (i) -*x*, -*y*+1, -*z*; (ii) -*x*, -*y*+1, -*z*+1; (iii) -*x*+1, -*y*+2, -*z*.

Yb1-O1	2.282(3)	O1-C1	1.244(5)
Yb1-O2^{i}	2.324(3)	O2-C1	1.246(5)
Yb1-O3	2.304(3)	O3-C2	1.248(5)
Yb1-O4^{ii}	2.359(3)	O4-C2	1.251(5)
Yb1-O5	2.321(3)	O5-C3	1.247(5)
Yb1-O6^{iii}	2.357(3)	O6-C3	1.262(5)
Yb1-O7	2.342(3)	C1-C1^{i}	1.540(8)
Yb1-O8	2.325(3)	C2-C2^{ii}	1.533(8)
Yb1-C3^{iii}	3.148(4)	C3-C3^{iii}	1.524(8)

O1-Yb1-O2^{i}	70.44(10)	O7-Yb1-O4^{ii}	105.05(13)
O1-Yb1-O3	120.73(12)	O7-Yb1-O6^{iii}	90.86(12)
O1-Yb1-O4^{ii}	77.04(12)	O7-Yb1-C3^{iii}	87.71(12)
O1-Yb1-O5	134.11(12)	O8-Yb1-O4^{ii}	79.93(12)
O1-Yb1-O6^{iii}	79.65(11)	O8-Yb1-O6^{iii}	103.55(11)
O1-Yb1-O7	67.77(11)	O8-Yb1-O7	147.86(12)
O1-Yb1-O8	142.51(12)	O8-Yb1-C3^{iii}	95.71(11)
O1-Yb1-C3^{iii}	97.46(11)	C1-O1-Yb1	119.2(3)
O2^{i}-Yb1-O4^{ii}	74.37(11)	C1-O2-Yb1^{i}	117.0(3)
O2^{i}-Yb1-O6^{iii}	72.11(11)	C2-O3-Yb1	118.9(3)
O2^{i}-Yb1-O7	137.03(11)	C2-O4-Yb1^{ii}	117.5(3)
O2^{i}-Yb1-O8	75.10(11)	C3-O5-Yb1	118.6(3)
O2^{i}-Yb1-C3^{iii}	88.14(10)	C3-O6-Yb1^{iii}	117.6(3)
O3-Yb1-O2^{i}	137.46(11)	O1-C1-Yb1^{i}	168.7(3)
O3-Yb1-O4^{ii}	69.67(11)	O1-C1-O2	126.7(4)
O3-Yb1-O5	77.78(11)	O1-C1-C1^{i}	116.1(4)
O3-Yb1-O6^{iii}	146.35(11)	O2-C1-Yb1^{i}	42.0(2)
O3-Yb1-O7	75.38(12)	O1-C1-C1^{i}	117.2(4)
O3-Yb1-O8	76.92(12)	C1^{i}-C1-Yb1^{i}	75.3(3)
O3-Yb1-C3^{iii}	126.16(10)	O3-C2-Yb1^{ii}	167.8(3)
O4^{ii}-Yb1-C3^{iii}	162.50(10)	O3-C2-O4	126.2(4)
O5-Yb1-O2^{i}	126.41(11)	O3-C2-C2^{ii}	117.5(5)
O5-Yb1-O4^{ii}	144.46(11)	O4-C2-Yb1^{ii}	41.8(2)
O5-Yb1-O6^{iii}	69.47(10)	O4-C2-C2^{ii}	116.3(5)
O5-Yb1-O7	79.34(12)	C2^{ii}-C2-Yb1^{ii}	74.6(3)
O5-Yb1-O8	79.17(12)	O5-C3-O6	125.9(4)
O5-Yb1-C3^{iii}	48.71(10)	O5-C3-C3^{iii}	117.8(4)
O6^{iii}-Yb1-O4^{ii}	143.97(10)	O6-C3-C3^{iii}	116.3(4)
O6^{iii}-Yb1-C3^{iii}	20.80(10)		

The Yb atom is eight coordinate, bonding with each of two O atoms on three different oxalates and two water molecules within its coordination sphere. Another interstitial water molecule lies within the Yb atom's coordination sphere. The entire Yb coordination sphere takes a Y-like shape, similar to that of Dy in its 3D MOF oxalate structure [71] (Figure 6.6). Hydrogen bonding further binds the Yb-centered moieties together.

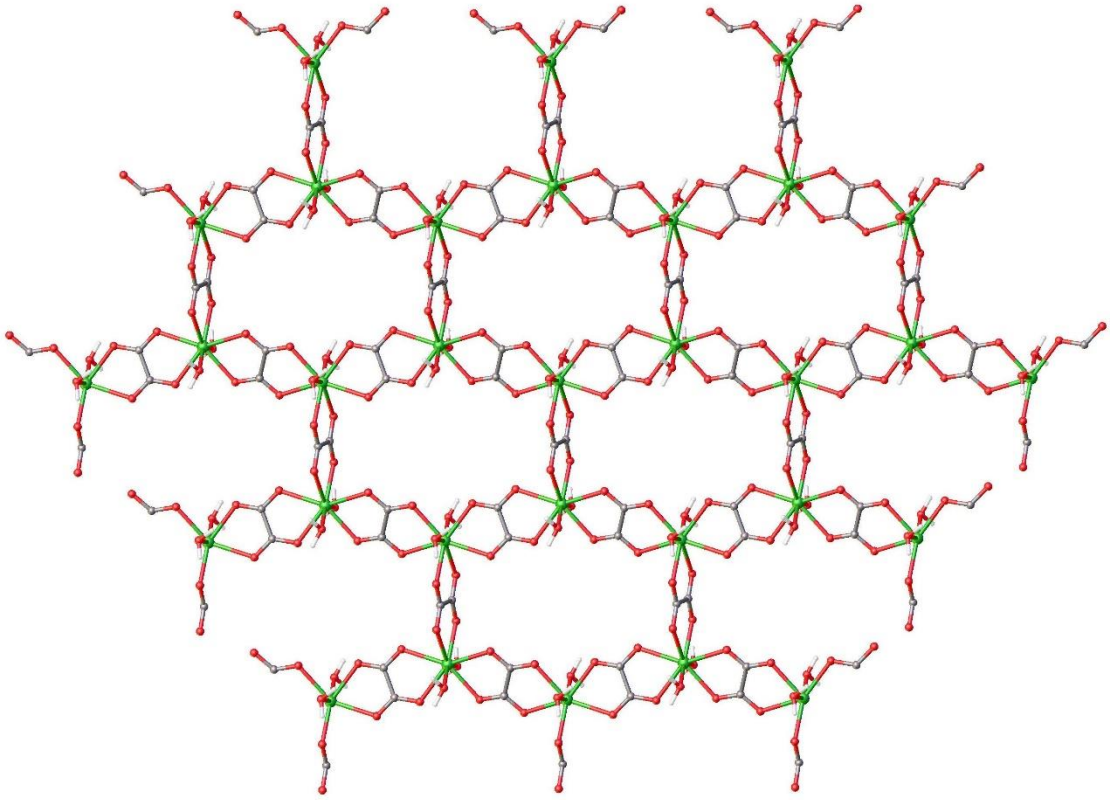

Figure 6.6: Crystal-packing diagram of **2**. Color coding: Yb green, C grey, O red, and H white.

6.5 Conclusion

Through the decomposition of rhodizonate we were able to form two previously unreported 3D MOFs. It is presumed that the specific pathway of rhodizonate decomposition to croconate, and further decomposition to oxalate, along with metal complexation during these steps is responsible for the formation of the 3D MOF structure.

The Cd(II) MOF has vertices that are composed of two Cd(II) atoms, with the parts of each pore held together through cross coordination and H-bonding. The Yb(III) MOF has a much simpler structure, with each Yb(III) atom serving as the center through which three oxalate molecules are coordinated.

6.6 References

[1] Yang, Y., Huang, H., Wang, Y., Qiu, F., Feng, Y., Song, X., Tang, X., Zhang, G., Liu, W., *Dalton Trans.,* **2018,** *47,* 13384-13390.

[2] Easterday, R., Sanchez-Felix, O., Losovyj, Y., Pink, M., Stein, B. D., Morgan, D. G., Rakitin, M., Doluda, V. Y., Sulman, M. G., Mahmoud, W. E., Al-Ghamdi, A. A., Bronstein, L. M., *Catal. Sci. Technol.,* **2015,** *5,* 1902.

[3] Tang, Q., Liu, Y., Liu, S., He, D., Miao, J., Wang, X., Yang, G., Shi, Z., Zheng, Z., *J. Am. Chem. Soc.,* **2014,** *136,* 12444-12449.

[4] Li, J.-R., Kuppler, R. J., Zhou, H.-C. *Chem. Soc. Rev.* **2009**, *38*, 1477−1504.

[5] Suh, M. P., Park, H. J., Prasad, T. K., Lim, D.-W. *Chem. Rev.* **2011**, *112*, 782−835.

[6] Li, J.-R., Sculley, J., Zhou, H.-C. *Chem. Rev.* **2011**, *112*, 869−932.

[7] Sadakiyo, M., Okawa, H., Shigematsu, A., Ohba, M., Yamada, T., Kitagawa, H., *J. Am. Chem. Soc.,* **2012,** *134,* 5472-5475.

[8] Matsuda, R., Kitaura, R., Kitagawa, S., Kubota, Y., Belosludov, R. V., Kobayashi, T. C., Sakamoto, H., Chiba, T., Takata, M., Kawazoe, Y., Mita, Y., *Nature*, **2005**, *436*, 238−241.

[9] Shimomura, S., Higuchi, M., Matsuda, R., Yoneda, K., Hijikata, Y., Kubota, Y., Mita, Y., Kim, J., Takata, M., Kitagawa, S., *Nat. Chem.,* **2010**, *2*, 633− 637.

[10] Bourrelly, S., Llewellyn, P. L., Serre, C., Millange, F., Loiseau, T., Ferey, G., *J. Am. Chem. Soc.*, **2005**, *127*, 13519−13521.

[11] Sadakiyo, M., Yamada, T., Kitagawa, H., *J. Am. Chem. Soc.* **2011**, *133*, 11050−11053.

[12] Kabachii, Y. A., Golub, A. S., Kochev, S. Y., Lenenko, N. D., Abramchuk, S. S., Antipin, M. Y., Valetsky, P. M., Stein, B. D., Mahmoud, W. E., Al-Ghamdi, A. A., Bronstein, L. M., *Chem. Mater.,* **2013,** *25,* 2434.

[13] Sadakiyo, M., Yamada, T., Kitagawa, H., *J. Am. Chem. Soc.,* **2009,** *131,* 9906-9907.

[14] Wang, H., Liu, S.-J., Tian, D., Jia, J.-M., Hu, T.-L., *Cryst. Growth Des.,* **2012,** *12,* 3263-3270.

[15] Biswas, S., Chakraborty, J., Parmar, V. S., Bera, S. P., Ganguli, N., Konar, S., *Inorg. Chem.,* **2017,** *56,* 4956-4965.

[16] Cui, Y., Yue, Y., Qian, G., Chen, B., *Chem. Rev.* **2012,** *112,* 1126.

[17] Allendorf, M. D., Bauer, C. A., Bhakta, R. K., Houk, R. J. T., *Chem. Soc. Rev.,* **2009,** *38,* 1330.

[18] Rocha, J., Carlos, L. D., Paz, F. A. A., Ananias, D., *Chem. Soc. Rev.,* **2011,** *40,* 926.

[19] Mahmoud, W. E., *Sens. Actuators B,* **2017,** *238,* 1001.

[20] Hu, Z., Deibert, B. J., Li, J., *Chem. Soc. Rev.,* **2014,** *43,* 5815.

[21] Mahmoud, W. E., *Mater. Lett.,* **2016,** *177,* 42.

[22] Bétard, A., Fischer, R. A., *Chem. Rev.,* **2012,** *112,* 1055.

[23] Ōkawa, H., Sadakiyo, M., Yamada, T., Maesato, M., Ohba, M., Kitagawa, H., *J. Am. Chem. Soc.,* **2013,** *135,* 2256-2262.

[24] Akutsu-Sato, A., Akutsu, H., Turner, S. S., Day, P., Probert, M. R., Howard, J. A. K., Akutagawa, T., Takeda, S., Nakamura, T., Mori, T., *Angew. Chem.,* **2005**, *117*, 296.

[25] Fujishima, M., Kanda, S., Mitani, T., Kitagawa, H., *Synth. Met.,* **2001**, *119*, 485.

[26] Nagao, Y., Ikeda, R., Kanda, S., Kubozono Y., Kitagawa, H., *Mol. Cryst. Liq. Cryst.,* **2002**, *379*, 89.

[27] Nagao, Y., Fujishima, M., Kanda, S., Ikeda, R., Kitagawa, H., *Synth. Met.*, **2003**, *133*, 431.

[28] Nagao, Y., Ikeda, R., Iijima, K., Kubo, T., Nakasuji, K., Kitagawa, H., *Synth. Met.*, **2003**, *135*, 283.

[29] Nagao, Y., Kubo, T., Nakasuji, K., Ikeda, R., Kojima, T., Kitagawa, H., *Synth. Met.,* **2005**, *154*, 89.

[30] Fujishima, M., Enyo, M., Kanda, S., Ikeda, R., Kitagawa, H., *Chem. Lett.,* **2006**, *35*, 546.

[31] Yamada, T., Sadakiyo, M., Kitagawa, H., *J. Am. Chem. Soc.*, **2009**, *131*, 3144.

[32] Morikawa, S., Yamada, T., Kitagawa, H., *Chem. Lett.*, **2009**, 654.

[33] Yamada, T., Morikawa, S., Kitagawa, H., *Bull. Chem. Soc. Jpn.*, **2010**, *83*, 42.

[34] Bureekaew, S., Horike, S., Higuchi, M., Mizuno, M., Kawamura, T. Tanaka, D., Yanai, N., Kitagawa, S., *Nat. Mater.*, **2009**, *8*, 831.

[35] Kanaizuka, K., Iwakiri, S., Yamada, T., Kitagawa, H., *Chem. Lett.*, **2010**, 28.

[36] Hurd, J. A., Vaidhyanathan, R., Thangadurai, V., Ratcliffe, C. I., Moudrakovski, I. L., Shimizu, G. K. H., *Nat. Chem.*, **2009**, *1*, 705.

[37] Taylor, J. M., Mah, R. K., Moudrakovski, I. L., Ratcliffe, C. I., Valdhyanathan, R., Shimizu, G. K. H., *J. Am. Chem. Soc.*, **2010**, *132*, 14055.

[38] Ōkawa, H., Sadakiyo, M., Shigematsu, A., Miyakawa, T., Ohba, M., Kitagawa, H., *J. Am. Chem. Soc.*, **2009**, *131*, 13516.

[39] Yang, A.-H., Zou, J.-Y., Wang, W.-M., Shi, X.-Y., Gao, H.-L., Cui, J.-Z., Zhao, B., *Inorg. Chem.*, **2014,** *53*, 7092-7100.

[40] Yan, Y., Wu, C. D., Lu, C. Z. Z., *Anorg. Allg. Chem.*, **2003**, *629*, 1991−1995.

[41] Zhang, X. M., Fang, R. Q., *Inorg. Chem.*, **2005**, *44*, 3955−3959.

[42] Zhang, X. M., *Coord. Chem. Rev.*, **2005**, *249*, 1201−1219.

[43] Sun, Y. Q., Zhang, J., Yang, G. Y., *Chem. Commun.*, **2006**, 1947−1949.

[44] Zheng, Y. Z., Tong, M. L., Chen, X. M., *J. Mol. Struct.*, **2006**, *796*, 9−17.

[45] Li, M., Xiang, J. F., Yuan, L. J., Wu, S. M., Chen, S. P., Sun, J. T., *Cryst. Growth Des.*, **2006**, *6*, 2036−2040.

[46] Wu, W. P., Wang, Y. Y., Wu, Y. P., Liu, J. Q., Zeng, X. R., Shi, Q. Z., Peng, S. M., *CrystEngComm*, **2007**, *9*, 753−757.

[47] Lisitsyn, A. S., *Appl. Catal., A*, **2007**, *332*, 166−170.

[48] Gooßen, L. J., Thiel, W. R., Rodríguez, N., Linder, C., Melzer, B., *Adv. Synth. Catal.*, **2007**, *349*, 2241−2246.

[49] Shepard, A. F., Wilson, N. R., Johnson, J. R., *J. Am. Chem. Soc.*, **1930**, *52*, 2083−2090.

[50] Kreno, L. E., Leong, K., Farha, O. K., Allendorf, M., van Duyne, R. P., Hupp, J. T., *Chem. Rev.*, **2012,** *112,* 1105.

[51] Yu-Cheng, Z., Liang, Z., Hong-Yan, L., Qui-Lei, X., Ming-Yu, T., You-Xuan, Z., Jing-Lin, Z., Hong-Jie, Z., Xiao-Zeng, Y., *Adv., Mater.*, **2011,** *23,* 4041.

[52] Mojgan, R., Xiao, Z., Jing, L., *Angew. Chem. Int. Ed.*, **2012,** *124,* 451.

[53] Luo, F., Wang, M.-S., Luo, M.-B., Sun, G.-M., Song, Y.-M., Li, P.-X., Guo, G.-C., *Chem. Commun.*, **2012,** *48,* 5989.

[54] Della Rocca, J., Liu, D., Lin, W., *Acc. Chem. Res.*, **2011,** *44,* 957.

[55] Zhao, J.-P., Xu, J., Han, S.-D., Wang, Q.-L., Bu, X.-H., *Adv. Mater.*, **2017,** *29,* 1606.

[56] Wang, H., Xu, J., Zhang, D.-S., Chen, Q., Wen, R.-M., Chang, Z, Bu, X.-H., *Angew. Chem. Int. Ed.*, **2015,** *54,* 5966.

[57] Gao, Q., Xu, J., Cao, D., Chang, Z, Bu, X.-H., *Angew. Chem. Int. Ed.*, **2016,** *55,* 15027.

[58] Gu, Z.-G., Fang, H.-C., Yin, P.-Y., Tong, L., Ying, Y., Hu, S.-J., Li, W.-S., Cai, Y.-P., *Cryst. Growth Des.*, **2011,** *11,* 2220-2227.

[59] Feng, X., Zhao, J., Liu, B., Wang, L., Ng, S., Zhang, G., Wang, J., Shi, X., Liu, Y., *Cryst. Growth Des.*, **2010,** *10,* 1399-1408.

[60] Akhtar, M. N., Chen, Y.-C., AlDamen, M. A., Tong, M.-L., *Dalton Trans.*, **2017,** *46,* 116.

[61] Orts-Arroyo, M., Rabelo, R., Carrasco-Berlanga, A., Moliner, N., Cano, J., Julve, M., Lloret, F., De Munno, G., Ruiz-Garcia, R., Mayans, J., Martinez-Lillio, J., Castro, I., *Dalton Trans.*, **2021,** *50,* 3801.

[62] Liu, C.-M., Zhang, D.-Q., Zhu, D.-B., *Chem. Commun.*, **2016,** *52,* 4804.

[63] Wang, J.-J., Si, P.-P., Yang, J., Zhao, S.-S., Li, P.-P., Li, B., Wang, S.-Y., Lu, M., Yu, S.-X., *Polyhedron*, **2019,** *162,* 255-26.

[64] West, R., *Isr. J. Chem.*, **1979,** *20,* 300-307.

[65] Zhang, S., Ke, H., Liu, X., Wei, Q., Xie G., Chen, S., *Chem. Commun.*, **2015**, *51*, 15188–15191.

[66] Wang, P., Fan, R.-Q., Liu, X.-R., Wang, L.-Y., Yang, Y.-L., Cao, W.-W., Yang, B., Hasi, W., Su, Q., Mu, Y., *CrystEngComm*, **2013**, *15*, 1931–1949.

[67] Liu, T.-F., Zhang, W., Sun W.-H., Cao, R., *Inorg. Chem.,* **2011**, *50*, 5242–5248.

[68] Meng, Y., Liu, J.-L., Zhang, Z.-M., Lin, W.-Q., Lin Z.-J., Tong, M.-L., *Dalton Trans.*, **2013**, *42*, 12853–12856.

[69] Meng, Y., Chen, Y.-C., Zhang, Z.-M., Lin Z.-J., Tong, M.-L., *Inorg. Chem.*, **2014**, *53*, 9052–9057.

[70] Sibille, R., Didelot, E., Mazet, T., Malaman B., François, M., *APL Mater.*, **2014**, *2*, 124402–124407.

[71] Biswas, S., Mondaland, A. K., Konar, S., *Inorg. Chem.,* **2016,** *55*, 2085-2090.

[72] Bruker, *APEX2* and *SAINT*, Bruker AXS Inc., Wisconsin, Madison, USA, **2015**.

[73] Sheldrick, G. M., *Acta Cryst.* **2015,** *A71*, 3–8.

[74] Sheldrick, G. M., *Acta Cryst.* **2015,** *C71*, 3–8.

[75] Dolomanov, O. V., Bourhis, L. J., Gildea, R. J., Howard, J. A. K. & Puschmann, H., *J. Appl. Cryst.*, **2009**, *42*, 339–341.

[76] Kovalchukova, O. & Strashnova, S., *Rev. Inorg. Chem.*, **2014**, *34*, 1–24.

CHAPTER VII. GENERAL CONCLUSIONS

In this dissertation, we have investigated the coordination chemistry of rhodizonate with several metals, and N-donating co-ligands. We have also investigated the rhodizonate decomposition in solution and how these decomposition products coordinate with select metals. In Chapter II, we reported on the coordination chemistry between Pb(II) and rhodizonate in relation to the sodium rhodizonate test. We were able to quantify the binding affinity of each reagent to the Pb(II)-rhodizonate complex as the sodium rhodizonate test is performed. XPS and FT-IR data further reveal the structure of each product from each step of the sodium rhodizonate test in the solid state. With this information in hand, we were able to formulate the structure of each compound formed at each step of the sodium rhodizonate test, which is different in solution *vs*. the solid state.

Chapter III extends the research of the coordination chemistry of rhodizonate to lanthanides. Several Ln were tested in both solution and in the solid state. While many of the Ln(III) complexes showed similar FT-IR absorption patterns, their elemental analysis and the results of their UV-Vis Job Plots show a variety of binding ratios between Ln(III) and rhodizonate. UV-Vis titrations give a broad range of binding constants among the various lanthanides, spanning almost three orders of magnitude. This wide variation in binding constants could potentially be exploited to separate lanthanides, and, if such variation were to occur in actinide rhodizonate complexes, facilitate An/Ln separations through selective precipitation.

In Chapter IV, we reported on the coordination chemistry of rhodizonate with Cd(II) and Hg(II) and what happens when N-donating co-ligands, such as bipy, phen, and imidazole are added to solutions of preformed binary M(II)-rhodizonate complexes. In all

the cases studied, the addition of such co-ligands showed favorable formation of ternary complexes of type M(rho)(coligand). Furthermore, of the three N-donating co-ligands tested, imidazole produced complexes that were of a markedly different color from both the complexes of the other two N-donating co-ligands and of the binary complexes. This difference was especially pronounced for Hg(II) ternary complexes.

Finally, Chapters V and VI explored the coordination chemistry of rhodizonate decomposition products croconate (Chapter V) and oxalate (Chapter VI). Chapter V introduced two recently published croconate crystal structures with Cd(II) and Pb(II). Cd(II)-croconate crystals consist of 1D zig-zag chains whose layers are held together through H-bonding. Pb(II)-croconate crystals, in contrast, consist of a similar appearing 1D chain that is bonded with actual chemical bonds to adjacent layers, forming a true 3D structure. Chapter VI introduced two new X-ray crystal structures of oxalate with Cd(II) and Yb(III). These oxalate MOFs owe their unique 3D shape to the decomposition of rhodizonate to croconate to oxalate. Chapter VI also reported more -in depth- studies quantifying the solvent-dependent decomposition of the rhodizonate dianion and determining rhodizonate stability in various solvent systems.

VITA

JOSHUA ALLEN SILVERMAN

Born, Fairfax, Virginia

2007	B.S., Electrical Engineering University of Florida Gainesville, Florida
2013	B.S., Chemistry Florida International University Miami, Florida
2016-2021	NRC Fellowship Grant numbers NRC-HQ-84-14-G-0040 and NRC-HQ-84-15-G-0038/0038B
2019	M.S., Chemistry Florida International University Miami, Florida
2021	Ph. D., Chemistry: Radiochemistry Track Florida International University Miami, Florida

PUBLICATIONS AND PRESENTATIONS

Joshua A. Silverman, Logesh Mathivathanan, Evgen V. Govor, Raphael G. Raptis, and Konstantinos Kavallieratos, Coordination polymers of Cd(II) and Pb(II) with croconate show remarkable differences in coordination patterns: a structural and spectroscopic study, Acta Cryst., C75, 2019, 935-940.

Joshua A. Silverman, Evgen V. Govor, and Konstantinos Kavallieratos, Coordination chemistry of the rhodizonate anion: Towards understanding the Na-rhodizonate test for Pb, 251st ACS National Meeting & Exposition, San Diego, CA, March 13-17, 2016.

Joshua A. Silverman, Evgen V. Govor, and Konstantinos Kavallieratos, Coordination chemistry of the rhodizonate anion with Pb(II) and lanthanides: From understanding complexation to analytical applications, 253rd ACS National Meeting & Exposition, San Francisco, CA, April 2-6, 2017.

Joshua A. Silverman, Evgen V. Govor, and Konstantinos Kavallieratos, Coordination of Lanthanides with the Rhodizonate Anion, 42nd Actinide Separations Conference, Charleston, SC, May 21-24, 2018.

Joshua A. Silverman, Logesh Mathivathanan, Evgen V. Govor, Raphael G. Raptis, and Konstantinos Kavallieratos, Coordination chemistry of the rhodizonate anion with Pb(II) and lanthanides: From understanding complexation to analytical applications (revised), Florida Inorganic and Materials Symposium, Gainesville, FL, September 28-29, 2018.

Joshua A. Silverman, and Konstantinos Kavallieratos, Investigation of Coordination Chemistry of Rhodizonate – Towards Understanding the Na-Rhodizonate Test for Pb, 92nd Florida Annual Meeting and Exposition, Tampa, FL, May 2016.

Joshua A. Silverman, and Konstantinos Kavallieratos, Coordination chemistry of the rhodizonate anion with divalent toxic metals: Binary and ternary rhodizonate complexes for spectrophotometric M(II) detection, 257th ACS National Meeting and Exposition, Orlando, FL, March 31-April 4, 2019.

Joshua A. Silverman, Logesh Mathivathanan, Evgen V. Govor, Raphael G. Raptis, Christopher J. Dares, Shannon J. Saluga, and Konstantinos Kavallieratos, Coordination Chemistry of the Rhodizonate and Croconate Oxocarbons with Toxic Metals: Structural and Spectroscopic Studies, FIMS, Gainesville, FL, October 12, 2019.